Journal of Morphological Sciences

ISSN: 0102-9010
eISSN: 2177-0298

Editor
Valéria Paula Sassoli Fazan

Number 2 • Volume 36 • Pages 55–144 • June 2019

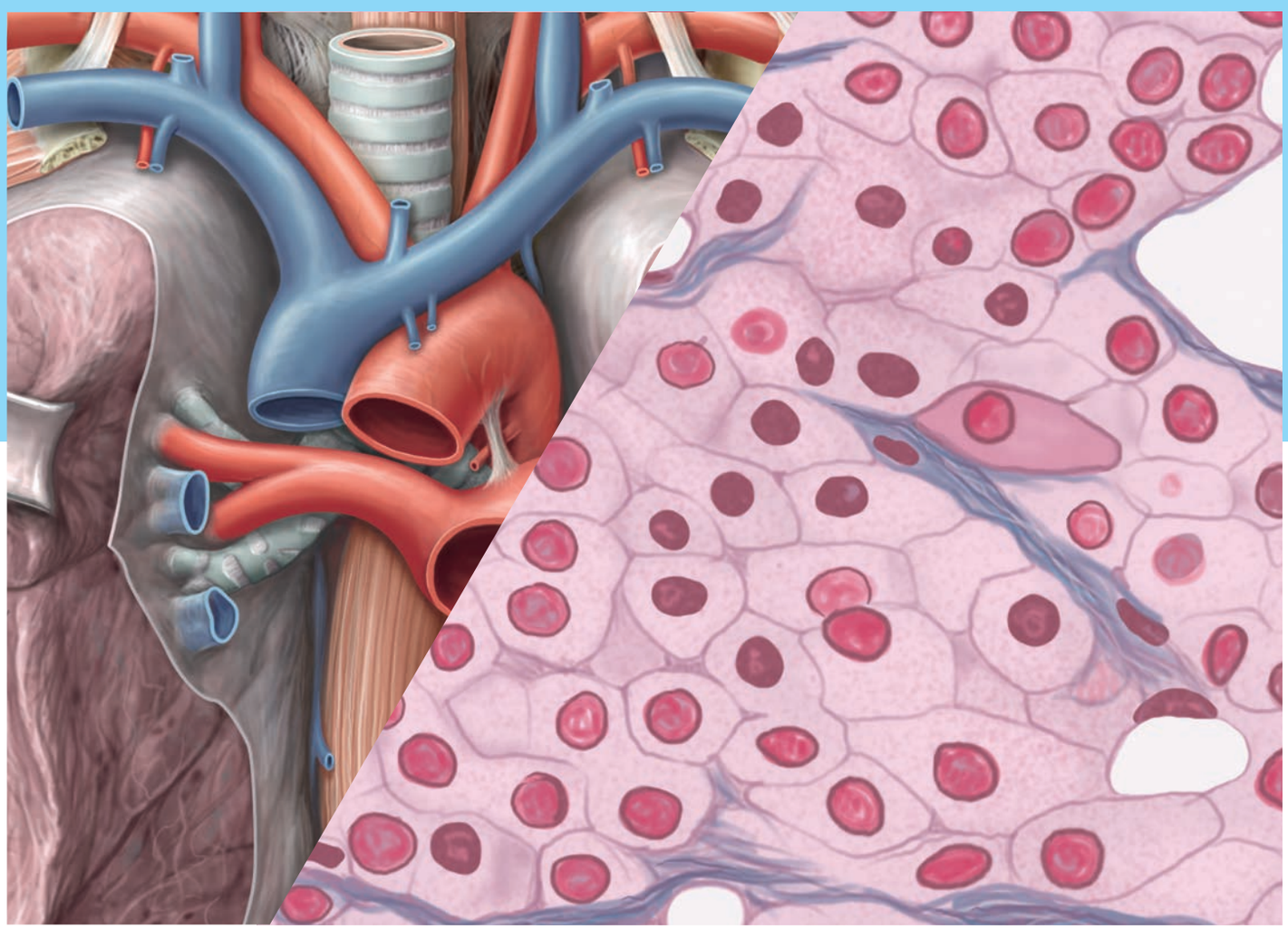

OPEN ACCESS

Thieme

ISSN 0102-9010

Journal of Morphological Sciences

Editor-in-chief

Profa. Dra. Valéria Paula Sassoli Fazan
Faculdade de Medicina de Ribeirão Preto, Universidade de São Paulo, São Paulo, Brazil

Associated Editors

Prof. Dr. Norberto Cysne Coimbra, MD, PhD
Faculdade de Medicina de Ribeirão Preto, Universidade de São Paulo, São Paulo, Brazil

Prof. Dr. João Paulo Mardegan Issa, DDS, PhD
Faculdade de Odontologia de Ribeirão Preto, Universidade de São Paulo, São Paulo, Brazil

Prof. Dr. Marco Aurélio Pereira Sampaio, DMV, PhD
Universidade Federal Fluminense, Niterói, Rio de Janeiro, Brazil

Editorial Board

Alberto Rodríguez Torres
Universidad De Chile, Santiago, Chile

Alessandro Riva
Department of Biomedical Science, Università degli studi di Cagliari, Cagliari, Italy

Alexandre Leite Rodrigues de Oliveira
Universidade Estadual de Campinas, Campinas, São Paulo, Brazill

Beverley Kramer
University of the Witwatersrand - Johannesburg, South Africa

Bruno König Júnior
Universidade de São Paulo, São Paulo, Brazil

Cagatay Barut
Department of Anatomy, Bahçeşehir University - Istambul, Turkey

Carlos Alberto Mandarim de Lacerda
Universidade do Estado do Rio de Janeiro, Rio de Janeiro, Rio de Janeiro, Brazil

David Brynmor Thomas
University of St Andrews, St Andrews, Scotland

David Kachlik
Charles University, Prague, Czech Republic

Diogo de Freitas Branco Pais
Universidade NOVA de Lisboa, Portugal

Fernando José Dias
Universidad de La Frontera, Temuco, Chile

Gilberto Cerqueira
Universidade Federal do Ceará, Fortaleza, Ceará, Brazil

Gordana Teofilovski-Parapid
University of Belgrade, Serbia

Guido Macchiarelli
Facoltà di Medicina e Chirurgia, Università dell'Aquila, L'Aquila, Italy

Hakan Hamdi Celik
Hacettepe University Faculty of Medicine, Turkey

Humberto Guiraldes del Canto
Facultad de Medicina Clínica Alemana de la Universidad del Desarrollo, Santiago, Chile

Jacques Patrick Barbet
Hôpital Saint Vincent de Paul, Paris, France

John F Morris
University of Oxford, England

José Aderval Aragão
Universidade Federal de Sergipe, São Cristovão, Sergipe, Brazil

José de Anchieta C Horta Júnior
Universidade Estadual Paulista Júlio de Mesquita Filho, Botucatu, São Paulo, Brazil

Luciana Sayuri Sanada
Universidade Federal de Santa Catarina, Florianópolis, Santa Catarina, Brazil

Manuel Angeles Castellanos
Universidad Nacional Autónoma de México, Mexico

Mariano del Sol
Universidad de La Frontera, Temuco, Chile

Marcelo Abidu Figueiredo
Universidade Federal Rural do Rio de Janeiro, Seropédica, Rio de Janeiro, Brazil

Marcelo Cavenaghi Pereira da Silva
Universidade federal de São Paulo, São Paulo, São Paulo, Brazil

Márcio Antônio Babinski
Universidade Federal Fluminense, Niterói, Rio de Janeiro, Brazil

Marco Antonio Stefani
Universidade Federal do Rio Grande do Sul, Porto Alegre, Rio Grande do Sul, Brazil

Mustafa F. Sargon
Hacettepe University, Turkey

Nalini Pather
UNSW EPICentre, Sidney, Australia

Ricardo Jorge Losardo
Universidad del Salvador, Buenos Aires, Argentina

Richard L. Drake
University of Mount Union, Ohio, USA

Robert W. Henry
University of Queensland, Brisbane, Australia

Stephen Carmichael
American Association of Clinical Anatomists, LaGrange, USA

Udo Schumacher
Department of Anatomy and Experimental Morphology, University Medical Center Hamburg, Germany

Editorial Office

Monise Moreno (e-mail: monise_moreno@yahoo.com.br)

Office Address

Journal of Morphological Sciences
Av. Prof. Lineu Prestes, 2415,
ICBIII, 05508-900, São Paulo - SP, Brazil
Phone: +55 11 3814-8266/3091-7369,
Fax: +55 11 3812-7216
E-mail: sba@icb.usp.br

Volume 36, Number 2/2019

Journal of Morphological Sciences

Thieme Revinter Publicações Ltda

online www.thieme-connect.com/products

Case Reports

Copyright © 2019 by Thieme Revinter Publicações Ltda, Rio de Janeiro, Brazil. *Journal of Morphological Sciences* is published four times a year in March, June, September, and December by Thieme-Revinter Publicações Ltda, Rua do Matoso, 170, Rio de Janeiro, 20270-135, Brazil.

Editorial comments should be sent to **journals@thieme.com**. Articles may be submitted to this journal on an open-access basis. For further information, please send an e-mail to openaccess@thieme.com. The content of this journal is available online at **www.thieme-connect.com/products.** Visit our Web site at **www. thieme.com** and the direct link to this journal at **www.thieme.com/jms.**

Journal of Morphological Sciences is issued by SBA-Sociedade Brasileira de Anatomia (Brazilian Society of Anatomy) and publishes scientific articles in the area of vertebrate and invertebrate animals.

Journal of Morphological Sciences is listed in Scopus, LILACS (Latin-American and Caribbean Center on Health Sciencies Information), IMLA (Index Medicus Latino-Americano), Veterinary Science Database, CAB Abstracts, CAB Health e BIOSIS (Biological Abstracts and Zoological Record).

ISSN 0102-9010

Some of the product names, patents, and registered designs referred to in this publication are in fact registered trade marks or proprietary names even though specific reference to this fact is not always made in the text. Therefore, the appearance of a name without designation as proprietary is not to be construed as a representation by the Publisher that it is in the public domain.

All rights, including the rights of publication, distribution, and sales, as well as the right to translation, are reserved. No part of this work covered by the copyrights hereon may be reproduced or copied in any form or by any means—graphic, electronic, or mechanical, including photocopying, recording, taping, or information and retrieval systems—without written permission of the Publisher.

Important Note: Medical knowledge is ever-changing. As new research and clinical experience broaden our knowledge, changes in treatment and drug therapy may be required. The authors and editors of the material herein have consulted sources believed to be reliable in their efforts to provide information that is complete and in accord with the standards accepted at the time of publication. However, in view of the possibility of human error by the authors, editors, or publisher of the work herein, or changes in medical knowledge, neither the authors, editors, or publisher, nor any other party who has been involved in the preparation of this work, warrants that the information contained herein is in every respect accurate or complete, and they are not responsible for any errors or omissions or for the results obtained from use of such information. Because of rapid advances in the medical sciences, independent verification of diagnoses and drug dosages should be made. Readers are encouraged to confirm the information contained herein with other sources. For example, readers are advised to check the product information sheet included in the package of each drug they plan to administer to be certain that the information contained in this publication is accurate and that changes have not been made in the recommended dose or in the contraindications for administration. This recommendation is of particular importance in connection with new or infrequently used drugs.

Although all advertising material is expected to conform to ethical (medical) standards, inclusion in this journal does not constitute a guarantee or endorsement of the quality or value of such product or of claims made by its manufacturer.

Editorial

The Journal of Morphological Sciences Presents the New Associate Editors

[1] Department of Surgery and Anatomy, Faculdade de Medicina de Ribeirão Preto, Universidade de São Paulo, Ribeirão Preto, SP, Brazil

J Morphol Sci 2019;36:55–56.

The Journal of Morphological Sciences is still sometimes referred to as the Brazilian Journal of Morphological Sciences among the colleagues in the anatomical field of expertise, due to its direct link to the Brazilian Society of Anatomy. Historical facts about the creation of the journal and how it changed with time was recently published,[1] and the name of the journal was changed to Journal of Morphological Sciences (in 2010) to broaden the readership and also to be an attractive journal for international contributors. Currently, more than 30% of the manuscripts published in the journal are from authors from outside of Brazil, and the journal will continue to work hard to expand its internationalization.

One challenge that the Journal of Morphological Sciences is facing is the variety of subjects of interest to our readers. We have detected three major areas of manuscripts submitted to our journal that need special attention from our editorial board to help speeding up the process of publication. Thus, three associate editors are reinforcing our editorial board to give particular attention to the manuscripts in their specific area of interest. They are highly qualified researchers in their fields, with national recognition and international prestige. These new associate editors are presented below.

João Paulo Mardegan Issa, DDS, M.S., PhD (http://lattes.cnpq.br/9557307818304730)

Graduated in dentistry from the University of São Paulo (2003), João Paulo Mardegan Issa holds a master's degree in dentistry (oral rehabilitation) from the University of São Paulo (2006) and a PhD in sciences from the University of São Paulo (2007). He was a postdoc fellow with a FAPESP Scholarship in Brazil (2010) and abroad, at the Princess Margaret Hospital, University of Toronto (2013). He is currently an Associate Professor 1 in Anatomy at the Dental School of Ribeirão Preto, Universidade de São Paulo. He has experience in the area of bone repair and of regenerative medicine.

Norberto Cysne Coimbra, MD, M.S., PhD (http://lattes.cnpq.br/7087724353350725)

Norberto Cysne Coimbra is a medical doctor graduated at the Faculdade de Medicina of the Universidade Federal do Espírito Santo (1988), has a master's degree in neuropsychobiology from the Ribeirão Preto School of Philosophy, Sciences and Literature of the Universidade de São Paulo (1991), and PhD in morphology-cellular biology from the Ribeirão Preto Medical School of the Universidade de São Paulo (1995). He was a postdoc in the Pain Imaging Neuroscience (PaIN) Group of the Department of Physiology, Anatomy & Genetics of the University of Oxford from 09/01/2006 to 30/06/2006, and in the Centre for Functional Magnetic Resonance Imaging of the Brain (FMRIB) of the Clinical

Address for correspondence Valéria Paula Sassoli Fazan, MD, PhD, Departamento de Cirurgia e Anatomia, Escola de Medicina de Ribeirão Preto, Universidade de São Paulo, Av. dos Bandeirantes 3900, Monte Alegre, Ribeirão, Preto, SP, 14049-900, Brazil (e-mail: vpsfazan@yahoo.com.br).

DOI https://doi.org/10.1055/s-0039-1692446.
ISSN 2177-0298.

Copyright © 2019 by Thieme Revinter Publicações Ltda, Rio de Janeiro, Brazil

License terms

Neurology Department of the University of Oxford (Oxford, England, United Kingdom), from 01/07/2006 to 08/01/2007. He is an Associate Professor (Level III) in the Department of Pharmacology of the Ribeirão Preto Medical School of the Universidade of São Paulo (2010), working mainly in the following subjects: neuroanatomy, neuropharmacology, psychopharmacology, neurotracing, fear defense, and behavior.

Marco Aurélio Pereira Sampaio, DMV, M.S., PhD (http://lattes.cnpq.br/2974617010463918)

Marco Aurélio Pereira Sampaio holds a bachelor's degree in veterinary medicine from the Universidade Federal Fluminense (1985), a master's degree in morphology from the State University of Rio de Janeiro (1995), a PhD in morphology from the State University of Rio de Janeiro, with a PhD fellowship at the University of Tennessee. He is currently an Associate Professor at the Universidade Federal Fluminense, President of the World Association of Veterinary Anatomists, Member of the Subcommittee of Splanchnology of the International Committee on Veterinary Gross Anatomical Nomenclature, Director of the Postgraduate Program in Pathophysiology and Surgical Sciences of the Universidade do Estado do Rio de Janeiro, and member of the editorial board of the journals Archives of Clinical Nephrology and Bulgarian Journal of Veterinary Medicine. Ad hoc reviewer of several international and national journals. He has experience in the area of morphology, with emphasis on plastination and comparative anatomy of the urogenital system, working mainly in the following subjects: animal anatomy, urology, surgical technique, experimental models in urology, teaching, and stereology.

Valéria Paula Sassoli Fazan
MD, PhD, Editor-in-Chief
Journal of Morphological Sciences

Reference

1 Rueff-Barroso et al. Profile Analysis of the Scientific Articles Published in the Journal of Morphological Sciences between 2000 and 2017: A Bibliometric Study. J Morphol Sci 2018;35 (04):255–260. Doi: 10.1055/s-0038-1676541

Human Mandible Prenatal Morphogenesis

Sergey Lvovich Kabak[1] Natalia Victorovna Zhuravleva[1] Yuliya Michailovna Melnichenko[1]

[1] Human Morphology Department, Belarusian State Medical University, Minsk, Belarus

J Morphol Sci 2019;36:57–62.

Address for correspondence Sergey Lvovich Kabak, PhD, Human Morphology Department, Belarusian State Medical University, Dzerzhinsky Avenue 83, 220116, Minsk, Belarus (e-mail: kabakmorph@gmail.com).

Abstract

Introduction This study was performed with the aim of detecting the interaction between cartilaginous and bone tissues in the process of mandible morphogenesis in human embryos.

Material and Methods Whole-mount skeletal preparations, stained with Alcian blue and Alizarin red, as well as serial histological sections impregnated with silver and stained with hematoxylin and eosin were studied. A total of 48 human embryos/fetuses from 5 to 29 weeks of age were used.

Results In the mandible anlage, in addition to the woven bone, cartilaginous and chondroid tissues are present. Cartilaginous tissue islets are localized at the tip of the condylar and coronoid processes and also in the region of the mandibular symphysis. The chondroid tissue is incorporated into the bone in the region of the mandibular symphysis, along the edge of the coronoid process, and also in the alveolar part of the mandible.

Conclusion Meckel's cartilage participates in the formation of the mandibular body, and its remains persist in the area of the mandibular symphysis until the second half of the prenatal development.

Keywords
- mandible
- human development
- Meckel's cartilage
- chondroid tissue
- condylar cartilage

Introduction

In an adult, the mandible is an unpaired bone that forms part of the facial skull. In newborns, it consists of two halves separated by a mandibular symphysis, which, in addition to fibrous connective tissue, includes fragments of cartilaginous tissue (chondriola symphysea), as well as one or more ossicula mentalia.[1] The two halves of the mandible and ossicula mentalia combine into a single bone in the first year of life (by 9–12 months).

The mandible as the derivative of the first pharyngeal arch develops from the cells of the neural crest, which migrate to the mandibular processes of the mandibular arch in the 4th week of embryonic development.[2] Differentiation of the cells of the ectomesenchyme of the first pharyngeal arch begins after ingrowth of the maxillary nerve, which, due to neurotropic factors, induces chondrogenesis and osteogenesis.

An important role in the mandible morphogenesis is played by Meckel's cartilage—"the primary lower jaw." It is a template by which the size of the primary ossification centers increases. In the experiment, external influences that disrupt the growth of Meckel's cartilage lead to mandibular hypoplasia.[3]

At present, the question of Meckel's cartilage ossification and its incorporation into the mandibular body remains controversial. In addition, the participation of secondary cartilage in the formation of the mandible has not been adequately described in the literature.

The purpose of this study is to detect an interaction between cartilaginous and bone tissues in the process of mandible morphogenesis in human embryos.

Material and Methods

Forty-eight human embryos/fetuses between 5 and 29 weeks in utero and without visible developmental anomalies were studied. Their age was determined by the crown-rump length (CRL) or according to obstetric anamnesis (►**Table 1**). Part of the material was totally stained with Alcian blue and Alizarin red, followed by clearing in an alkaline solution. Serial histological sections of entire embryos from the collection of the Normal Anatomy Department and Histology, Cytology and

received
August 12, 2018
accepted
February 15, 2019

DOI https://doi.org/10.1055/s-0039-1685456.
ISSN 2177-0298.

Copyright © 2019 by Thieme Revinter Publicações Ltda, Rio de Janeiro, Brazil

License terms

Table 1 Age of embryos/fetuses used in the study

Size (CRL, mm)	Age (days/weeks)	Number of embryos	Size (CRL, mm)	Age (days/weeks)	Number of embryos
5	28 days **	1 †	–	12 weeks ◊	1 ♦
6	28 days **	7†	–	12 weeks ◊	2 ‡
13	41 days**	6 †	–	13 weeks ◊	1 ♦
15	44 days**	1 †	–	13 weeks ◊	4 ‡
17	47 days **	4†	73	13 + 3 weeks^	1 †
19	49 days**	1 †	–	14 weeks ◊	1 ‡
27	54 days **	1 †	–	16 weeks ◊	1 ‡
–	10 weeks ^	1 ♦	–	20 weeks ◊	5 ‡
–	11 weeks◊	4 ♦	–	21 weeks ◊	1 ‡
48	11 + 3 weeks^	4 †	–	29 weeks◊	1 ‡

Abbreviation: CRL, crown-to-rump length.
Notes:
** www.ehd.org/developmental-stages/stage0.php.
^http://onlinelibrary.wiley.com/doi/10.1002/uog.13448/full.
◊ gestational age (according to obstetric anamnesis).
† - serial histological sections of the embryos.
‡ - histological sections of the mandible fragments.
♦ - whole-mount skeletal preparations.

Embryology Department of the Belarusian State Medical University together with individual fragments of the mandible—impregnated by silver nitrate, according to Bilshovsky-Buke, and stained with hematoxylin and eosin—were also studied. The present study was approved by the Medical Ethics Committee of the Belarusian State Medical University, Minsk, Belarus (Protocol No.: 2017/2).

The present study was approved by the Medical Ethics Committee of the Belarusian State Medical University, Minsk, Belarus (Protocol No.: 2017/2). Photos of anatomical and histological specimens were obtained using a Leica Microsystems stereomicroscope (Leica Microsystems, GmbH, Wetzlar, Germany) and an optical microscope Leica DM2500 (Leica Microsystems).

Results

By the beginning of the 5th week of embryogenesis, the lower wall of the stomodeum is formed from the fusion of the two mandibular processes. In human embryos with a CRL of 13 mm, in the mandibular processes, next to the third branch of the trigeminal nerve, a Meckel's cartilage anlage in the form of mesenchyme condensation is revealed. In the 7th week of prenatal development, Meckel's cartilage is a paired typical hyaline cartilage surrounded by perichondrium that extends from the ear capsule to the midline, where the cartilages of opposite sides are separated by a layer of mesenchymal tissue. On the lateral side of the Meckel's cartilage, there is the inferior alveolar nerve, on the medial side—the lingual nerve, which is directed toward the tongue anlage.

In embryos with a CRL of 13 mm (7 weeks), on the histological sections from both sides of the midline outside the Meckel's cartilage, the primary center of ossification appears in the thickness of the mesenchyme of the mandibular processes (►**Fig. 1A**). In this area, the bony trabeculae containing the oxyphilic extracellular matrix are formed. Presence of bony trabeculae indicates the beginning of organic matrix (osteoid) secretion by osteoblasts. The primary center of ossification first looks like a plate located on the lateral side of the Meckel's cartilage and is separated from it by the inferior alveolar nerve. In the following, the process of intramembranous ossification extends downward, backward, forward and upward. By the end of the embryonic period, the anlage of the mandibular body is formed by two bone plates. They partially merge, resulting in the formation of the Y-shaped structure, which, in the form of a groove, covers the inferior alveolar nerve from below (►**Fig. 1B**). The medial bone plate is in close contact with the perichondrium of Meckel's cartilage. There is a wide gap (the area of the future mental foramen) in the lateral bone plate. At this point, the inferior alveolar nerve turns to the side and appears outside the lateral bone plate continuing as the mental nerve (►**Fig. 1C, D**).

In the serial sections of the embryo with a CRL of 48 mm (12th week of development), mesenchymal condensation is revealed in the region of the future condylar process. It is located on the distal (posterior) end of the bony trabeculae of the mandibular body, covered with the periosteum. Soon the mesenchymal condensation is replaced by a cartilaginous tissue. Due to its rapid increase in volume in fetuses at 11 to 12 weeks of development, cartilage (the core of the condylar process) is formed, which looks like an inverted cone (►**Fig. 1E**). Its broad base is turned toward the mandibular fossa of the temporal bone, and the apex is directed in the opposite direction, reaching the level of the mandibular foramen. Outside the cartilage, a periosteal bone collar is formed. The collar causes dystrophic changes in the underlying cartilage that manifest hypertrophy of the

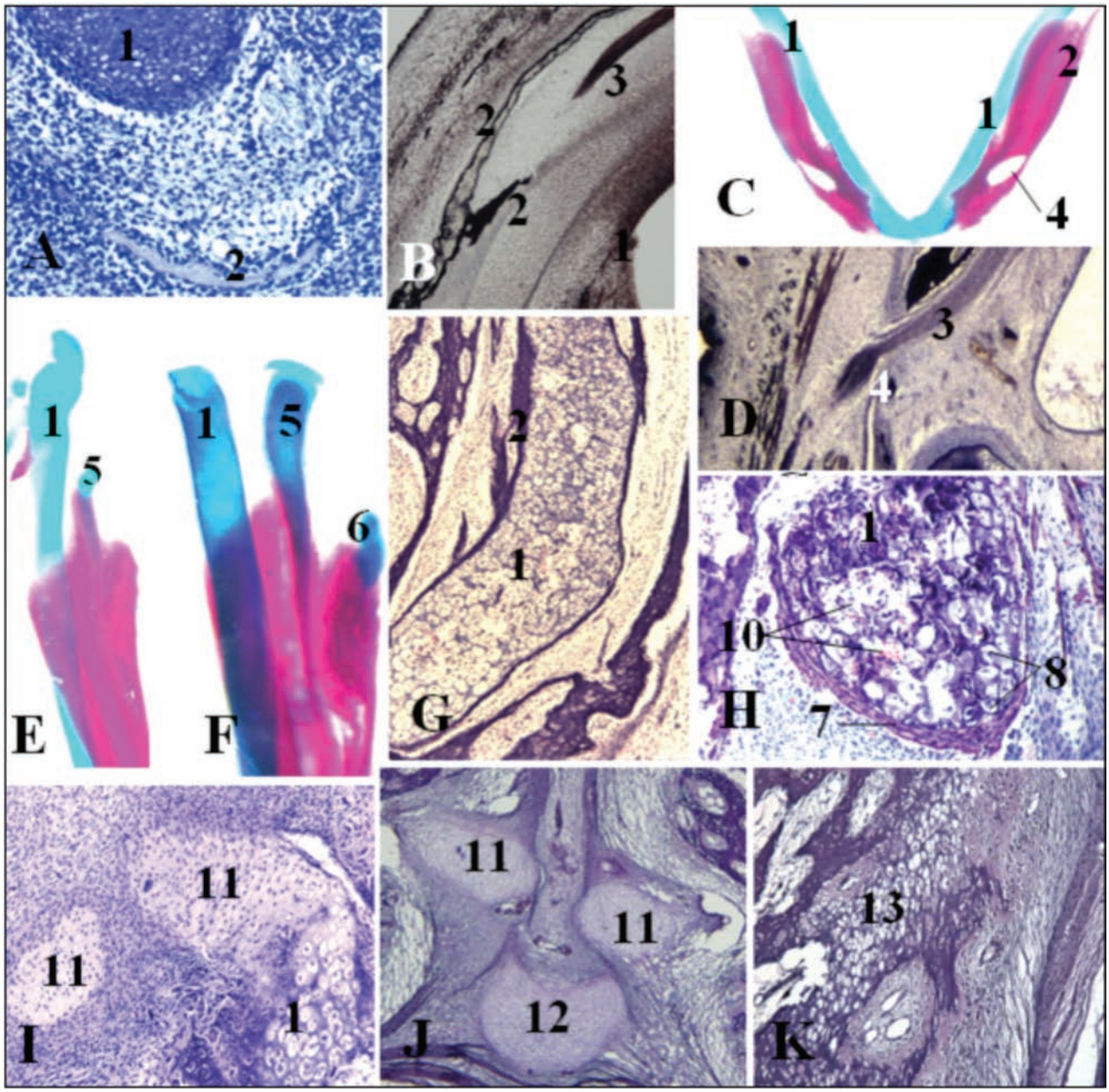

Fig. 1 Organogenesis and histogenesis of the mandible in human embryos (A – 13 mm CRL, B – 27 mm CRL, C – 10 weeks, D – 73 mm CRL, E – 11 weeks, F – 12 weeks, G, H – 13 weeks, I – 16 weeks; J, K – 20 weeks). 1–Meckel's cartilage, 2–bone plates, 3–inferior alveolar nerve, 4–mental foramen, 5–condylar cartilage, 6–coronoid cartilage, 7–periosteal bone collar, 8–hypertrophic chondrocytes, 9–calcified cartilage matrix, 10–mesenchyme with blood vessels; 11–Meckel's cartilage remnants, 12–secondary cartilage, 13–chondroid tissue in the mandibular symphysis. A, B, D, G-K – photomicrographs of histological preparations; stain: A, H, I-K – hematoxylin-eosin; B, D, G – impregnation with silver nitrate according to Bilshovsky-Buke, magnification: A, H – x200; B, D, G, I – x100; J, K – x40; C, E, F – total preparations; stain: Alcian blue and Alizarin red.

chondrocytes, the vacuolization of their cytoplasm and karyopycnosis, and the mineralization of the matrix in the form of deep purple spicules. Shortly after the appearance of condylar cartilage, the periosteal collar leaves only a small portion of it uncovered at the very end of the condylar process—the head of the mandible.

In the human fetus with a CRL of 73 mm (14th week of development), the head of the mandible and mandibular fossa form temporomandibular joint. An articular cleft completely separates the surfaces of the bony anlages from the articular disc. In human fetuses, starting at 12 weeks of age, the cartilage of the head gradually differentiates into several layers. Twenty-week-old fetuses have superficially located elongated cells—the perichondrium (fibroblastic layer), which extends into the periosteum of the mandibular ramus. A layer of polymorphic cells surrounded by a small amount of basophilic intercellular matrix lies deeper continuing in the wide zone of flat cells. The layer of hypertrophic chondrocytes borders on the zone of cartilage erosion. From the side of the mesenchyme surrounding the cartilage, vascular channels grow into the mandibular condyle. At 12 to 16 weeks of intrauterine development, the end of the

coronoid process of the mandible also reveals a site of cartilage, characterized by alzianophilia on cleared human embryos (►**Fig. 1F**). Histological examination of 20-week-old fetuses revealed the presence of groups of hypertrophic chondrocytes in partially mineralized matrix, surrounded by areas of woven bone, near which the cartilage is partially destroyed. In addition, a strip of cartilaginous tissue was found along the edge of the coronoid process. Within the oxyphilic bone matrix, simultaneously with osteocytes, populations of densely lying large cells located inside the lacunae are determined. The pericellular region around these cells is characterized by a weak basophilia.

Simultaneously with the appearance of cartilage in the condylar and coronary processes, the transformation of the microscopical structure of the Meckel's cartilage begins. In fetuses in the 11th week of intrauterine development, this structure remains intact from the middle ear to the mandibular symphysis, but somewhat changes the direction of its course. Closer to the distal end, the cartilage sharply deflects laterally and closely interacts with the mandibular body anlage. At this point, the cartilage is surrounded by bone trabeculae on three sides. Only its medial surface remains uncovered by bone. The distal end of the Meckel's cartilage is curved in the medial direction toward the cartilage of the opposite side, from which it is separated by a thin interlayer of mesenchyme. In embryos between 13 and 16 weeks, from the lateral side of the Meckel's cartilage through its direct contact with the bone plate of the jaw anlage, hypertrophic chondrocytes are revealed, the integrity of the cellular lacunae walls are broken, and the intercellular matrix is degraded. The described morphological features are the initial manifestations of the destructive degeneration, which gradually spreads across the cartilage (►**Fig. 1G, H**). As a result of the destruction of the Meckel's cartilage, cavities filled with an immature myeloid tissue appear, and areas of the calcified extracellular matrix and woven bone from the side of the perichondrium are identified on non-decalcified preparations. The most distal end of the Meckel's cartilage is separated as an independent structure located in the thickness of the mesenchyme separating the two halves of the mandibular body (►**Fig. 1I**).

In 16-week-old fetuses, in the region of the mandibular symphysis, next to the remains of the Meckel's cartilage, additional fragments of cartilaginous tissue of round or oval shape—consisting of large chondrocytes in the center and smaller cells along the periphery—are identified.

In fetuses between 20 and 29 weeks in utero, the mandibular body looks open from the part above the groove, which contains teeth and the inferior alveolar nerve and vessels. In the mesenchyme of the caudal portion of the mandibular symphysis, from its lingual side, several areas of the cartilaginous tissue are identified alongside the midline. At this point, the symphysis has the form of a triangular extension with the base facing its lingual side.

The paired cartilaginous structures located on both sides of the midline are considered to be the distal portions of the Meckel's cartilage, which undergo progressive atrophy. Microscopically, these structures look like a part of the Meckel's cartilage, located from the medial side of the body of the mandible closer to its angle. In addition to the remnants of the Meckel's cartilage, there is another unpaired cartilaginous rounded structure in the region of the mandibular symphysis, which is located along the midline (►**Fig. 1J**). According to the histological structure, this structure is a typical hyaline cartilage.

In the woven bone, at the distal end of the bone anlage of each half of the mandible facing the mandibular symphysis, areas of the cartilaginous tissue are identified, comprising large, densely located cells of oval shape surrounded by a small amount of a homogeneous matrix, which is slightly basophilic in the pericellular region (►**Fig. 1K**). The presence of a cartilaginous tissue was also found in the alveolar ridge on the lingual side of the mandibular body anlage.

Discussion

Embryogenesis of the mandible is at the top of the discussions among experts studying the morphogenesis of the maxillofacial region.

We have established that two primary ossification centers fused in the midline of the mandibular processes of the human embryos from outside the Meckel's cartilage, near the inferior alveolar nerve. The time and the place of their appearance are consistent with published data.[4,5] It indirectly confirms the inductive effect of the nerves and Meckel's cartilage on the appearance of the primary bone in the mesenchyme of the mandibular processes.

Meckel's cartilage is a transient embryonic structure. There are contradictory reports in the literature about the transformation in embryogenesis of its distal fragment, located from the medial side of the bone anlage of the mandible body. Amano et al (2010),[6] Bontemps et al (2001)[7] and Lee et al (2001)[4] believe that the Meckel's cartilage does not undergo endochondral ossification in humans, but atrophies and gradually disappears. According to Radlanski et al (2016)[8] a site of cartilage, at least along the length from the mental foramen to the midline (at the level of the canine and incisors), is incorporated into the mandible by endochondral ossification. In 14 to 16 week-old fetuses, we observed thinning and subsequent fragmentation of the middle segment of Meckel's cartilage, surrounded by bone tissue from three sides. Chondrocytes, which are the part of this segment, had varying degrees of destructive degeneration, similar to those in endochondral ossification. According to Yang et al. (2012)[9] the destruction of Meckel's cartilage begins with the accumulation of autophagic vacuoles in the cytoplasm of chondrocytes with products of destruction of the extracellular matrix, which subsequently leads to cell death. Classical apoptosis of the cartilaginous cells takes place during endochondral ossification. Authentic endochondral ossification is characterized by the proliferation of chondrocytes first, and then by their hypertrophy followed by calcification of the extracellular matrix. We observed the calcification of the Meckel's cartilage matrix and the formation of woven bone from the side of the perichondrium on non-decalcified preparations. Thus, we should agree with the opinion of the authors who assert that Meckel's cartilage takes part in the formation of the mandibular body.

The proximal extremity of Meckel's cartilage also undergoes ossification to form two of the auditory ossicles, the malleus and incus. In mammals the greater part of this embryonic cartilage between the proximal and distal ossified extremities degenerates to become a fibrous tissue in which amorphous remnants of cartilage may persist for some time. In man ossification of all or part of this fibrous tissue along the medial surface of the mandible results in the bony anomaly called mylohyoid bridge.[10] The ossified middle segment of Meckel's cartilage was present in the symmetrodont Zhangheotherium from Liaoning.[11,12] This fact supports the assumption that chondrocytes from all parts of Meckel's cartilage can transform into the bone. Yang et al (2014)[13] show that hypertrophic chondrocytes can survive the cartilage-to-bone transition and become osteoblasts and osteocytes during endochondral bone formation and in bone repair.

Most of the mandible in embryogenesis is formed by direct osteogenesis, although some of its parts develop on basis of secondary cartilage by indirect osteogenesis.[8] Secondary cartilages appear in embryogenesis later than the primary cartilages forming the chondroskeleton. The periosteum of the primary ossification centers is the source of their development. In the literature, the presence of secondary cartilages was found in the condylar and coronary process, in the mandibular symphysis and the angular region of the mandible, and also in the alveolar ridge at the level of i1, i2, m1, m2, and M1 tooth germs.[8,14,15] Our data about secondary cartilage origin time in embryogenesis are coincident with published data.[8]

There is a typical hyaline cartilage at the end of the condylar and coronary processes of the mandibular angle, as well as between its two halves in the mandibular symphysis region. We have identified the areas of cartilaginous tissue incorporated into the bone along the edge of the coronoid process, in the alveolar crest and in the region of the mandibular symphysis. It can be classified as cartilaginous (chondroid) tissue[1,16] considering its location and external resemblance to the cartilaginous and bone tissue simultaneously.

In 20 to 29 week-old-fetuses there are round shape fragments of cartilage—chondriola symphysea—between the mesial ends of the two halves of the mandible body. There are different opinions about the origin and subsequent modification of these structures in the process of embryogenesis in the literature.

Some authors[2] believe that the chondriola symphysea are the remains of the Meckel's cartilage (Meckelian islets), which turn into the mental ossicula (ossicula mentalia) during ossification. Other researchers hold the view that these cartilages are secondary cartilage, which are formed in the mesenchyme of the mandibular symphysis de novo,[17] and the distal segment of the Meckel's cartilage is a transient structure.[1] It has no physiological significance and by the 6th month of intrauterine development disappears as a result of an atrophic degeneration process in the cartilage.[7] We found the presence of both the primary (Meckel's) and secondary cartilages in the mandibular symphysis region of 16 to 20 week-old fetuses. At the same time, the morphological signs of Meckel's cartilage physiological atrophy, such as a decrease in its size, vacuolization and karyopycnosis of a part of the chondrocytes, the desolation and reduction of the area of the perichondrocytic lacunae, are revealed.

Condylar cartilage appears between the 11th and 12th week of intrauterine development and forms a cartilaginous core of the condylar process, which gradually "plunges" into the bone tissue. In the following, as a result of ossification, most of the cartilage integrates into the condylar process, undergoing endochondral ossification. Finally, cartilaginous tissue remains only in the head of the mandible. The condylar cartilage is an analogue of the epiphyseal cartilage. Proliferation of its cells provides an increase in the size of the mandible both in prenatal and postnatal ontogenesis.[14] Unlike the epiphyseal plate of long bones, the replacement of condyle cartilage by bone occurs only from the side facing the mandibular body.

The cartilage on the apex of coronoid process appears a bit later than the condyle cartilage. It is a transient structure, which is subsequently replaced by bone.

The transcription factor Sox9 and external mechanical effects such as pressure,[8] for example, are stimuli that affect the development of cartilage. The secondary cartilage appearance in the mandibular symphysis region in embryogenesis coincides with the first swallowing movements of the fetus. The movements in the temporomandibular joint are also likely to promote the differentiation of the mesenchymal cells of the mandibular condyle into the chondrocytes, as demonstrated in a study by Habib et al (2005).[18]

Conclusion

In humans, two centers of intramembranous ossification in the mandibular arch appear at the 7th week of embryogenesis. There is a cartilaginous and chondroid tissue in the mandible anlage in addition to the woven bone. Hyaline cartilage is localized at the end of the condylar and coronoid processes, and also as an independent structure in the mandibular symphysis region. The chondroid tissue is incorporated into the bone near the mandibular symphysis and along the edge of the coronoid process. It is also present in the alveolar part of the mandible. Meckel's cartilage is the "primary lower jaw" and persists in the development process until the morphogenesis of the temporomandibular joint is completed and the two halves of the mandible come closer along the midline. In the following, the cartilage undergoes involution and loses its integrity. By the 20 to 29th week of embryogenesis, its remnants persist near the distal part of the body of the mandible and in the mandibular symphysis region.

Funding
The present study had no sponsorship.

Conflicts of Interest
The authors declare that there are no conflicts of interest.

Acknowledgments
None.

References

1 Dhem A. The Mandible - Natural History of a Bone Completely Different from All the Others. Dental and Medical Problems 2004; 41(03):395–402
2 Collins P. 2015Embryogenesis. In: Standring S, ed. Gray's Anatomy E-Book: The Anatomical Basis of Clinical Practice. Philadelphia: Elsevier Limited; 32–226
3 Jaskoll T, Abichaker G, Sedghizadeh PP, Bringas P Jr, Melnick M. Cytomegalovirus induces abnormal chondrogenesis and osteogenesis during embryonic mandibular development. BMC Dev Biol 2008;8(08):33
4 Lee SK, Kim YS, Oh HS, Yang KH, Kim EC, Chi JG. Prenatal development of the human mandible. Anat Rec 2001;263(03):314–325
5 Wyganowska-Świątkowska M, Przystańska A. The Meckel's cartilage in human embryonic and early fetal periods. Anat Sci Int 2011;86(02):98–107
6 Amano O, Doi T, Yamada T, et al. Meckel's cartilage: discovery, embryology and evolution: overview of the specificity of Meckel's cartilage. Journal of Oral Biosciences 2010;52(02):125–135
7 Bontemps C, Cannistrà C, Hannecke V, Michel P, Fonzi L, Barbet JP. [The first appearance of Meckel's cartilage in the fetus]. Bull Group Int Rech Sci Stomatol Odontol 2001;43(03):94–99
8 Radlanski RJ, Renz H, Zimmermann CA, Schuster FP, Voigt A, Heikinheimo K. Chondral ossification centers next to dental primordia in the human mandible: A study of the prenatal development ranging between 68 to 270mm CRL. Ann Anat 2016;208:49–57
9 Yang RT, Zhang C, Liu Y, Zhou HH, Li ZB. Autophagy prior to chondrocyte cell death during the degeneration of Meckel's cartilage. Anat Rec (Hoboken) 2012;295(05):734–741
10 Hu Y, Wang Y, Luo Z, Li C. A new symmetrodont mammal from China and its implications for mammalian evolution. Nature 1997;390(6656):137–142
11 Meng JIN, Hu Y, Wang Y, Li C. The ossified Meckel's cartilage and internal groove in Mesozoic mammalian forms: implications to origin of the definitive mammalian middle ear. Zool J Linn Soc 2003;138(04):431–448
12 Ossenberg NS. The mylohyoid bridge: an anomalous derivative of Meckel's cartilage. J Dent Res 1974;53(01):77–82
13 Yang L, Tsang KY, Tang HC, Chan D, Cheah KS. Hypertrophic chondrocytes can become osteoblasts and osteocytes in endochondral bone formation. Proc Natl Acad Sci U S A 2014;111(33): 12097–12102
14 Leander D. Role of Growth Factors in the Development of Mandible. J Indian Orthod Soc 2011;45(02):51–60
15 Mérida Velasco JR, Rodríguez Vázquez JF, De la Cuadra Blanco C, Campos López R, Sánchez M, Mérida Velasco JA. Development of the mandibular condylar cartilage in human specimens of 10-15 weeks' gestation. J Anat 2009;214(01):56–64
16 Bailleul AM, Nyssen-Behets C, Lengelec B, Hall BK, Horner JR. Chondroid bone in dinosaur embryos and nestlings (Ornithischia: Hadrosauridae): Insights into the growth of the skull and the evolution of skeletal tissues. C R Palevol 2016;15(1–2):49–64
17 El Fouhil AF. 2012Development of the site of articulation between the two human hemimandibles (Symphysis Menti). In: Dr. Ken-Ichi Sato (ed). Embryogenesis, InTech 167–188
18 Habib H, Hatta T, Udagawa J, Zhang L, Yoshimura Y, Otani H. Fetal jaw movement affects condylar cartilage development. J Dent Res 2005;84(05):474–479

Dissection Course in Anatomy as Stimulus to Independent Research and to a Real Step into Medicine

Vladimir Nikolenko[1,2] Marine Oganesyan[1] Felix Zakirov[1] Valentina Kudryashova[1] Nelly Rizaeva[1] Polina Valiullina[1]

[1] Department of Human Anatomy, First Moscow State Medical University (Sechenov University), Moscow, Russia
[2] Department of Normal and Topographic Anatomy, Moscow State University, Moscow, Russia

Address for correspondence Felix Zakirov, Department of human anatomy, First Moscow State Medical University (Sechenov University), Mohovaya street, 11, 125009, Moscow, Russia (e-mail: nilski@mail.ru).

J Morphol Sci 2019;36:63–66.

Abstract

Objectives In the recent years, many strategies in anatomy education have appeared. However, these innovations reduce the time students can spend on cadaver-based classes, which are considered to be an effective method of learning anatomy. The aim of the present research was to observe the advantages and features of dissection sessions in medical universities.

Materials and Methods The comparative analysis of the academic performance of dissector ($n = 30$) and nondissector ($n = 105$) students and a survey questionnaire were conducted. The data was collected through the work of the Dissection Mastery School (DMS) of the Sechenov University, Moscow, Russia, between 2016 and 2018.

Results The data analysis showed significant higher examination results in the dissectors cohort ($p < 0.001$) and a strong opinion about dissection as a good tool to improve anatomy knowledge (95% of responders). Apart from that, prosection is proven to have advantages in comparison with alternative learning approaches, according to researches performed by colleagues.

Conclusion These data show that dissection still remains one of the most effective and beneficial methods of teaching anatomy in medical universities, and that it should be further integrated into the medical curriculum.

Keywords
- anatomy
- cross-sectional anatomy
- dissection
- medical education
- methodology

Introduction

Anatomy is a basic medical science that provides necessary knowledge and forms a solid foundation for future doctors. Since the ancient times, the structure of the human body has been a topic of great interest.[1] However, during the following centuries, dissection has faced criticism and oppression by religion and society.[2] But the will of researchers to understand the human body has managed to overcome these difficulties to enrich anatomy knowledge. Thus, all the anatomy we learn and study today is the result of great enthusiasm.

Through the ages, anatomy did not lose its importance and still remains one of the first disciplines taught in the medical universities, as it provides the learning of further subjects.[3] Obviously, there cannot be a qualified physician without knowledge of anatomy. Today, the process of teaching anatomy is being constantly improved and integrated with new technologies.[4] As a result of this rapid development of the anatomical sciences, more requirements relating to future doctors are imposed.

In addition to that, there is a tendency of reducing the curriculum of long-lasting disciplines, such as human anatomy.[5] Often, the time allocated to the teaching of anatomy is only enough for a theoretical introduction to the subject and for a short visual overview into the human body.[6] That is why, in spite of the large amount of available corpses, a significant shortage of time for cadaver prosection can be noticed. Under

received
August 19, 2018
accepted
February 15, 2019

DOI https://doi.org/10.1055/s-0039-1685222.
ISSN 2177-0298.

Copyright © 2019 by Thieme Revinter Publicações Ltda, Rio de Janeiro, Brazil

License terms

these circumstances, the necessity of practical classes with natural materials strongly increases, as anatomy is considered to be a classical morphological science.

The most detailed and comprehensive notion of the human body a future physician can get is only by being in contact with it.[7] Dissection sessions provide important illustrative materials and proper learning of the structure of the human body.[8] Therefore, today, cadaver dissection still remains an important aspect of teaching anatomy. Therefore, the aim of the present research was to value the role of practical dissection classes in learning anatomy by analyzing the academic performance of the students and summarizing their opinion regarding these classes.

Materials and Methods

In March 2016, the Dissection Mastery School (DMS) of the Sechenov University, Moscow, Russia, was launched. Any student was able to attend the School and learn the basics of dissection under the supervision of the human anatomy department professors. Two-hour length practical classes with cadavers were held twice a week in the evenings. During the classes, the students had an opportunity to work with cadavers individually or in groups.

Recruitment

Participation in the study was voluntary. During the 2017–2018 academic year, 135 first- and second-year students were selected for the research and divided into 2 groups, with 30 and 105 students, respectively. Members of the first group ($n = 30$) had been participating in current dissection schedule (dissectors). The second group of students ($n = 105$) did not attend the DMS classes (nondissectors). The academic performance in human anatomy of both groups was compared, according to the results of the diagnostic tests (DT), of the final exam (FE), and of the final test (FT). There was no bias for gender, for age, or for previous experience in anatomy. Informed consent was obtained from all of the participants.

Examinations Structure

The DT contained 20 questions of different types: multiple-choice, true/false, and matching. The FT included 30 questions of different types: multiple-choice, true/false, matching, and ordering. To observe the DT and FT results, a percentage of correct answers was calculated. The FE held in the end of the academic year included identifying anatomical structures, solving situational tasks, and an oral theoretical examination. After the interview with an independent examiner, the student was given a mark (excellent, average, or failure).

Statistical Analysis

To observe the efficiency of the dissection sessions and their impact on learning anatomy, the academic performance of the students on the FE was statistically analyzed. All of the data were collated and entered into Microsoft Excel (Microsoft Corporation, Redmond, WA, USA) and exported into STATA 13 software (StataCorp., College Station, TX, USA). To investigate the correlation, the chi-squared distribution (χ^2) was used. A value of $p \leq 0.005$ was considered statistically significant.

Subjective Data Collection

The survey was administered over a 3-day period at the conclusion of the course of DMS classes among students of the dissectors group ($n = 35$). All of the 35 students were asked to complete a questionnaire and share their opinion on dissection practice, measuring statements approval. To summarize the preferences and year of study distribution of the students, the review of two years of DMS work was composed. The results were compiled using Microsoft Excel.

Results

The results of the FE showed a significant difference between the 2 groups, with a higher performance in the 1st group ($n = 30$) (►**Table 1**). The DMS students demonstrated more comprehensive and confident knowledge and were given better marks overall.

The overall pooled distribution of the FE marks showed a strongly significant correlation between attending practical classes with cadavers and higher academic performance on the FE ($\chi^2 = 27.991$; df $= 3$; $p < 0.0001$).

The data analysis of the DT results (►**Table 2**) also showed that the DMS participants demonstrated more comprehensive knowledge about subject units such as musculoskeletal, angiology, and peripheral nerves anatomy. Obviously, this fact was due to the opportunity to dissect and see those structures naturally at the DMS.

The average FT result was 88% in the DMS participants group and 74% in the control group. This significant difference indicates the efficiency of practical classes with cadavers in learning anatomy and correlates with the mentioned data.

Table 1 The final exam results

Final exam result	Number of students	
	Dissectors	Nondissectors
Failure	0	1
Average	1	29
Excellent	29	75

Table 2 Academic performance of students according to diagnostic tests

Curriculum unit	Attended DMS classes	Average result, %
Musculoskeletal	+	87
	-	76
Splanchnology	+	82
	-	74
Neurology	+	86
	-	72
Angiology	+	85
	-	71

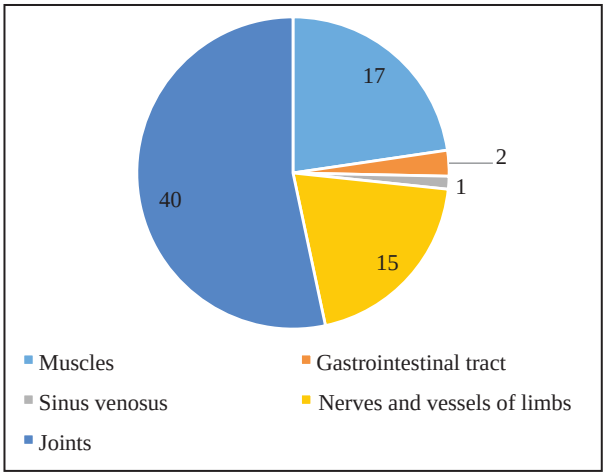

Fig. 1 The most preferred objects the students dissected.

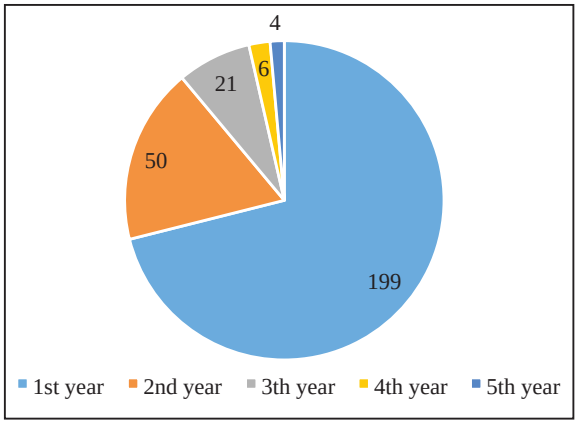

Fig. 2 Number of students who attended the DMS (year of study distribution).

According to the data of DMS work for 2 years, the most preferred objects for students to dissect were joints (total of 40 preparations). In addition to that, much attention was given to muscles, blood vessels and nerves (17 muscular and 15 preparations of blood vessels and nerves of limbs) (►**Fig. 1**).

The survey questionnaire results (summarized in ►**Table 3**) showed that the students described the dissection practice in positive terms. Most of the responders confirmed the benefits and the efficiency of practical classes with cadavers in understanding gross anatomy and its necessity for every medical student. A small number of students (2 out of 30) were indifferent to dissection sessions and did not consider them as an effective method for learning anatomy. Almost one third of the responders (9 out of 30) did not agree that dissection classes have any impact on memorizing anatomical terms. A total of 95% of the responders agreed that dissection was a useful approach to learning anatomy.

The increased interest in dissection classes was proven according to the number of students who attended at the DMS. In the 2017–2018 academic year, there were 280 students in comparison to 113 in 2016–2017. The distribution of students in 2017–2018 is symbolic: most of the contingent comprised first- and second-year students. However, the analysis showed several more adult students who attended the DMS classes (►**Fig. 2**).

Discussion

Dissection has a very long history, dating back to the first attempts to understand the structure of the human body.[9] Despite the new technologies and innovations integrated to the educational process, prosection still remains an effective method in teaching anatomy.[10] Data collected in the DMS show that dissection sessions improves academic performance and enriches the knowledge of human anatomy.

This point of view was also mentioned in other researches. Entwistle et al found that dissection classes helped students to combine their theoretical and practical skills to form the most comprehensive notion of the subject.[11]

The necessity of practical classes was also mentioned in the work of Pandey et al.[12] They suggested that students encounter some difficulties in learning anatomy using only one method. According to the research, a combination of memorizing, theoretical revision, and practical dissection sessions resulted in the best achievements of students. Findings similar to ours were made by Yeager.[13] That study included 4 examinations with 4 units in each, in which dissectors scored higher than nondissectors in 13 cases.

Despite the positive impact on the academic performance of the students, dissection classes have less obvious advantages, according to Crisp et al.[14] The researchers concluded that prosection in the dissecting room develops teamwork

Table 3 Survey questionnaire results

Statement about cadaveric dissection	Frequency, %				
	Strongly agree	Agree	Neutral	Disagree	Strongly disagree
A useful method of learning anatomy	69	26	5	–	–
Helped to better understand gross anatomy	57	34	9	–	–
Helped to memorize anatomical terms	14	23	34	20	9
Helped to develop manual skills	32	54	14	–	–
Is only necessary for future surgeons	–	–	5	9	86
Would recommend dissection to classmates	37	28	26	9	–

and cooperation among students. These skills might be useful for practice in hospitals and in future jobs.

To observe the psychological aspect of dissection practice in medical universities, Bertman et al studied how classes with cadavers adapt students to accepting death.[15] Researches stated that this experience would be useful in making an autopsy and dealing with terminal patients. Indeed, there are few medical specialties that do not face death during practice. Therefore, accepting death is an important stage of becoming a doctor, according to Marks et al.[16]

Another interesting finding that correlates with our results was made by Ellis.[17] The scientist noticed that the hours spent by the students with cadavers had a positive impact on their manual skills, as well as on their knowledge about gross anatomy. This aspect of dissection practice might be useful for students who choose the path of a surgeon. This opinion was also confirmed by Sheikh et al, who used a survey questionnaire among 80 practicing surgeons of different specialties.[18] Responders chose dissection as the most preferred method of learning human anatomy.

In the recent years, an impressive number of alternative methods of learning anatomy approach. Sometimes, dissection is being totally replaced by the use of new technologies, or changes in the medical curriculum leave a short amount of time for dissection, according to Bouwer et al and to Whelan et al.[19,20] Every method has its unique features and advantages, mostly because of opportunities of vital study, visual quality, and ethical aspects. However, according to Estai et al, who composed a comparative analysis of all teaching and learning techniques that are used in medical universities nowadays, these methods have serious disadvantages in comparison to dissection.[21] New technologies achieve high accuracy visualization, but still cannot replace the experience of tactile contact with the human body and of obtaining a correct notion of its texture, according to Van Wyk et al and to Burgess et al.[22,23]

Conclusion

Our study suggests that medical students consider dissection to have a positive impact on their knowledge and manual skills. According to the research results and data collected at the DMS of the Sechenov University, practical classes with cadavers provide students with an opportunity to improve academic performance and effectively learn human anatomy. Moreover, classical dissection demonstrates serious advantages in comparison to other methods used in the modern curriculum. The knowledge and skills obtained by the students from dissection can be useful for physicians of any specialty and qualification.

Conflicts of Interests

The authors have no conflicts of interests to declare.

Acknowledgment

The present research received no specific grant from any funding agency in the public, commercial, or not-for-profit sectors.

References

1 Ferngren G. Vivisection Ancient and Modern. Hist Med 2017;4 (03):243–254
2 Izutkin DA. History of forming fundamentals of scientific anatomy. Medicinskij al'manah 2017;(02):38–41
3 Ivanenko GA, Kuznetsov AV. Teaching of human anatomy in medical university: problems and prospects. Journal of Anatomy and Histopathology. 2017;6(05):16
4 Kuznecova MA, Miroshkin DV, Chilingaridi SN. Methodological approaches to the teaching of human anatomy in modern conditions. Morphology 2017;151(03):79–80(In Russian)
5 Winkelmann A. Anatomical dissection as a teaching method in medical school: a review of the evidence. Med Educ 2007;41(01):15–22
6 Borovleva OV, Martynchuk DV, CHerdanceva DD, Batuhtina NP, Efremova VP, Sindeeva LV. Classic and innovative methods in the educational-research work of students studying the discipline «human anatomy. Modern issues of science and education 2015;(05):190. (In Russian) Classic and innovative methods in the educational-research work of students studying the discipline «human anatomy
7 Nikolenko VN, Oganesyan MV, Kudryashova VA, Rizaeva NA, Shumak AV. What can bring teaching of anatomy to the requirements (needs) of medical practice? Modern issues of science and education 2017;(03):65–70
8 Griksaitis MJ, Sawdon MA, Finn GM. Ultrasound and cadaveric prosections as methods for teaching cardiac anatomy: a comparative study. Anat Sci Educ 2012;5(01):20–26
9 Ghosh SK. Human cadaveric dissection: a historical account from ancient Greece to the modern era. Anat Cell Biol 2015;48(03):153–169
10 Larkin TA, McAndrew DJ. Factors influencing students' decisions to participate in a short "dissection experience" within a systemic anatomy course. Anat Sci Educ 2013;6(04):225–231
11 Entwistle N, Tait H. Approaches to studying and perceptions of the learning environment across disciplines. New Dir Teach Learn 1995;•••:93–103
12 Pandey P, Zimitat C. Medical students' learning of anatomy: memorisation, understanding and visualisation. Med Educ 2007;41(01):7–14
13 Yeager VL. Learning gross anatomy: dissection and prosection. Clin Anat 1996;9(01):57–59
14 Crisp AH. The relevance of anatomy and morbid anatomy for medical practice and hence for postgraduate and continuing medical education of doctors. Postgrad Med J 1989;65(762):221–223
15 Bertman SL, Marks SC Jr. Humanities in medical education: rationale and resources for the dissection laboratory. Med Educ 1985;19(05):374–381
16 Marks SC Jr, Bertman SL, Penney JC. Human anatomy: a foundation for education about death and dying in medicine. Clin Anat 1997;10(02):118–122
17 Ellis H. Teaching in the dissecting room. Clin Anat 2001;14(02): 149–151
18 Sheikh AH, Barry DS, Gutierrez H, Cryan JF, O'Keeffe GW. Cadaveric anatomy in the future of medical education: What is the surgeons view? Anat Sci Educ 2016;9(02):203–208
19 Bouwer HE, Valter K, Webb AL. Current integration of dissection in medical education in Australia and New Zealand: Challenges and successes. Anat Sci Educ 2016;9(02):161–170
20 Whelan A, Leddy JJ, Ramnanan CJ. Benefits of extracurricular participation in dissection in a prosection-based medical anatomy program. Anat Sci Educ 2018;11(03):294–302
21 Estai M, Bunt S. Best teaching practices in anatomy education: A critical review. Ann Anat 2016;208:151–157
22 Van Wyk J, Rennie CO. Learning Anatomy Through Dissection: Perceptions of a Diverse Medical Student Cohort. Int J Morphol 2015;33(01):89–95
23 Burgess A, Ramsey-Stewart G. Elective anatomy by whole body dissection course: what motivates students? BMC Med Educ 2014;14:272

Estimation of the Humerus Length by its Proximal Segments: A South Indian Anatomical Study

Kasargod Umesh Prashanth[1] Mangala Manohar Pai[2] Bukkambudhi Virupakshamurthy Murlimanju[2] Latha Venkatraya Prabhu[2] Manoor Dass Prameela[2]

[1] Department of Anatomy, A.J. Institute of Medical Sciences and Research, Kuntikana, Mangalore, India
[2] Department of Anatomy, Kasturba Medical College, Manipal Academy of Higher Education, Karnataka, India

Address for correspondence Mangala Manohar Pai, MBBS, MD, Department of Anatomy, Kasturba Medical College, Manipal Academy of Higher Education, Centre for Basic Sciences, Bejai, Mangalore, 575004, Karnataka, India (e-mail: mangala.pai@manipal.edu).

J Morphol Sci 2019;36:67–71.

Abstract

Introduction To determine the morphometric data of the proximal segments of the humerus in the South Indian population, and to obtain the regression equations that will enable us to predict the whole length of humerus.

Materials and Methods The present study included 166 dried adult human humeri. Their lengths were measured by using the osteometric board. The seven proximal segment lengths of the humeri were assessed by using a digital Vernier caliper (Mitutoyo Corporation 150 mm/6 inch, model number 500-196-20, Kawasaki, Japan).

Results The mean humerus length in the present study was 30.75 $\pm$ 2.03 cm on the right side and 30.27 $\pm$ 2.28 cm on the left side. The comparison between the right and left sides of the proximal segments of the humerus did not yield statistically significant results ($p > 0.05$). The present study observed that the relationship between the dimensions of the proximal segments of the humerus and the length of humerus were strong ($p = 0.00$). The oblique length between the most proximal and distal points over the anatomical neck was the best parameter to predict the length of humerus (the Pearson coefficient was 0.78 for the right side and 0.77 for the left side).

Conclusion The simple regression formulae, which were derived in this study, are helpful in the estimation of the length of the humerus. The formulae can be used in forensic investigations, in which the stature of a person has to be determined and only bone fragments are available. The morphometric data of the present study have implications in archaeological and anthropological studies. The data are enlightening to orthopedicians, when planning reconstructive surgeries of the proximal end of the humerus in the South Indian population.

Keywords
- archeology
- forensic medicine
- humerus

Introduction

Identity is considered an important aspect in anthropology, forensic science and social demography. The stature is believed to be an integral part of identity. However, estimation of the identity of body parts and the stature of a person is complex, indeed. In archeology, the stature estimation of human skeletal remains is an essential step in assessing the general body size, health and sexual dimorphism.[1,2] However, variation exists among the intra- and interpopulation, as well as between the male and female individuals.[3,4] The ethnic, ancestral and geographical differences exist because of the hereditary, environmental and social factors. Krishan[5] reported that the stature of an individual is the variable that can be estimated with the greatest accuracy, even from the smallest bone available. However, long bones

received
August 2, 2018
accepted
February 15, 2019

DOI https://doi.org/10.1055/s-0039-1685223.
ISSN 2177-0298.

Copyright © 2019 by Thieme Revinter Publicações Ltda, Rio de Janeiro, Brazil

License terms

are preferred for stature determination because of their better accuracy.[5]

Steele[6] described that estimation of living stature can be done by using the humeral length in the absence of more accurate long bones, such as the femur or tibia. Salles et al.[7] opined that the forensic analysis of the modern population cannot be based on the formulas that were obtained from the ancient population. This is because of the rapid diachronic secular changes of limbs, and it has been observed by Salles et al.[7] that human beings are growing taller. In this context, developing a set of morphometric data from the modern population is considered to be essential to forensic investigations. There are several methods that can be used to estimate the stature of an individual by using his bones, among which the most reliable one is the regression analysis.[8,9] Regression analysis is more appropriate in defining the relationship between the length of long bone and living stature of an individual, as well as the relationship between the measurements of bone fragments and bone length.[9] The present study to collect the dimensions of the proximal segments of the humerus in the South Indian population and to obtain the regression equations that will enable us to predict the whole length of humerus.

Materials and Methods

The present study included 166 (82 right sided and 84 left sided) dried adult human cadaveric humeri, which were obtained from the collections of anatomy and forensic medicine departments of Kasturba Medical College, Mangalore, India. The humeri were carefully observed with respect to the proximal segments, which are vital in this present study. The humeri that presented significant deformities at the proximal end were excluded from the present study. The gender and age determination of the humeri were not performed in the present study. The present study was approved by the Time-Bound Research Ethics Committee of Kasturba Medical College, Mangalore (A Constituent Unit of Manipal Academy of Higher Education, Manipal, Karnataka, India) on July 28, 2010. The same researcher performed all the measurements, which prevented inter observer variation. Each measurement was performed three times and the average was calculated.

The maximum length of humerus (MLH) was measured by using the osteometric board. This was the maximum distance between the most proximal points over the caput humeri and the most distal point of the trochlea. The measurements of the proximal segments of the humeri were performed by using a digital Vernier caliper (Mitutoyo Corporation 150 mm/6 inch, model number 500-196-20, Kawasaki, Japan) (►**Fig. 1**).

S1 - distance between the most proximal part of the head of the humerus and the most distal part of the anatomical neck
S2 - oblique length between the most proximal and distal points in the anatomical neck
S3–distance between the most medial aspects of the lesser tubercle and the most lateral aspect of the greater tubercle
S4 - horizontal breadth of the humeral head, at its center
S5 - largest breadth of the greater tubercle
S6 - largest breadth of the lesser tubercle
S7 - the widest part of the proximal end of the humerus

The morphometric data were tabulated separately for the right and left sides of the humeri. The data were statistically analyzed by using the SPSS software, version 15 (SPSS Inc., Chicago, IL, USA). After obtaining the mean and standard

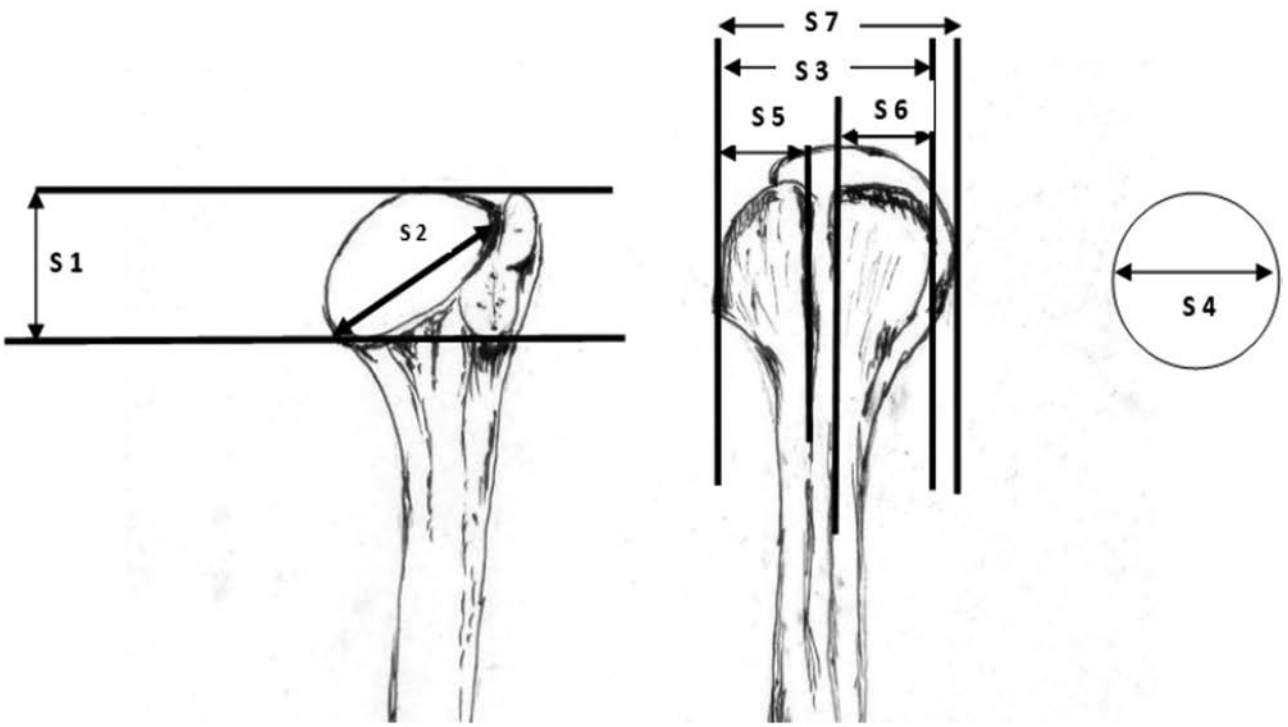

Fig. 1 Measurements of the proximal segments of the humerus performed in the present study.

Table 1 Morphometric data of the proximal segments of the humerus ($n = 166$)

Segment	Right side ($n = 82$)	Left side ($n = 84$)	*P*-value
S1	3.28 ± 0.31	3.25 ± 0.32	0.43
S2	4.12 ± 0.36	4.08 ± 0.35	0.45
S3	3.26 ± 0.47	3.29 ± 0.40	0.72
S4	3.84 ± 0.31	3.80 ± 0.35	0.46
S5	2.92 ± 0.29	2.84 ± 0.27	0.08
S6	1.36 ± 0.17	1.36 ± 0.19	0.78
S7	4.50 ± 0.36	4.42 ± 0.37	0.16

(values are given in cm, mean ± SD, independent samples test)

deviation (SD.) for each of the parameters, the association between the variables and the length of the humerus was investigated by means of the Pearson correlation coefficient (r). The linear regression was applied for the right and left humeri separately. The simple linear regression shows the regression coefficient (COE) and the significance (*p*-value) for the dimensions of the proximal segments of the right and left humeri, separately. The simple linear regression analysis shows the relationship of the dimensions of the individual proximal segment with the MLH. This analysis shows the coefficient of correlation (Pearson correlation coefficient) between a dependent variable and an independent variable. The Pearson coefficient determines the strength of the relationship between the variables. The *p*-value determines the statistical significance. A *p*-value 0.05 was considered statistically significant. The simple linear regression equations were formulated from the obtained data, which would predict the mean length of the humerus (MHL).

Results

From the 166 humeri (82 of right side and 84 of left side), the MHL on the right side was 30.75 cm, with a SD of 2.03 cm. The MHL on the left side was 30.27 cm, with a SD of 2.28 cm.

The descriptive statistics represented in ►**Table 1** shows the mean values of the proximal segments of the humeri of both the sides. The data were compared by using, independent samples test. The analysis showed that the comparison between the right and left sides was not statistically significant. The 2-tailed *p*-values were higher than 0.05 ($p > 0.05$).

The Pearson coefficient dictates the quantitative relation of each of the segment with the length of humerus. The Pearson coefficient, coefficient of determination (R^2) and *p*-values obtained in the present study are given in ►**Table 2**. The present study observed that the relationship between the dimensions of the proximal segments of the humerus and the length of the humerus were proportional. The relationship was real and did not occur by chance ($p = 0.00$, which is statistically highly significant).

►**Table 3** shows the Pearson coefficient in decreasing order of values. Among all the measurements performed, the S2 segment of both sides was the best parameter. The Pearson coefficient was 0.78 on the right side and 0.77 on the left side. The second best parameter was the S7 segment (The Pearson coefficient was 0.77 on both the sides). The lowest Pearson coefficient value was for the S6 segment on the right side, which was 0.38, and on the left side, it was for the S3 segment, which was 0.41.

The simple regression was formulated, $Y = (a + bX) \pm SD$, in which *Y* is the maximum humeral length (dependent variable); *X* is the dimension of the proximal segment of the humerus (independent variable), *b* is the multiplying factor and *a* is the constant, which was obtained by using the SPSS software (SPSS Inc.). The simple regression formula, which has highest multiplying factor, is considered to be the best. The simple regression formulae, which were obtained in the present study are given in ►**Table 4**. The formula applied to the S4 segment was the best for predicting the length of humerus on the right side (the multiplying factor was 4.67). On the left side, the formula that was applied to the S5 segment was considered the best (the multiplying factor was 6.19).

Discussion

In the absence of the cranium and the pelvis, the fragments of long bones can be used during the anthropology and forensic science investigations.[10–12] The simple regression formulae are considered important during the determination of the stature from the available anthropometric dimensions.[13,14] Singhal and Rao[15] reported that the length of the humerus can be used to estimate the stature of an individual with an error margin of less than 2 cm. They also reported that their

Table 2 Pearson coefficient and *p*-values of the right ($n = 82$) and left ($n = 84$) sides of the proximal humeral segments

Segment	Pearson coefficient		R^2		Significance (*p*-value)	
	Right side	Left side	Right side	Left side	Right side	Left side
S1	0.54	0.50	0.30	0.25	0.00	0.00
S2	0.78	0.77	0.62	0.59	0.00	0.00
S3	0.39	0.41	0.15	0.17	0.00	0.00
S4	0.71	0.72	0.50	0.51	0.00	0.00
S5	0.63	0.73	0.40	0.53	0.00	0.00
S6	0.38	0.46	0.15	0.21	0.00	0.00
S7	0.77	0.77	0.60	0.59	0.00	0.00

Table 3 Pearson coefficient of the proximal segments in decreasing order

Right humerus	Pearson coefficient	*P*-value	Left humerus	Pearson coefficient	*P*-value
S2	0.78	0.00	S2	0.77	0.00
S7	0.77	0.00	S7	0.77	0.00
S4	0.71	0.00	S5	0.73	0.00
S5	0.63	0.00	S4	0.72	0.00
S1	0.54	0.00	S1	0.50	0.00
S3	0.39	0.00	S6	0.46	0.00
S6	0.38	0.00	S3	0.41	0.00

Table 4 Simple regression formulae to determine the mean humeral length (MHL) from the data of the proximal segments

Right humerus	Left humerus
MHL = 19.06 + 3.55 (S1) ± 1.71	MHL = 18.60 + 3.60 (S1) ± 1.98
MHL = 12.35 + 4.46 (S2) ± 1.26	MHL = 9.89 + 5.00 (S2) ± 1.47
MHL = 25.28 + 1.67 (S3) ± 1.88	MHL = 22.62 + 2.33 (S3) ± 2.09
MHL = 12.84 + 4.67 (S4) ± 1.44	MHL = 12.32 + 4.73 (S4) ± 1.60
MHL = 18.06 + 4.35 (S5) ± 1.58	MHL = 12.68 + 6.19 (S5) ± 1.56
MHL = 24.57 + 4.55 (S6) ± 1.89	MHL = 22.78 + 5.55 (S6) ± 2.03
MHL = 11.13 + 4.36 (S7) ± 1.30	MHL = 9.27 + 4.75 (S7) ± 1.47

regression formula, which was derived from the longer segments of the humerus, can be used with other samples of the Indian population. However, if there are shorter segments, new equations are required. Somesh et al[16] studied the distance between the most proximal point of the humeral head and the greater tuberosity. They also determined the distance between the head of the humerus and the surgical neck of the humerus in the South Indian population. The present study did not measure these segments of the humerus. The best parameters in the present study were, the oblique length between the most proximal and the most distal points on the anatomical neck (S2), the horizontal breadth of the humeral head at its center (S4), and the widest part of the proximal end of the humerus (S7). These horizontal dimensions are different from the ones reported by Somesh et al,[16] who measured the vertical segments, which had lower coefficient values. This suggests that the horizontal segments of the present study gave better results. Salles et al[7] also reported that the oblique length between the most proximal and the most distal points on the anatomical neck, and the horizontal breadth of the humeral head at its center had good correlation to the MLH.

The forensic, anthropologic and archaeological studies suggest that the MHL offers important data to study the characteristics of a population.[17] In the present South Indian study, the MHL was 30.75 ± 2.03 cm on the right side and 30.27 ± 2.28 cm on the left side, respectively. These data are almost similar to the data from the Turkish population.[18] However, the MHL of the present study was lower in comparison to that of other European population. This is due to the ancestral variation, as the Europeans are tall and robust.[13,19] In a Brazilian study, the oblique length between the most proximal and the most distal points on the anatomical neck were 4.9 ± 0.5 cm and 4.8 ± 0.4 cm for the right and left sides, respectively.[7] These dimensions are much higher than the ones obtained in the present study, which were 4.12 ± 0.36 cm and 4.08 ± 0.35 cm, respectively. However, the horizontal breadth of the humeral head at its center was 3.84 ± 0.31 cm for the right side and 3.8 ± 0.35 cm for the left side, in the present study. This is similar to the data observed in the Brazilian study by Salles et al, which was 4.0 ± 0.4 cm and 3.9 ± 0.3 cm, respectively.[7]

By using the derived regression formulae, one can fairly estimate the full length of humerus. This is useful when only a few segments of a long bone are available. By using the MLH, it is possible to determine the stature of an individual. In the present study, the correlation between the measurements of the proximal segments of the humerus and the stature of an individual was not possible, due to lack of information about the dried bones. The stature of an individual is extremely variable and can be affected by ethnic differences. The regression formula of one population cannot be applied to another.[16] In this context, the data and formulae of the present study are important as they provide data about the South Indian population. The morphometric data of the humeral segments have implications in the identification of missing persons during the medico-legal investigations.[17,20] The morphometric data of the humerus segments are enlightening to orthopedic surgeons during the treatment of humeral fractures and reconstruction of the humerus.[16] The data are also enlightening during procedures like prosthetic designing, sizing and positioning.[21,22]

Conclusions

We believe that the data in the present study will contribute to estimation of the humeral length and the length of its proximal segments in a subset of the South Indian population. The derived formulae of the present study may be useful in forensic investigations in which the stature of an

individual has to be determined and there are only few segments of bone are available. The data can be of help in archaeological and anthropological studies in which excavations often yield only a few incomplete skeletal remains. The data in the present study are also essential to orthopedicians, who can utilize them during the planning of reconstructive surgeries involving the proximal end of the humerus.

Note

Mangala M. Pai is presently working as Professor and Head of the Anatomy Department and is interested in the field of human morphology. She has more than 50 research articles published on human morphology and anthropology.

Sources of Support

None.

Conflicts of Interest

The authors declare that they have no conflicts of interest.

References

1 Hoppa RD, Gruspier KL. Estimating diaphyseal length from fragmentary subadult skeletal remains: implications for palaeodemographic reconstructions of a southern Ontario ossuary. Am J Phys Anthropol 1996;100(03):341–354
2 Raxter MH, Auerbach BM, Ruff CB. Revision of the Fully technique for estimating statures. Am J Phys Anthropol 2006;130(03): 374–384
3 Pearson OM. Activity, climate, and postcranial robusticity: implications for modern human origins and scenarios of adaptive change. Curr Anthropol 2000;41(04):569–607
4 Ruff CB. Body size, body shape, and long bone strength in modern humans. J Hum Evol 2000;38(02):269–290
5 Krishan K. Anthropometry in forensic medicine and forensic science - 'forensic anthropometry'. The Internet Journal of Forensic Science 2006;2:1
6 Steele DG. Estimation of stature from fragments of long limb bones. In: Stewart TD, ed. Personal Identification in Mass Disaster. Washington, D.C.: Smithsonian Institution Press; 1970: 85–97
7 Salles AD, Carvalho CRF, Silva DM, Santana LA. Reconstruction of humeral length from measurements of its proximal and distal fragments. Braz J Morphol Sci 2009;26:55–61
8 Işcan MY. Global forensic anthropology in the 21st century. Forensic Sci Int 2001;117(1-2):1–6
9 Iscan MY. Forensic anthropology of sex and body size. Forensic Sci Int 2005;147:107–112
10 Beddoe J. On the stature of the older races of England, as estimated from the long bones. J Anthropol Inst G B Irel 1888; 17:201–209
11 Nath S, Badkur P. Reconstruction of stature from long bone lengths. Anthropologist 2002;4:109–114
12 Petersen HC. On the accuracy of estimating living stature from skeletal length in the grave and by linear regression. Int J Osteoarchaeol 2005;15:106–114
13 Willey P, Falsetti T. Inaccuracy of height information on driver's licenses. J Forensic Sci 1991;36(03):813–819
14 Williams PL, Warwick R, Dyson M, Bannister LH. The humerus. In: Gray's Anatomy. 37th ed,. Edinburgh: Churchill Livingstone; 1989:406
15 Singhal S, Rao V. Estimation of total length of humerus from its segments. Med Sci Law 2011;51(01):18–20
16 Somesh MS, Prabhu LV, Pai MM, Shilpa K, Krishnamurthy A, Murlimanju BV. Morphometric study of the humerus in Indian population. Int J Morphol 2011;29:1174–1180
17 Wright LE, Vásquez MA. Estimating the length of incomplete long bones: forensic standards from Guatemala. Am J Phys Anthropol 2003;120(03):233–251
18 Muñoz JI, Liñares-Iglesias M, Suárez-Peñaranda JM, et al. Stature estimation from radiographically determined long bone length in a Spanish population sample. J Forensic Sci 2001;46(02):363–366
19 Zverev Y, Chisi J. Estimating height from arm span measurement in Malawian children. Coll Antropol 2005;29(02):469–473
20 Ross AH, Konigsberg LW. New formulae for estimating stature in the Balkans. J Forensic Sci 2002;47(01):165–167
21 Murlimanju BV, Prabhu LV, Pai MM, et al. Anthropometric study of the bicipital groove in Indians and its clinical implications. Chang Gung Med J 2012;35(02):155–159
22 Robertson DD, Yuan J, Bigliani LU, Flatow EL, Yamaguchi K. Three-dimensional analysis of the proximal part of the humerus: relevance to arthroplasty. J Bone Joint Surg Am 2000;82-A(11):1594–1602

Comparative Morphological Studies of the Stifle Menisci in Donkeys, Goats and Dogs

Mohamed M.A. Abumandour[1] Naglaa Fathi Bassuoni[1] Samir El-Gendy[1] Ashraf Karkoura[1] Raafat El-Bakary[1]

[1] Department of Anatomy and Embryology, Faculty of Veterinary Medicine at Alexandria University, Behera, Egypt

J Morphol Sci 2019;36:72–84.

Address for correspondence Mohamed M. A. Abumandour, Assistant Professor of Anatomy and Embryology, Faculty of Veterinary Medicine at Alexandria University, Rashid, Edfina, Behera, Egypt, Postal Box: 22785 (e-mail: m.abumandour@yahoo.com).

Abstract

The present work aims to provide more anatomical information on the stifle joint of the investigated species using computed tomography with gross anatomical cross-sections. The current work analyzed the stifle joint of the pelvic limbs of 12 adult donkeys, goats and dogs of both genders. The medial condyle of the femur was larger than the lateral one in the donkey, while it was smaller and lower than the lateral one in the goat and in the dog. The unsuitable femoral and tibial condyles were adapted by the presence of menisci. In the donkey, the medial meniscus was crescentic in shape, but it was semicircular in the goat, while in the dog, the medial and lateral menisci were C-shaped. In the donkey, the medial meniscus was larger than the lateral one, but in the goat and in the dog, the lateral meniscus was the largest, and more concave and thicker. The lateral meniscus was semicircular in the donkey, but it was shaped like an elongated kidney in the goat. In the goat and in the dog, the central border of two menisci was thin, concave and notched centrally. The meniscal ligaments included cranial and caudal ligaments of the medial and lateral menisci, and meniscofemoral ligament of the lateral meniscus. In the dog, the cranial ligament of the medial meniscus was absent, and the medial meniscus had no bony attachment to the tibia but it attached to the transverse intermeniscal ligament, which connected the cranial horn of the medial meniscus with the cranial ligament of the lateral meniscus. The meniscofemoral ligament connected the caudal pole of the lateral meniscus with the intercondyloid fossa of the femur.

Keywords
- stifle joint
- meniscal ligaments
- computed tomography
- anatomical sections

Introduction

Anatomically, the stifle meniscus is described as a crescentic-shaped or semilunar fibrocartilaginous plate wedged between the femoral and tibial condyles. Its role is to provide structural integrity to the stifle joint during joint tension and torsion due to unsuitable articulation between the femoral and tibial condyles as well as to provide joint stabilization, shock absorption and protection of the articular surface.[1–6]

It is of vital importance to understand the morphological appearance of the stifle meniscus in animals because they are used as medical models to measure the degree of success of treatment options for meniscal injury [7] in humans and to know more about surgery of the stifle joint in animals.[8,9] A few examples of meniscal surgery models most frequently used are small animals (dog and pig), small ruminants (goat, sheep) and large ruminants (cow).[4,7,10–13]

The stifle joint is usually exposed to many problems that may require surgical treatment, such as patellar luxation, gonitis (stifle arthritis), synovitis, fracture, meniscal tearing and cruciate ligament sprain in the bovine.[14] Most commonly, sheep, goats, pigs, dogs, and rabbits are used as models of the human knee to test implants or to discover determinants of disease progression.[15–18]

Computed tomography (CT) is an efficient imaging modality that provides a cross-sectional image with superior soft

received
November 5, 2018
accepted
February 15, 2019

DOI https://doi.org/10.1055/s-0039-1685487.
ISSN 2177-0298.

Copyright © 2019 by Thieme Revinter Publicações Ltda, Rio de Janeiro, Brazil

License terms

tissue differentiation and no superimposition of the overlying structures, which can be used for better diagnosis of foot and foot pad abnormalities.[19,20] The CT is considered an important diagnostic tool in the human diagnosis, but due to its high cost, it is not used as often in veterinary diagnosis.[21] Moreover, the CT technique is useful for evaluation of the osseous structure, and it also gives three-dimensional CT images to provide a better view of the ligaments during surgery.[22]

The purpose of the present study was to provide a detailed anatomic reference of CT images interpreted with gross anatomical cross-sections of the normal stifle menisci of donkeys, goats and dogs for anatomists, surgeons and veterinary students.

Material and Methods

Samples

Six healthy adult animals of both genders, from each species, were used in the current study. The used animals were free of any anatomical abnormalities and any stifle joint affection. They were collected from the farms near the Kafr El-Sheik government. Joints from the right and left limbs were used. The current study was performed according to the guidelines for the care and use of laboratory animals and the Animal Welfare and Ethics Committee of the Faculty of Veterinary Medicine at Alexandria University, following the Egyptian's laws. The anatomical terms follow the Nomina Anatomica Veterinaria (NAV).[23]

Gross Morphology Examination

Four pelvic limbs from each animal species were used for studying the articular surfaces of the femorotibial joint. The animals were bled after being anesthetized; then, the three pelvic limbs were separated and buried in soil until complete decomposition of the tissues. After that, the bones of the two joints were collected, washed thoroughly using water and soap, and then bleached with hydrogen peroxide for 1 day and left to dry. The bones were then photographed after studying the characteristics of the articular surfaces of the stifle joint. Finally, the characteristic features of the bones were photographed with a Canon IXY 325 digital camera (Canon, Tokyo, Japan) after studying the characteristics of the articular surfaces of the stifle joint.

Four pelvic limbs from each species were used for studying the stifle meniscus ligaments. The animals were bled after being anesthetized, and, then, they underwent routine preservative technique (10% formalin mixed with 4% glycerin and 1% phenol) for 10 to 15 days until complete fixation. Finally, the two pelvic limbs were separated and the stifle meniscus ligaments were dissected.

Computed Tomography

Four pelvic limbs from each animal species were obtained, and the stifle joint was severed and used for studying it by means of a CT. The animas were anesthetized and then bled, and the joints were separated and transferred to the CT center within 24 hours, where they were analyzed using a Toshiba ASTEION SUPER-4 multi slice 4 CT scanner (Toshiba Corp., Minato, Tokyo, Japan) at 120 KV and 150 mAs. The distance between the slices taken was 0.5 cm. Three-dimensional images were also taken by the CT scanner for reconstruction of the stifle joint. Bone and soft tissue window images were taken.

Statistical Analysis

The IBM SPSS Statistics for Windows, Version 21.0 software (IBM Corp., Armonk, NY, USA)[24] was used for making a correlation between the articular surfaces of the femorotibial joint and the body weight of the donkey, the goat and the dog.

Results

Articular Surface

Anatomically, the stifle joint consists of two main joints: the femorotibial and femoropatellar joints. The femorotibial articulation (articulatio femorotibialis) is formed between the condyles of the femur, the condyles of the tibia and the medial and lateral menisci.

Medial and Lateral Condyles of the Femur (Condylus Medialis and Lateralis)

The head of the femur has two condyles: medial and lateral. The medial condyle was larger than the lateral one in the donkey (►**Fig. 1A/4**), while it was smaller and lower than the lateral one in the goat (►**Fig. 2A/4**) and in the dog (►**Fig. 3A/4**). Furthermore, the correlation between the length and weight of the medial and lateral condyles of the femur was demonstrated in ►**Fig. 4**.

In the three examined animals, the medial condyle of the femur was semispherical in shape and oblique in direction; on the other hand, the lateral condyle was sagittal in direction (►**Fig. 1A**; **2A** and **3A/5**). In the dog, the articular surfaces of the two condyles were continuous proximocaudally with small articular facet for sesamoid bones (►**Fig. 7C** and **12B/ms** and **Is**), which present in the tendons of the medial and lateral head of the gastrocnemius muscle.

In the three species, we observed a fossa located between the lateral ridge of the trochlea of the femur and the lateral condyle. This is called the extensor fossa (►**Fig. 1A**; **2A** and **3A/9**), which marks the origin of the long digital extensor muscle and peroneus tertius in the donkey and goat but the origin of the long digital extensor muscle only in the dog. The intercondyloid fossa (►**Fig. 1A**, **2A** and **3A/8**) was deep and sagittal in direction. In the dog, this fossa was deeper caudally than cranially. The length and width were calculated as means and recorded in ►**Table 1**.

Medial and Lateral Condyles of the Tibia (Condylus Medialis and Lateralis)

These condyles were not adapted with the condyles of the femur and there was only a small contact area with them. This adaptation was compensated by the presence of the menisci. In the donkey (►**Fig. 1A/10**) and in the goat (►**Fig. 2A/10**), the articular surface of the medial condyle of the tibia was triangular in outlines, while the lateral condyle was quadrilateral, but in the dog, the medial condyle (►**Fig. 3B/10**) was oval in shape, and the lateral condyle (►**Fig. 3B/11**) was nearly

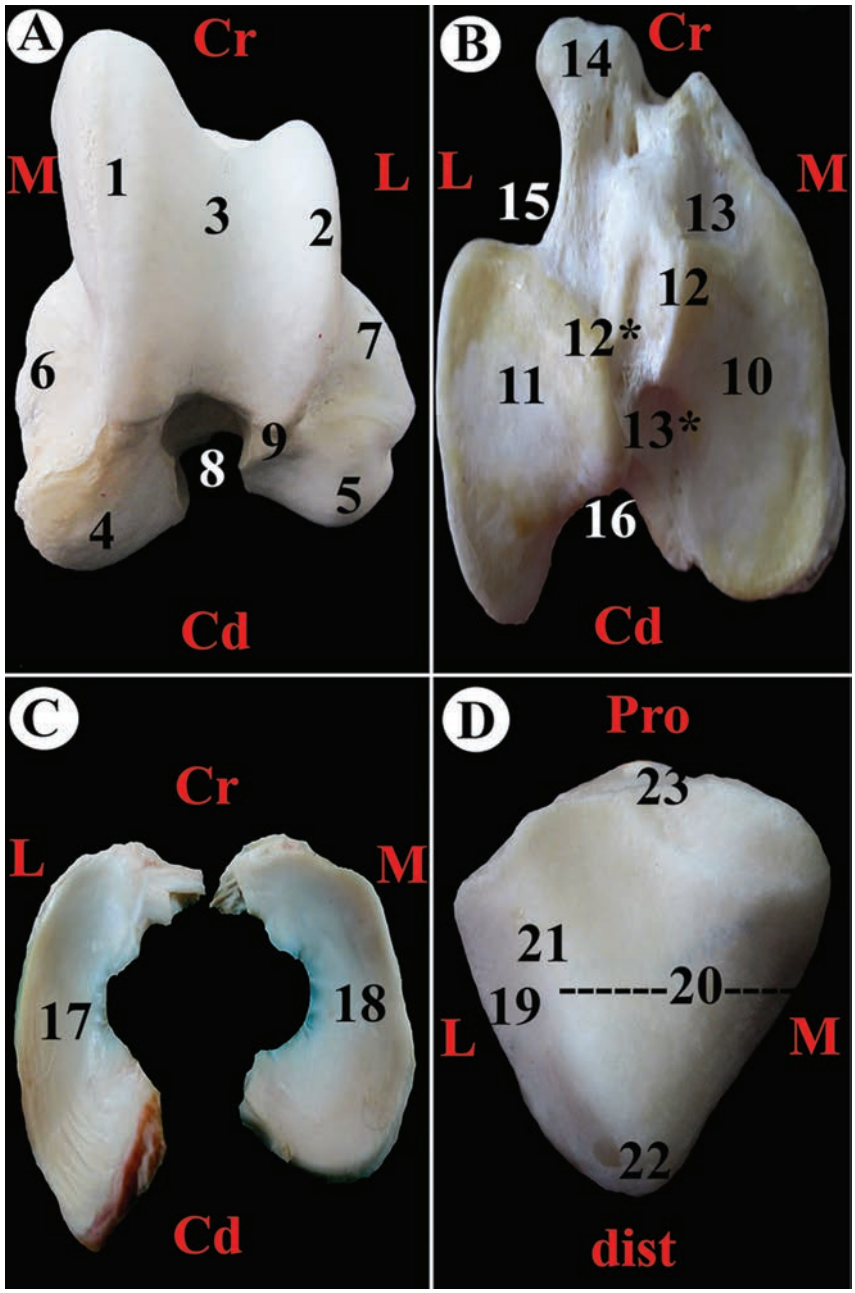

Fig. 1 Gross morphological views of the articular surfaces of the left stifle joint of the donkey: (View A) clarifies the distal extremity of the femur, (View B) clarifies the proximal extremity of the tibia, (View C) clarifies the menisci, (View D) clarifies the articular surface of the patella. 1- Medial ridge of the trochlea of the femur. 2- Lateral ridge of the trochlea of the femur. 3- Trochlear groove. 4- Medial condyle. 5- Lateral condyle. 6- Medial epicondyle. 7- Lateral epicondyle. 8- Intercondyloid fossa. 9- Extensor fossa. 10- Medial condyle. 11- Lateral condyle. 12- Medial part of the intercondyloid eminence. 12*- lateral part of the intercondyloid eminence. 13- Cranial part of intercondyloid fossa. 13*- Caudal part of intercondyloid fossa. 14- Tibial tuberosity. 15- Extensor groove. 16- Popliteal notch. 17- Lateral meniscus. 18- Medial meniscus.19- Medial articular surface. 20- Lateral articular surface. 21- Ridge. 22- Apex. 23- Base.

circular in shape. In the donkey, the medial condyle was larger than the lateral one, while in the goat (►**Fig. 2B/11**) and in the dog (►**Fig. 3B/11**), the lateral condyle was larger than the medial one. Furthermore, the correlation between the length and weight of the medial and lateral condyle of the tibia was demonstrated in ►**Fig. 5**.

The two condyles were separated by an intercondylar eminence that divided the intercondylar area into a medial and a lateral part. The medial intercondyloid eminence was more elevated than the lateral one in the donkey (►**Fig. 1B/12**) and in the goat (►**Fig. 2B/12**), while the lateral intercondyloid eminence (►**Fig. 3B/12***) was higher than the medial one in the dog (►**Fig. 3B/12**). In the three species, there was a fossa (►**Fig. 1B**, **2B** and **3B/13** and **13***) cranial and caudal to the intercondyloid eminence named the intercondyloid fossa. The lateral condyle separated from tibial tuberosity by the extensor groove that clear in (►**Fig. 1B**, **2B** and **3B/15**). The two condyles of the tibia separated caudally by the popliteal notch (►**Fig. 1**, **2** and **3**). The length and width were calculated as means and recorded in ►**Table 1**.

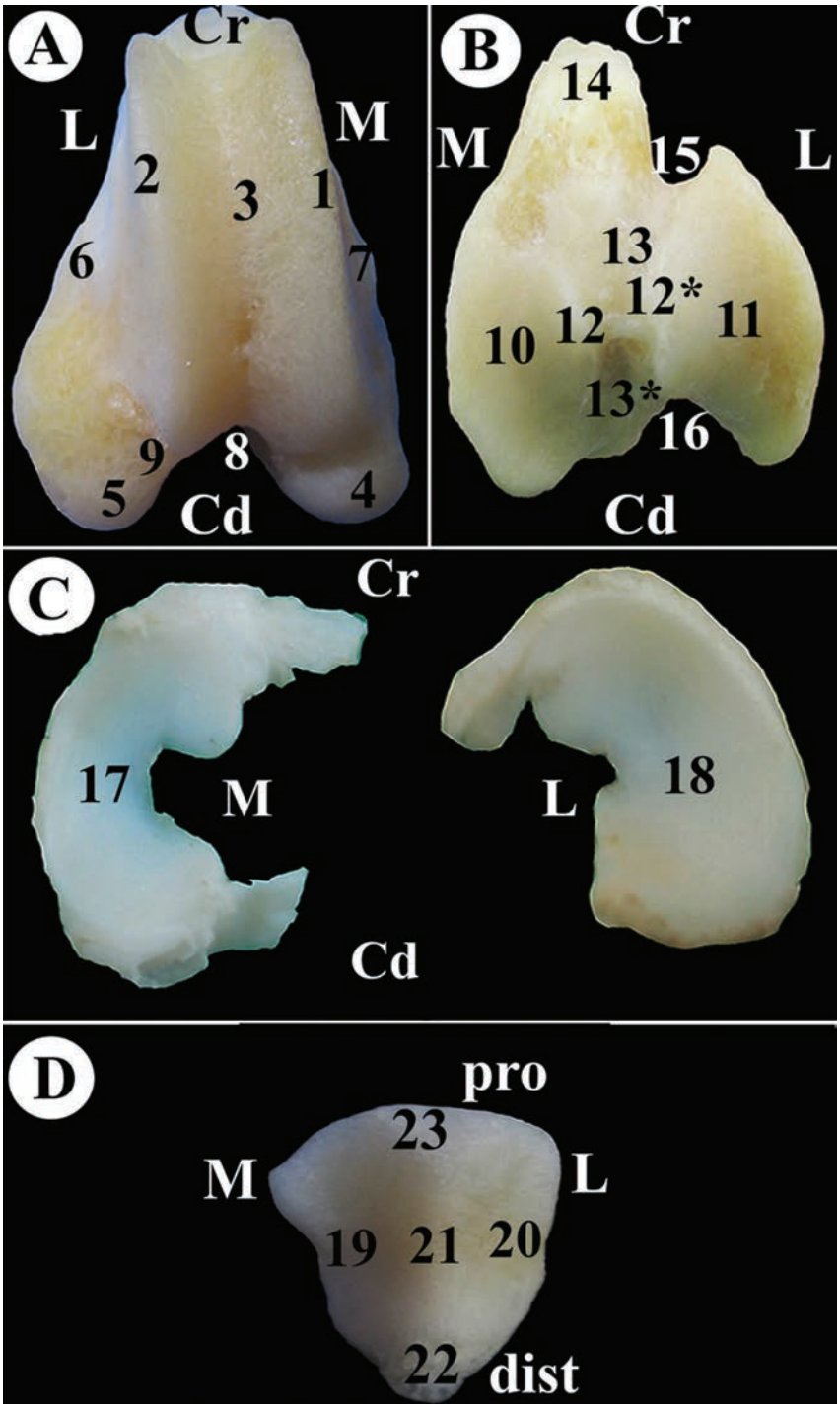

Fig. 2 Gross morphological views of the articular surfaces of the right stifle joint of the goat: (View A) clarifies the distal extremity of the femur, (View B) clarifies the proximal extremity of the tibia, (View C) clarifies the menisci, (View D) clarifies the articular surface of the patella. 1- Medial ridge of the trochlea. 2- Lateral ridge of the trochlea. 3- Groove. 4- Lateralcondyle.5- Medial condyle. 6- Lateral epicondyle. 7- Intercondyloid fossa. 8- Medial condyle. 9- Extensor fossa. 10- Medial condyle. 11- Lateral condyle. 12- Medial part of intercondyloid eminence. 12*- Lateral part of intercondyloid eminence. 13- Cranial intercondyloid fossa. 13*- Caudal intercondyloid fossa. 14- Tibial tuberosity. 15- Extensor groove. 16- Popliteal notch. 17- Medial meniscus. 18- Lateral meniscus. 19- Medial articular surface. 20- Lateral articular surface. 21- Ridge. 22- Apex. 23- Base.

Medial and Lateral Menisci (Meniscus Medialis and Lateralis)

Generally, the medial and lateral menisci were normal, smooth, white and glistening fibrocartilage that located between the two condyles of the femur and tibia. They presented cranial and caudal poles, axial and abaxial borders and proximal and distal articular surfaces. Their proximal surface was concave to adapt to the condyles of the femur, while the distal surface was convex to the condyles of the tibia. In the donkey, the medial meniscus (►**Fig. 1C/18**) was crescentic in shape, while in the goat (►**Fig. 2C/18**), it was semicircular, and in the dog, the medial (►**Fig. 3C/18**) and lateral menisci (►**Fig. 3C/19**) were C-shaped.

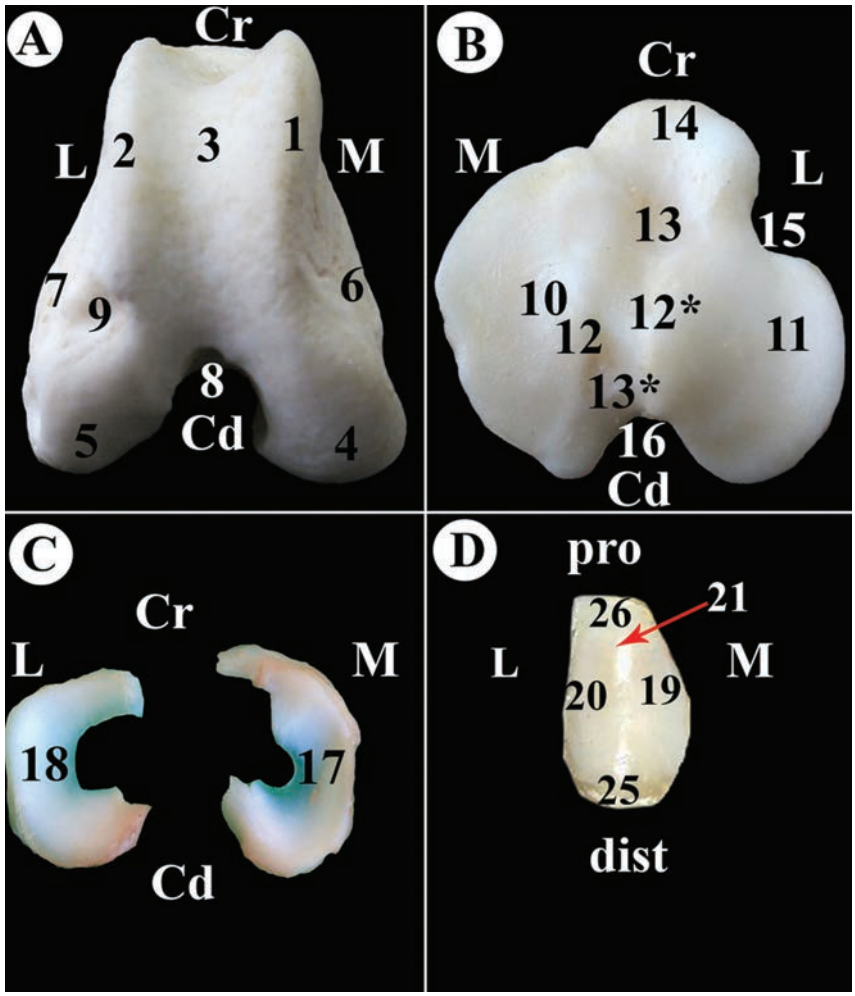

Fig. 3 Gross morphological views of the articular surfaces of the right stifle joint of the dog: (View A) clarifies the distal extremity of the right femur, (View B) clarifies the proximal extremity of the right tibia, (View C) clarifies the left menisci, (View D) clarifies the articular surface of the left patella. 1- medial ridge of the trochlea. 2- lateral ridge of the trochlea. 3- groove of the trochlea. 4- medial condyle. 5- lateral condyle. 7- popliteal fossa. 8- intercondyloid fossa. 9- extensor fossa. 10-Medial condyle. 11- lateral condyle. 12- medial part of the intercondyloid eminence. 12*- lateral part of the intercondyloid eminence. 13- cranial part of the intercondyloid fossa. 13*- caudal part of the intercondyloid fossa. 14- tibial tuberosity. 15- extensor groove. 16- popliteal notch.17-Medial meniscus. 18- lateral meniscus.19- medial articular surface. 20- lateral articular surface. 21- ridge. 22- Lateral sesamoid bone of the tendon of the gastrocnemius muscle. 23- Medial sesamoid bone of the tendon of the gastrocnemius muscle.24- sesamoid bone of the tendon of the popliteus muscle. 25- apex. 26- base.

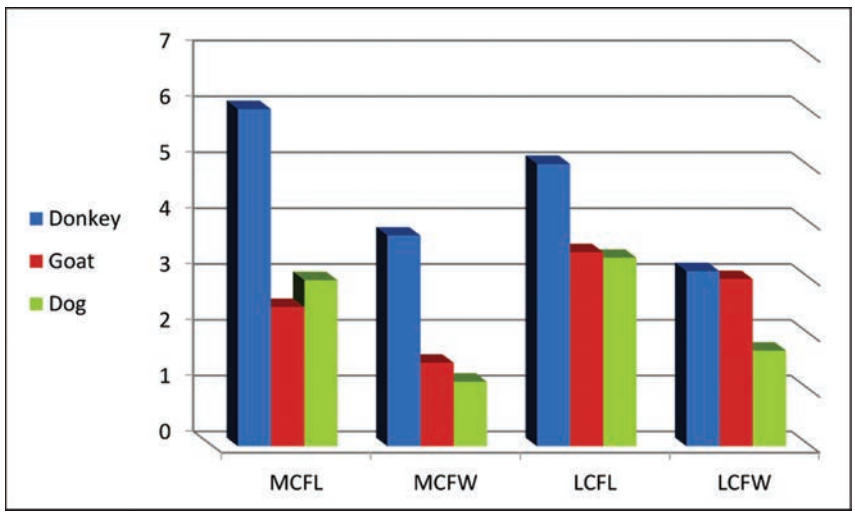

Fig. 4 Diagram to clarify the correlation between the length (MCFL) and weight (**MCFW**) of the medial condyle of the femur in addition to the correlation between the length (**LCFL**) and weight (**LCFW**) of the lateral condyle of the femur between the three examined animals: donkey (blue), goat (red) and dog (green).

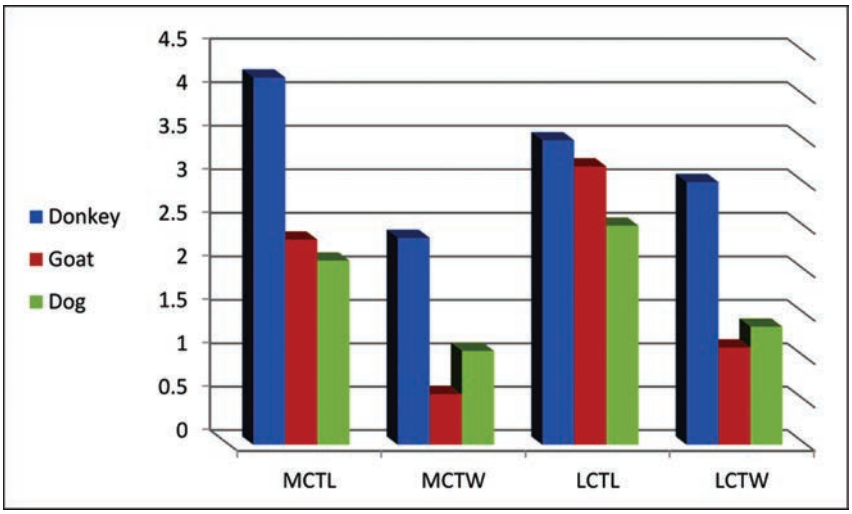

Fig. 5 Diagram to clarify the correlation between the length (**MCTL**) and weight (**MCTW**) of the medial condyle of the tibia in addition to, the correlation between the length (**LCTL**) and weight (**LCTW**) of the lateral condyle of the tibia between the three examined animals: donkey (blue), goat (red) and dog (green).

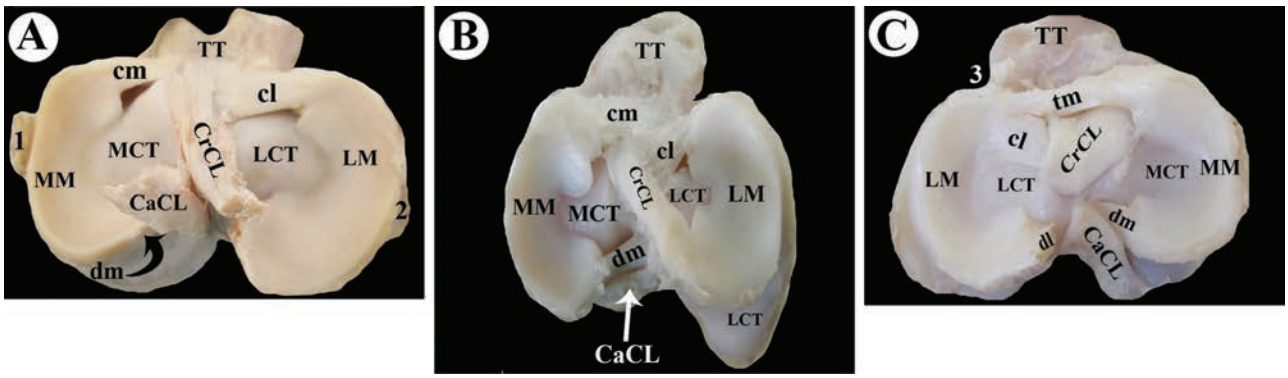

Fig. 6 Gross morphological views of the right stifle joint of the donkey (View A), right stifle joint of the goat (View B), and left stifle joint of the dog (View C) TT- tibial tuberosity. MM- medial meniscus. LM- lateral meniscus. MCT- medial condyle of the tibia. LCT- lateral condyle of the tibia. MFL- meniscofemoral ligament. CrCL- cranial cruciate ligament. CaCL- caudal cruciate ligament. cm- cranial ligament of the medial meniscus. cl- cranial ligament of the lateral meniscus. dm- caudal ligament of the medial meniscus. dl- caudal ligament of the lateral meniscus. tm- transverse meniscal ligament. 1- stump of the medial collateral ligament. 2. stump of the lateral collateral ligament. 3. Extensor groove.

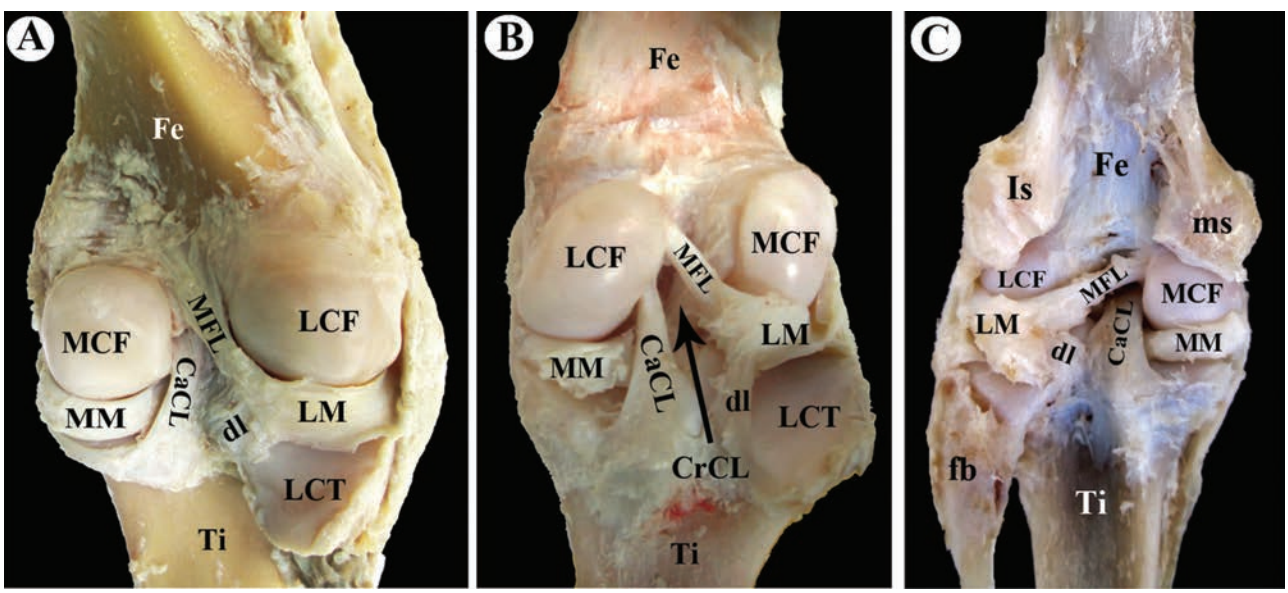

Fig. 7 Gross morphological views of the caudal view of the; right stifle joint of the donkey (View A), right stifle joint of the goat (View B), and left stifle joint of the dog (View C) Fe- femur. Ti- tibia. MM- medial meniscus. LM- lateral meniscus. MCF- medial condyle of the femur. LCF- lateral condyle of the femur. LCT- lateral condyle of the tibia. MFL- meniscofemoral ligament. CrCL- cranial cruciate ligament. CaCL- caudal cruciate ligament. dl- caudal ligament of the lateral meniscus.

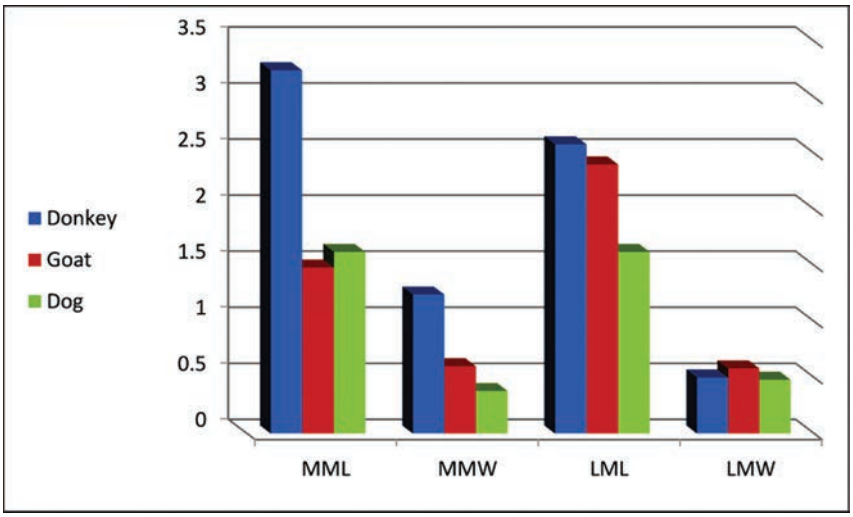

Fig. 8 Diagram to clarify the correlation between the length (MML) and weight (MMW) of the medial meniscus in addition to the correlation between the length (LML) and weight (LMW) of the lateral meniscus between the three examined animals: donkey (blue), goat (red) and dog (green).

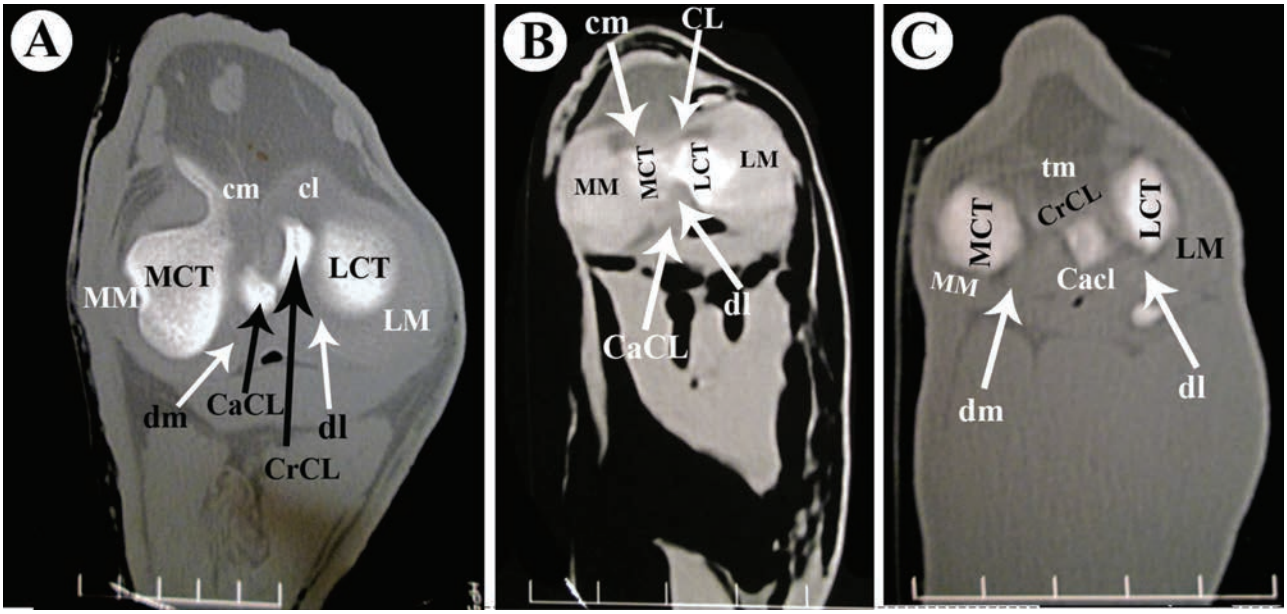

Fig. 9 Transverse computed tomography images of the right stifle joint of the donkey (view A), left stifle joint of the goat (View B), and left stifle joint of the dog (View C) TT- tibial tuberosity. MM- medial meniscus. LM- lateral meniscus. MCT- medial condyle of the tibia. LCT- lateral condyle of the tibia. MFL- meniscofemoral ligament. CrCL- cranial cruciate ligament. CaCL- caudal cruciate ligament. cm- cranial ligament of the medial meniscus. cl- cranial ligament of the lateral meniscus. dm- caudal ligament of the medial meniscus. dl- caudal ligament of the lateral meniscus. tm- transverse meniscal ligament. 1- stump of the medial collateral ligament. 2. stump of the lateral collateral ligament. 3. Extensor groove.

In the donkey, the medial meniscus was larger than the lateral one, but in the goat and in the dog, the lateral one was the largest, and more concave and thicker. In the three species, the central border of the medial meniscus was deeper than that of the lateral one, and the peripheral border was thicker and more convex than the lateral one.

The lateral meniscus was semicircular in shape in the donkey (►**Fig. 1C/19**), but it was shaped like and elongated kidney in the goat (►**Fig. 2C/19**). In the three examined species, the medial meniscus was firmly attached to the joint capsule while the lateral one was not. In the goat and in the dog, the central border of the two menisci was thin, concave and notched centrally. The length and width were calculated as means and recorded in ►**Table 1**. Furthermore, the correlation between the length and weight of the medial and lateral stifle menisci was demonstrated in ►**Fig. 8**.

The correlation between the body weight and dimensions of the articular surfaces of the stifle joint of the donkey, the goat and the dog are recorded in ►**Tables 2**, **3** and **4**.

Meniscal Ligaments

They included the cranial and caudal ligaments of the medial and lateral menisci, and the meniscofemoral ligament of the lateral meniscus. The cranial ligament of the medial meniscus connected the cranial pole of the medial meniscus with the cranial intercondyloid fossa of the tibia, and it measured

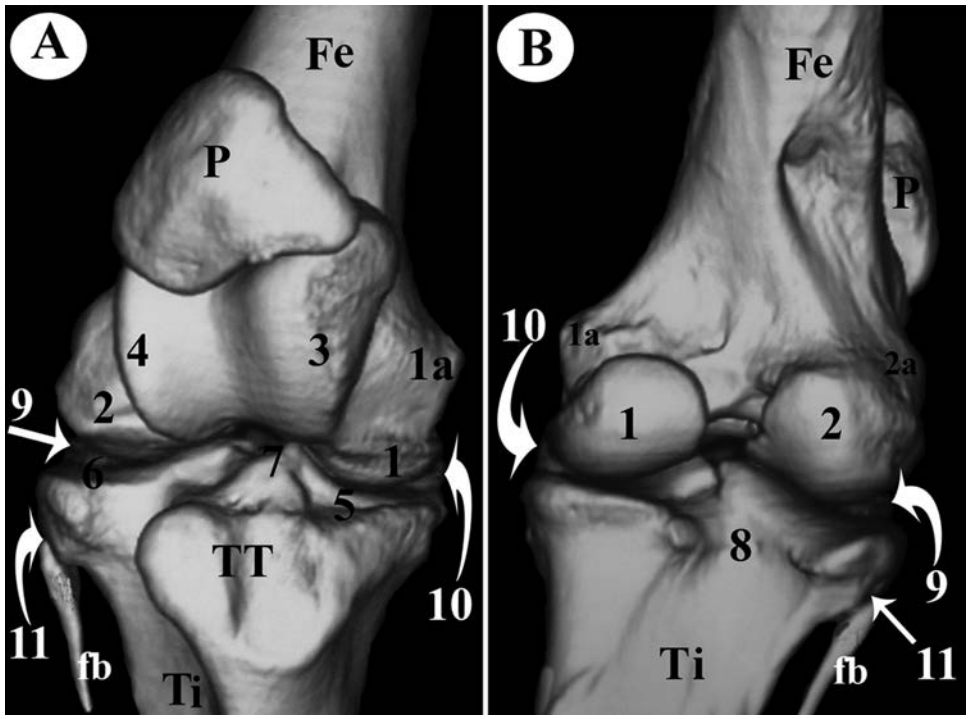

Fig. 10 Volume-rendered images (reconstruction) of the right stifle joint of the donkey: (View A) cranial and (View B) caudal views. F- femur. T- Tibia. P- patella. fb- fibula. TT- tibial tuberosity. EF- extensor fossa. 1- Medial condyle of the femur. 1a- Medial epicondyle. 2- Lateral condyle of the femur. 2a- lateral epicondyle. 3- Medial ridge of the trochlea of the femur. 4- Lateral ridge of the trochlea of the femur. 5- Medial condyle of the tibia. 6- Lateral condyle of the tibia. 7- Intercondyloid eminence. 8- Popliteal notch. 9- Extensor groove. 10- Proximal tibiofibular joint.

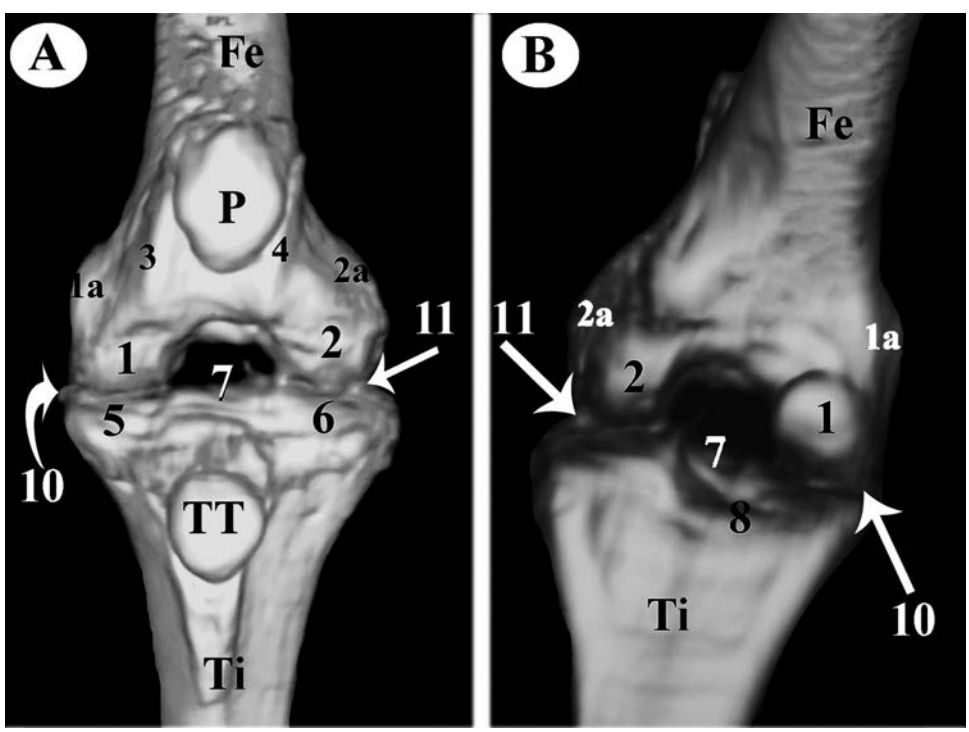

Fig. 11 Volume-rendered images (reconstruction) of the left stifle joint of the goat: (View A) cranial and (View B) caudal views. F- femur. T- tibia. P- patella. fb- fibula. TT- tibial tuberosity. 1- Medial condyle of the femur. 1a- Medial epicondyle. 2- Lateral condyle of the femur. 2a- Lateral epicondyle. 3- Medial ridge of the trochlea of the femur. 4- Lateral ridge of the trochlea of the femur. 5- Medial condyle of the tibia. 6- Lateral condyle of the tibia. 7- Intercondyloid eminence. 8- Popliteal notch. 9- Extensor groove. 10- Lateral meniscus.

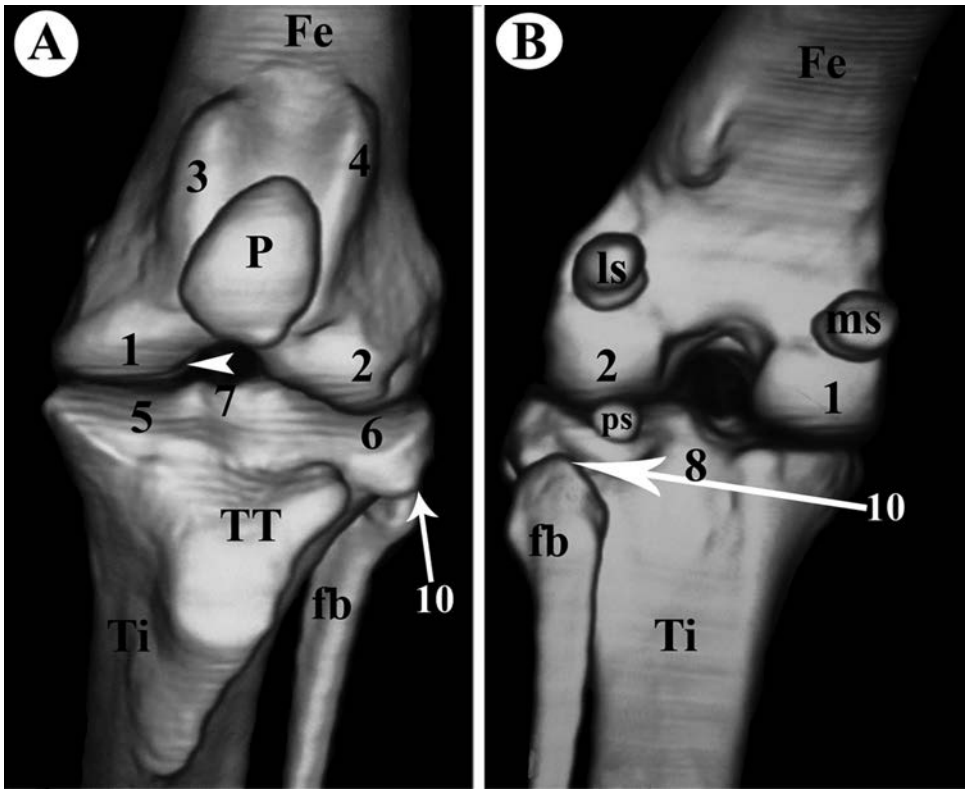

Fig. 12 Volume-rendered images (reconstruction) of the left stifle joint of the dog: (View A) cranial and (View B) caudal views. F- femur. T- tibia. P- patella. fb- fibula.TT- Tibial tuberosity. ms- medial sesamoid bone of the tendon of the gastrocnemius muscle. ls- Lateral sesamoid bone of the tendon of the gastrocnemius muscle. ps- Sesamoid bone of the tendon of the popliteus muscle. EF- extensor fossa. 1- Medial condyle of the femur. 2- Lateral condyle of the femur. 3- Medial ridge of the trochlea of the femur. 4- Lateral ridge of the trochlea of the femur. 5- Medial condyle of the tibia. 6- Lateral condyle of the tibia. 7- Intercondyloid eminence. 8- Popliteal notch. 9- Extensor groove. 10- Proximal tibiofibular joint.

Table 1 Average measurements of length (L) and weight (W) of the medial and lateral condyles of the femur and tibia in addition to the lateral and medial meniscus

Item	Donkey		Goat		Dog	
Medial femoral condyle	L	6 ± 0.3	L	2.5 ± 0.31	L	3 ± 0.29
	W	4 ± 0.5	W	1.5 ± 0.29	W	1.2 ± 0.2
Lateral femoral condyle	L	5 ± 0.35	L	3 ± 0.31	L	3.5 ± 0.21
	W	3 ± 0.48	W	3 ± 0.2	W	1.6 ± 0.21
Medial tibial condyle	L	4.5 ± 0.35	L	2.6 ± 0.22	L	2 ± 0.23
	W	2.6 ± 0.25	W	0.8 ± 0.25	W	1.2 ± 0.3
Lateral tibial condyle	L	3.5 ± 0.19	L	3.3 ± 0.21	L	2.9 ± 0.25
	W	3.2 ± 0.25	W	1 ± 0.3	W	1.3 ± 0.24
Medial meniscus	L	4 ± 0.5	L	1.4 ± 0.34	L	1.5 ± 0.4
	W	1.2 ± 0.2	W	0.8 ± 0.35	W	0.6 ± 0.34
Lateral meniscus	L	2.5 ± 0.21	L	2.4 ± 0.21	L	1.5 ± 0.2
	W	0.6 ± 0.19	W	0.5 ± 0.19	W	0.5 ± 0.24

∼ 1.3 cm long and 0.7 cm wide in the donkey (►**Fig. 6A** and **9A/cm**). In the goat, is measured ∼ 1.8 cm in length and 0.8 cm in width (►**Fig. 6B** and **9B/cm**). In the dog, the cranial ligament of the medial meniscus was absent, and the medial meniscus had no bony attachment to the tibia, but it was attached to the transverse or intermeniscal ligament that connected the cranial horn of the medial meniscus with the cranial ligament of the lateral meniscus, and it was located immediately cranial to the cranial ligament of the lateral meniscus, and the tibial attachment of the cranial cruciate ligament. It was ∼ 1.4 cm long and 0.2 cm wide (►**Fig. 6C** and **9C/tm**).

The caudal ligament of the medial meniscus attached the caudal pole of the medial meniscus with the caudal

Table 2 Correlation between the body weight and dimensions of the articular surfaces of the stifle joint of the donkey

	BW Vs MCFL	BW Vs MCFW	BW Vs LCFL	BW Vs LCFW	BW Vs MCTL	BW Vs MCTW	BW Vs LCTL	BW Vs LCTW
Correlation	0.535	0.076	.561	0.165	.425	.625	0.633	0.412
	BW Vs MML	BW Vs MMW	BW Vs LML	BW Vs LMW				
Correlation	0.798	-0.710	0.472	0.374				

There is positive correlation between body weight and MCFL, MCFW, LCFL, LCFW, MCTL, MCTW, LCTL, LCTW, MML, LML, LMW, and negative correlation with MMW.
Abbreviations: LCFL, length of the lateral femoral condyle; LCFW, Width of the lateral femoral condyle; LCTL, length of the lateral tibial condyle; LCTW, width of the lateral tibial condyle; LML, length of the lateral meniscus; LMW, width of the lateral meniscus; MCFL, length of the medial femoral condyle; MCFW, width of the medial femoral condyle; MCTL, length of the medial tibial condyle; MCTW, width of the medial tibial condyle; MML, length of the medial meniscus; MMW, width of the medial meniscus.

intercondyloid fossa of the tibia. In the donkey, it measured ~ 1 cm in length and width (►**Fig. 6A/dm**), while it was ~ 0.5 cm in length and 0.3 cm in width in the goat (►**Fig. 6B** and **9B/dm**). In the dog (►**Fig. 6C** and **9C/dm**), it attached cranial to the tibial attachment of the caudal cruciate ligament and it was ~ 0.2 cm in length and 0.1 cm in width.

The cranial ligament of the lateral meniscus connected the cranial pole of the lateral meniscus with the cranial intercondyloid fossa of the tibia. It was longer and thicker than that of the medial meniscus in the donkey (►**Fig. 6A** and **9A/cl**), it measured ~ 1.5 cm long and 1.3 cm wide. In the goat, it was ~ 0.7 cm in length and width (►**Fig. 6B** and **9B/cl**), while in the dog, it was ~ 0.3 cm in length and 0.1cm in width(►**Fig. 6C/cl**). In the dog, the cranial ligament of the lateral meniscus was located caudal to the transverse ligament, the caudal one was longer than the caudal ligament of the medial meniscus. The caudal ligament of the lateral meniscus connected the caudal pole of the lateral meniscus and divided into two parts, one attached to the medial part of the medial condyle of the tibia and the other to the popliteal notch. It measured ~ 1.5 cm long and 0.9 cm wide in the donkey (►**Fig. 5A** and **9A/dl**). In the goat, it measured 0.5 cm in length and 0.2 cm in width (►**Fig. 7B** and **9B/dl**), while in the dog, it was ~ 0.3 cm long and 0.2 cm wide (►**Fig. 7C** and **9C/dl**).

The meniscofemoral ligament connected the caudal pole of the lateral meniscus with the intercondyloid fossa of the femur. It measured ~ 2.7 cm in length and 0.8 cm in width in the donkey (►**Fig. 10A/MFL**); ~ 1.5 cm in length and 0.5 cm in width in the goat (►**Fig. 10B/MFL**), and ~ 1.3 cm long and 0.4 cm wide in the dog (►**Fig. 10C/MFL**). The length and width were calculated as means and recorded in ►**Table 5**.

The correlation between the body weight and dimensions of the articular surfaces of the stifle joint of the donkey, the goat and the dog are recorded in ►**Table 2**, **3** and **4**.

With volume-rendering reconstruction techniques, 3D-CT (►**Fig. 10**, **11** and **12**) images were produced, rotated and sectioned as desired. In 3D images (reconstruction), the characteristic features of the articular surfaces of the joint of each species evaluated (donkeys, goats and dogs), in which the lateral condyle of the femur appeared larger in the goat and in the dog.

Discussion

The present study was performed to describe the morphological features of the stifle menisci of donkeys, goats and dogs using gross anatomy, and CT, with special references to the articular surfaces. The animals have been chosen on the basis of the donkey being of the equine species, which is knows for carrying heavy loads for long distances; the goat being of the ruminant species, known for its limited mobility, and the dog of the carnivores that characterized by its fast-moving.

Table 3 Correlation between the body weight and dimensions of the articular surfaces of the stifle joint of the goat

	BW Vs MCFL	BW Vs MCFW	BW Vs LCFL	BW Vs LCFW	BW Vs MCTL	BW Vs MCTW	BW Vs LCTL	BW Vs LCTW
Correlation	0.226	0.042	.325	0.510	0.082	-0.075	0.246	0.0742
	BW Vs MML	BW Vs MMW	BW Vs LML	BW Vs LMW				
Correlation	0.344	0.283	0.356	0.439				

There is positive correlation between body weight and MCFL, MCFW, LCFL, LCFW, MCTL, LCTL, LCTW, MML, LML, LMW, and negative correlation with MCTW.
Abbreviations: LCFL, length of the lateral femoral condyle; LCFW, width of the lateral femoral condyle; LCTL, length of the lateral tibial condyle; LCTW, width of the lateral tibial condyle; LML, length of the lateral meniscus; LMW, width of the lateral meniscus; MCFL, length of the medial femoral condyle; MCFW, width of the medial femoral condyle; MCTL, length of the medial tibial condyle; MCTW, width of the medial tibial condyle; MML, length of the medial meniscus; MMW, width of the medial meniscus.

Table 4 Correlation between the body weight and dimensions of the articular surfaces of the stifle joint of the dog

	BW Vs MCFL	BW Vs MCFW	BW Vs LCFL	BW Vs LCFW	BW Vs MCTL	BW Vs MCTW	BW Vs LCTL	BW Vs LCTW
Correlation	0.247	0.403	0.449	0.054	0.037	0.165	0.322	0.453
	BW Vs MML	BW Vs MMW	BW Vs LMW	BW Vs LMW				
Correlation	0.559	0.505	0.559	0.291				

There is a positive correlation between body weight and MCFL, MCFW, LCFL, LCFW, MCTL, MCTW, LCTL, LCTW, MML, LML, LMW.
Abbreviations: LCFL, length of the lateral femoral condyle; LCFW, width of the lateral femoral condyle; LCTL, length of the lateral condyle of the tibia; LCTW, width of the lateral condyle of the tibia; LML, length of the lateral meniscus; LMW, width of the lateral meniscus; MCFL, length of the medial femoral condyle; MCFW, width of the medial femoral condyle; MCTL, length of the medial condyle of the tibia; MCTW, width of the medial condyle of the tibia; MML, length of the medial meniscus; MMW, width of the medial meniscus.

Table 5 Average measurements of length (L) and weight (W) of the meniscal ligament of the stifle joint

	Donkey		Goat		Dog	
Cranial ligament of the medial meniscus	L	1.3 cm	L	0.5 cm	Absent	
	W	0.7 cm	W	1.8 cm		
Transverse ligament	Absent		Absent		L	1.4 cm
					W	0.2 cm
Caudal ligament of medial meniscus	L	1 cm	L	0.5 cm	L	0.2 cm
	W	1 cm	W	0.3 cm	W	0.1 cm
Cranial ligament of lateral meniscus	L	1.5 cm	L	0.7 cm	L	0.3 cm
	W	1.3 cm	W	0.7 cm	W	0.1 cm
Caudal ligament of lateral meniscus	L	1.5 cm	L	0.5 cm	L	0.3 cm
	W	0.9 cm	W	0.2 cm	W	0.2 cm
Meniscofemoral ligament	L	2.7 cm	L	1.5 cm	L	1.3 cm
	W	0.8 cm	W	0.5 cm	W	0.4 cm

Concerning the articular surfaces of the femorotibial joint, they were the condyles of the femur and tibia and the menisci. The medial condyle of the femur of the donkey, goat and dog was oblique in direction and smaller than the lateral in the donkey and goat, this was observed by [25] in the donkey and mule and like that of the horse [26] and camel [27] while, the lateral condyle was sagittal in direction, this agreed with that observed by [25] in the donkey and mule,[26] in the horse and [28] in the dog.

The current investigation mentioned that the medial condyle of the femur was larger than the lateral one in the donkey, while it was smaller and lower than the lateral one in the goat and in the dog. The results in the dog and in the goat are similar to those obtained by[29] in the marsh deer and [9,30] in the ovine.

In the dog, the articular surfaces of the two condyles were continuous proximocaudally with small articular facet for sesamoid bones, which present in the tendons of the medial and lateral head of the gastrocnemius muscle; however, this is absent in the horse and in the goat. Similar results were noted by [9,29] in sheep and deer. In the dog, the femoral condyles were articulated with the sesamoid bones of the tendons of the gastrocnemius muscle, this agreed with that described by [28] in the dog.

The medial condyle of the tibia was triangular in shape in the donkey and goat likes that of the donkey and mule [25] and in the camel, [27] while that of the dog was oval in shape and the lateral condyle was circular as noted by.[28] The adaptation of the condyles of the femur and tibia was compensated by the presence of the menisci, which increase femorotibial joint stability and congruency and serve as the shock absorbers of the stifle.[31,32] The medial meniscus of the donkey was crescentic in shape, as mentioned by ,[25] while in the goat, it was semicircular, and in the dog, the medial and lateral menisci were C-shaped.

In general, the normal medial and lateral menisci were smooth, white and located between the two condyles of the femur and tibia to improve joint adaptation.[2,4,5,9,10,33] In the examined donkey and goat, the meniscal ligaments included the cranial and caudal ligaments of the medial and lateral menisci and the meniscofemoral ligament of the lateral meniscus, similar to that observed by[26,34,35] in horse,[36,37] in ovine, [27] in camel and [4] in humans, sheep and rabbits. In the dog, the cranial ligament of the medial meniscus was absent, and the medial meniscus had no bony attachment to the tibia, but it was attached to the transverse intermeniscal ligament, which connected the cranial horn of the medial

meniscus to the cranial ligament of the lateral meniscus. This did not agree with the findings of [28] in the dog. Moreover, the absence of the caudal ligament of the lateral menisci was recorded in rabbits by.[4,38]

In the current study, there is a transverse intermeniscal ligament that connects the cranial horn of the medial meniscus with the cranial ligament of the lateral meniscus in the dog, but the present study did not record this ligament in the donkey and the goat. The transverse intermeniscal ligament was also observed by[33] in tigers,[4,38] rabbits and [39–42] in dogs and cats. They also [43] described this ligament in the dog and pig, but reported that it was absent in sheep. The transverse intermeniscal ligament was also absent in donkey and goat, in the current study, and sheep [9] and deer.[29]

The meniscofemoral ligament connected the caudal pole of the lateral meniscus with the intercondyloid fossa of the femur. The similar observations were recorded in all animal species [25,29,33,39,42]

Conclusion

The medial condyle of the femur was larger than the lateral one in the donkey, while it was smaller and lower than the lateral one in the goat and in the dog. In the donkey, the medial meniscus was larger than the lateral one, but in the goat and in the dog, the lateral meniscus was the largest, more concave and thicker. The meniscus ligaments included cranial and caudal ligaments of the medial and lateral menisci, and the meniscofemoral ligament of the lateral meniscus. In the dog, the cranial ligament of medial meniscus was absent, and the medial meniscus had no bony attachment to tibia, but it attached to the transverse intermeniscal ligament, which connected the cranial horn of the medial meniscus with the cranial ligament of lateral meniscus. The meniscofemoral ligament connected the caudal pole of the lateral meniscus with the intercondyloid fossa of the femur.

Contribution of the Authors to the Manuscript

All authors confirm their contribution. Mohamed Abumandour was responsible for the data collection, data analysis, manuscript writing/editing, anatomical dissection and protocol/project development. Samir El-Gendy was responsible for the protocol/project development and the manuscript revision. Ashraf Karkoura was responsible for following up the protocol/project and for the manuscript revision. Raafat El-Bakary was responsible for following up the data analysis and the manuscript preparation. Naglaa Fathi was responsible for the manuscript writing/editing, protocol/project development, data collection, data analysis and anatomical dissection.

Ethics Approval and Consent to Participate

The present article was performed with the approval of the Bioethics Committee and in accordance with the guidelines for the care and use of laboratory animals and the Animal Welfare and Ethics Committee of the Faculty of Veterinary Medicine at Alexandria University, following the Egyptian laws.

Data and Material Availability

All data used in this study were included in this published article.

Conflicts of Interest

The authors have no conflicts of interest to declare.

Acknowledgment

The authors thank Dr. Sahar El-Naggar for the help in the process of statistical analysis during this study.

References

1 Parsons FG. The joints of mammals compared with those of man: a course of lectures delivered at the Royal College of Surgeons of England. J Anat Physiol 1899;34(Pt 1):41–68
2 Messner K, Gao J. The menisci of the knee joint. Anatomical and functional characteristics, and a rationale for clinical treatment. J Anat 1998;193(Pt 2):161–178
3 McDevitt CA, Webber RJ. The ultrastructure and biochemistry of meniscal cartilage. Clin Orthop Relat Res 1990;(252):8–18
4 Chevrier A, Nelea M, Hurtig MB, Hoemann CD, Buschmann MD. Meniscus structure in human, sheep, and rabbit for animal models of meniscus repair. J Orthop Res 2009;27(09):1197–1203
5 Fithian DC, Kelly MA, Mow VC. Material properties and structure-function relationships in the menisci. Clin Orthop Relat Res 1990;(252):19–31
6 Rath E, Richmond JC. The menisci: basic science and advances in treatment. Br J Sports Med 2000;34(04):252–257
7 Deponti D, Di Giancamillo A, Scotti C, Peretti GM, Martin I. Animal models for meniscus repair and regeneration. J Tissue Eng Regen Med 2015;9(05):512–527
8 Walmsley JP. Vertical tears of the cranial horn of the meniscus and its cranial ligament in the equine femorotibial joint: 7 cases and their treatment by arthroscopic surgery. Equine Vet J 1995;27(01):20–25
9 Allen MJ, Houlton JE, Adams SB, Rushton N. The surgical anatomy of the stifle joint in sheep. Vet Surg 1998;27(06):596–605
10 Aspden RM, Yarker YE, Hukins DW. Collagen orientations in the meniscus of the knee joint. J Anat 1985;140(Pt 3):371–380
11 Ghadially FN, Thomas I, Yong N, Lalonde JM. Ultrastructure of rabbit semilunar cartilages. J Anat 1978;125(Pt 3):499–517
12 Ghadially FN, Wedge JH, Lalonde JM. Experimental methods of repairing injured menisci. J Bone Joint Surg Br 1986;68(01):106–110
13 Krause WR, Pope MH, Johnson RJ, Wilder DG. Mechanical changes in the knee after meniscectomy. J Bone Joint Surg Am 1976;58(05):599–604
14 Weaver A. Bovine medicine diseases and husbandry of cattle. In Andrews A, Blowey R, Boyd H, Eddy R, Eds. 2nd ed. Oxford: Blackwell Science Ltd.; 435–652004
15 Huangfu X, Zhao J. Tendon-bone healing enhancement using injectable tricalcium phosphate in a dog anterior cruciate ligament reconstruction model. Arthroscopy 2007;23(05):455–462
16 Meller R, Kendoff D, Hankemeier S, et al. Hindlimb growth after a transphyseal reconstruction of the anterior cruciate ligament: a study in skeletally immature sheep with wide-open physes. Am J Sports Med 2008;36(12):2437–2443
17 Spindler KP, Murray MM, Carey JL, Zurakowski D, Fleming BC. The use of platelets to affect functional healing of an anterior cruciate ligament (ACL) autograft in a caprine ACL reconstruction model. J Orthop Res 2009;27(05):631–638
18 Murray MM, Magarian E, Zurakowski D, Fleming BC. Bone-to-bone fixation enhances functional healing of the porcine anterior cruciate ligament using a collagen-platelet composite. Arthroscopy 2010;26(9, Suppl)S49–S57

19 Badawy AM. Computed Tomographic anatomy of the fore foot in one-humped camel (Camelus dromedrus). Glob Vet 2011;6: 417–423
20 Widmer WR, Buckwalter KA, Braunstein EM, Hill MA, O'Connor BL, Visco DM. Radiographic and magnetic resonance imaging of the stifle joint in experimental osteoarthritis of dogs. Vet Radiol Ultrasound 1994;35:371–383
21 Baird DK, Hathcock JT, Rumph PF, Kincaid SA, Visco DM. Low-field magnetic resonance imaging of the canine stifle joint: normal anatomy. Vet Radiol Ultrasound 1998;39(02):87–97
22 Pretorius ES, Fishman EK. Volume-rendered three-dimensional spiral CT: musculoskeletal applications. Radiographics 1999;19 (05):1143–1160
23 Nomina AnatomicaVeterinaria (NAV). International Committee on Veterinary Gross Anatomical Nomenclature and authorized by the general assembly of the world Association of veterinary Anatomist. Knoxville, 3rd Ed. Ghent. Published by the Editorial Committee Hanover (Germany), Ghent (Belgium), Columbia, MO (U.S.A.), Rio de Janeiro (Brazil)2017
24 corporation I. IBM SPSS statistics for Windows, version 21.0. IBM Corporation Armonk eNY NY; 2012
25 El-Bakary R. Comparative anatomical and clinical studies on the stifle joint of the mule and donkey. Zagazig Veterinary Journal (Egypt) 1993
26 Getty R. The Anatomy of the Domestic Animals. Vol.1, 5th Ed. W.B. Saunders CompanyPhiladelpshia, USA1975
27 Karkoura AA. Applied Anatomical Studies On The Stifle Joint Of The One-Humped Camel (Camelus Domedrius). alex. J Vet Sci 1991;6:19–38
28 Evans HE, de Lahunta A. Miller's ANATOMY of the DOG fourth edition. W. B. Saunders CompanyPhiladelphia11812013
29 Shigue DA, Rahal SC, Schimming BC, et al. Evaluation of the marsh deer stifle joint by imaging studies and gross anatomy. Anat Histol Embryol 2015;44(06):468–474
30 Hette K, Rahal SC, Mamprim MJ. Volpi RdS, Silva VCd, Ferreira DOL. Radiographic and ultrasonographic evaluations of the ovine stifle joint. Pesqui Vet Bras 2008;28:393–398
31 Brantigan OC, Voshell AF. The mechanics of the ligaments and menisci of the knee joint. J Bone Joint Surg Am 1941;23:44–66
32 Bylski-Austrow DI, Ciarelli MJ, Kayner DC, Matthews LS, Goldstein SA. Displacements of the menisci under joint load: an in vitro study in human knees. J Biomech 1994;27(04):421–431
33 Arencibia A, Encinoso M, Jáber JR, et al. Magnetic resonance imaging study in a normal Bengal tiger (Panthera tigris) stifle joint. BMC Vet Res 2015;11:192
34 De Lahunta A, Habel RE. Applied veterinary anatomy. Library of Congress Cataloging in Publication Data. W.B. Saunders Company. Philadelphia, London, Toronto, Mexico City, Rio de Janeiro, Sydney, Tokyo, Hong Kong.1986
35 Hoegaerts M, Nicaise M, Van Bree H, Saunders JH. Cross-sectional anatomy and comparative ultrasonography of the equine medial femorotibial joint and its related structures. Equine Vet J 2005;37 (06):520–529
36 Vandeweerd JM, Kirschvink N, Muylkens B, et al. Magnetic resonance imaging (MRI) anatomy of the ovine stifle. Vet Surg 2013;42(05):551–558
37 Rosvold JM, Atarod M, Heard BJ, O'Brien EJ, Frank CB, Shrive NG. Ligament and meniscus loading in the ovine stifle joint during normal gait. Knee 2016;23(01):70–77
38 Orhan IO, Haziroglu RM, Gultiken ME. The ligaments and sesamoid bones of knee joint in New Zealand rabbits. Anat Histol Embryol 2005;34(02):65–71
39 Dyce KM, Sack WO, Wensing CJG. Text book of Veterinary anatomy. W.B. Saunders CompanyPhiladelphia, London and Toronto2010
40 Nickel R, Schummer A, Seiferle E, Frewein J, Wilkens H, Wille KH. The Locomotor System of the Domestic Mammals "Skeleton of the Head of Ruminants'' 149-154. Verlag Paul PareyBerlin-Hamburg, Germany1986
41 Soler M, Murciano J, Latorre R, Belda E, Rodríguez MJ, Agut A. Ultrasonographic, computed tomographic and magnetic resonance imaging anatomy of the normal canine stifle joint. Vet J 2007;174(02):351–361
42 Gupte CM, Bull AM, Murray R, Amis AA. Comparative anatomy of the meniscofemoral ligament in humans and some domestic mammals. Anat Histol Embryol 2007;36(01):47–52
43 Barone R. Articulation fémoro-tibio-rotulienne. Anatomie Comparée des Mammifères Domestiques 1968;2:296

Morphometrics Analysis of Sagitta Otolith in Pool Barb, *Puntius sophore* (Hamilton, 1822)

Anju Rani[1] Deepak Rai[1] Anil K. Tyor[1]

[1] Department of Zoology, Kurukshetra University, Kurukshetra, Haryana, India

Address for correspondence Anju Rani, Research Scholar, Department of Zoology, Kurukshetra University, Kurukshetra 136119, Haryana, India (e-mail: thaakran2101@gmail.com).

J Morphol Sci 2019;36:85–90.

Abstract

Introduction The use of otolith morphometrics could prove to be a powerful tool in fish identification. The aim of the present study was to analyze the shape of the otolith in pool barb, *Puntius sophore*.

Materials and Methods To accomplish the present study, samples of various sizes were collected from the Yamunanagar and from the Faridabad fish markets in Haryana, India. The sagitta otoliths were extracted by making a horizontal cut across the head of the fish.

Results The independent *t*-test revealed no statistically significant difference between the values of otolith length and width of both the right and left otoliths ($p > 0.05$). Furthermore, various shape indexes, such as form factor (FF); circularity (C); rectangularity (REC), and aspect ratio (AR) were calculated, and the general shape of the otoliths of *P. sophore* was described as rectangular and less elongated. The otolith length (OL) was found to be positively correlated with the AR, whereas the FF was found to be negatively correlated with REC and C. The present study expresses the relationship between the total length (TL) and the head length (HL) of the fish with the OL and the otolith width (OW) by a linear regression model. The results depicted that the OL and the OW were linearly correlated to the TL and to the HL of the fish.

Conclusion The present study also provides a better understanding in identification of fish stock.

Keywords

- linear regression
- otolith dimensions
- shape indices

Introduction

Puntius sophore (Hamilton, 1822), commonly known as pool barb, stigma barb, and swamp barb, is a freshwater to brackish-water fish belonging to the cypriniformes order and to the cyprinidae family.[1] Cypriniformes are the largest group of fishes, with an estimated number of ~ 3,500 species.[2] *Puntius sophore* is widely distributed in inland waters of Asia, including Bangladesh, Pakistan, India, Nepal, Myanmar, Bhutan, Afghanistan, and China. This fish is benthopelagic (demersal), inhabiting rivers, streams, and ponds of plains.[3] It is considered as a chief food source for poor people in Bangladesh,[4] and is used as an aquarium fish.[5] According to the red list (2010) of the International Union for Conservation of Nature (IUCN), the status of this fish is regarded as of least concern.[6] However, studies from the Indian waters depicted that the fish is at lower risk to near threatened in the Western Ghat and in the Harike wetland, due to heavy fishing pressure.[7,8] Otoliths are paired calcified, aragonitic mineralizations located in the inner ear of the fish, which contribute to audition and equilibrium.[9,10] Amongst the three otoliths, the sagitta is the largest, followed by the astericus and by the lapillus.[11] The otolith continues to grow throughout the life of the fish, and its growth generally follows an allometric increase with respect to fish size.[12] The variations in the shape of the sagitta otolith are immense and are species specific, ranging from pinhead size to massive pieces of calcium carbonate ($CaCO_3$).[11] Due to its interspecific variations and larger size, the sagitta otolith has been used to estimate the taxon, age, size, migration, and feeding habits of fishes.[10,13,14]. Hence, knowledge of fish otolith morphometry is considered a valuable tool for the identification of the stock,[15,16] population management,[17] determination of diet

received
September 4, 2018
accepted
January 9, 2019

DOI https://doi.org/10.1055/s-0039-1683911.
ISSN 2177-0298.

Copyright © 2019 by Thieme Revinter Publicações Ltda, Rio de Janeiro, Brazil

License terms

Table 1 Variables utilized to study otolith morphology[22]

Variables	Measurements	Description
Relative dorsal length, (D)	d-d'	$D=\frac{d-d'}{l-l'}X\,100$
Relative medial length, (M)	m-m'	$M=\frac{m-m'}{l-l'}X\,100$
Relative antirostrum height, (A)	m-a	$A=\frac{m-a}{h-h'}X\,100$
Relative rostrum height, (R)	m-r	$R=\frac{m-r}{h-h'}X\,100$
Relative antirostrum length, (AL)	al-d	$AL=\frac{al-d}{l-l'}X\,100$
Relative rostrum length, (RL)	rl-l	$RL=\frac{rl-l}{l-l'}X\,100$

in predatory fishes,[18] ontogenic research,[19] ecomorphological studies,[20] and for the identification of specific species.[21]

Although the otolith chemistry of marine fishes has been extensively studied, information on otolith of freshwater fishes concerning the Indian subcontinent is limited. Therefore, the purpose of the present study was aimed to analyze the shape and morphometrics measurements of the otolith of *P. sophore*.

Materials and Methods

A total of 41 specimens ranging between 66 and 109 mm in total length (TL) were procured from the fish markets of the Faridabad (28.4211° N and 77.3078° E) and of the Yamunanagar (30.133° N and 77.288° E) regions of Haryana, India, and brought to the laboratory in an ice box. All of the fish specimens were cleaned and measured for TL, standard length, HL, and body weight, nearest to 0.1 mm and 1 g, respectively. The sagitta otoliths were removed by making a horizontal cut across the head of the fish. The otoliths were cleaned manually by using 1% potassium hydroxide (KOH) solution to remove otic fluid, blood, and tissue, and were air dried. The right and left otoliths were kept separately in different labeled envelopes.

Table 2 Shape indices calculated using otolith morphometric parameters[23,24]

Parameters	Shape indices	Formulae
Area (Ar)	Aspect ratio (AR)	OL/OW
Perimeter (P)	Form factor (FF)	$4\pi Ar/P^2$
Otolith length (OL)	Rectangularity (REC)	Ar/OL/OW
Otolith width (OW)	Circularity (C)	P^2/Ar

Digital images of both the right and left otoliths were obtained over a dark background using a Magnus MSZ-TR stereo microscope (Magnus Analytics, New Delhi, India (fitted with a Magcam DCS 5.1MP, ½.5" CMOS SENSOR camera. Various morphometric measurements of the otoliths,[22] as shown in ►**Table 1**, were acquired using ProgRes CapturePro, version 2.80, software (Jenoptik AG, Jena, Germany), in which the otolith length (OL) was the maximum distance from the rostrum to the postrostrum, and the otolith width (OW) was the distance perpendicular to the length passing through the dorsal and ventral rim (►**Fig. 1**).

For the analysis of the shape of the otoliths, morphometric parameters such as OL, OW, area (Ar) and perimeter (P) were utilized to calculate four dimensionless shape indices (form factor (FF); circularity (C); rectangularity (REC); and aspect ratio (AR)[23,24] (►**Table 2**). Form factor is a mean to estimate the surface area irregularity, C gives information on the similarity of various features to a perfect circle, REC describes the variations of length and width with respect to the area, and AR expresses the shape tendency of the otolith.[23] To statistically analyze the data, SPSS for Windows, Version 16.0 (SPSS Inc, Chicago, IL, USA) and Microsoft Excel, version 2007 (Microsoft Corp., Redmond, WA, USA) were employed. The difference between the OL and the OW of the right and left otoliths was examined by employing the independent *t*-test. The relationship between the TL and the HL of the fish and the OL and OW was described by a linear equation.

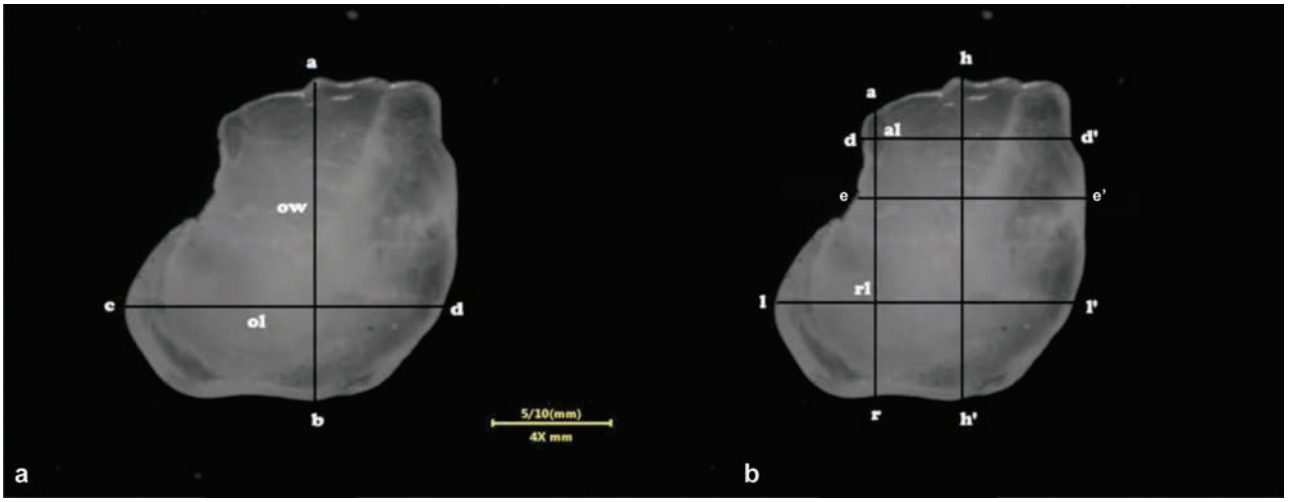

Fig. 1 Otolith of *Puntius sophore* (a) The distance between a and b is the otolith width, and the distance between c and d is the otolith length, (b) various otolith morphometric measurements used for the present study.

Table 3 Mean, standard deviation, standard error, minimum and maximum values of various body measurements of *Puntius sophore*

Parameter	Mean	SD	SE	Min	Max
Total length (TL)	83.9	10.4	1.6	66	109
Standard length (SL)	67.5	8.6	1.3	52	89
Head length (HL)	15	2.1	0.3	12	20
Body weight (BW)	104	36.9	5.8	40	210

Abbreviations: Max, maximum range; Min, minimum range; SD, standard deviation.
All of the values depicted in the table are in millimeters (mm)

Table 4 Mean, standard error, minimum and maximum values of various parameters of otolith dimensions

Parameters	Mean ± SE	Min	Max
Otolith length (OL)	0.74 ± 0.1	0.54	1.07
Otolith width (OW)	0.91 ± 0.0.2	0.61	0.98
Relative antirostrum height (A)	28.8 ± 1.68	14.03	65.74
Relative antirostrum length (AL)	8.51 ± 0.60	17.89	2.75
Relative rostrum height (R)	55.4 ± 2.05	18.10	75.79
Relative rostrum length (RL)	14.3 ± 1.25	4.53	33.27

Abbreviations: Max, maximum range; Min, minimum range; SE, standard error.
All the values depicted in table are in millimeters (mm).

Results

A total of 82 otolith samples were collected from 41 specimens. The OLs and OWs ranged between 0.54 and 1.07 mm, and between 0.61 and 0.98 mm, respectively. Various morphometric parameters of the fish were taken into consideration (►**Table 3**). The measurements of Otolith length (OL) and otolith width (OW) of both right and left otoliths were tested and no statistically significant difference was observed ($p > 0.05$). Therefore, either the left or right sagitta otolith can be used for the analysis. For the present study, the left sagitta otolith was utilized. The shape of the otolith of *P. sophore* was described as rectangular and less elongated, possessing well-defined antirostrum and rostrum. The antirostrum was observed as short and narrow, with average height and length of 28.8 ± 1.68 and 8.51 ± 0.6 0mm, respectively, whereas the rostrum was noticed to be wide and round with a mean height and length of 55.4 ± 2.05 and 14.3 ± 1.25 mm, respectively (►**Table 4**). The otolith has smooth dorsal and ventral margins with an obtuse excisural notch. The sulcus was found to be round and deep (►**Fig. 2b**). By comparing the mean values of 4 shape indices of the otolith of *P. sophore* (►**Table 5**), it was concluded that the average value of REC was the highest, while the value of AR was the lowest (AR: 0.82 < C: 1.36 < FF: 31.91 < REC: 34.03). Furthermore, the OL was found to be positively correlated with the AR, whereas the FF was found to be negatively correlated with REC and C. The present study explains the relationship between the TL and the HL of the fish with the OL and the OW described by the linear equations $y = 0.0052x + 0.309$ (►**Fig. 3a**); $y = 0.0095x + 0.1114$ (►**Fig. 3b**); $y = 7.2851x + 9.5285$ (►**Fig. 3c**), respectively. The results depicted that the OL and the OW were linearly correlated to the TL and to the HL of the fish.

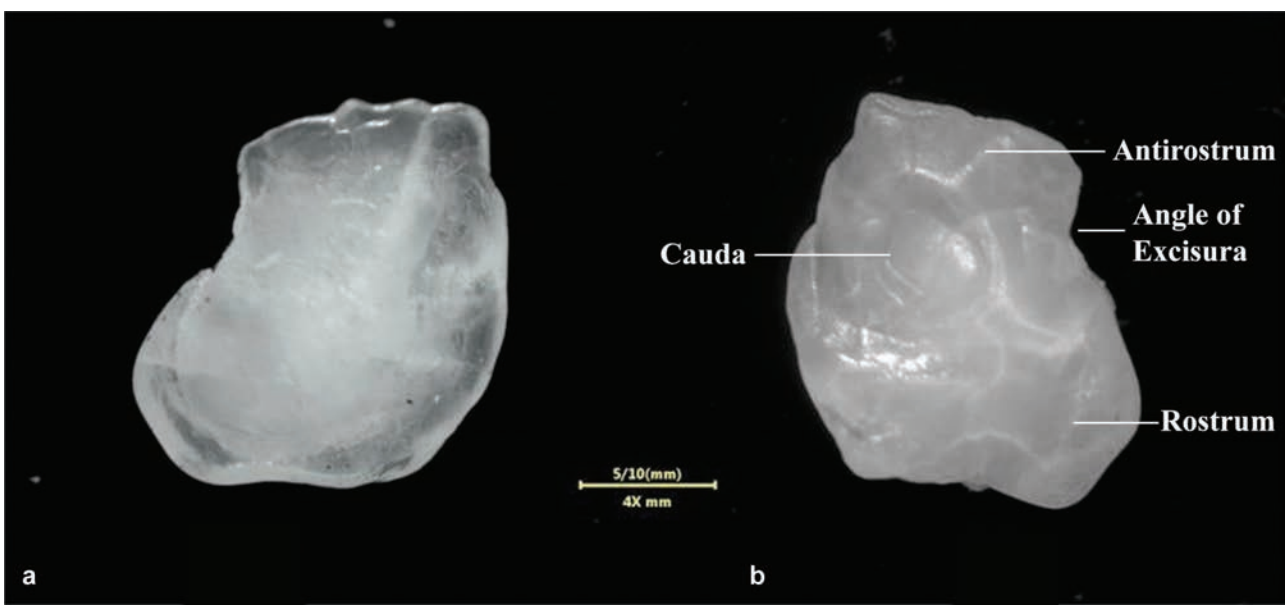

Fig. 2 *Puntius sophore* otolith (a) dorsal view of the left sagitta otolith, (b) ventral view of left sagitta otolith showing the cauda, the rostrum, the antirostrum, and the angle of excisura.

Table 5 Descriptive statistics of shape indices of *Puntius sophore*

Shape indices	Mean	SD	SE	Min	Max
Form factor	31.91	5.20	0.81	0.31	34.57
Aspect ratio	0.82	0.1	0.02	0.61	0.98
Rectangularity	34.03	2.57	0.40	28.52	39.86
Circularity	1.36	3.93	0.61	2.35	27.72

Abbreviations: Max, maximum range; Min, minimum range; SD, standard deviation; SE, standard error.

The OW was found to be a better parameter in estimating fish length than the OL.

Discussion

Otolith morphology has proven to be a powerful and vital tool in various taxonomic studies. Among the three otoliths, the sagitta otolith has been extensively utilized in various taxonomic studies related to age, growth, feeding habits, and stock identification, due to its larger size and great interspecific variability.[10,13,14,25] The present study has aimed to examine the relationship of fish TL and HL with otolith dimensions (OL and OW) by a linear regression model. The otolith dimensions (OL and OW) and fish body relationships have been studied in various marine fish species by linear regression models.[15,26–32] The results of the present study depicted that the OL and the OW were linearly correlated to the TL of the fish. The HL of the fish also showed positive correlation with the OL. The OW was found to be a better parameter than the OL in estimating fish length. Hence, it is suggested that otolith dimensions increase as fish length increase and, therefore, otolith growth can be correlated with fish growth. These results are similar to previous studies.[33,34]. However, other studies depicted that the relationship of otolith variables and fish somatic growth are not necessarily linear.[35,36] In studies on the relationship between otolith and fish size, the OL was usually used.[15,26,37–39] The present study supplies supplementary information by considering both the OL and the OW, as well as the HL of the fish. The present study also described various other morphometric parameters to give a detailed observation of the shape of the otolith. When comparing the values of the OL and of the OW of both right and left otoliths, no statistically significant difference was observed, which was consistent with the previous findings of different authors.[29,32,35,40] But some studies of sciaenid fishes, such as *Micropogonias furnieri* and *Macrodon ancylodon*, and of teleost fishes, such as *Lycodes palearis* (Zoarcidae) revealed inverse findings.[15,41] Concerning the findings of the present study, it becomes evident that the knowledge of the otolith morphometrics is considered an important marker in the identification of species and in many other ecological studies that aimed to determine the prey size based on otoliths obtained from the stomach contents of piscivorous predators, because, when the relationship between the OL and the TL in a

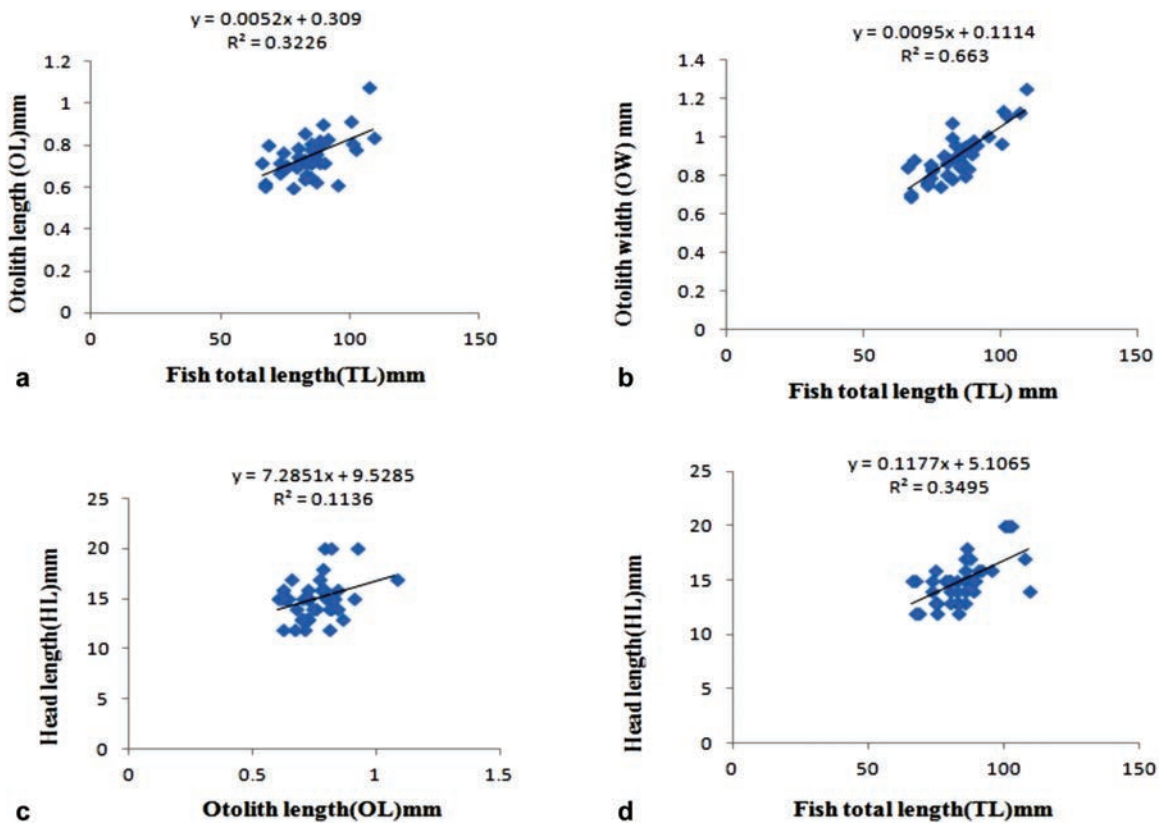

Fig. 3 Relationship between (a) otolith length and fish total length, (b) otolith width and fish total length, (C) head length and otolith length, and (d) head length and fish total length.

species is determined, the TL or standard length of a fish can be easily estimated from its OL, or vice versa.[28,31,33] The present study also provides a better understanding in the identification of the stock.

Conflicts of Interest

The authors have no conflicts of interest to declare.

Acknowledgments

The authors are highly grateful to the Department of Zoology of the Kurukshetra University, Kurukshetra, India, for providing the necessary laboratory facility for the accomplishment of the present study. The authors are also thankful to the local fishermen for providing suitable help during the sampling.

References

1 Redie K. Global register of migratory species from global to regional scales. Final report of R&D Project 808 05 081. Bonn, Germany: Fedral Agency for Nature Conservation; 2004:330
2 Nelson JS. Fishes of the World. 4th ed. Hoboken, NY, USA: John Wiley & Sons, Inc.; 2006
3 Menon AGK. Check list - fresh water fishes of India. Rec ZoolSurv India. 1999;175:234–259
4 Roos N, Leth T, Jakobsen J, Thilsted SH. High vitamin A content in some small indigenous fish species in Bangladesh: perspectives for food-based strategies to reduce vitamin A deficiency. Int J Food SciNutr 2002;53(05):425–437
5 Froese R, Pauly D. EDS. http://www.fishbase.org2011
6 Dahanukar N*Puntiussophore*. The IUCN Red List of Threatened Species 2010; e.T166623A6249514.
7 Balasundaram C, Arumugam R, Murugan PB. Fish diversity of Kolli hills, Western Ghats, Salem district, Tamil Nadu. Zoos' Print. 2000;16(1):403–406
8 Dua A, Parkash C. Distribution and abundance of fish populations in Harike wetland–a Ramsar site in India. J Environ Biol 2009;30 (02):247–251
9 Popper AN, Ramcharitar J, Campana SE. Why otoliths? Insights from inner ear physiology and fisheries biology. Mar Freshw Res 2005;56:497–504
10 Mendoza RPR. Otoliths and their applications in fishery science. Ribarstvo 2006;64(03):89–102
11 Paxton JR. Fish otoliths: do sizes correlate with taxonomic group, habitat and/or luminescence? Philos Trans R SocLond B BiolSci 2000;355(1401):1299–1303
12 Chilton DE, Beamish RJ. Age determination methods for fishes studied by the groundfish program at the Pacific Biological Station.Ottowa. Can Spec Publ Fish AquatSci 1992;60:1–102
13 Campana SE. 2005Otolith elemental composition as a natural marker of fish stocks. In *Stock Identification Methods Applications in Fishery Sciences*, edited by Cadrin SX, Friedland K, Waldman JR. Massachusetts: Elsevier Academic Press; 227–245
14 Morat F, Banaru D, Merigot B, et al. Relationship between Fish Length for nine teleost from Mediterranean basin, Kerguelen Islands and Pacific ocean. Cybium 2008;32:265–269
15 Harvey JT, Oughlin TR, Perez MA, Oxman DS. Relationship between fish size and otolith length for 63 species of fishes from the eastern North Pacific Ocean. NOAA Technical Report 2000;150:1–36
16 Campana SE, Thorrold SR. Otoliths, increments, and elements: Keys to a comprehensive understanding of fish populations? Can J Fish AquatSci 2001;58:30–38
17 Vasconcelos J, Vieira AR, Sequeira V, Gonzalez JA, Kaufmann M, Serrano Gordo L. Identifying populations of the blue jack mackerel (Trachurus picturatus) in the Northeast Atlantic by using geometric morphometrics and otolith shape analysis. Fish Bull 2018;116:81–92
18 Lilliendahl K, Solmundsson J. Feeding ecology of symparic European shags *Phalacrocorax artistotelis* and great cormorants *P. carbo* in Iceland. Mar Biol 2006;149:979–990
19 Capoccioni F, Costa C, Aguzzi J, Menesatti P, Lombarte A, Ciccotti E. Ontogenetic and environmental effects on otolith shape variability in three Mediterranean European eel (*Anguilla anguilla*, L.) local stocks. J Exp Mar Biol Ecol 2011;397(01):1–7
20 Tuset VM, Piretti S, Lombarte A, Gonzalez JA. Using sagittal otoliths an deye diameter for ecological characterization of deep-sea fish: *Aphanopus carbo* and *A. intermedius* from NE Atlantic waters. Sci Mar 2010;74:807–814
21 Bani A, Poursaeid S, Tuset VM. Comparative morphology of the sagittal otolith in three species of south Caspian gobies. J Fish Biol 2013;82(04):1321–1332
22 Reichenbacher B, Sienknecht U, Küchenhoff H, Fenske N. Combined otolith morphology and morphometry for assessing taxonomy and diversity in fossil and extant killifish (Aphanius, Prolebias). J Morphol 2007;268(10):898–915
23 Tuset VM, Lombarte A, González JA, Pertusa JF, Lorente MJ. Comparative morphology of the sagittal otolith in *Serranus spp.*. J Fish Biol 2003;63(06):1491–1504
24 Lord C, Morat F, Lecomte-Finiger R, Keith P. Otolith shape analysis for three Sicyopterus (Teleostei: Gobioidei: Sicydiinae) species from New Caledonia and Vanuatu. Environ Biol Fishes 2012;93 (02):209–222
25 Rodgveller CJ, Hutchinson CE, Harris JP, Vulstek SC, Guthrie CM. Otolith shape variability and associated body growth differences in giant grenadier, Albatrossiapectoralis. PLoS One 2017;12(06): e0180020
26 Şen D, Aydin R, Çalta M. Relationships between fish length and otolith length in the population of *Capoetacapoetaumbla* (Heckel, 1843) inhabiting Hazar Lake, Elazig, Turkey. Arch Pol Fisheries 2001;9:267–272
27 Bostanci D. Otolith biometry-body length relationships in four fish species (chub, pikeperch, crucian carp, and common carp). J FreshwatEcol 2009;24:619–624
28 Battaglia P, Malara D, Romeo T, Andloro F. Relationships between otolith size and fish size in some mesopelagic and bathypelagic species from Mediterranean Sea (Strait of Messina, Italy). Sci Mar 2010;74:605–612
29 Jawad LA, Ambuali A, Al-Mamyr JM, Albusaidi HK. Relationships between fish length and otolith length, width and weight of the Indian mackerel *Rastrelligerkanagurta*(Cuvier, 1817) collected from the Sea of Oman. Ribarstvo 2011;69(2):51–61
30 Bostanci D, Yilmaz S, Polat N, Kontas S. The otolith biometry characteristics of black scorpionfish, *Scorpaenaporcus*, 1758.*The Black Sea*.International. J Engineering Science 2012;2:59–68(in Turkish)
31 Basusta A, Bal H, Aslan E. Otolith biometry – total length relationships in the population of Hazar Bleak, *Alburnusheckeli*(Battalgil, 1943) inhabiting Lake Hazar, Elazig, Turkey. Pak J Zool 2013; 45:1180–1182
32 Félix VR, Martínez-Pérez JA, Molina JR, Emiliano R, Zuñiga Q, López JF. Morphology and morphometric relationships of the sagitta of Diapterusauratus (Perciformes: Gerreidae) from Veracruz, Mexico. Rev Biol Trop 2013;61(01):139–147
33 Yilmaz S, Yazicioglu O. Saygin (Ayaydin) S, Polat N. Relationships of otolith dimensions with body length of European perch, *Percafluviatilis* L, 1758 from Lake Ladik, Turkey. Pak J Zool 2014;46:1231–1238
34 Yilmaz S, Yazicioglu O, Yazici R, Polat N. Relationships between fish length and otolith size for five cyprinid species from Lake Ladik, Samsun,Turkey. Turk J Zool 2015;39:438–446
35 Dehghani M, Kamrani E, Salarpouri A, Kamali E. Age and growth of Sind sardine (Sardinellasindensis) using otolith

from Qeshm Island (Persian Gulf). Iran J Fish Sci 2015;14(1): 217–231
36 Campana SE. Photographic atlas of fish otoliths of the northwest atlantic ocean. Ottawa: NRC Research Press; 2004
37 Echeverria TW. Relationship of otolith length to total length in rockfishes from northern and central California. Fish Bull 1987; 85:383–387
38 Gamboa DA. Otolith size versus weight and bodylength relationships for eleven fish species of Baja California, Mexico. Fish Bull 1991;89:701–706
39 Şahin T, Güneş E. Relationship between otolith and total lengths of flounder (*Pleuronectesflesusluscus*Pallas, 1811) collected in eastern Black Sea coasts of Turkey. Turkish Journal of Maritime and Marine Sciences 1998;4:117–123
40 Škeljo F, Ferri J. The use of otolith shape and morphometry for identification and size-estimation of five wrasse species in predator-prey studies. J Appl Ichthyology 2012;28:524–553
41 Waessel JA, Lasta CA, Bavero M. Otolith morphology and body size relationship for juvenile sciaenidae in the rio de la plate esturay (35–36°s). Sci Mar 2003;67(02):233–240

Effects of Supraphysiological Doses of Steroids on the Left Ventricle of Sedentary Mice: Morphometric Analysis

Érika Larissa Poscidônio de Souza[1] Rodrigo Leandro Dias[1] Raíssa Santiago Rios[1] Tânia Martins Vieira[1] Bruno Damião[1] Wagner Costa Rossi Junior[1] Alessandra Esteves[1]

[1] Department of Anatomy, Universidade Federal de Alfenas, Alfenas, MG, Brazil

J Morphol Sci 2019;36:91–96.

Address for correspondence Alessandra Esteves, PhD, Departmento de Anatomia, Universidade Federal de Alfenas. Rua Gabriel Monteiro da Silva, n°700, Centro, Alfenas, MG, Brazil, CEP 37130-820 (e-mail: aesteves015@gmail.com).

Abstract

Anabolic androgenic steroids (AAS) are synthetic compounds derived from testosterone, which are widely used in supraphysiological doses by people seeking an aesthetic effect. The objective of the present experiment was to evaluate the possible morphometric changes in the cardiac left ventricle caused by the administration of supraphysiological doses of the anabolic steroids testosterone cypionate and stanozolol in the hearts of young sedentary mice, to serve as a comparative parameter with young mice that were submitted to exercise. We have used 60 hearts of sedentary young Swiss mice, aged ~ 90 days old (young-adult), with a body weight between 40 and 50 g. The animals were divided into three groups: the control group, the testosterone cypionate group, and the stanozolol group. For the analysis, 10 distinct sections of the apex, of the middle region, and of the base of the heart were selected, followed by an optical microscope measurement with a 2.5x magnification. The results obtained show an increase in both myocardial thickness and left ventricular cavity diameter in the two groups of male animals in relation to the control group; however, in females, an increase in the thickness of the left ventricular myocardium was observed only for the stanozolol group. These results suggest that the cardiac alterations observed in the present study may be directly related to some signs and symptoms already described in the literature, such as hypertension, arrhythmias, infarction, sudden death, and other cardiovascular diseases.

Keywords

- heart
- morphometric analysis
- left ventricle
- steroids

Introduction

Androgenic anabolic steroids (AAS) are hormones that function in the differentiation, growth, and development of the male reproductive tract, as well as in the development and maintenance of secondary sexual characteristics. However, they also have anabolic effects, stimulating body growth and increasing muscle mass.[1] AAS are synthetic compounds derived from this hormone, which mimic the anabolic effects of testosterone, while at the same time minimizing androgenic effects.[2]

In the 1950s, the first reports of abuse in the administration of AAS for non-therapeutic purposes by Russian athletes appeared in the literature.[3] Since then, AAS hormones have been used usually by people with good health, in order to increase muscle mass and potency, as well as to provide improvement in their physical condition and appearance.[4]

Illicit long-term and supraphysiologic use of AAS may cause adverse cardiovascular effects, such as pathological hypertrophy, as well as ventricular and atrial arrhythmic events, among which atrial fibrillation is the most frequently observed in bodybuilders. Additionally, several reports of atrial fibrillation suggest a causal link in the use of AAS in athletes.[5]

The compounds selected for the present study are synthetic, commonly used for aesthetic purposes, with testosterone cypionate being one of the most widely used AAS in the market.[6]

One of the mechanisms described in the literature regarding the use of supraphysiological doses is associated with the

received
August 22, 2018
accepted
January 28, 2019

DOI https://doi.org/10.1055/s-0039-1681109.
ISSN 2177-0298.

Copyright © 2019 by Thieme Revinter Publicações Ltda, Rio de Janeiro, Brazil

License terms

temporary nitrogen retention of ingested proteins, as well as with the competition of receptors of glucocorticoids released during intense exercise, leading to the inhibition of protein catabolism.[7]

Increased erythropoiesis is also a risk factor for erythropoietin stimulation and hepcidin suppression. Erythropoietin is the erythrocyte stimulating hormone, whereas hepcidin is a protein that regulates iron absorption, so the erythropoietin produced is more active due to the higher concentration of serum iron.[8]

Understanding the ease of obtaining anabolic agents, the indiscriminate use of these drugs and their possible side effects, it was proposed to evaluate in a specific and controlled way the effects of supraphysiological doses of these AAS in sedentary mice for comparison with a group of animals treated with the same drugs, but performing physical exercise, in order to obtain accurate information and, with this, to raise awareness, mainly to the generation of young adolescents, about the possible causes and effects of the indiscriminate use of these substances.

Materials and Methods

For the present experiment, 60 Swiss mice were used (30 males and 30 females) from the Universidade Federal de Alfenas (UNIFAL, in the Portuguese acronym) (Committee for Ethics in Animal Experimentation [CEEA], Universidade Federal de Alfenas, registry number 505/2013). These were housed in boxes containing 5 animals each, and were treated with commercial feed and ad libitum water and kept in a light-dark 12-hour cycle.

The treatment consisted of the intraperitoneal application of two AAS, as follows: Group 1: testosterone cypionate (Deposteron [EMS, São Bernardo do Campo, SP, Brazil]) (0.8 mg/kg); group 2: stanozolol ([Winstrol-Stanozolol Depot, Landerlan, Lambaré, Paraguay]) (1.8 mg/kg), and group 3: physiological solution (1 ml/kg). The animals were treated for 2 months, with doses applied twice a week at 2-day intervals.

After the euthanasia of the animals by means of the halothane anesthetic and the identification of each animal, the thoraxes were opened and the hearts were entirely removed. Finally, the organs were stored in glass containers containing paraformaldehyde (pH 7.4). They remained immersed in this fixative solution for 24 hours.

The hearts were processed following the standardized histological procedures. The paraffin-embedded samples were cut in a thickness of 7µm in a Yidi microtome ([Jinhua YIDI Medical Appliance CO., LTD, Jinhua City, Zhejiang province, China]) and stained with hematoxylin and eosin (H&E).

For the morphometric analysis, 10 distinct sections of the apex, of the middle region, and of the base of the heart were selected (►**Fig. 1**). To measure ventricular cavity diameter, was selected the entire area of ventricular cavity by means of one of the tools of the software Axiovision Version. 4.8.2 (Carl Zeiss Microscopy LLC, Peabody, MA, USA). To measure the myocardical thickness, three areas (anterior, posterior and lateral) were selected and was used the same software for analysis [Axiovision Version. 4.8.2 (Carl Zeiss Microscopy LLC, Peabody, MA, USA)]. The values were measure in μm^2.

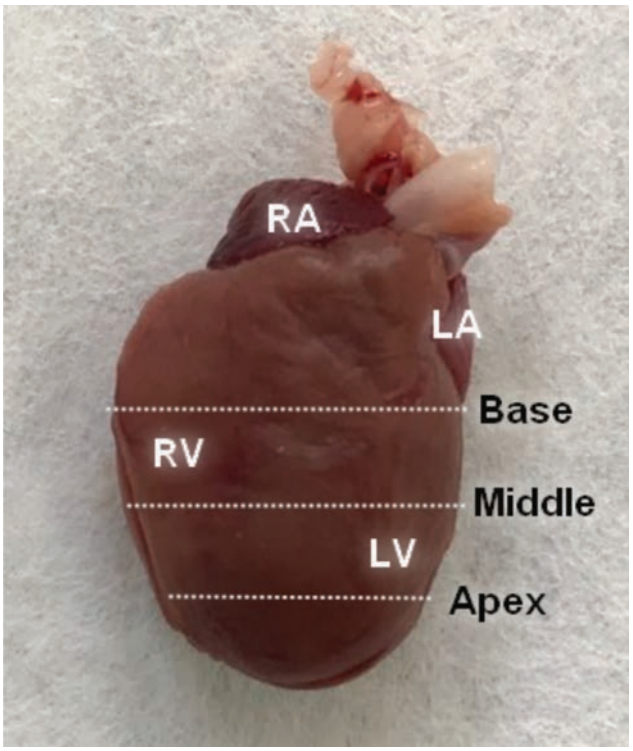

Fig. 1 Heart of a normal mouse demonstrating the regions to be analyzed (white trace): the apex, the middle region, and the base. Abbreviations: LA, left atrium; LV, left ventricle; RA, right atrium; RV, right ventricle.

The analysis was performed using an optical microscope model Axion Scope A1 (Carl Zeiss Microscopy LLC, Peabody, MA, USA) coupled to Axiovision Version. 4.8.2 (Carl Zeiss Microscopy LLC, Peabody, MA, USA) and to the Axiovision 4 Module Interactive Measurement software (Carl Zeiss Microscopy LLC). To capture the selected images, a 2.5x objective lens (Carl Zeiss Microscopy LLC, Peabody, MA, USA) was used (►**Fig. 1**).

To evaluate the mean values of the left ventricle areas, according to the gender of the mice and to the treatment imposed (research groups), the analysis of variance (ANOVA) was used. When a significant difference ($p < 0.01$) was observed among the groups when comparing different variables, the Tukey test was used to discriminate differences and/or similarities among the evaluated means.[9]

Results

As shown in the graphics, no significant result was observed in the diameter of the left ventricle cavity of the hearts of female mice in the control group in relation to the treated groups (►**Fig. 2A**).

However, when analyzing the myocardial thickness, a significant difference was observed, showing a decrease in the myocardial thickness of the stanozolol group in relation to the control group ($p < 0.00001$), as well as in the group treated with testosterone cypionate in relation to the group treated with stanozolol ($p < 0.0001$). However, when the testosterone

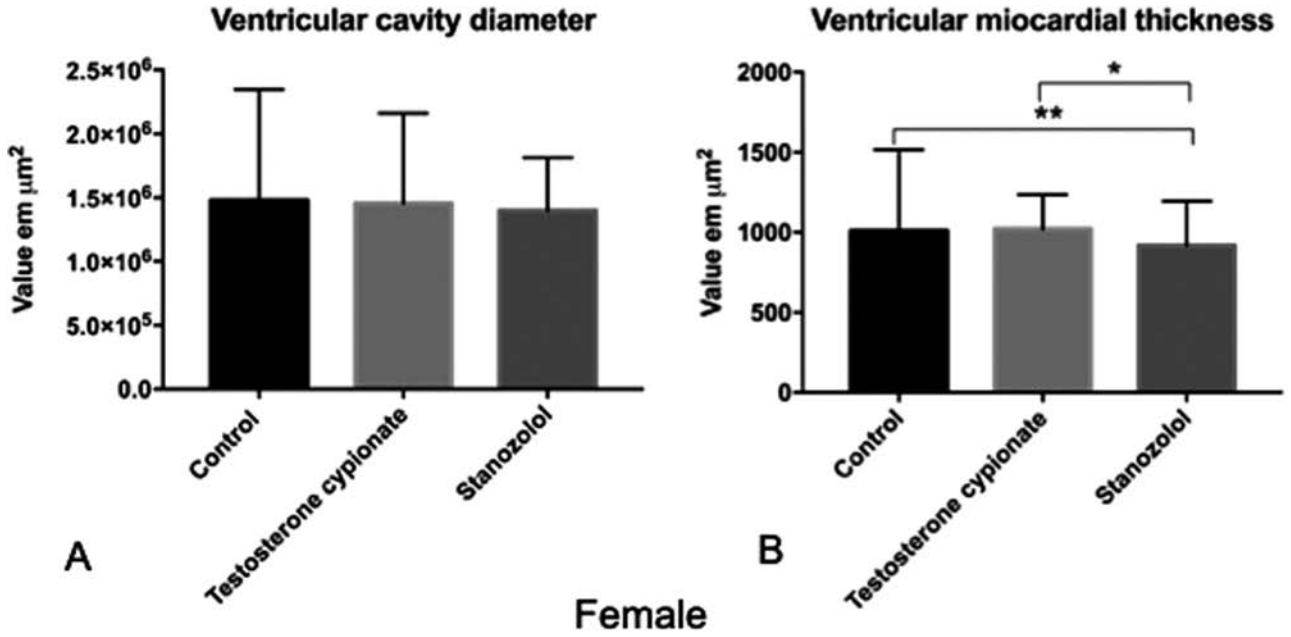

Fig. 2 (A) The graphics demonstrate the nonsignificant difference in the left ventricular cavity diameter of female mice between the experimental groups.(B) Shows the significant difference in the left ventricular myocardial thickness observed between the control group in relation to the group treated with stanozolol (Winstrol Depot) (**), and the group treated with testosterone cypionate (Deposteron) in relation to the Stanozolol (Winstrol) group (*).

cypionate group was compared with the control group, no statistically significant result was obtained (►**Fig. 2B**).

When comparing the diameter of the left ventricle in male mice, significant differences were observed, showing that both of the AAS evaluated increased the diameter of the left ventricular cavity, both in the testosterone cypionate group in relation to the control group ($p < 0.0001$), and in the stanozolol group in relation to the testosterone cypionate group ($p = 0.0009$) (►**Fig. 3A**).

Regarding the analysis of the thickness of the left myocardial ventricle, the male mice presented significant differences between the control group and the 2 treated groups: testosterone cypionate ($p < 0.0001$) and stanozolol ($p = 0.0008$). A statistically significant difference was also observed

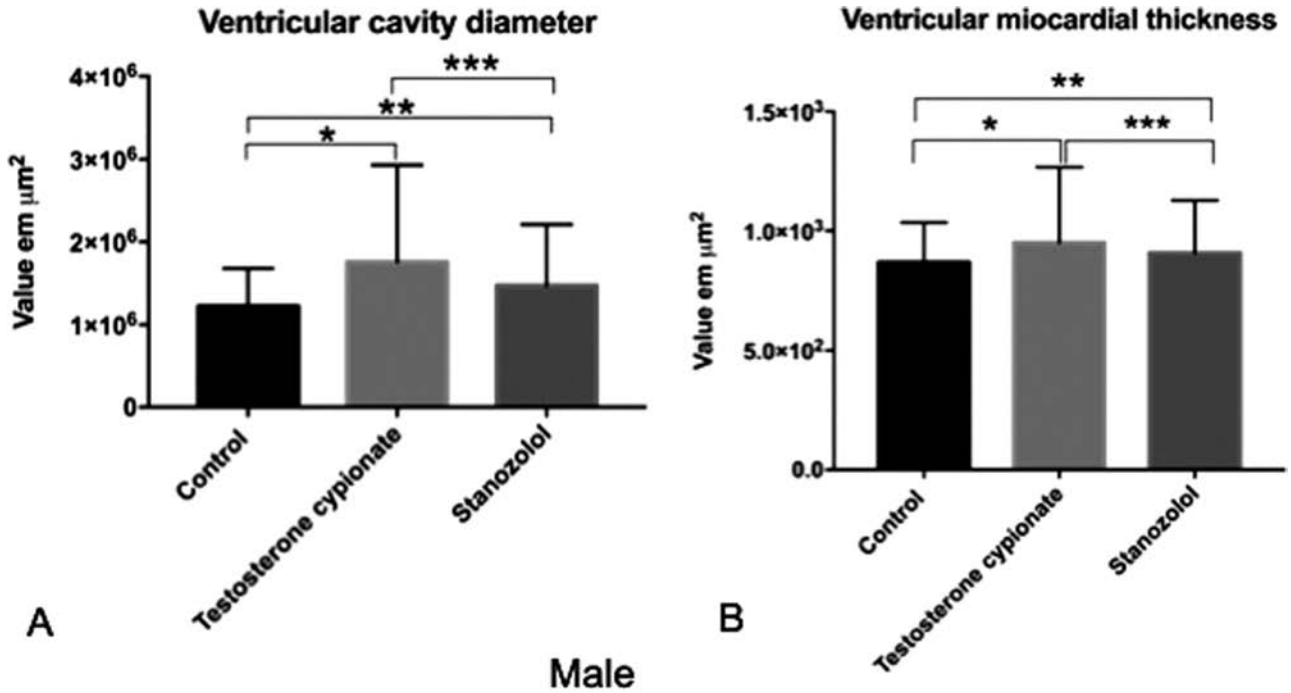

Fig. 3 The graphics show the statistically significant difference found in the left ventricular cavity diameter (A) and in the left ventricular myocardial thickness (B) between male mice in the control group and in the testosterone cypionate (Deposteron) group (*), between the control group and the Stanozolol (Winstrol) group (**), and between the two groups treated with the different steroids (***).

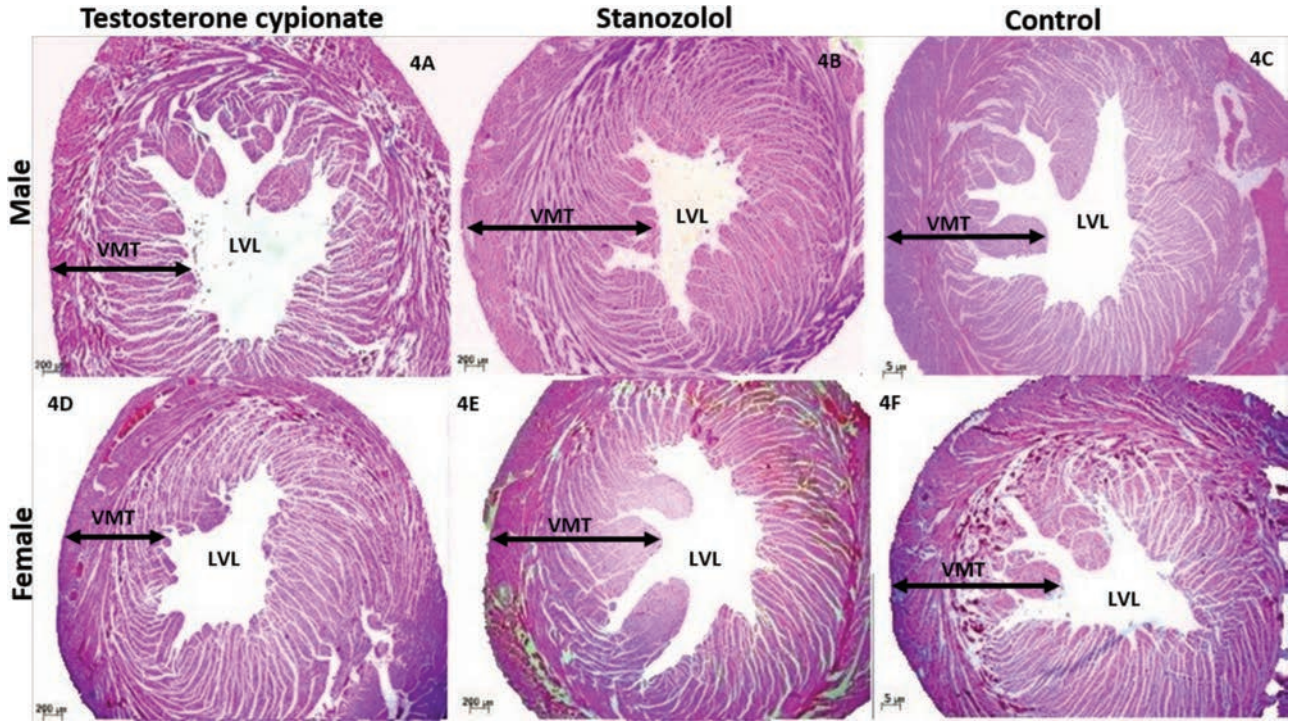

Fig. 4 Histological section of the left ventricles of some of the mice studied, (**A**) male mouse treated with testosterone cypionate, (**B**) stanozolol-treated male mouse, (**C**) male mouse in the control group, (**D**) testosterone cypionate-treated female mouse, (**E**) stanozolol-treated female mouse, and (**F**) female mouse in the control group, Abbreviations: LVL: left ventricular cavity; VMT, ventricular myocardial thickness.

between the stanozolol group and the testosterone cypionate group ($p = 0.0004$) (►**Fig. 3B**).

►**Fig. 4** represents histological section of the left ventricules of some of the male and female mice studied, stained in H&E, with a 2.5x magnification, of all in the groups studied for comparation.

Discussion

Left ventricular hypertrophy is directly related to increased blood pressure and systemic by compensatory mechanism. High blood pressure is associated with a three to four fold increase in the risk of stroke, fibrillation, and ventricular arrhythmia.[10,11] This study corroborates the results found Seara et al.[15], showing a significant increase in myocardial thickness and ventricular cavity diameter, in male mices.

According to literature, the use of nandrolone, another AAS widely used, promotes changes in endothelium of blood vessels, both at the sedentary and exercised female mice, indicating that physical exercise does not decrease the effects caused by AAS, and that sedentary users also suffer significant damage.[12] Other damages are also described by some authors, which demonstrated increased levels of LDL, HDL, NADPH oxidase in association with ventricular hypertrophy in rats treated with nandrolone, doing or not doing exercises.[13,14]

For Seara et al,[15] this cardiac hypertrophy is due to the thickening of the posterior wall of the left ventricle and of the interventricular septum in addition to fibrosis, even with discontinuation of the AAS treatment, thus reporting irreversible cardiac damage. And this can occur through several mechanisms, one of which is the increase in cardiac angiotensin due to the stimulus of the activity of the converting enzyme, and angiotensin II has been related to cardiac remodeling by cellular hypertrophy and collagen deposition.

The studies of Nascimento et al[16] showed that the deposition of collagen in cardiac cells can lead to a loss of the contractile function, with increased rigidity; moreover, an increase in the left ventricular systolic pressure has been reported, whereas a decrease in the diastolic function was observed, causing left ventricular isovolumic relaxation failure in rats treated with AAS. This failure in relaxation is one of the major etiological factors of ischemia and heart failure.

The possible increase in the erythrocytes count due to the stimulation caused by these hormones can also be seen as a risk factor because it leads to an increase in blood volume. Consequently, the heart would need more force to pump the blood to the tissues, causing hypertrophy.[17]

The results obtained in this study did not significantly alter the diameter of the left ventricular cavity of female mice, which can be explained by a cardiac and vascular protective effect of the endogenous estrogen, contributing to the maintenance of caliber and myocardial diameter, suggesting a possible compensation mechanism.[12,18]

According to Barp,[19] the cardiovascular protective effect of estrogen occurs in several ways, such as the stimulation of nitric oxide (NO), which is a vasodilatation gas that prevents platelet aggregation, endothelial leukocyte adhesion, endothelin production, and control of the vascular tone. Another protective factor is that estrogen can decrease cell proliferation in the tunica intima and in the tunica adventitia in the vessel wall, inhibiting protein kinase, which is in line with the results obtained in the present study.

Another probable hypothesis for the results found in females is the same as reported by Clark,[20] who states that, unlike testosterone cypionate, stanozolol has the ability to interfere with the production of estrogen by central action, as well as the potential to inhibit the hypothalamus-pituitary-gonadal axis, thus decreasing the production of estrogen, which explains the fact that the myocardial thickness of female mice changes once they no longer have the protective action of the hormone.

In patients with deficiency in testosterone levels, a deficiency of myocardial contraction is noted. In contrast, studies indicate that, at high levels, testosterone can be harmful because it acts directly on androgen receptors, which in turn act on genes that make the transcription of alpha-myosin heavy chain (α-MHC) and of transforming growth factor beta (TGF-β) proteins, which act respectively on atrial contraction and on the control of cell proliferation and differentiation.[21]

The results found by Pirampol et al.[21] may explain the results found in this study, which present a difference between the studied genders, showing that, in female mice, the use of AAS, such as stanozolol, may decrease the thickness of the left ventricular myocardium, while the results were the opposite in male mice.

The use of AAS causes changes in normal physiological adaptations that occur after exercise, from compen- sated to uncompensated hypertrophy and is related to several pathological processes according to Nascimento and Medei[22], such as heart failure, reduced tolerance to ischemia, and ventricular dilatation, which can also be demonstrated by the results found in the present study.

The use of AAS causes hypertrophy of cardiomyocytes, and a decrease in capillary density and increased capillary spacing was observed. It is presumed that these alterations affect the supply of oxygen to the myocardium by subjecting it to ischemia.[23]

Some researchers report the development of stress and cellular damage caused by the chronic use of AAS. In biochemical tests, it is known that troponin isoenzymes (cTnI) and creatine kinase MB (CK-MB) are specific indicators of cell lysis and are elevated in users of anabolic steroids.[24,25]

The heart rate also decreases after exercise, according to dos Santos,[26] who also reports that this may be an effect of changes in the parasympathetic nervous system, suggesting that these effects may also occur at rest in the case of sedentary mice, due to the changes already mentioned. The decrease in heart rate is a predisposing factor to cardiovascular pathologies.

Conclusion

The alterations found in the left ventricular cavity and thickness of the left ventricular myocardium allow to conclude that innumerable pathologies, such as vascular and cardiac hypertension, arrhythmias, acute myocardial infarction, and sudden death, may be associated with the findings described in the present study and that, beyond these alterations, it is also suggested that the indiscriminate use of AAS may bring serious risks to the user in relation to general health.

It is possible to see the great importance of studies related to AAS due to the increasing use of these substances in supraphysiological doses for non-medical purposes also by sedentary individuals who believe in the increase of muscular mass without physical effort.

Financial Support
The authors thank the financial support for accomplishment of this work provided by the Foundation of Support to Research of State of Minas Gerais (FAPEMIG, in the Portuguese acronym - Fundação de Amparo à Pesquisa do Estado de Minas Gerais).

Conflicts of Interest
The authors have no conflicts of interest to declare.

References

1 Armstrong JM, Avant RA, Charchenko CM, et al. Impact of anabolic androgenic steroids on sexual function. Transl Androl Urol 2018;7 (03):483–489. Doi: 10.21037/tau.2018.04.23
2 Yu JG, Bonnerud P, Eriksson A, Stål PS, Tegner Y, Malm C. Effects of long term supplementation of anabolic androgen steroids on human skeletal muscle. PLoS One 2014;9(09):e105330. Doi: 10.1371/journal.pone.0105330
3 Cunha TS, Cunha NS, Moura MJCS, et al. Esteroides anabólicos androgênicos e sua relação com a prática desportiva. Revista Brasileira de Ciências Farmacêuticas 2014;40(02):165–179
4 Molero Y, Bakshi AS, Gripenberg J. Illicit Drug Use Among Gym-Goers: a Cross-sectional Study of Gym-Goers in Sweden. Sports Med Open 2017;3(01):31
5 Akçakoyun M, Alizade E, Gündoğdu R, et al. Long-term anabolic androgenic steroid use is associated with increased atrial electromechanical delay in male bodybuilders. BioMed Res Int 2014; 2014:451520. Doi: 10.1155/2014/451520
6 Lima AP. CARDOSO FB. Alterações fisiológicas e efeitos colaterais decorrentes da utilização de esteroides anabolizantes androgênicos. Revista Brasileira de Ciências da Saúde 2011;9(29):39–46. Doi: 10.13037/rbcs.vol9n29.1252
7 Ferreira UMG, Ferreira ACD, Azevedo AMP, et al. Esteroides Anabólicos Androgênicos. Rev Brasileira em Promoção da Saúde 2007;20(04):267–275
8 Bachman E, Travison TG, Basaria S, et al. Testosterone induces erythrocytosis via increased erythropoietin and suppressed hepcidin: evidence for a new erythropoietin/hemoglobin set point. J Gerontol A Biol Sci Med Sci 2014;69(06):725–735. Doi: 10.1093/gerona/glt154
9 Alves DM, Silva MSO, Zavan B, et al. Morphometric analysis of mice's ventricular myocardium submitted to androgenic anabolizing steroids use. Journal of Morphological Science 2015;32(01): 33–36. Doi: 10.4322/jms.071614
10 Lip GYH, Felmeden DC, Li-Saw-Hee FL, Beevers DG. Hypertensive heart disease. A complex syndrome or a hypertensive 'cardiomyopathy'? Eur Heart J 2000;21(20):1653–1665. Doi: 10.1053/euhj.2000.2339
11 Nucci RAB, Tanasov VS, Krause Neto W, et al. Testosterone Administration Alters Hepatic Blood Flow Across Age: Systematic Review of Animal Experimental Studies. J Morphol Sci 2018;35 (02):96–100. Doi: 10.1055/s-0038-1669470
12 Caliman IF, Bernabe CS, de Melo AF Jr, et al. Long-term treatment with Nandrolone Decanoate impairs mesenteric vascular relaxation in both sedentary and exercised female rats. Steroids 2017; 120:7–18. Doi: 10.1016/j.steroids.2017.02.001
13 Tofighi A, Shirpoor M, Ansari MHK, Shirpoor A, Zerehpoosh M. The effect of nandrolone treatment with and without enforced

swimming on histological and biochemical changes in the heart and coronary artery of male rats. Anatol J Cardiol 2017;17(03): 176–183. Doi: 10.14744/AnatolJCardiol.2016.7333
14 Moreira WF, Scoss DM. Risco do Uso Indiscriminado de Esteróides Androgênicos Anabolizantes na Hipertrofia Muscular. Revista ENAF Science 2016;11(01):371–383
15 Seara FAC, Barbosa RAQ, de Oliveira DF, et al. Administration of anabolic steroid during adolescence induces long-term cardiac hypertrophy and increases susceptibility to ischemia/reperfusion injury in adult Wistar rats. J Steroid Biochem Mol Biol 2017; 171:34–42. Doi: 10.1016/j.jsbmb.2017.01.012
16 Nascimento AM, Lima EM, Brasil GA, et al. Serca2a and Na(+)/Ca (2+) exchanger are involved in left ventricular function following cardiac remodelling of female rats treated with anabolic androgenic steroid. Toxicol Appl Pharmacol 2016;301:22–30. Doi: 10.1016/j.taap.2016.04.001
17 Unver S, Kavlak E, Gümüsel HK, et al. Correlation between hypervolemia, left ventricular hypertrophy and fibroblast growth factor 23 in hemodialysis patients. Ren Fail 2015;37(06): 951–956. Doi: 10.3109/0886022X.2015.1052945
18 Rosano GMC, Spoletini I, Vitale C. Cardiovascular disease in women, is it different to men? The role of sex hormones. Climacteric 2017; 20(02):125–128. Doi: 10.1080/13697137.2017.1291780
19 BARP. J. 2007. Avaliação do dano oxidativo e função cardiovascular em diferentes modelos de hiperhomocisteinemia: papel protetor do folato e do estrogênio. Porto Alegre: Instituto de Ciências Básicas da Saúde; Universidade Federal do Rio Grande do Sul. 134 p. Tese de doutorado em Ciências Biológicas: Fisiologia
20 Clark AS, Blasberg ME, Brandling-Bennett EM. Stanozolol, oxymetholone, and testosterone cypionate effects on the rat estrous cycle. Physiol Behav 1998;63(02):287–295. Doi: 10.1016/s0031-9384(97)00443-5
21 Pirompol P, Teekabut V, Weerachatyanukul W, Bupha-Intr T, Wattanapermpool J. Supra-physiological dose of testosterone induces pathological cardiac hypertrophy. J Endocrinol 2016; 229(01):13–23. Doi: 10.1530/JOE-15-0506
22 Nascimento JH, Medei E. Cardiac effects of anabolic steroids: hypertrophy, ischemia and electrical remodelling as potential triggers of sudden death. Mini Rev Med Chem 2011;11(05): 425–429. Doi: 10.2174/138955711795445899
23 Tagarakis CV, Bloch W, Hartmann G, Hollmann W, Addicks K. Anabolic steroids impair the exercise-induced growth of the cardiac capillary bed. Int J Sports Med 2000;21(06):412–418. Doi: 10.1055/s-2000-3835
24 Arazi H, Mohammadjafari H, Asadi A. Use of anabolic androgenic steroids produces greater oxidative stress responses to resistance exercise in strength-trained men. Toxicol Rep 2017;4(04):282–286. Doi: 10.1016/j.toxrep.2017.05.005
25 Karbasi S, Zaeemi M, Mohri M, Rashidlamir A, Moosavi Z. Effects of testosterone enanthate and resistance training on myocardium in Wistar rats; clinical and anatomical pathology. Andrologia 2018;50(03):1–15. Doi: 10.1111/and.12908
26 dos Santos MR, Dias RG, Laterza MC, et al. Impaired post exercise heart rate recovery in anabolic steroid users. Int J Sports Med 2013;34(10):931–935. Doi: 10.1055/s-0032-1331741

Morphometric Analysis of the Foramen Magnum in Dry Human Skulls in Northeastern Brazil

Jalles Dantas de Lucena[1] João Victor Souza Sanders[2] Hudson Martins de Brito[2] Gilberto Santos Cerqueira[3] Ivson Bezerra da Silva[4] André de Sá Braga Oliveira[4]

[1] Department of Morphofunctional Sciences, Universidade Federal do Ceará, Fortaleza, CE, Brazil
[2] Medical School, Universidade Federal do Ceará, Fortaleza, CE, Brazil
[3] Department of Morphology, Medical School, Universidade Federal do Ceará, Fortaleza, CE, Brazil
[4] Department of Morphology, Health Science Center, Universidade Federal da Paraíba, João Pessoa, PB, Brazil

Address for correspondence Ivson Bezerra da Silva, PhD, Departamento de Morfologia, Universidade Federal da Paraíba – UFPB, Conj. Pres. Castelo Branco III, S/N, João Pessoa, PB 58033-455, Brasil (e-mail: ivsonbsilva@ccs.ufpb.br).

J Morphol Sci 2019;36:97–104.

Abstract

Introduction The successful identification of the deceased is vital to the progress of any forensic investigation. This process of identification is facilitated by the determination of age, gender, and ethnicity. One of the main biological traits to be established from skeletal remains is the gender of the individual. In situations in which there are fragmented and mutilated skeletal remains, gender determination is relatively difficult, and it becomes important to establish the accuracy of individual bones. The basal region of the occipital bone is covered by a large volume of soft tissue and is therefore in a relatively well-protected anatomical position and, as such, classification of gender using the occipital bone may prove to be useful in cases of significantly disrupted remains. The present study aims to describe and analyze the morphological aspects of the foramen magnum (FM) in the population of the northeastern region of Brazil.

Material and Methods A total of 159 dry skulls (88 males and 71 females) were subjected to measurement by a digital caliper (DIGIMESS®, Instrumentos de Precisão Ltda., São Paulo, Brazil) and was assessed for anteroposterior diameter (APD) and transverse diameter (TD), FM area, FM index (FMI), anterior, posterior and maximum lateral intercondylar distance. The measurement of all of these parameters sought to classify the FM in nine different types.

Results The pentagonal type was the most found in males (11.31%), and the biconvex in females (18.86%). The less frequent type in males was the pear type (2.53%), and in females the less frequent types were the pentagonal and the heptagonal types (2.53% each). Using the traditional anthropological classification of Martin et al,[13] the most common type of FM was the brachytrematous, with 49.68% of the total skulls. The APD, TD and FM area were higher in males than in females, only in the oval FM type.

Conclusion The sexual dimorphism of the dimensions of the FM is established. However, there is a wide variability in the shape and measures in different populations, and to our knowledge this is the first study that shows the different types of the FM in the population of the northeastern region of Brazil.

Keywords
- anatomy and anthropology
- brazil
- foramen magnum
- occipital bone
- skull

received
September 24, 2018
accepted
March 28, 2019

DOI https://doi.org/10.1055/s-0039-1688694.
ISSN 2177-0298.

Copyright © 2019 by Thieme Revinter Publicações Ltda, Rio de Janeiro, Brazil

License terms

Introduction

The foramen magnum (FM) is a large opening located at the base of the skull, belonging to the occipital bone. Its borders are very variable in shape and are formed by the anatomical regions of the occipital bone. The anterior border of the FM consists of the basilar process, the lateral border is formed by the right and left occipital condyles, and the posterior border is composed by the supraoccipital portion.[1]

Numerous noble and hard-to-access structures enter the skull through this foramen, the main ones being the medulla bulb, the spinal cord, the meninges, the vertebral arteries, and some spinal nerve roots.[2] In addition, other structures essential for the support and for the movement of the skull in relation to the spine are associated with the limits of the FM, such as the complex that forms the atlanto-occipital joint and the membranes associated with it.[3]

The correlation between the morphological patterns of the FM and the gender of the corpse to which the skull belongs is relevant to the forensic practice. This approach is a relatively simple and economically accessible alternative for the sexual recognition of bodies in an advanced state of degradation, in which this identification cannot be made from superficial characteristics, as is the case of carbonized victims.[4,5]

The understanding of the anatomy of the FM and its variations allows for a broader view in the radiological study of pathologies associated with it, as well as a better planning and technical refinement of the neurosurgical approaches to this region,[6] such as, for example, the herniations of structures of the central nervous system (CNS) through the foramen in Arnold-Chiari Syndrome, foramen stenoses in achondroplastic patients, specific meningiomas related to this structure, bulbar tumors, and cases of platybasia with invagination of the odontoid process through the FM.[7,8]

The present article aims to describe and analyze the morphological aspects of the FM in the population of the northeastern region of Brazil. This knowledge can serve as a basis for therapeutic behavior in several serious neurological conditions, related or not to sexual dimorphism, as well as to forensic medicine.

Material and Methods

The present study corresponds to quantitative and qualitative research. The morphometric analysis of the FM was conducted in the Department of Morphology of the Universidade Federal da Paraíba, João Pessoa, state of Paraíba, Brazil, in the Department of Morphology of the Universidade Federal do Ceará, Fortaleza, state of Ceará, Brazil, and in the Laboratory of Anatomy of the Faculdades Integradas de Patos, Patos, state of Paraíba, Brazil. All of the universities are located in the northeastern region of Brazil. The present study involved 88 male skulls and 71 female skulls, with the gender confirmation done previously from the records of the departments. All of the skulls belonged to adults $\geq$ 18 years old.

Only skulls in a good state of conservation, allowing the identification of the gender, derived from the northeastern region of Brazil, were used in the present study. Skulls of children, damaged skulls, skulls with pathological conditions, incomplete skulls, and skulls without gender identification were excluded from the study.

The skulls were classified according to their gender, based on the following Vanrell criteria:[9] 1–massivity; 2–supraorbital margin shape; 3–size of the occipital condyles; 4–degree of inclination of the forehead; 5–size of the mastoid process size; and 6–degree of prominence of anatomical accidents.

The FM had its form classified according to the criteria of Aragão et al:[10] 1– pear; 2–oval; 3–rounded; 4–tetragonal; 5–pentagonal; 6–hexagonal; 7–heptagonal; 8–biconvex; or 9–irregular. Then, with a digital caliper (DIGIMESS®, Instrumentos de Precisão Ltda., São Paulo, Brazil) of 0.01 mm accuracy, the following FM morphometric parameters were measured (►**Fig. 1**):

- The criterion for the measurement of the anteroposterior diameter (APD) of the FM was the distance between the basion (the midpoint of the anterior margin of the FM) and the opisthion (the midpoint of the posterior margin of the FM). The criterion for measuring the transverse diameter (TD) was the distance between the lateral margins of the FM, at the point of the greatest lateral curvature (►**Fig. 1**). The area of the FM was calculated using the equations by Teixeira:[11]: Area $= \pi \times [(APD \times TD)/4]^2$; and by Routal et al[12]: Area $= ¼ \times \pi \times APD \times TD$.
- The anterior intercondylar distance (AID), which is the minimum distance between the medial margins of the occipital condyles, the posterior intercondylar distance (PID), which is the maximum distance between the medial margins of the occipital condyles, and the maximum lateral intercondylar distance (MLID), which is the maximum distance between the lateral margins of the occipital condyles, were measured.
- Using an original anthropological formula by Martin et al,[13] the FM index (FMI) was calculated as follows: FMI $=$ TD/APD [absolute value] or $= 100 \times$ [foramen magnum breadth (FmB)/foramen magnum length (FmL)] [relative value; %]).
- Based on the APD and on the DT of the FM, its shape was divided into oval or rounded. The rounded shape was defined as a TD/APD quotient between 0.9 and 1.1 (90–110%). Skulls with a value below or above this range were included within the oval-longitudinal or oval-horizontal types, respectively.
- Based on the FMI,[13] the FM was classified into 1 of 3 three groups: dolichocephalous (oval, index $<$ 81.9), mesocephalous (flat oval, index $=$ 81.9–85.9), and brachycephalous (rounded index $>$ 86.0).

Data were presented as: mean, maximum and minimum values, standard deviation (SD) and standard error of mean (SEM). The distribution of these data was evaluated by the Kolmogorov-Smirnov test. Differences between males and females were analyzed using the Student-t test. A level of significance of $p < 0.05$ was used as a criterion of significance. The IBM SPSS Statistics for Windows, Version 20.0 (IBM Corp., Armonk, NY, USA) was used for the statistical analyzes.

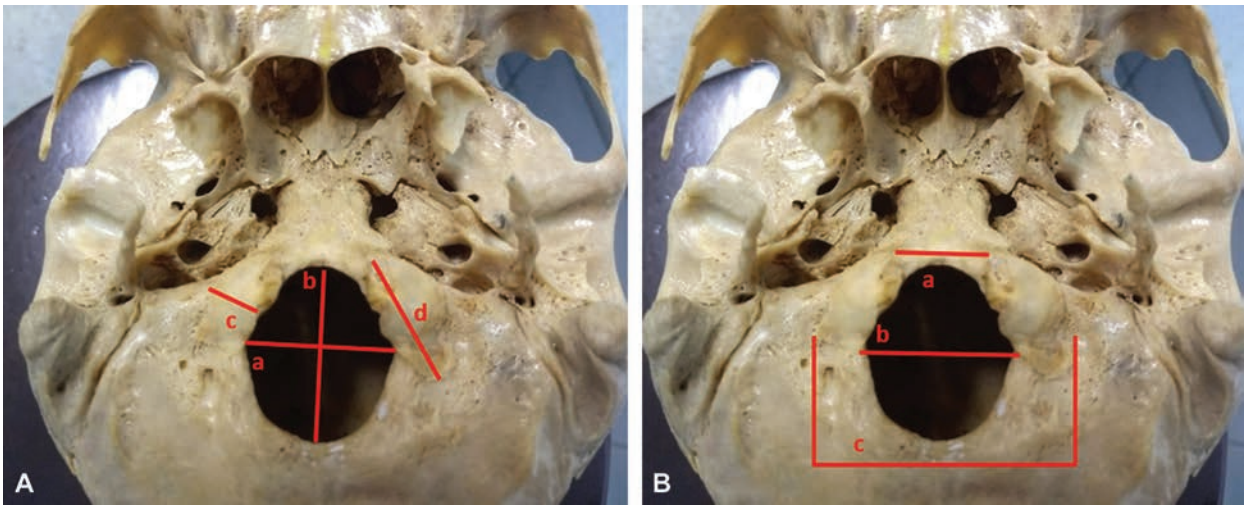

Fig. 1 An adult human skull base view. Occipital measurements. (**A**) a. Anteroposterior distance of the foramen magnum (APD), b. Transversal diameter of the foramen magnum (TD). (**B**) Adult human skull base view. Occipital measurements. a. Anterior intercondylar distance (AID), b. Posterior intercondylar distance (PID), c. Maximum lateral intercondylar distance (MLID).

Results

All of the 9 FM types that were identified by Aragão et al[10] were seen in the present study, in the evaluated population (►**Table 1**). In males, the FM types were separated by tetragonal, pentagonal and hexagonal, with 15, 18 and 16 cases, respectively. In females, the biconvex FM was the most common, with 19 cases. The pear type was the least frequent type in males, with 4 cases; in females, the pentagonal and heptagonal types were the least frequent, both with 4 cases (►**Table 1**).

The morphometric parameters of the FM recorded in dry skulls are represented in ►**Table 2**. Differences between male and female FMs were calculated, and it was found that the dimensions were significantly higher in males compared with females ($p < 0.05$), except for the FMI and for the PID.

Table 1 Frequencies of the different morphological types of the foramen magnum according the classification by Aragão et al,[10] in relation to gender among the examined skulls

Shapes of the foramen magnum	Gender					
	Male		Female		Total	
	n	%	*n*	%	*n*	%
Pear	4	2.53	9	5.67	13	8.2
Oval	5	3.13	9	5.67	14	8.8
Rounded	9	5.67	6	3.76	15	9.43
Tetragonal	15	9.44	5	3.13	20	12.57
Pentagonal	18	11.31	4	2.53	22	13.84
Hexagonal	16	10.06	9	5.67	25	15.73
Heptagonal	5	3.13	4	2.53	9	5.66
Biconvex	11	6.95	19	11.93	30	18.86
Irregular	5	3.13	6	3.76	11	6.91
Total	**88**	**55.35**	**71**	**44.65**	**159**	**100.0**

Using the traditional anthropological classification of Martin et al,[13] the most common type of FM was brachytrematous, which was observed in 79 cases in males and females. Less frequently, mesothematous (18 male and 12 female) and dolichotrematous (26 male and 24 female) types were also seen (►**Table 3**).

When the oval-type FM was analyzed, it was observed that the APD, the TD, and the FM area were higher in males than in females. However, there was no difference between these parameters in the genres studied when the FM of the rounded type was analyzed (►**Table 4**).

When the APD and the TD were compared between the oval and rounded forms of the FM, higher values of APD were observed in both genders in the oval form and higher values of TD were observed in both genders in the rounded form. There were no differences between the oval and rounded forms with respect to the FM area in both genders (►**Table 4**).

Discussion

The differences in shape of the FM seem to be related to gender and ethnicity.[14] Various studies suggest different shapes of the FM; however, the most common shapes are the oval, hexagonal, and round shapes.[15,16] Based on the results of the present study, the most common forms of the FM are the tetragonal, the pentagonal and the hexagonal shapes in males, and the biconvex in females.

The FM is a morphologically variable osteological feature in the skull that has undergone evolutionary changes.[16–18] The shape and morphological variations of the FM are important in neurological interpretation. In an ovoid type of the FM, for example, the surgeon may find it difficult to explore the anterior portion of the FM.[19]

The shape of the FM can also be determined by using the FMI. Muthukumar et al have considered the FM to be oval when the FMI was > 1.2, and they considered the rest (FMI < 1.2) as round.[20] A similar sized lesion located anterior to the

Table 2 Gender difference for the foramen magnum and other craniometric measurements in males and females

Variables	Male ($n = 88$)				Female ($n = 71$)				*p-value* (t *test)*
	Range	Mean	SD	SEM	Range	Mean	SD	SEM	
Foramen magnum anteroposterior diameter (mm)	29.16–43.81	35.01	3.03	0.32	22.08–41.17	33.92	3.19	0.37	0.028
Foramen magnum transverse diameter (mm)	22.63–37.84	30.12	2.95	0.31	20.37–36.32	28.91	2.83	0.33	0.010
Foramen magnum area of Teixeira (mm^2)	576.93–1174.47	839.83	131.75	13.44	429.46–1154.21	773.13	127.94	14.21	0.001
Foramen magnum area of Routal (mm^2)	570.01–1169.24	833.46	131.34	13.40	370.73–1150.26	765.47	130.52	14.50	0.001
Foramen magnum index (mm)	67.92–123.98	86.74	8.61	0.87	46.00–132.60	85.36	10.82	1.20	0.348
Anterior intercondylar distance (mm)	13.08–27.16	18.81	2.67	0.33	9.32–28.93	17.00	3.71	0.50	0.0028
Posterior intercondylar distance (mm)	26.97–39.38	32.36	3.08	0.40	25.54–45.99	32.86	5.75	0.78	0.564
Maximum lateral intercondylar distance (mm)	42.05–58.19	48.73	3.52	0.45	38.36–57.38	45.67	3.85	0.51	0.0001

Abbreviations: SD, Standard deviation; SEM, Standard error of mean.

Table 3 Frequency of the dolichotrematous, mesotrematous and brachytrematous foramen magnume in male and female skulls

FM type (Fm index)*	Male ($n = 88$)			Female ($n = 71$)		
	n	Mean	SD	*n*	Mean	SD
Dolichotrematous (< 81.9)	26	76.81	4.03	24	74.72	8.36
Mesotrematous (81.9–85.9)	18	84.30	1.15	12	83.62	1.37
Brachytrematous (> 86.0)	44	92.75	6.07	35	92.83	8.35

Abbreviation: FM, foramen magnum.
*FM index (%) according to the Martin et al[13] formula = (FmTD / FmAPD) × 100. *Standard deviation (SD).

Table 4 Diameters of the foramen magnus (mean ± standard deviation) in male and female skulls with longitudinal oval- and round-like types of the foramen magnus

Variables	Oval-like			Round-like		
	Male	Female	*p-value*	Male	Female	p
Anteroposterior diameter (mm)	36.02 ± 2.97*	34.63 ± 2.56	0.010	33.09 ± 2.22#	32.14 ± 2.54#	0.0001; 0.001
Transverse diameter (mm)	29.41 ± 2.86*	27.98 ± 3.34	0.018	31.00 ± 2.07#	30.50 ± 2.29#	0.011; 0.003
Foramen magnum area of Routal (mm^2)	836.67 ± 140.85*	764.34 ± 132.38	0.007	791.82 ± 91.84	773.56 ± 116.54	
Foramen magnum area of Teixeira (mm^2)	846.08 ± 141.01*	774.63 ± 128.13	0.007	792.79 ± 91.96	774.42 ± 116.61	

*male versus female; #oval-like versus round-like.

Table 5 Comparison of the anteroposterior diameter, of the transverse diameter (mm), and of the area (mm^2) of the foramen magnus in different populations

Author and year	Origin	Gener	Sample size	Anteroposterior diameter (mm)	Transverse diameter (mm)	Area of the foramen magnus (mm^2)
	South America					
Present study	Brazil	Male	88	35.01 ± 3.03	30.12 ± 2.95	839.83 ± 131.75[a] 833.46 ± 131.34[b]
		Female	71	33.92 ± 3.19	28.91 ± 2.83	773.13 ± 127.94[a] 765.47 ± 130.52[b]
Pires et al, 2016[36]	Brazil	Male/ Female	77	34.23 ± 2.54	28.62 ± 2.83	772.4 ± 116.7[c]
Damiani et al, 2012[37]	Brazil	Male/ Female	17/23	34.78 ± 2.19	28.69 ± 2.73	907,25 ± 192
Manoel et al, 2009[28]	Brazil	Male	139	35.7 ± 0.29	30.3 ± 0.20	n/a
		Female	76	35.1 ± 0.33	29.4 ± 0.23	n/a
Suazo et al, 2009[38]	Brazil	Male	144	36.5 ± 2.6	30.6 ± 2.5	n/a
		Female	71	35.6 ± 2.5	29.5 ± 1.9	n/a
Teixeira, 1982[11]	Brazil	Male	20	n/a	n/a	963.73 ± 140[a]
		Female	20	n/a	n/a	805.65 ± 105[a]
Espinoza et al, 2011[39]	Chile	Male	50	37.4 ± 3.3	31.9 ± 2.6	877 ± 125
		Female	50	35.6 ± 3.0	30.1 ± 2.4	798 ± 115
Isaza et al, 2014[40]	Columbia	Male	121	22.66 ± 2.17	30.27 ± 2.02	n/a
		Female	128	20.97 ± 1.86	27.75 ± 2.29	n/a
	North America					
Wanebo et al 2001[41]	USA	Male/ Female	32	36 ± 3	31 ± 2	608.4 ± 121
Milhorat et al, 2010[42]	USA	Male/ Female	25/55	32.5 ± 3.17	30.8 ± 5.74	787.70 ± 118.4
	Europe					
Catalina-Herrera, 1987[43]	Spain	Male	74	36.2 ± 0.3	31.1 ± 0.3	888.4 ± 13.9[e]
		Female	26	34.3 ± 0.4	29.6 ± 0.3	801 ± 17.4[e]
Macaluso, 2011[44]	France	Male	36	35.38 ± 2.27	30.72 ± 2.11	860.27 ± 94.54[a] 854.80 ± 93.79[b]
		Female	32	34.90 ± 2.26	29.40 ± 2.63	815.13 ± 106.29[a] 807.86 ± 107.58[b]
Gapert et al, 2009[5]	UK	Male	82	35.91 ± 2.41	30.51 ± 1.77	868.95 ± 96.36[a] 862.41 ± 94.79[b]
		Female	76	34.71 ± 1.91	29.36 ± 1.96	808.14 ± 85.40[a] 801.78 ± 85.43[b]
Gapert et al, 2013[35]	UK	Male	69	35.79 ± 2.36	30.48 ± 1.86	n/a
		Female	66	34.78 ± 1.97	29.35 ± 2.06	n/a
Gruber et al, 2009[45]	Central European	Male	28	37.1 ± 2.7	32.4 ± 2.4	n/a
		Female	21	35.8 ± 3.5	31.0 ± 2.8	n/a
Burdan et al, 2012[24]	Eastern European	Male	142	37.06 ± 3.07	32.98 ± 2.78	877.40 ± 131.64
		Female	171	35.47 ± 2.60	30.95 ± 2.71	781.57 ± 93.74
	Asia					
Murshed et al, 2003[16]	Turkey	Male	57	37.2 ± 3.43	31.6 ± 2.99	931.7 ± 144.29
		Female	53	34.6 ± 3.16	29.3 ± 2.19	795.0 ± 99.32

(*Continued*)

Table 5 (*Continued*)

Author and year	Origin	Gener	Sample size	Anteroposterior diameter (mm)	Transverse diameter (mm)	Area of the foramen magnus (mm^2)
Aghakhani et al, 2016[34]	Iran	Male	50	37.71 ± 1.00	31.68 ± 1.26	946.66 ± 61.94[a] 939.47 ± 62.48[b]
		Female	50	34.37 ± 1.46	28.34 ± 1.43	773.96 ± 70.39[a] 766.81 ± 70.30[b]
Routal et al, 1984[12]	India	Male	104	35.5 ± 2.8	32.0 ± 2.8	819.0 ± 94[b]
		Female	37	29.6 ± 1.9	27.1 ± 1.6	771.0 ± 90[b]
Jain et al, 2014[29]	India	Male	70	36.2 ± 3.0	31.3 ± 2.4	909 ± 129[a] 895 ± 126[b]
		Female	70	34.0 ± 2.7	28.3 ± 2.0	775 ± 107[a] 759 ± 102[b]
Vinutha et al, 2016[21]	India	Male	100	33.37 ± 2.33	27.4 ± 2.44	727.5 ± 83.12[a] 718.41 ± 83.75[b]
		Female	100	29.72 ± 1.89	24.73 ± 2.05	583.71 ± 63.58[a] 577.52 ± 64.36[b]
Madadin et al, 2017[46]	Saudi Arabia	Male	100	37.21 ± 2.15	31.65 ± 2.25	925.84 ± 98.20
		Female	100	36.10 ± 2.65	30.60 ± 2.47	869.80 ± 122.75
	Africa					
Ukoha et al, 2011[47]	Nigeria	Male	90	36.26 ± 2.39	30.09 ± 2.58	857.30[d]
		Female	10	34.39 ± 3.88	28.16 ± 1.99	760.94[d]
Osunwoke et al, 2012[48]	Nigeria	Male/ Female	120	36.11 ± 2.60	29.56 ± 2.60	n/a

[a]Area = $\pi \times [(APD + TD) / 4]^2$ (Teixeira formula).[11]
[b]Area = $¼ \times \pi \times APD \times TD$ (Routal formula).[12]
[c]Area = $¼ \times \pi \times TD \times APD$ (Radinsky formula).[49]
[d]Area = $\pi \times r^2$, $C = 2 \times \pi \times r$ (Gapert formula).[5]
[e]Mean ± standard error of mean instead of standard deviation. n/a - unknown data.

brainstem will require more extensive bone removal in a person with an ovoid FM than in a person with a round FM. In 20% of the skulls, the occipital condyle protruded significantly into the FM. As a result, a patient with a round FM, without significant protrusion of the occipital condyles into the FM, will require less bony resection than a patient with an ovoid FM with medially protuberant and sagittaly inclined occipital condyles, even though both patients present similar lesions.[21]

In our study, the FMI suggested by Martin et al was considered.[13] The round-like form is characterized by the index between 0.9 and 1.1 (90–110%), while structures with a value below or above this index are called longitudinal and horizontal oval-like, respectively. Based on the index value, it is also possible to classify the FM into one of the three groups: dolichotrematous (oval; index < 81.9), mesotrematous (flattened oval; index $= 81.9–85.9$) and brachytrematous (round, index > 86.0). In our study, a high predilection of brachytrematous in male and female FMs was found (79 cases). In adult native South Africans, the most common type of FM was dolichotrematous, with a low frequency of meso- and brachytrematous.[22] However, a much higher value of the index (71.0–111.0%) was present in other populations.[5,13,23–26]

The parameters associated with the FM, such as the APD of the FM, the TD of the FM, the AID, the MLID, and the FM area had a high sensitivity and specificity for the determination of gender; however, the FMI and the PID had less specificity.

In our study, the APD was 35.01 mm in males and 33.92 mm in females. The index shows some varieties in different studies. The APD values vary from 29.16 mm to 43.81 mm in men and from 22.08 mm to 41.17 mm in women. According to some reports, the APD is larger in men than in women.[5,15,16,24,27–33]

The TD was 28.91 mm in women and 30.12 mm in men. In other studies, the mean TD was reported differently, from 29.5 mm to 31.6 mm in men and from 27.1 to 29.4 in women; the reported diameters are larger in men than in women.[5,15,16,18,24,27–33]

The FM area has been calculated between 862.41 and 931.7 mm^2 in men and between 765.29 and 819.01 mm^2 in women.[4,5,16,30–33] In our study, various diameters were relatively smaller than those found in other studies, and it is likely that the FM in the Iranian community would be larger than in other ethnic groups.[34] It seems that different ethnic groups have differences in the dimensions of the FM. Hence, it is not possible to set a specific cutoff point for all human beings. Another reason for these differences could be due to the method of measurement (via computed tomography [CT]

scan or direct measurement of the skull). After puberty, age does not affect the size of the FM. Therefore, differences in the results of various studies could not be due to the age of the samples and there is no need to consider age while determining gender based on the dimensions of the FM.[35]

The degree of expression of sexual dimorphism within the FM dimensions may be explained by its development. Compared with many other skeletal elements, the FM reaches its adult size rather early in childhood and is unlikely to respond to significant secondary sexual changes. No muscles act upon the shape and size of the FM, its prime function is to accommodate the passage of structures into and out of the region of the cranial base, particularly the medulla oblongata, which occupies the greatest proportion of the space of the foramina. As the nervous system is the most precocious of all of the body systems, it reaches maturity at a very young age and, therefore, has no requirement to increase in size. This is evidenced by the completion of fusion of the different elements of the occipital bone by between 5 and 7 years of age.[5,21]

Conclusion

Gender determination in missing or damaged skeletal remains is a major problem in forensic medicine. To this end, numerous anatomic parameters, such as shape and dimensions of the FM, should be taken into consideration to solve this problem. Since the FM has a regular structure and is located in an area that is less prone to injury, it can be used as a helpful tool for gender determination. Nevertheless, to utilize these indicators, it is required to have local data of each country and their specific regions, as there are countries, Brazil being one example, that have an extensive population. By combining qualitative data with quantitative ones, performing these studies is of great value for forensic medicine as well as for neurosurgeons.

Funding

The present research did not receive any specific grant from funding agencies in the public, commercial, or nonprofit sectors.

Conflict of Interest

The authors declare that there are no competing or financial interests associated with the present manuscript.

Acknowledgments

The authors are grateful to Mr. Benjamin D. Adam for providing help with the language.

References

1 Scheuer L, Black S. The juvenile skeleton. New York: Elsevier Academic Press; 2004
2 Moore KL, Dalley AF, Agur AMR. Anatomia Orientada para a Clínica. 7th ed. Rio de Janeiro: Guanabara Koogan; 2014
3 Bruneau M, George B. Foramen magnum meningiomas: detailed surgical approaches and technical aspects at Lariboisière Hospital and review of the literature. Neurosurg Rev 2008;31(01):19–32, discussion 32–33
4 Günay Y, Altinkök M. The value of the size of foramen magnum in sex determination. J Clin Forensic Med 2000;7(03):147–149
5 Gapert R, Black S, Last J. Sex determination from the foramen magnum: discriminant function analysis in an eighteenth and nineteenth century British sample. Int J Legal Med 2009;123(01): 25–33
6 Kanodia G, Parihar V, Yadav YR, Bhatele PR, Sharma D. Morphometric analysis of posterior fossa and foramen magnum. J Neurosci Rural Pract 2012;3(03):261–266
7 Goel A. Can foramen magnum decompression surgery become historical? J Craniovertebr Junction Spine 2015;6(02):49–50
8 Ozcetin M, Arslan MT, Karapinar B. An achondroplasic case with foramen magnum stenosis, hydrocephaly, cortical atrophy, respiratory failure and sympathetic dysfunction. Iran J Pediatr 2012;22(01):121–124
9 Vanrell JP. Odontologia legal e antropologia forense. Rio de Janeiro: Guanabara Koogan; 2002
10 Aragão JA, Pereira RO, Moraes RZC, Reis FP. Morphological Types of Foramen Magnum. Annu Res Rev Biol 2014;4:1372–1378
11 Teixeira WR. Sex identification utilizing the size of the foramen magnum. Am J Forensic Med Pathol 1982;3(03):203–206
12 Routal RR, Pal GP, Bhagawat SS, Tamankar BP. Metrical studies with sexual dimorphism in foramen magnum of human crania. J Anat Soc India 1984;2:85–89
13 Martin R, Saller K. Lehrbuch der Anthropologie. Stuttgart: Gustav Fischer Verlag; 1959
14 Burdan F, Dworzanska A, Dworzanski W, et al. Foramen Magnum - New and Old Anthropological Data. G J Anthropol Res 2014; 1:25–34
15 Chethan P, Prakash KG, Murlimanju BV, et al. Morphological analysis and morphometry of the foramen magnum: an anatomical investigation. Turk Neurosurg 2012;22(04):416–419
16 Murshed KA, Çiçekcibaşi AE, Tuncer I. Morphometric evaluation of the foramen magnum and variations in its shape: a study on computerized tomographic images of normal adults. Turk J Med Sci 2003;33:301–306
17 Nevell L, Wood B. Cranial base evolution within the hominin clade. J Anat 2008;212(04):455–468
18 Tubbs RS, Griessenauer CJ, Loukas M, Shoja MM, Cohen-Gadol AA. Morphometric analysis of the foramen magnum: an anatomic study. Neurosurgery 2010;66(02):385–388, discussion 388
19 Sandeep A, Sharma SK, Siddiqui SW, Khatri S. Morphometry and surgical importance of foramen magnum. Int J Anat Res 2017; 5:3464–3469
20 Muthukumar N, Swaminathan R, Venkatesh G, Bhanumathy SP. A morphometric analysis of the foramen magnum region as it relates to the transcondylar approach. Acta Neurochir (Wien) 2005;147(08):889–895
21 Vinutha SP, Shubha R. Morphometry and sexual dimorphism in foramen magnum: a study of human skull bones. Int J Anat Res 2016;4:2593–2599
22 De Villiers H. The Skull of the South African Negro: A Biometrical and Morphological Study. 1st ed. Johannesburg: Witwatersrand University Press; 1968
23 Richards GD, Jabbour RS. Foramen magnum ontogeny in Homo sapiens: a functional matrix perspective. Anat Rec (Hoboken) 2011;294(02):199–216
24 Burdan F, Szumiło J, Walocha J, et al. Morphology of the foramen magnum in young Eastern European adults. Folia Morphol (Warsz) 2012;71(04):205–216
25 Calvy TM, Segall HD, Gilles FH, et al. CT anatomy of the craniovertebral junction in infants and children. AJNR Am J Neuroradiol 1987;8(03):489–494
26 Coqueugniot H. Le crane d'Homo sapiens em Eurasie: Croissance et variation depuis 100 000 ans. In: British Archaelogical Reports International Series, London: British Archaelogical Reports: 1999
27 Shanthi CH, Lokanadham S. Morphometric Study on Foramen Magnum of Human Skulls. Med Sci 2013;2:792–798

28 Manoel C, Prado FB, Caria PHF, Groppo FC. Morphometric analysis of the foramen magnum in human skulls of brazilian individuals: its relation to gender. Braz J Morphol Sci 2009;26:104–108
29 Jain D, Jasuja OP, Nath S. Evaluation of foramen magnum in sex determination from human crania by using discriminant function analysis. El Med J 2014;2:89–92
30 Uysal S, Gokharman D, Kacar M, Tuncbilek I, Kosa U. Estimation of sex by 3D CT measurements of the foramen magnum. J Forensic Sci 2005;50(06):1310–1314
31 Sendemir E, Savci G, Cimen A. Evaluation of the foramen magnum dimensions. Kaibogaku Zasshi 1994;69(01):50–52
32 Burdan F, Umławska W, Dworzański W, et al. Anatomical variances and dimensions of the superior orbital fissure and foramen ovale in adults. Folia Morphol (Warsz) 2011;70(04):263–271
33 Raghavendra Babu YP, Kanchan T, Attiku Y, Dixit PN, Kotian MS. Sex estimation from foramen magnum dimensions in an Indian population. J Forensic Leg Med 2012;19(03):162–167
34 Aghakhani K, Kazemzadeh N, Ghafurian F, Soltani B, Soltani S. Gender determination using diagnostic values of foramen magnum. Int J Med Toxicol Forensic Med 2016;6:29–35
35 Gapert R, Black S, Last J. Test of age-related variation in the craniometry of the adult human foramen magnum region: implications for sex determination methods. Forensic Sci Med Pathol 2013;9(04):478–488
36 Pires LAS, Teixeira AR, Leite TFO, Babinski MA, Chagas CAA. Morphometric aspects of the foramen magnum and the orbit in Brazilian dry skulls. Int J Med Res Health Sci 2016;5:34–42
37 Damiani D, Borelli NS, Melo HJF, Lima RS, Nobeschi L. Morphometry and spatial correlation of the foramen magnum and spinal cord through the magnetic resonance in normal young adults – anatomical and clinical aspects. J Morphol Sci 2012;29:87–90
38 Suazo GIC, Russo PP, Zavando MDA, Smith RL. Sexual dimorphism in the foramen magnum dimensions. Int J Morphol 2009;27:21–23
39 Espinoza EG, Ayala CP, Ortega LB, Collipal LE, Silva HM. Tomographic morphometry of the foramen magnum and its relation to sex and Mapuche ethnicity. Rev Anacem 2011;5:28–31
40 Isaza J, Díaz CA, Bedoya JF, Monsalve T, Botella MC. Assessment of sex from endocranial cavity using volume-rendered CT scans in a sample from Medellín, Colombia. Forensic Sci Int 2014;234:186.e1–186.e10
41 Wanebo JE, Chicoine MR. Quantitative analysis of the transcondylar approach to the foramen magnum. Neurosurgery 2001;49 (04):934–941, discussion 941–943
42 Milhorat TH, Nishikawa M, Kula RW, Dlugacz YD. Mechanisms of cerebellar tonsil herniation in patients with Chiari malformations as guide to clinical management. Acta Neurochir (Wien) 2010;152 (07):1117–1127
43 Catalina-Herrera CJ. Study of the anatomic metric values of the foramen magnum and its relation to sex. Acta Anat (Basel) 1987; 130(04):344–347
44 Macaluso PJ Jr. Metric sex determination from the basal region of the occipital bone in a documented French sample. Bull Mem Soc Anthropol Paris 2011;23:19–26
45 Gruber P, Henneberg M, Böni T, Rühli FJ. Variability of human foramen magnum size. Anat Rec (Hoboken) 2009;292(11):1713–1719
46 Madadin M, Menezes RG, Al Saif HS, et al. Morphometric evaluation of the foramen magnum for sex determination: A study from Saudi Arabia. J Forensic Leg Med 2017;46:66–71
47 Ukoha U, Egwu OA, Okafor IJ, Anyabolu AE, Ndukwe GU, Okpala I. Sexual dimorphism in the foramen magnum of Nigerian adult. Int J Biol Med Res 2011;2:878–881
48 Osunwoke EA, Oladipo GS, Gwunireama IU, Ngaokere JO. Morphometric analysis of the foramen magnum and jugular foramen in adult skulls in southern Nigerian population. Am J Sci Ind Res 2012;3:446–448
49 Radinsky L. Relative brain size: a new measure. Science 1967;155 (3764):836–838

Three-dimensional Cat Virtual Anatomy: Development of an Interactive Virtual Anatomical Software

Juan Sebastián Osorio-Echeverri[1] Diana Alexandra Orrego-Metaute[2] Juan Pablo Murillo-Escobar[2] Lynda Tamayo-Arango[1]

[1] CIBAV Research Group, Faculty of Agrarian Sciences, University of Antioquia, Medellín, Colombia
[2] Biomedical Research and Innovation Group, Faculty of Exact and Applied Sciences, Metropolitan Technological Institute, Medellín, Colombia

Address for correspondence Lynda Tamayo-Arango, VM, PhD, CIBAV Research Group, Faculty of Agrarian Sciences, University of Antioquia, 65-87, Medellín, Colombia (e-mail: lynda.tamayo@udea.edu.co).

J Morphol Sci 2019;36:105–114.

Abstract

Background Three-dimensional (3D) virtual models are novel tools to teach veterinary anatomy.

Objective The aim of the present study was to create a 3D cat image software and a library of cross-sectional images.

Methods Modeling of the 3D cat organs and structures was done with Autodesk Maya, version 2017 (Autodesk Inc., San Rafael, California, USA) and ZBrush, version 4R7 (Pixologic, Los Angeles, CA, USA) software. In order to obtain the images for the library, three cadavers of adult cats were used, with the following techniques: 1) scanning by magnetic resonance imaging (MRI) at 3-mm intervals, 2) scanning by computed tomography (CT) at 2-mm intervals, and 3) photographing of 178 transverse cuts at 2.5-mm intervals from the frozen cadavers. Out of all the images, thirty images of each technique were selected. An interactive software was developed with the modeled 3D cat and the selected images using Unity, version 5.4 (Unity Technologies, San Francisco, CA, USA).

Results A virtual 3D cat model was obtained with 418 labeled structures of the skeletal, muscular, circulatory, nervous, respiratory, digestive, urinary, and integumentary systems. The virtual interface enables the manipulation of the 3D cat in all views and the visualization of the selected images in a chosen localization along the body of the cat. The library of images allows comparison among CT, MRI and photographs of transverse cuts.

Conclusions The software interface facilitates the access to the content for the user. Sectional images of the cat and of its body structures can be easily understood. This new 3D software of cat anatomy is another tool that can be used in teaching veterinary anatomy.

Keywords
- three-dimensional anatomy
- education in anatomy
- multimedia anatomy resources

Introduction

Virtual models are interesting tools that show anatomy in a hyper-realistic way through three-dimensional (3D) virtual objects representing anatomical structures.[1–5] Compared with static images or videos, 3D virtual objects allow the creation of realistic and interactive virtual spaces.[3–5]

These models allow taking out parts or systems of the body, such as the skeleton, organs, or vascular structures, virtually mimicking a body dissection. The user can visualize and manipulate the structures according to their interest, even beyond what reality allows.[5–8] In addition, a large number of structures and organs can be shown in a simplified, clear, and illustrative way, due to interfaces that facilitate their display and manipulation according to the particular interest of the user.[4–7] In this respect, the use of virtual models is a new tool that facilitates the understanding of the localization of anatomical structures.[8–10]

received
August 2, 2018
accepted
February 11, 2019

DOI https://doi.org/10.1055/s-0039-1683964.
ISSN 2177-0298.

Copyright © 2019 by Thieme Revinter Publicações Ltda, Rio de Janeiro, Brazil

License terms

It is important to highlight the quality and realism of 3D models compared with traditional anatomical drawings, and the possibility of viewing from several angles for easier interpretation and understanding.[4,5,8,11] Additionally, these models allow the simulation or the visualization of physiological and dynamic processes.[11–13] For example, recreating natural processes such as the heartbeat or the movement of the body or of a limb in a virtual way allows analyzing them in more detail.[13,14]

The increasing use of advanced imaging diagnostic techniques such as computed tomography (CT) and magnetic resonance imaging (MRI) in veterinary medicine, especially in small animal practice, requires a deep knowledge of anatomy.[6,8,15] Interactive virtual models based on cross-sections, MRI, and CT images facilitate the understanding of the anatomy and, consequently, a better interpretation of the image for future diagnosis purposes.[10,15]

The complexity of 3D models requires the development of navigation systems that provide fast and dynamic exploration of scenes.[1,4,5,13] User interface approaches facilitate a precise composition of the scene and its exploration according to the conditions considered appropriate. In addition, the animation combined with the interaction facilitates the rapid exploration of complicated scenes.[4–7]

In human anatomy, multiple virtual 3D models of the body have been developed to support teaching in a detailed way, allowing the development of simulators of physiological cycles.[11–13,16–20] In veterinary medicine, several models that cover the entire body of the animal have been developed for dogs and mice.[14,21–23]

The aim of the present work was to develop an interactive 3D cat virtual model and an image library using transverse MRI, CT, and photograph images of the entire body of the cat.

Materials and Methods

Ethics

The present study was approved by the Ethics Committee for Animal Experimentation of the Universidad de Antioquia (CEEA-03/10/2014).

Preparation of the Cadaver

A fresh cadaver of an adult 4 Kg male mongrel cat was donated to the Hospital Veterinario de la Universidad de Antioquia. The cause of death was an acute infectious process that did not affect its anatomy. It was kept refrigerated (between 4 and 0°C) for ~ 10 hours, while the initial positioning and freezing process was started. No fixation or vascular perfusion with any substance was performed to avoid any alteration in the anatomy. The cadaver was prepared as follows: positioned in left lateral decubitus with the head slightly elevated on a blanket above the level of the trunk, the forelimbs parallel and flexed at the humeral, ulnar and carpal joints; similarly, both hind limbs were parallel and flexed at the hip, stifle and tarsus joints. Finally, the tail was flexed laterally, parallel to the trunk (►**Fig. 1A**). The cadaver was frozen at - 20°C for 48 hours. An open wooden box was wrapped with polystyrene (►**Fig. 1B**), filled with ~ 2 cm of embedding fluid (94.5% water, 5% gelatin, 0.5% methylene blue), and put into a deep freezer at - 20°C. When the fluid was frozen, the cadaver was placed inside the box (►**Fig. 1C**), and embedding fluid was added until 50% of the body was covered to be frozen again. Finally, the remaining space of the box was completed with embedding fluid and frozen at - 20°C for 1 week. A frozen block of embedding fluid was obtained with the cadaver positioned inside (►**Fig. 1D**).

Sectioning of the Cadaver

A band saw (Generic butcher cutter band) was used for the cutting process. The band saw had a load tray, adjustable stop, guides for the band, and rubber feet. The load tray had a raised edge on one of its sides and moved on a rail in the direction of the saw, the adjustable stop allowed to limit the cutting space as desired, the guides for the band kept the position of the cutting blade stable preventing displacements and keeping the cut on the same plane, and the rubber feet were non-slip to avoid machine movements that deflect the band at the time of cutting. The band used was a 27 mm wide, 1.6 mm thick steel blade (Baileigh Industrial, California, USA), with 4 teeth per inch of length. The sectioning process was made from cranial to caudal, making serial cross-sections of the animal with a thickness of 2.5 mm between cuts. The frozen block was removed from the wooden box, inside the polystyrene. Before starting the sectioning, and using a digital caliper (Mitutoyo Corporation, Tokio, Japan) (accuracy of 0.01 mm) to measure the distance, the adjustable stop was fixed to a space of 2.5 mm from the cutting blade to fix the cuts to this thickness. Then, the frozen block was carefully placed on the load tray, keeping the left side of the face resting on the raised edge of the tray and the cranial face supported by the adjustable stop, the machine was turned on, the tray was moved, a complete cut of the surface was made and then the machine was turned off. No slices were obtained but ground tissues, because of the low temperature of the block. The frozen block was taken to the photograph table and positioned with the freshly-cut side facing the camera. The surface was cleaned with 80% ethyl alcohol cooled to - 20°C, to remove the remaining frost and debris, and the photographic capture of the cut surface was made. Each cutting process involved measuring again the thickness of the cut and carefully positioning the block in the machine. The block was frozen again at - 20°C after 2 hours of work, preventing melting. The cutting process was performed until the entire cat was sectioned and photographed.

Image Capture and Photography

Artificial lighting under white light fluorescent lamps was used to photograph each sectioned surface with a Nikon D5500 (Nikon Corporation, Tokyo, Japan) digital camera equipped with a 55–300 lens. As the laboratory had several windows, the photographs were taken at night to avoid the effect of natural light. The camera was installed on a Beston 3560 tripod (Beston, Bogotá, Colombia) stand at a fixed distance and height from the metal table, so that the framing included the area of the cut surface of the block, and the plane of the cut surface was parallel to the framing plane of the photograph. After cutting, the frozen block was placed on

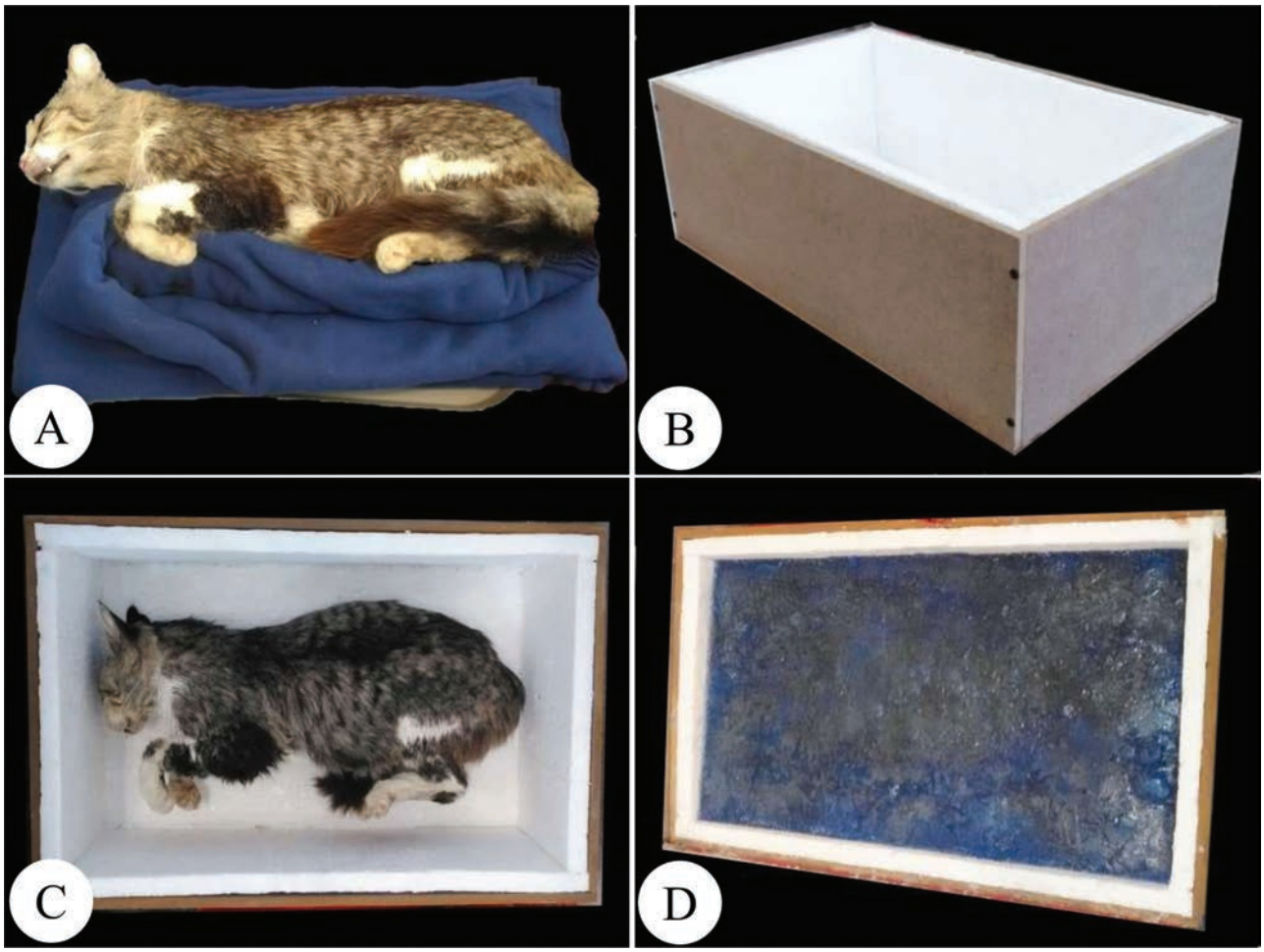

Fig. 1 Preparation of the cadaver. (A) Cadaver positioned with flexed limbs and tail. (B) Wooden box made with polystyrene cover. (C) Cadaver frozen and positioned inside the box before the embedding process. (D) Box with frozen block of embedded fluid with the cadaver inside.

the metal table in a predetermined position, the surface was cleaned as already mentioned, and the photographs were taken (automatic focus, aperture f 9, ISO 400, shooting speed 1/15). All of the photographs had the same technical and lighting characteristics, and were stored in the internal memory of the camera and in a computer.

Computed Tomography and Magnetic Resonance Imaging Images

The Universidad Nacional de Colombia provided 2 cadavers of adult male mongrel cats (approximate weight: 4 Kg, no age data available), one for scanning by CT, and the other for scanning by MRI. The cadavers were preserved at - 20°C until usage. For the scanning procedures, the animals were thawed and placed in sternal recumbency with the limbs and neck in hyperextension. One of the cadavers was scanned by CT with a Philips Tomoscan AV (Philips Healthcare, Amsterdam, Netherlands) at 2 mm intervals, while the other cadaver was scanned by MRI with an Esaote Vet-MR 0.25 Tesla (Esaote, Genoa, Italy) at 3-mm intervals.

Three-dimensional Modeling

The modeling of the complete anatomy of a feline was made using Autodesk Maya, version 2017, (Autodesk Inc., San Rafael, California, USA) and ZBrush, version 4R7 (Pixologic, Los Angeles, CA, USA) software. Three-dimensional objects for the structures and organs of the animal were created and then linked to form a complete 3D cat.

Development of the Interactive Virtual Software

An interactive virtual software was developed with the 3D cat and images library using Unity, version 5.4 (Unity Technologies, San Francisco, CA, USA). For the image library, 30 representative equivalent images from each technique were selected, for a total of 90 images of the entire body of the animal. All of the images were edited to match the same resolution characteristics (1,024 × 1,024 pixels), filter, background, and labels. The CT and MRI images were transformed from the DICOM format to JPG.

Results

Sectioning and Photography

A total of 178 cross-sectional photographs of the frozen block of the entire cat cadaver were obtained with 2.5-mm intervals. The images were converted to JPG files (file size 13.4 MB/image, total file size 2.3 GB) with a resolution of 6,000 × 4,000 pixels (►**Table 1**).

Table 1 Quantity and characteristics of the different types of images obtained

Images Type	Quantity	Intervals	Resolution (Pixels)	Size	Format
Magnetic resonance imaging	135	3 mm	512 × 512	146 KB	DICOM
Computed tomography	330	2 mm	512 × 512	329 KB	DICOM
Photographs	178	2.5 mm	6,000 × 4,000	13.4 MB	JPG
Total	643				

Abbreviations: DICOM, digital imaging and communications; JPEG, joint photographic experts group.

The photographs showed the anatomy of the animal with detail. All of the organs and many of the structures throughout the body could be identified and differentiated. The color of the photographs facilitated the differentiation of a great variety of structures – for example, the gray and white matter (►**Fig. 2A**). The continuity of structures, such as of the trachea, of the cranial vena cava, of the aorta, and of the spinal cord, could be appreciated. Differentiated structures included individual muscles (i.e., the supraspinatus, the triceps brachii, and the quadriceps femoris muscles), bones (i.e., the femur, the ulna, and the sternum), and organs (i.e., the mucosa of the stomach, the parenchyma of the liver, and the renal marrow and cortex). Some small (i.e., the meninges, and the skin) and large structures (i.e., coxal, intestines) could also be recognized, but others, such as small blood vessels, were not discernible (►**Fig. 2**).

Computed Tomography and Magnetic Resonance Imaging Images

A total of 135 MRI images were obtained at 3-mm intervals (file size 146 KB/image, total file size 20 MB) with a resolution of 512 × 512 pixels. The images showed in detail several anatomical structures and organs of the cat (►**Fig. 3**). The different gray gradations allowed the differentiation between tissue types (muscle, bone, air, and fluids), cavities (i.e., the frontal sinus), solid organs (i.e., the liver, the lungs) and hollow organs (i.e., the stomach). The continuity of structures such as of the trachea and of the spinal cord was easily discerned. Among others, some of the structures that were easily recognized included: muscle groups (i.e., the sublumbar muscles), bones (i.e., the jawbone, the ribs, the sternum), the interior of some organs (i.e., lumen of the bowel, parenchyma of the liver, interior of the eye), structures of medium (i.e., vertebral bodies) and large dimensions (i.e., intestines). No small structures, such as blood vessels of medium and small caliber, could be identified. In nervous tissues, the gray matter was not distinguished from the white matter.

A total of 330 CT images were obtained using 2-mm intervals (file size 329 KB/image, total file size 108 MB) with a resolution of 512 × 512 pixels. The gray scales allowed the differentiation of soft tissue structures with poor detail (i.e., the liver, the stomach), but muscles could not be differentiated. Spaces occupied by bone tissue and air were clearly delineated. As with the MRI images, the continuity of structures, such as of the trachea and of the spinal cord, could be clearly demarcated. Other easily identified structures included air cavities (i.e., acoustic meatus, segmental bronchi, gas in the intestine), bones (i.e., the radius, the femur, the sternum, the skull, the ribs), organs (i.e., the heart, the lungs), and structures of medium (i.e., vertebrae) and large size (i.e., coxal). No small structures, such as blood vessels of medium or small caliber, could be identified. In nervous tissue, the gray matter was not differentiated from the white matter. In the abdominal cavity, the organs were not easily recognized – for example, the kidney and the spleen could not be identified (►**Fig. 4**).

Three-dimensional Modeling

A total of ∼ 418 structures were modeled for the skeletal, muscular, circulatory, nervous, respiratory, digestive, urinary, and integumentary systems (►**Fig. 5**).

Development of the Interactive Virtual Software

Two user interfaces were created, one for viewing organ systems of the 3D cat, another for viewing selected images. A panel with icons for the visualization of every organ system of the 3D cat was provided. The systems are activated by clicking on the icon of each organ system and are deactivated by clicking on the button again. Any system can be activated individually, or several systems can be activated at the same time. The images can be zoomed in and out, and can be moved and rotated according to the interest of the user of the 3D cat panel. Additionally, several structures of different systems stand out and their names are indicated when the mouse is scrolled over them (►**Fig. 6**). The muscular system structures have an additional command that allows them to fade and reappear for easier visualization.

The interface for displaying the image library has an initial screen that shows a cat with several points for the plane of interest. By selecting a point, the user gains access to the next screen, which shows the image of the corresponding CT slice (by default), and a panel with buttons to compare every image for any technique (MRI, photograph, or CT). When scrolling the mouse over the selected image, the names of some of the structures are disclosed (►**Fig. 7**).

A demo of the software is shown in a published YouTube video (https://www.youtube.com/watch?v=Qr4XazpMCEg) and a link is provided in it to allow free downloading.

Discussion

The preparation of a cadaver is crucial to obtain an animal without alterations in anatomy, shape, and color. Embedding was conducted in several stages to avoid air chambers that could change the shape of the animal,[16,18,23] and fixation

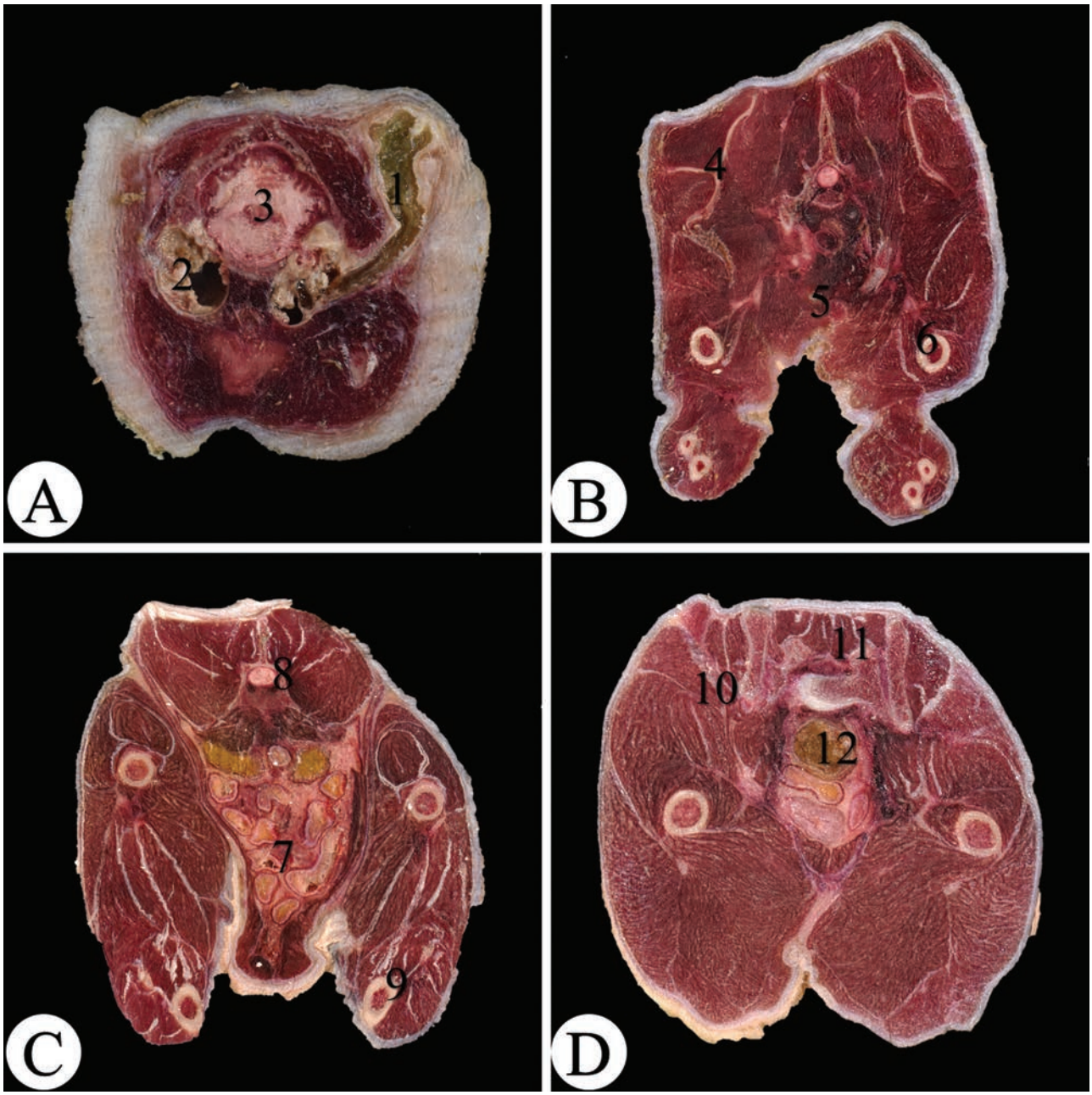

Fig. 2 Photographs of cross-sections of a cat cadaver. (A) Cranial region at the level of the brain, (B) thoracic region at the level of the second thoracic vertebra, (C) abdominal region at level of the kidneys, and (D) the pelvic region at the level of the coxal joint. (1) Brain, (2) jawbone, (3) masseter muscle, (4) humerus, (5) ulna and radius, (6) scapula, (7) right kidney, (8) stomach, (9) liver, (10) femur, (11) coxal, (12) rectum.

avoided alternations in the colors of the tissues.[22,23] Heparin could not be injected previously to death in the cat we have used; therefore, no substances were injected to highlight the blood vessels, because the presence of clots in the circulatory system may prevent the movement of any perfused substance and cause an obstruction that could alter the anatomy.[16,18,19]

Proper sectioning requires freezing the cadaver at the lowest possible temperature to obtain flat uniform surfaces and avoid quick thawing. Although similar projects have used freezing temperatures of - 80°C,[16,18,19,22,23] in our case the freezer could only attain temperatures of - 20°C. Despite this limitation, there were no problems with sectioning due to thawing of the block, suggesting that - 20°C can also be used as an alternative temperature. To avoid rapid thawing, a layer of polystyrene was used to wrap and isolate the block, the sectioning was performed at night to avoid daytime higher temperatures, and the surface was cleaned with 70% alcohol cooled to - 20°C.[16,18,19]

For image capturing, the body must be in an adequate position so that the images recreate the actual anatomy.[19,21] For the photographs, a quilted blanket was used to avoid deformation of the area on which the cadaver was lying. Because the cutting area of the bandsaw was limited, the position was chosen to occupy the smallest space possible that would be totally covered by the frozen block and by the width of the cutting area.

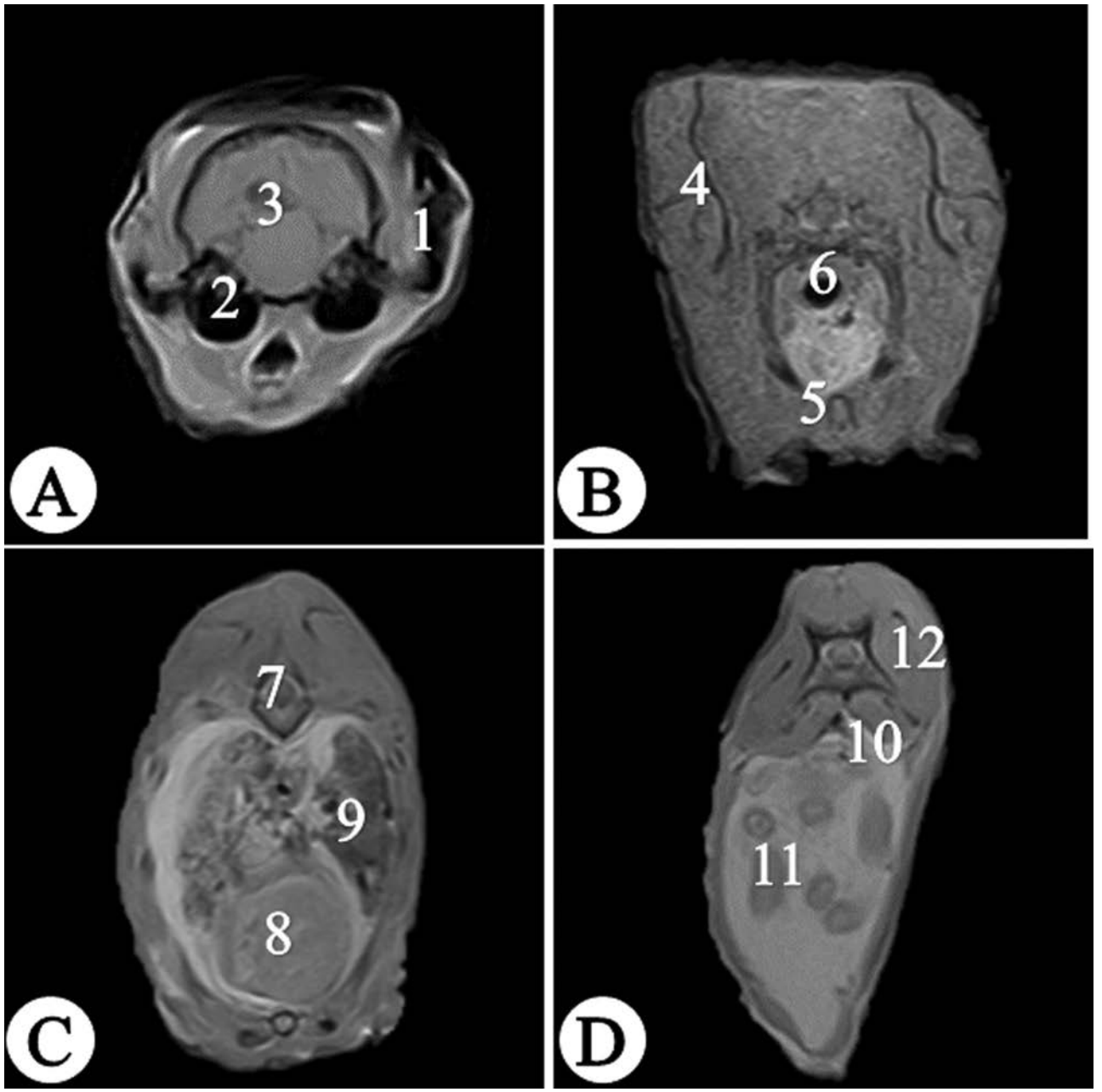

Fig. 3 Magnetic resonance imaging of (A) cranial region at the level of the frontal sinus, (B) thoracic region at the level of the second thoracic vertebra, and the region of the abdomen (C) at the level of the liver and (D), at the level of the last lumbar vertebrae. (1) Frontal sinus, (2) nasal cavity with turbinates, (3) jawbone, (4) scapula, (5) trachea, (6) sternum, (7) liver, (8) right lung, (9) vertebral body, (10) sublumbar muscles (10), intestines, (12) epaxial muscles.

For absolute correspondence among the images, all of the captions by every technique (MRI, CT and digital photographs) should be taken on the same animal and positions.[18,21,22] We have obtained images with each method from a different animal, in different positions, and at different section intervals. A major limitation was the availability of CT and MRI machines for veterinary use in the country. The only available machines were in another city, so there was no possibility of using the same animal due to the difficulty of transporting a cadaver from one city to another. Additionally, it was not possible to coordinate the two scanning processes for the same day with the same animal. Even using the same cadaver in similar projects report slight changes in position between different types of images.[16,18,19] The images were taken at different intervals due to the technical restrictions of the MRI and CT machines. Although there was no complete correspondence between the three techniques, a group of images equivalent to each other was obtained, which also allowed comparisons between the methods used.

The characteristics of the digital camera and of the lighting are decisive factors for the proper quality of the photographs. The capacity of the camera determines the resolution of the photograph, which is determined by the number of pixels. In the present study, a 24.2 megapixel camera was

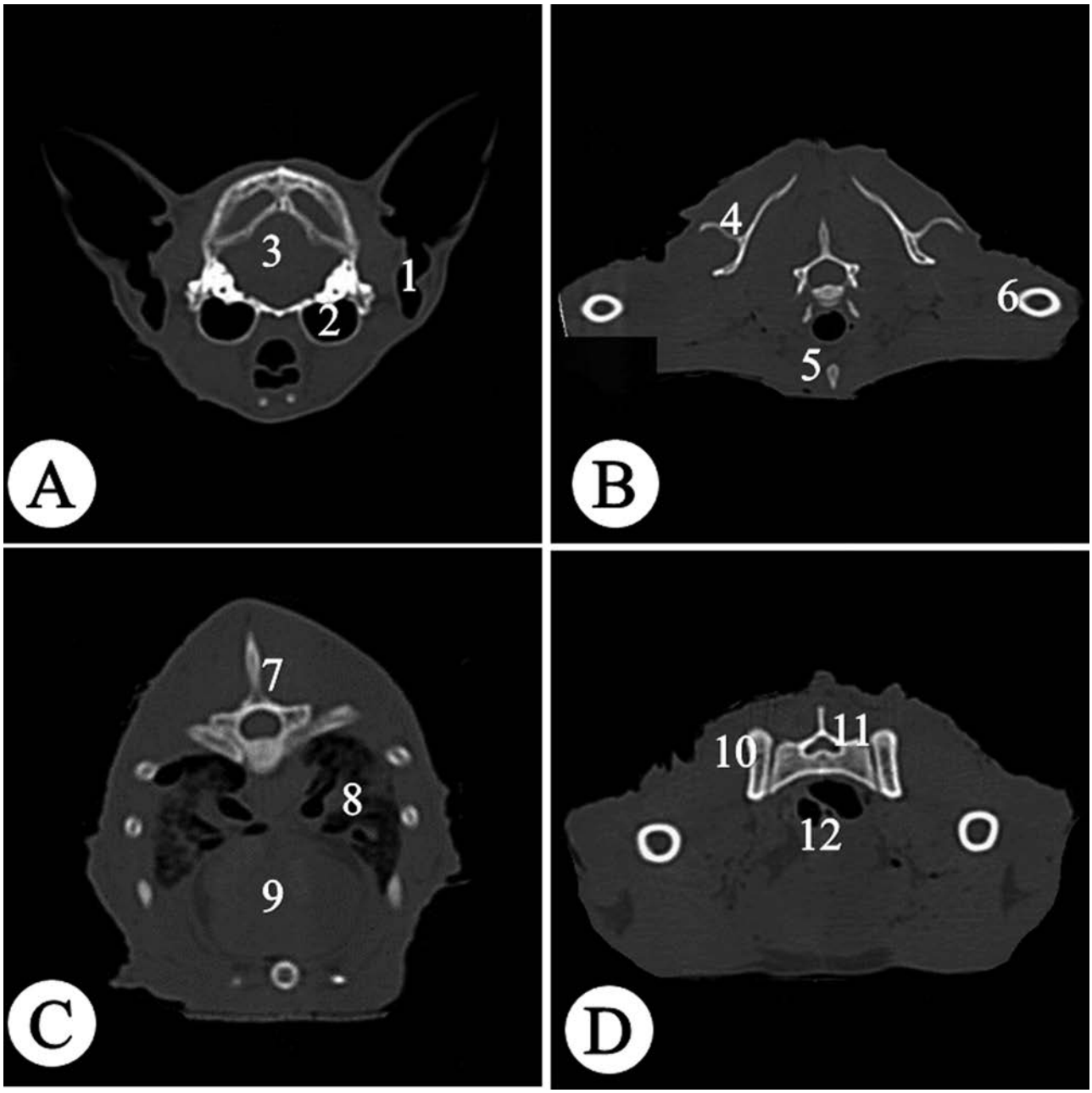

Fig. 4 Computed Tomography images of (A) cranial region at the level of the tympanic bulla, thoracic region (B) at the level of the second thoracic vertebra, (C) at the level of the heart, and (D) pelvic region at the level of the coxal joint (D). (1) Acoustic meatus, (2) tympanic bulla, (3) encephalon, (4) scapula, (5) sternum, (6) humerus, (7) thoracic vertebra, (8) heart, (9) left lung, (10) femur, (11) coxal, and (12) rectum.

used, providing an excellent resolution of the photographs.[16,18,19,23] Because the lighting should be constant and unchanged, the pictures were taken at night under constant artificial light.[21,22]

The software developed in the present study has two interfaces for easier navigation, one to explore the 3D cat and another to explore the image library. The interface approach for the 3D cat facilitates visualization and precise scene composition. The user can create any scene of interest, with the possibility of exploring the whole cat, a certain region of interest, or a particular structure. Text labels provide the name of the structure and the highlighting in color facilitates its recognition and location. The interface of the image library allows comparing equivalent images by CT, MRI and digital photographs, and rapid changes between planes to facilitate the understanding of sectional anatomy.

Compared with interactive virtual models, printed images have the limitation that they are static and not expandable, the labeling is often limited or incomplete, the number of views is limited, and the spatial relationships are difficult to understand.[4,5] Interactive virtual models reduce these limitations and become a valuable educational tool. If this type of interactive virtual resource is incorporated into the curricula, it can help to create a user-controlled learning experience that is customized and adapted to different types of learners.[2,5,21]

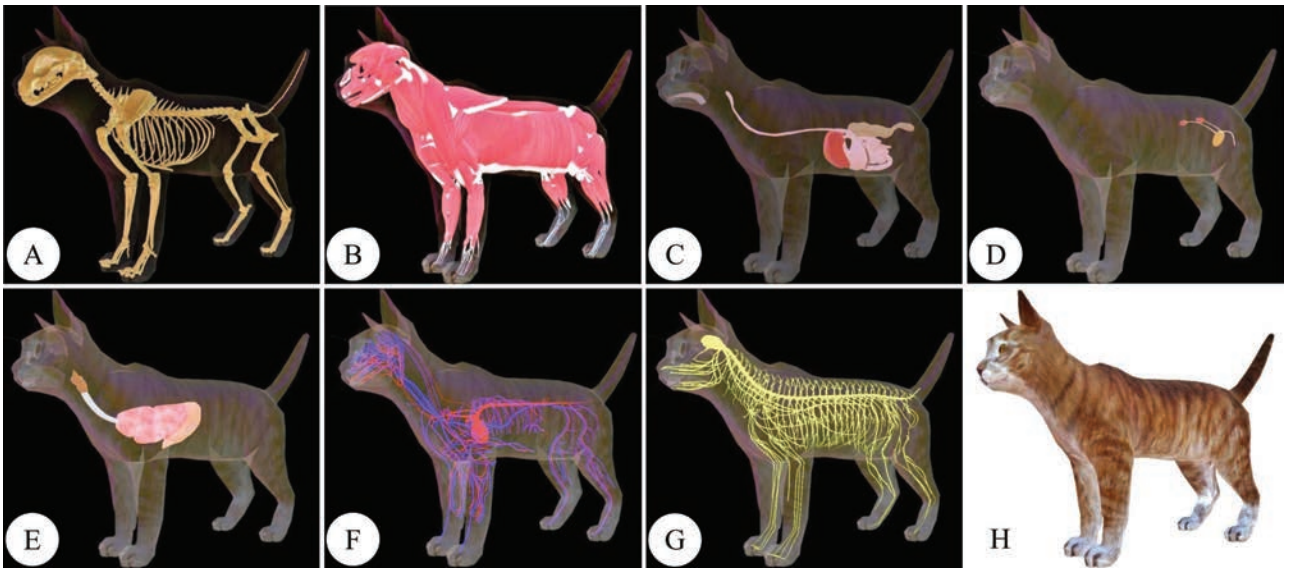

Fig. 5 Three-dimensional cat model of the anatomical systems. (A) Skeletal, (B) muscular, (C) digestive, (D) urinary, (E) respiratory, (F) circulatory, (G) nervous systems, and (H) skin and exterior model of the cat.

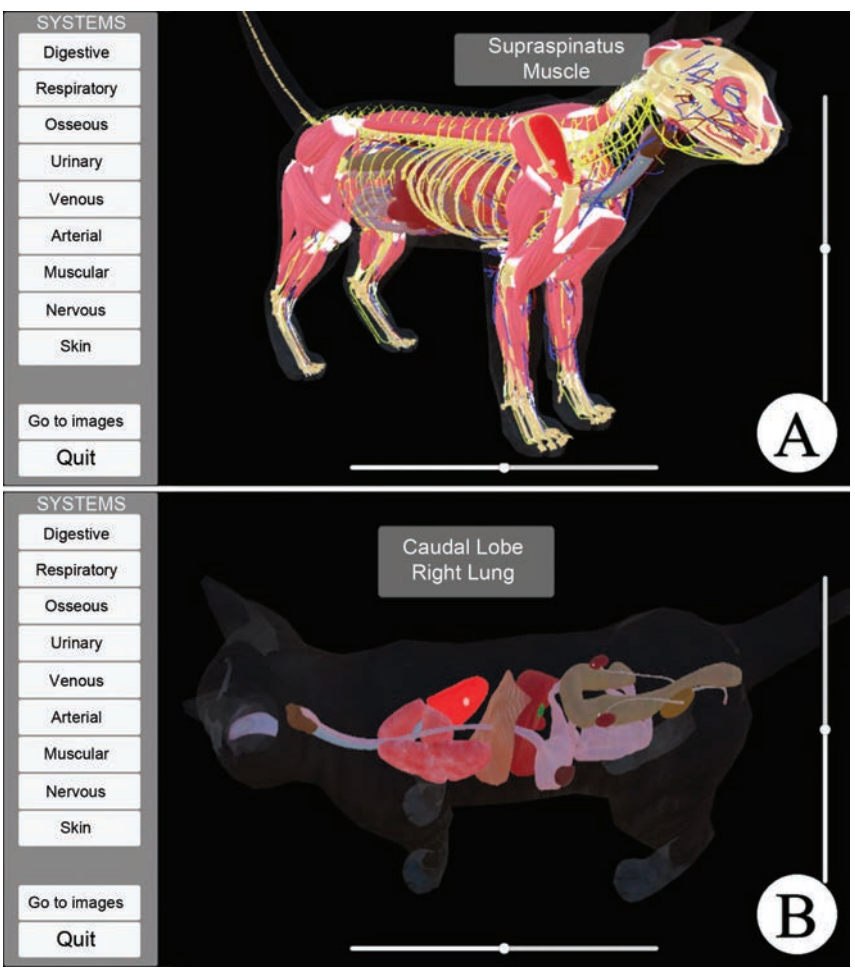

Fig. 6 User interface for the visualization of anatomical structures and systems. (A) Three-dimensional cat with zoom in, rotation, several organic systems activated and some hidden muscles, with the pointer indicating the infraspinatus muscle. (B) Three-dimensional cat with zoom in, and rotation, with the digestive, urinary and respiratory systems activated, with the pointer on the cranial lobe of the right lung.

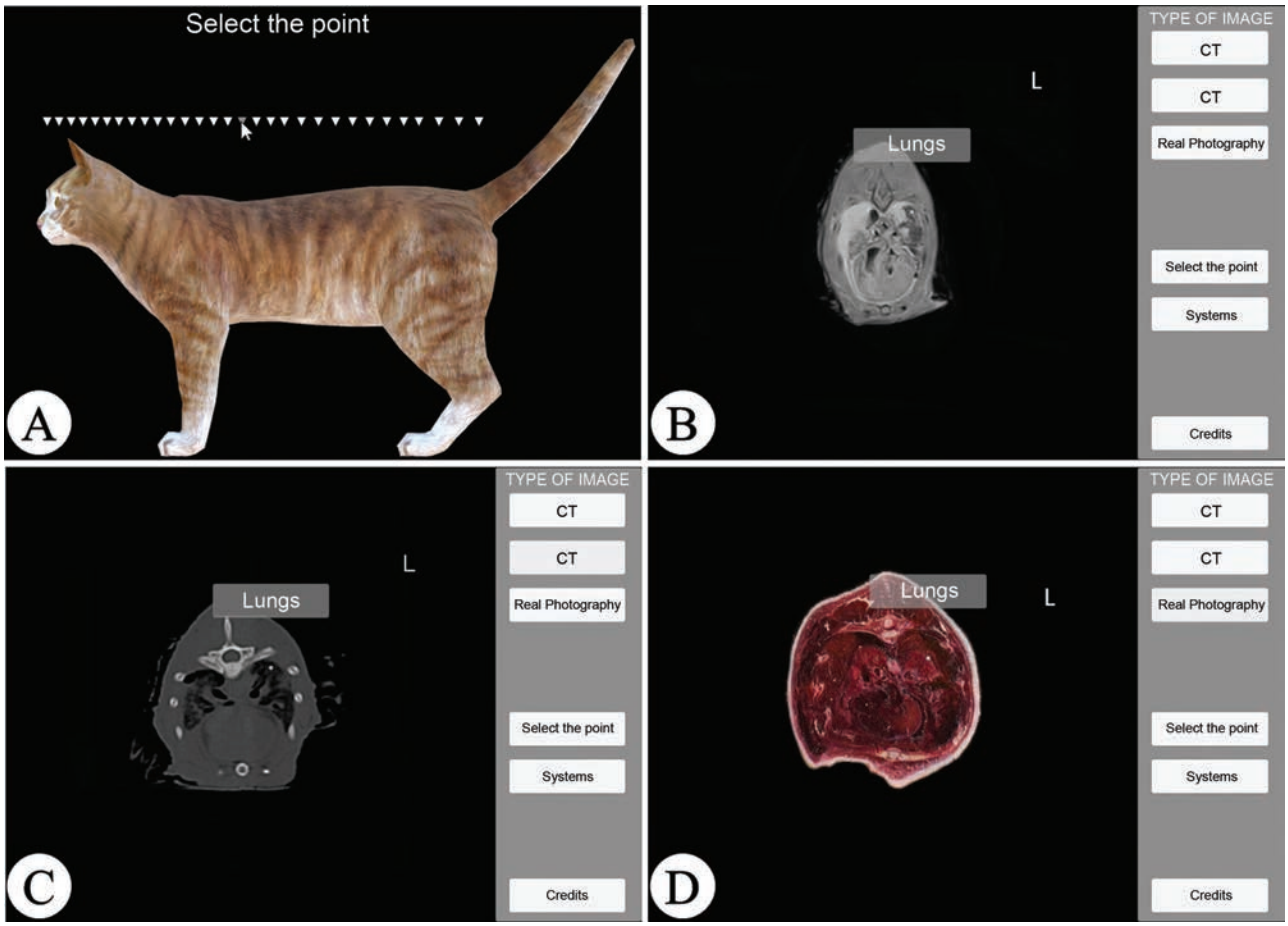

Fig. 7 User interface for displaying the image library. (A) Screen of selection of the plane of interest (thorax region). Screen with magnetic resonance imaging (B) and computed tomography (C) of the selected region with the pointer located above the lungs. (D) Screen with a photograph of a transverse section of the thorax region with the pointer located on the lungs.

This 3D virtual model software of the cat will simplify learning anatomy in veterinary education.

Conclusions

A thorough knowledge of veterinary anatomy is an important prerequisite for a proper interpretation of modern medical images. When interpreting images, knowledge of the dimensions and of the localization of anatomical structures is essential. For veterinary students and practitioners, it is difficult to envision 3D objects in space. The use of 3D virtual models can facilitate the interpretation of modern techniques of body imaging. In addition, these models reduce the difficulties of visualizing some anatomical structures, as occurs with 2D images.

There is a need to shorten the learning curve for students in the acquisition of basic anatomical knowledge. Three-dimensional virtual models could help to achieve this goal, allowing recognizing structures, exploring the body, making topographical relationships, simplifying structures, isolating regions or body parts with the possibility of easily changing the point of view.

Future studies must evaluate the efficacy of the software as a learning tool in veterinary anatomy, as well as students and faculty perceptions.

Conflicts of Interest

The authors have no conflicts of interest to declare.

Acknowledgments

We wish to thank the Comité para el Desarollo de la Investiacíon de la Universidad de Atioquia (CODI-UdeA) for the funding grant to develop the present work. We also wish to thank professor Hugo Gutiérrez, from Universidad Nacional de Colombia, for all the collaboration to this work.

References

1 Lewis TL, Burnett B, Tunstall RG, Abrahams PH. Complementing anatomy education using three-dimensional anatomy mobile software applications on tablet computers. Clin Anat 2014;27 (03):313–320
2 Nicholson DT, Chalk C, Funnell WRJ, Daniel SJ. Can virtual reality improve anatomy education? A randomised controlled study of a computer-generated three-dimensional anatomical ear model. Med Educ 2006;40(11):1081–1087
3 Jang HG, Chung MS, Shin DS, et al. Segmentation and surface reconstruction of the detailed ear structures, identified in sectioned images. Anat Rec (Hoboken) 2011;294(04):559–564
4 Allen LK, Bhattacharyya S, Wilson TD. Development of an interactive anatomical three-dimensional eye model. Anat Sci Educ 2015;8(03):275–282

5 Nowinski WL, Thirunavuukarasuu A, Volkau I, et al. A new presentation and exploration of human cerebral vasculature correlated with surface and sectional neuroanatomy. Anat Sci Educ 2009;2(01):24–33
6 Geyer LL, Schoepf UJ, Meinel FG, et al. State of the art: iterative CT reconstruction techniques. Radiology 2015;276(02):339–357
7 Henn JS, Lemole GM Jr, Ferreira MA, et al. Interactive stereoscopic virtual reality: a new tool for neurosurgical education. Technical note. J Neurosurg 2002;96(01):144–149
8 Martinsen S, Jukes N. Towards a humane veterinary education. J Vet Med Educ 2005;32(04):454–460
9 Preece D, Williams SB, Lam R, Weller R. "Let's get physical": advantages of a physical model over 3D computer models and textbooks in learning imaging anatomy. Anat Sci Educ 2013;6 (04):216–224
10 Leung KK, Lu KS, Huang TS, Hsieh BS. Anatomy instruction in medical schools: connecting the past and the future. Adv Health Sci Educ Theory Pract 2006;11(02):209–215
11 Shin DS, Chung MS, Park JS, et al. Three-dimensional surface models of detailed lumbosacral structures reconstructed from the Visible Korean. Ann Anat 2011;193(01):64–70
12 Park JS, Chung MS, Hwang SB, Lee YS, Har DH. Technical report on semiautomatic segmentation using the Adobe Photoshop. J Digit Imaging 2005;18(04):333–343
13 Segars WP, Mahesh M, Beck TJ, Frey EC, Tsui BM. Realistic CT simulation using the 4D XCAT phantom. Med Phys 2008;35(08): 3800–3808
14 Segars WP, Tsui BM, Frey EC, Johnson GA, Berr SS. Development of a 4-D digital mouse phantom for molecular imaging research. Mol Imaging Biol 2004;6(03):149–159
15 Lauridsen H, Hansen K, Wang T, et al. Inside out: modern imaging techniques to reveal animal anatomy. PLoS One 2011;6(03): e17879
16 Spitzer V, Ackerman MJ, Scherzinger AL, Whitlock D. The visible human male: a technical report. J Am Med Inform Assoc 1996;3 (02):118–130
17 Schiemann T, Freudenberg J, Pflesser B, et al. Exploring the Visible Human using the VOXEL-MAN framework. Comput Med Imaging Graph 2000;24(03):127–132
18 Zhang SX, Heng PA, Liu ZJ. Chinese visible human project. Clin Anat 2006;19(03):204–215
19 Park JS, Chung MS, Hwang SB, Shin BS, Park HS. Visible Korean Human: its techniques and applications. Clin Anat 2006;19(03): 216–224
20 Paul Segars W, Tsui BM. MCAT to XCAT: The Evolution of 4-D Computerized Phantoms for Imaging Research: Computer models that take account of body movements promise to provide evaluation and improvement of medical imaging devices and technology. Proc IEEE Inst Electr Electron Eng 2009;97(12): 1954–1968
21 Dogdas B, Stout D, Chatziioannou AF, Leahy RM. Digimouse: a 3D whole body mouse atlas from CT and cryosection data. Phys Med Biol 2007;52(03):577–587
22 Böttcher P, Maierl J. Macroscopic cryosectioning: a simple new method for producing digital, three-dimensional databases in veterinary anatomy. Anat Histol Embryol 1999;28(02): 97–102
23 Park HS, Shin DS, Cho DH, Jung YW, Park JS. Improved sectioned images and surface models of the whole dog body. Ann Anat 2014; 196(05):352–359

Effects of Supraphysiological Doses of Testosterone Cypionate and Stanozolol on Neuronal Density of Basolateral and Medial Amygdala and on the Anxious Behavior of Mice

Melissa Ribeiro[1] Ariane Freitas[1] Bruno Damião[1] Wagner Costa Rossi Junior[2] Flávia da Ré Guerra[1] Evelise Aline Soares[1] Petrus Pires Marques[2] Alessandra Esteves[1]

[1] Department of Anatomy, Universidade Federal de Alfenas, Alfenas, MG, Brazil
[2] Departament of Morphology, Universidade José do Rosário Vellano, Unifenas, Alfenas, MG, Brazil

Address for correspondence Alessandra Esteves, PhD, Departamento de Anatomia, Universidade Federal de Alfenas, Rua Gabriel Monteiro da Silva, n°700, Centro, Alfenas, MG, Brasil, CEP 37130-000. (e-mail: aesteves015@gmail.com).

J Morphol Sci 2019;36:115–121.

Abstract

Supraphysiological doses of anabolic-androgenic steroids (AAS) have been associated to possible nerve tissue damage and behavioral effects. Considering the lack of knowledge of the neural aspects involved in these behavioral alterations, this work aimed to analyze the anxious behavior response or aggressiveness, besides quantifying the neuronal density of the basolateral amygdala (BLA) and of the ventral posterior nucleus (VPN) of the medial amygdala. The animals received doses of testosterone cypionate (CT Group) and stanozolol (ST Group) twice a week for 33 days. The effects of chronic administration of AAS related to anxious behavior (as determined by the elevated plus maze [EPM] test) in male animals are observed in a lower number of entries (45.25%), and a shorter staying time spent in the open arms (41.9%) was observed in the ST. In female animals, a longer staying time spent in the closed arms of the EPM test was observed in the CT (15%) as well as a shorter staying time spent in the open arms for CT (17.1%) also to ST (52.1%). Regarding the neuronal density in BLA, a significant reduction in neuronal density of male animals (17.55%) was observed only in CT, whereas for females, significant differences were found in CT (19.16%) and ST (18.36%). The reduction of neuronal density in VPN in male animals was 13.55% in CT and 17.68% in ST, whereas in group of females it was 13.53% and 14.32%, respectively for CT and ST. Therefore, the two steroids used in this experiment were able to significantly reduce neuronal density in two analyzed areas, regardless of sex, suggesting that indiscriminate use of these substances causes death of brain amygdala neurons.

Keywords
- anabolic-androgenic steroids
- basolateral amygdala
- medial amygdala
- anxiety
- density neuron

Introduction

Abusive use of anabolic-androgenic steroids (AAS) is based on supraphysiological doses that are 10 to 100 times greater than therapeutic doses,[1,2] and which have been associated with a wide spectrum of adverse physical and psychic effects. Little is known about the effect of AAS in the human brain, with reports of changes in behavior, such as aggressiveness, anxiety and depression, among others.[3–5]

received
August 22, 2018
accepted
March 28, 2019

DOI https://doi.org/10.1055/s-0039-1688809.
ISSN 2177-0298.

Copyright © 2019 by Thieme Revinter Publicações Ltda, Rio de Janeiro, Brazil

License terms

Some studies have shown that AAS may have deleterious effect on the central nervous system (CNS).[6] The few in vitro data obtained suggest that the influence of androgenic drugs on neurodegeneration depends critically on the treatment regimen, concentration and cell phenotype. A single application of testosterone in supraphysiological concentration promoted cell death by apoptosis in nerve cells by means of altering their Ca^{2+} signaling.[7]

Recent animal models have demonstrated that chronic use and abuse of stanozolol have reduced levels of brain-derived neurotrophic factor (BDNF) and dopamine in the hippocampus and prefrontal cortex of rodents, in addition to the reduction in glucocorticoid receptor expression in the hippocampus and in plasma, and an increase in basal morning plasma cortisol levels. These metabolic changes have been related to mood disorders, such as depression.[8,9]

As the monoaminergic system regulates aggression, sexual behavior, fear and anxiety, one can suggest a possible correlation between changes in the monoamines generated by AAS and behavioral alterations and mood disorders.[9,10]

From the above mentioned, it is evident that there are considerable negative neurological effects due to abusive and/or chronic use of AAS that can lead to serious complications and damages, both physical and behavioral. Regarding the lack of knowledge of the neural mechanisms involved in the wide range of deleterious effects that may involve the CNS, it is necessary to carry out new research aiming to elucidate the underlying brain mechanisms associated to them.

Material and Methods

Ninety-two Swiss mice from the Central Biotery of the Universidade Federal de Alfenas (UNIFAL-MG) were used, with 46 being male and 46 female, ~ 90 days old (young adults), weighting between 40 and 50 g. All animals were fed with commercial ration and water *ad libitum* (at will) and kept in a 12-hour light-dark cycle. The animals were divided as follows:

CT group - Animals receiving testosterone cypionate (SigmaPharm Laboratories, Philadelphia, Pensilvania, USA) at a dose of 0.8 mg/kg/day.
ST group - Animals receiving stanozolol (Winstrol Depot [Winthrop Chemical Company, New York, NY, USA]) at a dose of 1.8 mg/kg/day.
Control group - Animals receiving sterile saline solution at 0.9% at a dose of 0.05 ml/day.

The treatment consisted of intraperitoneal (IP) injection of the drugs to be tested for 33 days, with applications performed twice a week. On intercalated days, they were submitted to swimming for an initial period of 5 minutes, gradually increasing up to 15 minutes. The swimming was performed in a container measuring 43 × 34 × 26 cm, containing in its interior water in the temperature of 24 to 26°C to the edge. Swimming training was performed in an attempt to generate the same stress conditions as body-building. From the 33rd day of treatment, the elevated plus maze (EPM) test was performed in all groups to study the effects of these substances on the anxiety level of the animals.[11,12]

After the days of behavioral testing, the animals were euthanized by inhalation of isoflurane for later craniotomy. The brains were removed entirely, washed in saline solution and fixed in 4% paraformaldehyde in phosphate buffer for 24 hours. After this period, the material underwent the conventional histological processes: alcohol dehydration, xylol diaphanization and paraffin inclusion.

From each brain so obtained, serial and homotypic samples were taken in frontal sections[13,14] with a thickness of 7 µm in a Yidi YD-315 microtome. To evaluate the areas selected for the study, the material was stained with Cresyl violet.[14,15] The determination of the studied areas matches the representation of plate 43 of Franklin and Paxinos' mouse brain stereotactic atlas.[15,16] For the quantitative analysis of neuron body cells, the simple random sample counting method was used.[17–19] Each division of the amygdala (basolateral amygdala [BLA] or ventral posterior nucleus [VPN]) had two areas quantified per hemisphere, totaling four areas per section. To avoid counting the same cell more than once, 3 semi-serial sections per animal were analyzed, totaling 12 histological fields per nucleus studied for each animal. As 2 divisions (BLA) and (VPN) were quantified, a total of 24 areas per animal were obtained. Thus, for the sample used, a total of 960 areas was quantified at a 400X magnification. All analyzes were performed by means of the software Axiovision 4 Module Interactive Measurement (Carl Zeiss Microscopy LLC, Thornwood NY, USA), an analyzing image system, coupled to the AxioScope A1 microscope (Carl Zeiss Microscopy LLC).

The study represents a completely randomized design (CRD); therefore, the statistical analysis was performed through a one-way analysis of variance (ANOVA) followed by Tukey averages comparison test. Values of $p < 0.05$ were considered as indicative of significance.

Ethics Statement

This work is in accordance with the ethical principles of experiment animal use and has been approved by the Commission for Ethics in Animal Experimentation of UNIFAL-MG, under the registration number 505/2013.

Results

The effects of chronic administration of AAS related to anxious behavior (determined by the EPM test) in male animals are shown in ►**Fig. 1**. A lower number of entries (45.25%) and a shorter staying time spent in the open arms (41.9%) of the EPM were observed in the stanozolol (Winstrol Depot) group when compared with the control group (►**Table 1**). These data indicate a greater anxiogenic response to stanozolol (Winstrol Depot) in the male animals group in relation to the control.

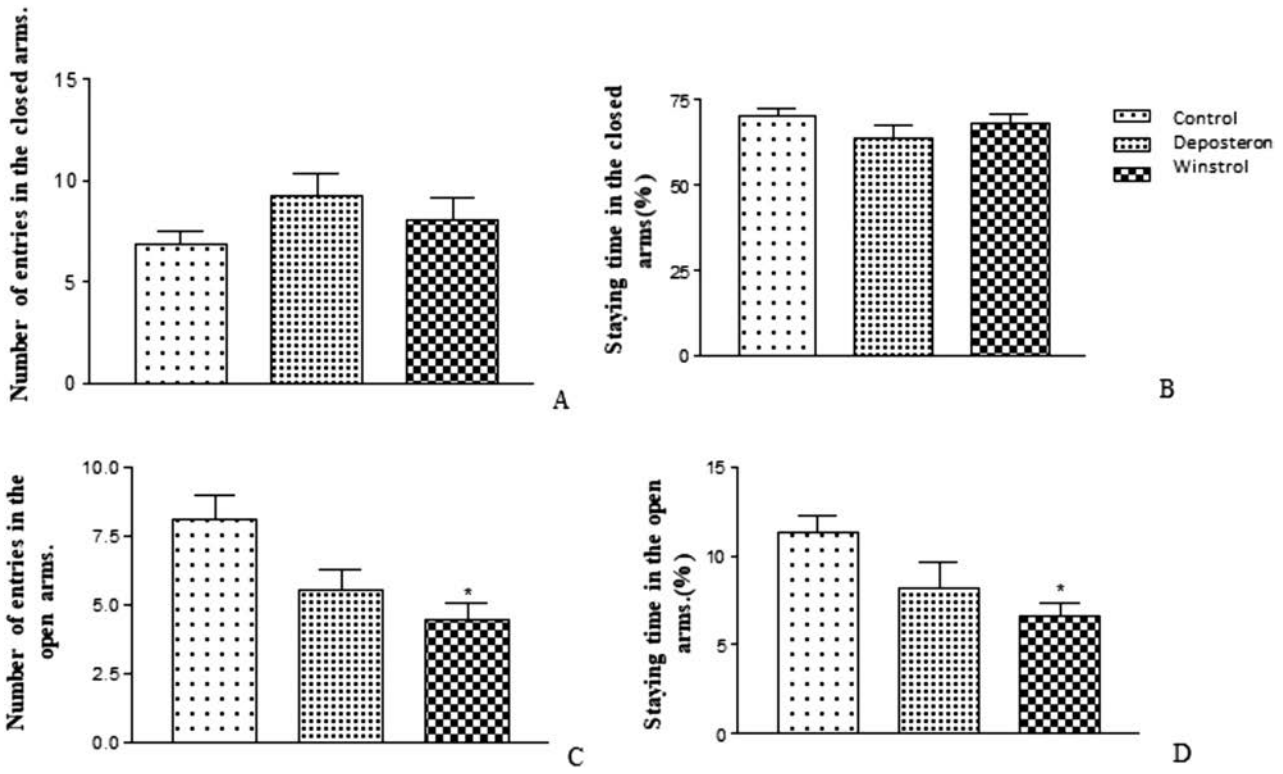

Fig. 1 Graphs illustrating analyzed elevated plus maze test parameters (male animals). Effect of testosterone cypionate (Deposteron), stanozolol (Winstrol Depot) or saline solution administration in relation to the number of entries in the closed arm (A), staying time in the closed arm (B), number of entries in the open arm (C) and staying time in the open arm (D). Means and respective standard deviations (*= $p < 0.01$) are depicted in relation to the control group.

The effects of chronic administration of AAS related to anxious behavior (EPM) in female animals are shown in ►**Fig. 2**. A longer staying time spent in the closed arms of the EPM was observed for the testosterone cypionate (Deposteron) group (15%) in relation to the control one, as well as a shorter staying time spent in the open arms of the EPM for the testosterone cypionate (Deposteron) group (17.1%) when compared with the control and the stanozolol (Winstrol Depot) groups (52.1%). These data indicate a higher anxiogenic response to testosterone cypionate (Deposteron) in the female animals group when compared with the control group (►**Table 1**).

In relation to neuronal density in the basolateral amygdala (ABL), a decrease in the number of neuron body cells in the testosterone cypionate (Deposteron) (17.55%) male animals group was observed when compared with the control group, as shown in ►**Fig. 3A** and ►**Table 2**. However, in female animals, significant differences were found in

Table 1 Number of entries and staying time in the arms of the elevated plus maze (EPM)test

	Number of entries (open arms)	Number of entries (closed arms)	% staying time (open arms)	% staying time (closed arms)
Male				
Control	8.11[a]	6.88[a]	11.34[a]	70.28[a]
Deposteron	5.57[a]	9.28[a]	8.2[a]	63.81[a]
Winstrol	4.44[b] (45.25%)	8.00[a]	6.58[b] (41.9%)	68.12[a]
Female				
Control	6.2[a]	7.1[a]	8.04[a]	65.46[a]
Deposteron	6.00[a]	7.5[a]	3.85[b] (52.1%)	75.64[b] (15%)
Winstrol	5.7[a]	8.1[a]	6.66[b] (17.1%)	70.63[a]

Different letters in superscript refer to statistical difference using Tukey test at the significance level of 5%.

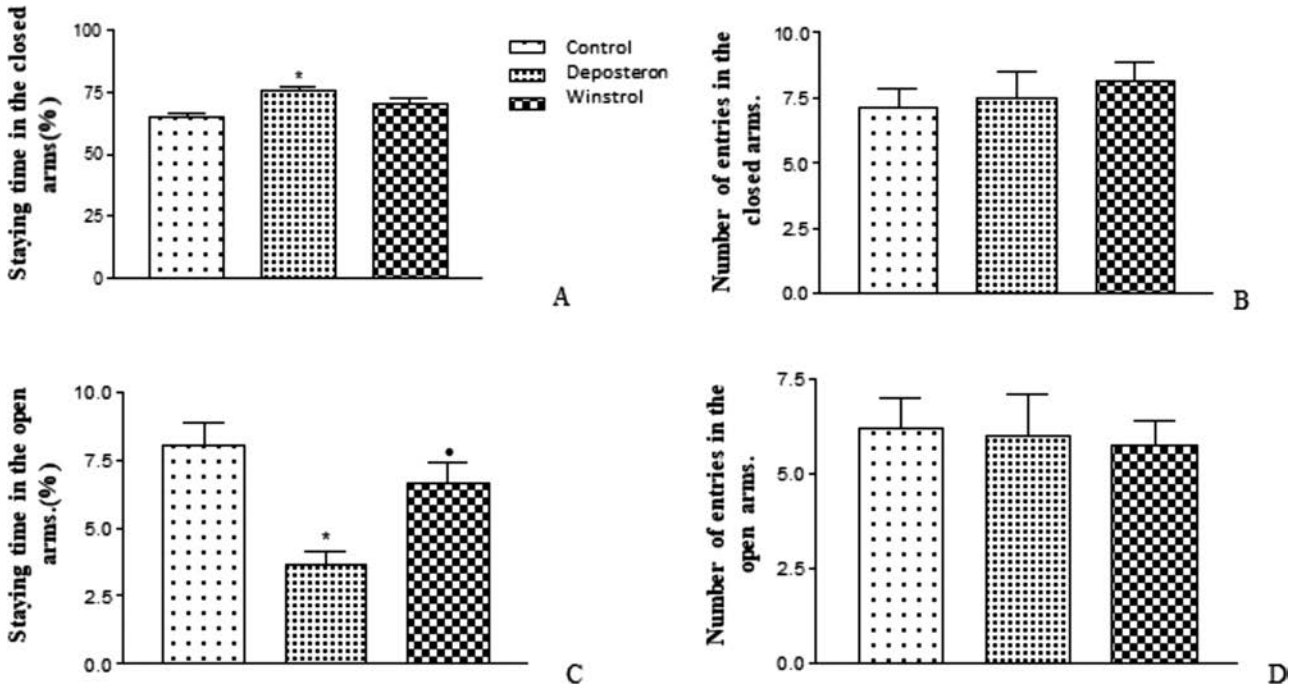

Fig. 2 Graphs illustrating analyzed elevated plus maze test parameters (female animals). Effect of testosterone cypionate (Deposteron), stanozolol (Winstrol Depot) or saline solution administration in relation to the number of entries in the closed arm (A), staying time in the closed arm (B), number of entries in the open arm (C) and staying time in the open arm (D). Means and respective standard deviations (*= $p < 0.01$) are depicted in relation to the control group (• = $p < 0.05$ is in relation to stanozolol group).

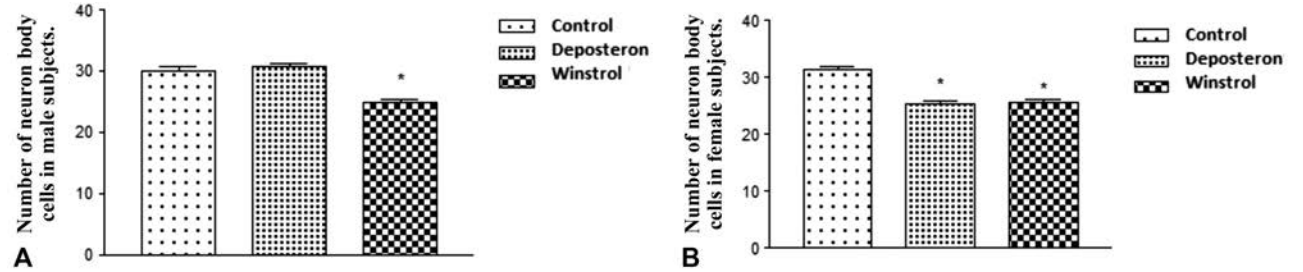

Fig. 3 Neuron body cells counting in the basolateral amygdala (BLA) of male and female animals. (A) shows comparative graphs of neuronal density in BLA of male mice in each analyzed experimental group (*= $p < 0.001$) for testosterone cypionate in relation to the control group. (B) shows comparative graphs of neuronal density in BLA of female mice in each analyzed experimental group (*= $p < 0.001$) for testosterone cypionate and stanozolol in relation to the control group.

Table 2 Mean of basolateral amygdala and percentage of reduction neuron cells quantification

Groups	Mean BLA neuron cell	Percentage of reduction
Male		
Control	30.07[a]	–
Deposteron	30.79[a]	–
Winstrol	24.79[b]	17.55%
Female		
Control	31.36[a]	–
Deposteron	25.35[b]	19.16%
Winstrol	25.60[b]	18.36%

Abbreviation: BLA, basolateral amygdala.
BLA neuron cells quantification exhibited as mean value.
Different letters in superscript refer to statistical difference using Tukey test at the significance level of 5%.

both testosterone cypionate (Deposteron) (19.16%) and stanozolol (Winstrol Depot) (18.36%) groups when compared with the control group, as shown in ►**Fig. 3B** and ►**Table 2**.

The decrease in neuronal density in the ventral posterior nucleus (VPN) of the medial amygdala was observed in both testosterone cypionate (Deposteron) and stanozolol (Winstrol Depot) groups when compared with the control group, for male (Deposteron-13.55% and Winstrol Depot-17.68%) and female animals (Deposteron 13.53% and Winstrol Depot 14.32%), as shown in ►**Fig. 4** and ►**Table 3**.

Discussion

From the general analysis of the results in the EPM test, we can suggest that both testosterone cypionate (Deposteron) and stanozolol (Winstrol Depot) are associated with the

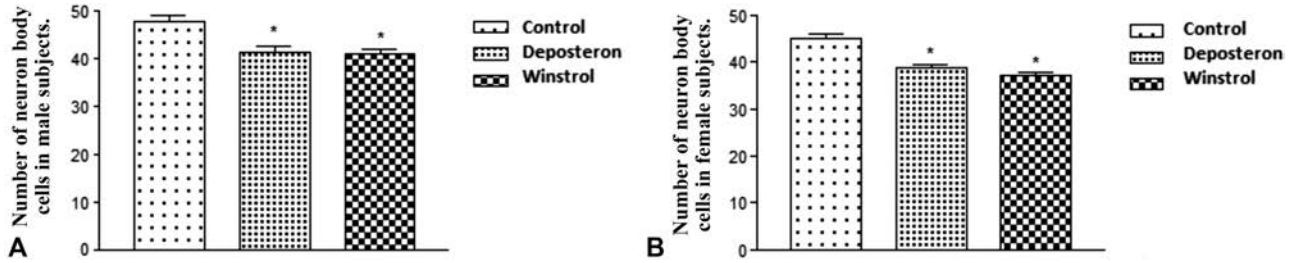

Fig. 4 Neuron body cells counting in the ventral posterior nucleus (VPN) of male and female animals. (A) shows comparative graphs of neuronal density in VPN of male mice in each analyzed experimental group ($^{*}= p < 0.001$) for testosterone cypionate and stanozolol in relation to the control group. (B) shows comparative graphs of neuronal density in VPN of female mice in each analyzed experimental group ($^{*}= p < 0.001$) for testosterone cypionate and stanozolol in relation to the control group.

Table 3 Mean of ventral posterior nucleus and percentage of reduction neuron cells quantification

Groups	Mean BLA neuron cell	Percentage of reduction
Male		
Control	45.00[a]	–
Deposteron	38.90[b]	13.55%
Winstrol	37.04[b]	17.68%
Female		
Control	48.03[a]	–
Deposteron	41.53[b]	13.53%
Winstrol	41.15[b]	14.32%

Abbreviation: BLA, basolateral amygdala.
Ventral posterior nucleus neuron cells quantification exhibited as mean value.
Different letters in superscript refer to statistical difference using Tukey test at the significance level of 5%.

generation of anxiogenic responses. The stanozolol (Winstrol Depot) male animals group, as well as the testosterone cypionate (Deposteron) female animals group presented responses indicative of greater anxiety. In the first group, the animals presented a lower number of entries and a shorter staying time spent in the open arms of the EPM (more aversive area). In the second group, the animals had a longer staying time spent in the closed arms of the EPM (less aversive area) and a shorter staying time spent in the open arms of the EPM (more aversive area). No significant results were found for the testosterone cypionate (Deposteron) male animals group and stanozolol (Winstrol Depot) female animals group.

The generation of an anxiogenic response is in agreement with the results obtained in a study in which adult male C57Bl/6J mice receiving a daily subcutaneous injection of 15 mg/kg of nandrolone decanoate presented an anxiogenic behavior in the EPM test after 19 days of treatment.[20] Anxiogenic response in the EPM test was also observed in a study in which male Wistar rats received nandrolone decanoate (5 mg/kg) twice a week for 6 weeks and were submitted to the EPM test at the end of this period.[21]

In another study, albino male mice receiving daily subcutaneous injections of nandrolone decanoate in the supraphysiological concentration of 15 mg/kg did not present changes in anxiety levels when submitted to the EPM test on the 14th day of treatment[6]. Some authors have reported that the treatment of Long-Evans rats with subcutaneous testosterone propionate through silicone implants for prolonged administration of supraphysiological doses (6 days) promoted an increase in the open arms exploration of the EPM, in relation to the control, indicating reduction on the level of anxiety. However, in the same study, treatment for 14 days did not promote anxiogenic effects. According to these authors, this variation of responses is due to the development of tolerance to AAS, a very common phenomenon in chronic users of psychoactive drugs.[22]

It has been demonstrated that serotonin activates inhibitory GABAergic interneurons in the amygdala, exerting a generalized inhibitory tonus on neuronal excitability, which suggests that serotonin functions as a brake mechanism that limits neuronal excitability.[23] There is a possibility that an inhibitory effect of the AAS on the serotonergic system may contribute to a greater excitability of the amygdala, which, in turn, could be responsible for the behavioral responses observed in the AAS prolonged use.[20]

Since a high dose (1 mg/kg) of AAS binds to glucocorticoid receptors,[21,24] the effects of these drugs could be related to their actions on these receptors. Glucocorticoids may act in the modulation of anxiety by their actions in the CNS, especially in the hippocampus.[25]

Some studies have attempted to correlate behavioral changes to the AAS effects on central serotonergic and GABAergic neurotransmission, among others, in several areas of the brain.[26]

In view of fact that there are synergistic interactions between glutamate and gonadal steroids coordinating several hypothalamic and limbic functions, the amygdaloid structures of treated groups, even with a lower number of neurons in relation to control group, may, through high local concentrations of AAS, stimulate glutamatergic transmission, increasing the excitatory signals in these neurons and keeping the aggressiveness responses statistically equal to those of control group. At the same time, it is also necessary to take into account the capacity of AAS to affect the gabaergic and serotoninergic transmissions, and may also

result in a greater excitation of these neurons. In view of this situation, it is necessary to carry out new studies seeking to highlight how the AAS have led to these changes in behavioral responses.

In one study, it was observed that the AAS chronic use in mice has been shown to induce dose-, sex- and age-dependent changes in the GABA-receptor subunit gene expression in anterior brain areas.[27] As observed in the present study, when evaluating neuronal density, it can be noted that both stanozolol and testosterone cypionate may lead to a decrease in the number of neuron body cells in mice. A statistically significant decrease in this number was observed in BLA of the stanozolol male animals group, testosterone cypionate and stanozolol female animals groups when compared with their respective control ones. We also observed the same result in the VPN of all experimental groups. These results are in agreement with previously published outcomes.[28,29]

In general, it seems that AAS physiological doses have the ability to play a neuroprotective role; however, when AAS is administered in high concentrations, they appear to exert a deleterious effect on neuron body cells, and most studies show an excitotoxic effect when using concentrations. The same was observed by some other authors, who found that pre-treatment with high doses of testosterone increased N-methyl-D-aspartate (NMDA) toxicity. Low testosterone concentrations, on other hand, exerted neuroprotective role, but became neurotoxic in presence of aromatase inhibitors.[7,30]

Another study has shown that hippocampal neurogenesis in adult male rats occurs via dihydrotestosterone (DHT) mediation,[31] while other authors have demonstrated that in mouse hippocampal cell culture, high concentrations of testosterone increased the toxicity induced by millimolar concentrations of glutamate, whereas dehydroepiandrosterone (DHEA), a metabolite precursor of testosterone, exerted a neuroprotective role.[32,33]

In vivo studies, androgenic neurosteroids, such as DHEA, testosterone and DHT, play a protective role in the hippocampus against damage induced by excitotoxins, kainic acid and domoic acid.[34,35] Neuroprotection was totally dependent on the availability of the enzyme aromatase, which converts testosterone to stradiol.[36]

Surprisingly, little is known about how androgens affect excitotoxic neuronal death, despite the large numbers of data obtained with female steroids. Excitotoxicity refers to a particular mechanism of neuronal death triggered by excessive stimulation of glutamatergic receptors.[37,38]

N-methyl-D-aspartate receptors are located on the postsynaptic membrane of excitatory synapses and exhibit greater permeability to Ca^{2+} than α-amino-3-hydroxy-5-methyl-4-isoxazolepropionic acid (AMPA) and kainic acid (KA) receptors, a feature that gives them a more active role in neurotoxic mechanisms. When the postsynaptic membrane is in resting potential, the NMDA channels are blocked by a magnesium (Mg^{2+}) ion that prevents the influx of Ca^{2+} to the postsynaptic receptors. However, in postsynaptic depolarization (which may be caused by the activation of AMPA receptors, among others), Mg^{2+} ions are expelled from the NMDA channels, which thus allow the influx of Ca^{2+} in favor of its concentration gradient.[39] In the cytosol, Ca^{2+} is an important second messenger and influences a large number of cellular functions, exerting a regulatory role in cellular proliferation and survival processes, as well as in cell death due to necrosis or apoptosis.[40] The Ca^{2+} influx regulates membrane excitability and the intensity of synaptic transmission through the activation of intracellular signaling cascades dependent on this ion. Excessive concentrations of L-Glu in the synaptic cleft result in hyperstimulation of its receptors and an excessive Ca^{2+} entrance at the postsynaptic receptors, which, together with the release of Ca^{2+} from intracellular reserves, raise the Ca^{2+} concentration above the triggering threshold of regulatory mechanisms by activating the intracellular mechanisms of excitotoxicity that culminate in neuronal death.[41]

Other published data have shown that neuron body cells regulated by glutamate in the hypothalamus are direct targets of gonadal steroids, both androgens and estrogens. Thus, they can easily influence excitatory neurotransmission in these areas in a sexually dimorphic manner.[42] The present work may explain the fact that testosterone cypionate led to a reduction in the number of neuron body cells in the BLA of female subjects but not in that of males.

Conclusion

The results obtained in the quantitative analyzes show that testosterone cypionate and stanozolol in supraphysiological doses are able to cause a significant reduction in the number of neuron body cells in the BLA and in the VPN of the medial amygdala of mice, and these results, added to the behavioral outcomes, may stimulate directly related anxiety-related emotional responses.

Conflicts of Interest

The authors have no conflicts of interest to declare.

References

1 Brower KJ. Anabolic steroids. Psychiatr Clin North Am 1993;16 (01):97–103
2 Clark AS, Fast AS. Comparison of the effects of 17 alpha-methyltestosterone, methandrostenolone, and nandrolone decanoate on the sexual behavior of castrated male rats. Behav Neurosci 1996; 110(06):1478–1486
3 Bahrke MS, Yesalis CE III, Wright JE. Psychological and behavioural effects of endogenous testosterone levels and anabolic-androgenic steroids among males. A review. Sports Med 1990;10(05): 303–337
4 Pope HG Jr, Katz DL. Affective and psychotic symptoms associated with anabolic steroid use. Am J Psychiatry 1988;145(04):487–490
5 Schulte A, Ernst H, Peters L, Heinrich U. Induction of squamous cell carcinomas in the mouse lung after long-term inhalation of polycyclic aromatic hydrocarbon-rich exhausts. Exp Toxicol Pathol 1994;45(07):415–421. Doi: 10.1016/S0940-2993(11)80369-6
6 Kalinine E, Zimmer ER, Zenki KC, et al. Nandrolone-induced aggressive behavior is associated with alterations in extracellular glutamate homeostasis in mice. Horm Behav 2014;66(02): 383–392. Doi: 10.1016/j.yhbeh.2014.06.005
7 Estrada M, Varshney A, Ehrlich BE. Elevated testosterone induces apoptosis in neuronal cells. J Biol Chem 2006;281(35):25492–25501. Doi: 10.1074/jbc.M603193200

8 Talih F, Fattal O, Malone D Jr. Anabolic steroid abuse: psychiatric and physical costs. Cleve Clin J Med 2007;74(05):341–344, 346, 349–352

9 Tucci P, Morgese MG, Colaianna M, et al. Neurochemical consequence of steroid abuse: stanozolol-induced monoaminergic changes. Steroids 2012;77(03):269–275. Doi: 10.1016/j.steroids.2011.12.014

10 Henderson LP, Penatti CA, Jones BL, Yang P, Clark AS. Anabolic androgenic steroids and forebrain GABAergic transmission. Neuroscience 2006;138(03):793–799. Doi: 10.1016/j.neuroscience.2005.08.039

11 Carobrez AP, Bertoglio LJ. Ethological and temporal analyses of anxiety-like behavior: the elevated plus-maze model 20 years on. Neurosci Biobehav Rev 2005;29(08):1193–1205. Doi: 10.1016/j.neubiorev.2005.04.017

12 Lister RG. The use of a plus-maze to measure anxiety in the mouse. Psychopharmacology (Berl) 1987;92(02):180–185

13 Ribeiro CM, Silva DK, Damião B, et al. Análise quantitativa de células de Purkinje em camundongos sob o uso dos esteroides anabolizantes. Revista Neurociências 2014;22(03):432–437. Doi: 10.4181/RNC.2014.22.03.969.6p

14 von Bartheld CS, Bahney J, Herculano-Houzel S. The search for true numbers of neurons and glial cells in the human brain: A review of 150 years of cell counting. J Comp Neurol 2016;524(18): 3865–3895https://doi.org/doi. Doi: 10.1002/cne.24040

15 Franklin KBJ, Paxinos G. Paxinos and Franklin's The mouse brain in stereotaxic coordinates, 3rd edn. Academic Press, an imprint of ElsevierNew York

16 Kádár A, Sánchez E, Wittmann G, et al. Distribution of hypophysiotropic thyrotropin-releasing hormone (TRH)-synthesizing neurons in the hypothalamic paraventricular nucleus of the mouse. J Comp Neurol 2010;518(19):3948–3961https://doi.org/doi. Doi: 10.1002/cne.22432

17 Mandarim-de-Lacerda CA. Stereological tools in biomedical research. An Acad Bras Cienc 2003;75(04):469–486

18 Boyce RW, Dorph-Petersen KA, Lyck L, Gundersen HJ. Design-based stereology: introduction to basic concepts and practical approaches for estimation of cell number. Toxicol Pathol 2010;38(07):1011–1025https://doi.org/doi. Doi: 10.1177/0192623310385140

19 Mühlfeld C, Papadakis T, Krasteva G, Nyengaard JR, Hahn U, Kummer W. An unbiased stereological method for efficiently quantifying the innervation of the heart and other organs based on total length estimations. J Appl Physiol (1985) 2010;108(05): 1402–1409https://doi.org/doi:10.1152/japplphysiol.01013.2009

20 Ambar G, Chiavegatto S. Anabolic-androgenic steroid treatment induces behavioral disinhibition and downregulation of serotonin receptor messenger RNA in the prefrontal cortex and amygdala of male mice. Genes Brain Behav 2009;8(02):161–173. Doi: 10.1111/j.1601-183X.2008.00458.x

21 Rocha VM, Calil CM, Ferreira R, Moura MJ, Marcondes FK. Influence of anabolic steroid on anxiety levels in sedentary male rats. Stress 2007;10(04):326–331. Doi: 10.1080/10253890701281344

22 Bitran D, Kellogg CK, Hilvers RJ. Treatment with an anabolic-androgenic steroid affects anxiety-related behavior and alters the sensitivity of cortical GABAA receptors in the rat. Horm Behav 1993;27(04):568–583. Doi: 10.1006/hbeh.1993.1041

23 Rainnie DG. Serotonergic modulation of neurotransmission in the rat basolateral amygdala. J Neurophysiol 1999;82(01):69–85

24 Friedel A, Geyer H, Kamber M, et al. 17beta-hydroxy-5alpha-androst-1-en-3-one (1-testosterone) is a potent androgen with anabolic properties. Toxicol Lett 2006;165(02):149–155. Doi: 10.1016/j.toxlet.2006.03.001

25 Oliveira M, Bessa JM, Mesquita A, et al. Induction of a hyperanxious state by antenatal dexamethasone: a case for less detrimental natural corticosteroids. Biol Psychiatry 2006;59(09): 844–852. Doi: 10.1016/j.biopsych.2005.08.020

26 Hallberg M, Johansson P, Kindlundh AM, Nyberg F. Anabolic-androgenic steroids affect the content of substance P and substance P(1-7) in the rat brain. Peptides 2000;21(06):845–852

27 McIntyre KL, Porter DM, Henderson LP. Anabolic androgenic steroids induce age-, sex-, and dose-dependent changes in GABA(A) receptor subunit mRNAs in the mouse forebrain. Neuropharmacology 2002;43(04):634–645

28 Damião B, Souza GG, Nogueira DA, et al. Quantificação de Corpos de Neurônios em Camundongos Submetidos ao Uso de Esteroides Anabolizantes. Revista de Neurociências 2012;20(01):68–72

29 Freitas AC, Damiao B, Alves DM, et al. Efeitos dos anabolizantes sobre a densidade de neurônios dos núcleos da base. Rev Bras Med Esporte 2017;23(03):213–216. Doi: 10.1590/1517-869220172303151688

30 Orlando R, Caruso A, Molinaro G, et al. Nanomolar concentrations of anabolic-androgenic steroids amplify excitotoxic neuronal death in mixed mouse cortical cultures. Brain Res 2007; 1165:21–29. Doi: 10.1016/j.brainres.2007.06.047

31 Okamoto M, Hojo Y, Inoue K, et al. Mild exercise increases dihydrotestosterone in hippocampus providing evidence for androgenic mediation of neurogenesis. Proc Natl Acad Sci U S A 2012;109(32):13100–13105. Doi: 10.1073/pnas.1210023109

32 Yang P, Lones BL, Henderson LP. Mechanisms of anabolic androgenic steroid modulation of GABAA receptors. Neuropharmacology 2002;43(04):619–633. Doi: 10.1016/S0028-3908(02)00155-7

33 Cardounel A, Regelson W, Kalimi M. Dehydroepiandrosterone protects hippocampal neurons against neurotoxin-induced cell death: mechanism of action. Proc Soc Exp Biol Med 1999;222(02): 145–149

34 Frye CA, Reed TA. Androgenic neurosteroids: anti-seizure effects in an animal model of epilepsy. Psychoneuroendocrinology 1998; 23(04):385–399

35 Ramsden M, Shin TM, Pike CJ. Androgens modulate neuronal vulnerability to kainate lesion. Neuroscience 2003;122(03):573–578

36 Azcoitia I, Sierra A, Veiga S, Honda S, Harada N, Garcia-Segura LM. Brain aromatase is neuroprotective. J Neurobiol 2001;47(04): 318–329

37 [REMOVED HYPERLINK FIELD]Choi DW. Glutamate neurotoxicity and diseases of the nervous system. Neuron 1988;1(08):623–634

38 Rothman SM, Olney JW. Excitotoxicity and the NMDA receptor–still lethal after eight years. Trends Neurosci 1995;18(02):57–58

39 Kubo M, Ito E. Structural dynamics of an ionotropic glutamate receptor. Proteins 2004;56(03):411–419. Doi: 10.1002/prot.20154

40 Orrenius S, Ankarcrona M, Nicotera P. Mechanisms of calcium-related cell death. Adv Neurol 1996;71:137–149, discussion 149–151

41 Sattler R, Tymianski M. Molecular mechanisms of calcium-dependent excitotoxicity. J Mol Med (Berl) 2000;78(01):3–13. Doi: 10.1007/s001090000077

42 Diano S, Naftolin F, Horvath TL. Gonadal steroids target AMPA glutamate receptor-containing neurons in the rat hypothalamus, septum and amygdala: a morphological and biochemical study. Endocrinology 1997;138(02):778–789. Doi: 10.1210/endo.138.2.4937

Cadaveric Study of Anatomical Variations in the Musculocutaneous Nerve and in the Median Nerve

Abhilasha Priya[1] Chandni Gupta[2] Antony Sylvan D'souza[3]

[1] Department of Anatomy, School of Medical Sciences, Sharda University, Greater Noida, Uttar Pradesh, India
[2] Department of Anatomy, Kasturba Medical College, Manipal, Udupi, Karnataka, India
[3] Department of Anatomy, Wayanad Institute of Medical Sciences, Wayanad, Kerala, India

Address for correspondence Abhilasha Priya, MBBS, MD, Department of Anatomy, School of Medical Sciences and Research, Sharda University, Knowledge Park 3, Greater Noida, UP 201310, India (e-mail: abhilasha.priya@sharda.ac.in; dr.abhilashapriya@gmail.com).

J Morphol Sci 2019;36:122–125.

Abstract

Introduction The musculocutaneous nerve and the median nerve are branches from the lateral cord of the brachial plexus with a root value of C5, C6, and C7. The medial root of the median nerve is a branch of the medial cord. The present study aims at observing any variations in these peripheral nerves, so that this knowledge can be utilized by surgeons, anesthesiologists, and orthopedicians during surgical procedures and nerve block.

Materials and Methods The present study was carried on 30 adult embalmed cadavers (60 upper limbs) in the department of anatomy of the Kasturba Medical College , Manipal, India. The infraclavicular part of the brachial plexus was dissected, and any anatomical variations in the formation and in the branching pattern of the musculocutaneous nerve and of the median nerve were noted and photographs were taken.

Results The median nerve was noted to be formed from 3 roots in 8 out of 60 dissected upper limbs (13.33%). The musculocutaneous nerve was absent in 5% of the dissected limbs, and communications between these 2 nerves were noted in 13.33% of the dissected limbs.

Conclusions Noted variations of the nerves may be of help to surgeons operating in the axillas and in the arms.

Keywords
- communication
- lateral cord
- macroscopic human anatomy
- median nerve
- musculocutaneous nerve

Introduction

The brachial plexus is formed by the ventral rami of the lower four cervical nerves and by the first thoracic nerve, and it supplies the upper limbs. C5, C6, C7, C8 and T1 roots unite to form trunks (upper, middle, and lower) that divide into anterior and posterior divisions. The anterior divisions of the upper and middle trunks unite to form the lateral cord, which lies laterally to the axillary artery. The musculocutaneous nerve is a continuation of the lateral cord and leaves the axilla by piercing the coracobrachialis muscle. It supplies all of the muscles of the anterior compartment of the arm and continues as a lateral cutaneous nerve of the forearm. The median nerve is formed by two roots; the medial root of the median nerve from the medial cord, and the lateral root of the median nerve from the lateral cord. Both roots join to form

Abhilasha Priya's ORCID is https://orcid.org/0000-0003-4739-2526.

received
July 24, 2018
accepted
March 28, 2019

DOI https://doi.org/10.1055/s-0039-1688799.
ISSN 2177-0298.

Copyright © 2019 by Thieme Revinter Publicações Ltda, Rio de Janeiro, Brazil

License terms

the median nerve in front of the third part of the axillary artery. The median nerve crosses the brachial artery from the lateral to the medial side in the middle of the arm and does not originate any branches in the arm. In the literature, various anatomical variations were described by many authors. The knowledge regarding these variations can serve as a useful guide for surgeons operating in the axillas and in the arms.[1]

Materials and Methods

The present study was conducted on 60 upper limbs dissected in the anatomy department of the Kasturba Medical College, Manipal, India, over a period of 2 years. The cadavers were embalmed and preserved in a weak formalin solution. The infraclavicular part of the brachial plexus was dissected according to the guidelines of the Cunningham's manual of Practical Anatomy.[2] During the dissection, the normal pattern, as well as variations from the normal pattern, were noted and photographed. The number of the variations was noted and the result was tabulated using a regular statistics method. The study was started after obtaining the Institutional Ethical Clearance. Any variations from normal was noted and tabulated (►**Table 1**).

Results

1) Formation of the median nerve by three roots was seen in 8 out of 60 cases. Out of the three roots of median nerve, two roots was given by the lateral cord of the brachial plexus and one root was given by the lateral cord of brachial plexus as seen in ►**Figure 1**.
2) Absence of the musculocutaneous nerve was seen in 3 out of 60 cases (5%). In the absence of the musculocutaneous nerve, the muscles of the anterior compartment of the arm were innervated by the median nerve as seen in ►**Figure 2**.
3) Communication between the median and the musculocutaneous nerves was seen in 8 specimens out of 60 (13.33%). There was a case in which the formation of the median nerve by three roots as well as communication between the median and the musculocutaneous nerve was observed, as seen in ►**Figure 3**.

Discussion

Variations of the lateral cord are not rare and have been reported by many authors in the past, such as Venieratos et al,[3] Beheiry,[4] Budhiraja et al,[5] and Chitra.[6] The comparison with similar studies has been shown in ►**Table 2**. The causes for these anatomical variations in these peripheral nerves are not well understood. It is mentioned that, in humans, the muscles of the upper limbs are derived from the paraxial mesoderm during the 5th week of development.[7] The axons of the spinal nerves grow toward the mesenchyme. If there is any altered signaling between them, it results in significant variations in the nerve pattern.[8]

Venieratos et al[3] described three different types of communications between the musculocutaneous and median nerves in relation to the coracobrachialis muscle. In 16 out of 79 cadavers, 22 communications were found between the musculocutaneous and median nerves. In six subjects, they were present bilaterally. There were three types based on the sites of communications.

Type I: The communication was proximal to the entrance of the musculocutaneous nerve into the coracobrachialis muscle;
Type II: The communication was distal to the coracobrachialis muscle;
Type III: The nerve, as well as the communicating branch, did not pierce the coracobrachialis muscle. Bilateral communications were not necessarily of the same type.

In the present study, the communication between the median nerve and the musculocutaneous nerve was distal to the coracobrachialis muscle.

In the present study, the musculocutaneous nerve was absent in 3 cases out of 60 (5%). Among these three cases, one case of bilateral absence of musculocutaneous nerve was seen. The coracobrachialis muscle was innervated by a thin branch directly from the lateral cord. The rest of the muscles of the anterior compartment were supplied by the median nerve and, finally, one branch from the median nerve continued as a lateral cutaneous nerve of the forearm. This case was similar to one reported by Beheiry.[4] There was no communication between the median nerve and the musculocutaneous nerve observed in this case. The third case of absence of musculocutaneous nerve in the present study was seen in the right upper limb of an adult male cadaver. In the absence of the musculocutaneous nerve, all of the muscles of the anterior compartment of the arm were supplied by the median nerve, which later originated a branch that continued as a lateral cutaneous nerve of the forearm. Budhiraja et al[5] reported the absence of the musculocutaneous nerve in 13 cases out of 116 (11%). In the present study, the

Table 1 Showing all the noted variations

Specimen number	Observed variations	Present in number of dissected upper limbs ($n = 60$)	Percentage
1	Extralateral root of Median nerve	8	13.33%
2	Absence of musculocutaneous nerve	3	5%
3	Communication between the median nerve and themusculocutaneous nerve	8	13.33%

Table 2 Showing comparison of present study with the other studies done by other authors

Authors	Sample size	Absent musculocutaneous nerve	Innervation to muscles of anterior compartment of the arm	Communiction between the median nerve and the musculocutaneous nerve
Beheiry[4]	60	1.66%	Median nerve except coracobrachialis which is supplied by direct branch of lateral cord	5%
Chitra[6]	50	–	–	26%
Joshi[13]	170	5.5%	Median nerve except coracobrachialis which is supplied by direct branch of lateral cord	14%
Budhiraja et al[7]	116	11%	Median Nerve supplying all muscles of anterior compartment of arm in absence of musculocutaneous nerve except coracobrachialis which is supplied by direct branch of lateral cord	26.7%
Dahiphale et al[11]	40	–	–	25%
Balachandra et al[17]	20	–	–	5%
Sah SK et al[9]	26	19..23%	_	_
Naveen Kumar et al[10]	70	3%	–	–
Present Study	60	5%	In absence of musculocutaneous nerve all muscles were supplied by median nerve and not by any direct branch from lateral cord	13.33%

musculocutaneous nerve was seen piercing the coracobrachialis muscle in all of the cases in which it was present.

Communication between the median and the musculocutaneous nerves was observed in 8 cases out of 60 (13.33%). Among these noted communications, five were seen on the left side, and three on the right side. In 1 case out of 60 communications between the median and the musculocutaneous nerves was seen on both arms of an adult male cadaver. According to the studies of Beheiry,[4] Budhiraja et al,[5] Dahiphale et al.,[11] Chitra,[6] and Choi et al.,[12] communications between the median and the musculocutaneous nerves was seen in 5% of the cases, in 20.7% of the cases, in 25% of the cases,

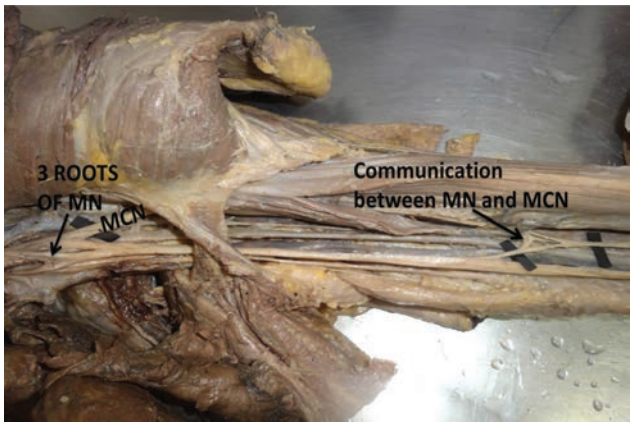

Fig. 1 Three roots of the median nerve with communication between the median nerve (MN)and the musculocutaneous nerve (MCN).

Fig. 2 Absence of musculocutaneous nerve and muscles of the anterior compartment of the arm supplied by the median nerve. Abbreviations: LCNF, lateral cutaneous nerve of the forearm; MN, median nerve.

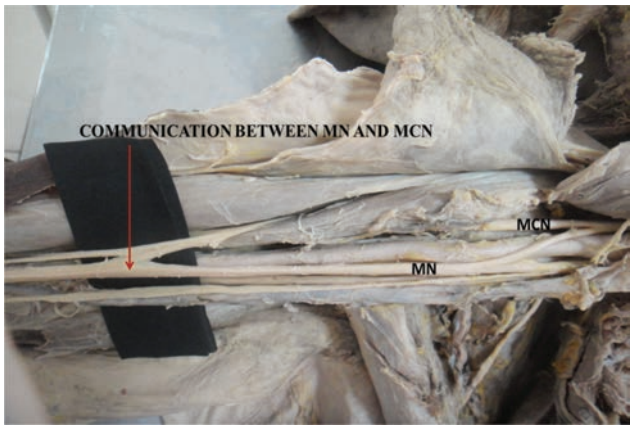

Fig. 3 Communication between the median nerve (MN) and the musculocutaneous nerve(MCN). Absence of musculocutaneous nerve. Median nerve supplying all of the muscles of the anterior compartment of the arm.

in 26% of the cases, and in 46.4% of the cases, respectively. Joshi et al[13] reported absence of the musculocutaneous nerve in 5.5% of the cases, and communication between the median and musculocutaneous nerves was noted in 14% of the cases. The result of the present study is related very closely to this study. In the present study, the communication between the median and the musculocutaneous nerves was more common on the left side, as seen in the study by Choi et al.[12]

In the present study, formation of the median nerve by three roots was noted in 8 out of 60 cases (13.33%). In all of these cases, two roots were coming from the lateral cord, and one root from the medial cord (four on the left side and four on the right side). In one case, there was also communication between the median and the musculocutaneous nerves. A similar case of formation of the median nerve by three roots was described by Sargon et al.,[14] Saeed et al.,[15] and by Das et al.[16]; with two roots from the lateral cord and one from the medial cord. Balachandra et al (2015) observed 3 roots of the median nerve in 5% of the cases with absence of the musculocutaneous nerve.[17]

The variations reported in the present study are of importance to surgeons during arthroscopic shoulder reconstructive surgery, nerve block, and in any surgery performed for pathologies involving the coracobrachialis muscles. Knowledge regarding these nerve variations may also be of use in case of treatment for fractures of the midshaft of the humerus. Chances of damage to these nerves can be due to trauma, to tractions, and to compression. It is observed that variant nerves are more prone to compression neuropathy. The knowledge of these variations also helps in correlating particular clinical manifestations with the involved nerve damage. In patients of breast carcinoma undergoing mastectomy, the coracobrachialis muscle is used as a flap to cover the defect after the mastectomy. Therefore, it becomes important to have knowledge regarding the normal anatomy as well as any observed variations in the muscle.[18]

Conflicts of Interests
The authors have no conflicts of interests to declare.

References

1 Maheria PB, Chinna NG, Khubchandani PR, et al. A Study of Anatomical Variations of the musculocutaneous nerve. Int J Res Med 2013;2(02):1–4
2 Romanes GJ. Cunningham's Manual of Practical Anatomy. Vol 1. 15th edition. London: Oxford University; 1986
3 Venieratos D, Anagnostopoulou S. Classification of communications between the musculocutaneous and median nerves. Clin Anat 1998;11(05):327–331
4 Beheiry EE. Anatomical variations of the median nerve distribution and communication in the arm. Folia Morphol (Warsz) 2004; 63(03):313–318
5 Budhiraja V, Rastogi R, Asthana AK. Anatomical variations of median nerve formation: embryological and clinical correlation. J Morphol Sci. 2011;28(04):283–286
6 Chitra R. Various types of intercommunications between musculocutaneous and median nerve: An analytical study. Ann Indian Acad Neurol 2007;10:100–104
7 Larsen WJ. Human Embryology. 12th edition. Edinburg: Churchil Livingstone; 1997
8 Le Minor JM. A rare variation of the median and musculocutaneous nerves in man. Arch Anat Histol Embryol 1990; 73:33–42
9 Sah SK, Chaudhary D, Pandey N. Prevalence of Absence of Musculocutaneous Nerve among Nepalese Cadaver. Int Journal of Scientific and Research Publication 2016;6(08):222–225
10 Kumar Naveen B, Sirisha V, Kumar Udaya P, Kalpana T. The formation of lateral cord of Brachial Plexus and it's Branches- A Cadaveric Study. Int J. Anat Res 2018;6(1.1):4836–4839
11 Dahiphale VP, Porwal SS, Joshi DS. Variations in the infraclavicular part of brachial plexus- a dissection study. Anatomica Karnataka 2012;6(01):62–65
12 Choi D, Rodríguez-Niedenführ M, Vázquez T, Parkin I, Sañudo JR. Patterns of connections between the musculocutaneous and median nerves in the axilla and arm. Clin Anat 2002;15(01): 11–17
13 Joshi SD, Joshi SS, Athavale SA. Hitch hiking fibres of lateral cord of brachial plexus and the median nerve in search of their destination. J Anat Soc India 2008;57(01):26–29
14 Sargon MF, Uslu SS, Celik HH, Akşit D. A variation of the median nerve at the level of brachial plexus. Bull Assoc Anat (Nancy) 1995;79(246):25–26
15 Saeed M, Rufai AA. Median and musculocutaneous nerves: variant formation and distribution. Clin Anat 2003;16(05): 453–457
16 Das S, Paul S. Anomalous Branching Pattern of Lateral Cord of Brachial Plexus. Int J Morphol 2005;23(04):289–292
17 Balachandra N, Kulkarni V, BR Ramesh. Absence of musculocutaneous nerve- a study of its incidence and clinical implications. International Journal of Basic and Applied Medical Sciences. 2015;5(01):42–47
18 Butz JJ, Shiwlochan DG, Brown KC, Prasad AM, Murlimanju BV, Viswanath S. Bilateral variations of brachial plexus involving the median nerve and lateral cord: An anatomical case study with clinical implications. Australian Medical J 2014;7(05): 227–231

Anatomical Variation of Hepatic Vascularization: Case Report

Cristiane Regina Ruiz[1] Sergio Ricardo Rios Nascimento[1] Alex Kors Vidsiunas[1]
Cristiano Cirqueira de Souza[2] Lilian Andrades[3]

[1] Macroscopical and Imaging Anatomy Postgraduate Course, Centro Universitário São Camilo, São Paulo, SP, Brazil
[2] Human Anatomy Laboratory, Centro Universitário São Camilo, São Paulo, SP, Brazil
[3] Faculty of Medicine, Hospital das Clínicas da Universidade de São Paulo, São Paulo, SP, Brazil

Address for correspondence Sergio R.R. Nascimento, Master, Avenida Nazaré 1501, Ipiranga., CEP: 04263-200. São Paulo – SP, Brasil (e-mail: srrnascimento@gmail.com).

J Morphol Sci 2019;36:126–128.

Abstract

Anatomical variations in the hepatic arteries and in the celiac trunk are important in liver transplants, laparoscopic surgeries, abdominal radiological interventions, and perforating injuries in the abdomen. The goal of the present report is to describe an abdominal vascular variation observed during a routine dissection in the Anatomy Laboratory of the Centro Universitário São Camilo, São Paulo, state of São Paulo, Brazil, in a male individual. The superior mesenteric artery had its origin in the celiac trunk and originated a right accessory hepatic artery that followed its path all the way to the liver. Several authors described variations in the origin and in the path of the hepatic artery and even created specific classifications. The advance of imaging methods that increase the number of studied individuals, without the need of dissection, aids exponentially the quantifying studies that seek to determine a pattern in the variations present in certain populations. The variations of the hepatic artery, as well as of the celiac trunk, have been extensively described in the literature; however, there is no pattern in the number of variations found both in the celiac trunk and in the regular hepatic artery, what leads to a need of description in each case found.

Keywords
- anatomical variation
- clinical anatomy
- macroscopic human anatomy
- morphology applied to other sciences

Introduction

Anatomical variations in the hepatic arteries and in the celiac trunk are of significant importance in liver transplants, laparoscopic surgeries, abdominal radiological interventions, and perforating injuries in the abdomen.[1–4] It is known that the arterial supplying pattern for the liver is variable, even with the occurrence of modifications in the standard organization through which the liver receives its total blood flow, through branches of the celiac trunk, in 25 to 75% of the cases .[2]

The celiac trunk, from which the left gastric arteries, the standard and splenic hepatic, normally originate, can also, in some cases, originate the inferior phrenic arteries and the superior mesenteric artery.[5]

In the literature, we have found numerous quotations about accessory hepatic arteries, when they bring blood to a lobe that is already irrigated by its regular artery, and about the substitute hepatic artery, which is a vase that has an unorthodox origin and irrigates a lobe by itself.

When present, the hepatic accessory artery or the right accessory branch of the hepatic artery originate in the superior mesenteric artery.[5]

The present paper reports a case in which, besides the superior mesenteric artery having an origin in the celiac

received
September 25, 2018
accepted
February 15, 2019

DOI https://doi.org/10.1055/s-0039-1685225.
ISSN 2177-0298.

Copyright © 2019 by Thieme Revinter Publicações Ltda, Rio de Janeiro, Brazil

License terms

trunk, there is a right accessory hepatic artery supplying the liver and originating in the superior mesenteric artery.

Case Report

In a routine dissection in the Anatomy Laboratory of the Centro Universitário São Camilo, São Paulo, state of São Paulo, Brazil, with the intent of removing a few internal organs in a male cadaver, a variation in the number of hepatic arteries, as well as in their origin, was observed. The medical history of the cadaver was not available.

The common hepatic artery originated in the celiac trunk and had a length of 39.01 mm from its origin all the way to its entry on the porta hepatis. From the origin of the common hepatic artery in the celiac trunk all the way to the origin of its gastroduodenal branch, the distance was of 16.41 mm. The superior mesenteric artery also had an anatomic variation, originating from the celiac trunk, and the distance between its origin and the appearance of a right accessory hepatic artery was of 21.77 mm. The right hepatic artery, from its origin in the superior mesenteric artery all the way to its entry on the door of the liver, had 71.99 mm of length (►**Fig. 1**).

Discussion

Several authors have described variations in the origin and in the path of the hepatic artery, and even created specific classifications.[2,6] With the advance in imaging methods, we were able to increase the number of studied individuals without the need of dissection, a fact that aided exponentially the quantitative studies that established a variation pattern in certain populations. Regarding the celiac trunk, Chen et al[7] found its standard formation in 974 cadavers (89.8%), and Ugurel et al,[4] in 50 out of 100 patients (50%). Concerning the origin of the common hepatic artery from the celiac trunk, the study of Hiatt et al[2] found this pattern in 75.7% of the cases, Michels et al[6] in 27.5% of the cases, and Song et al,[8] in 96.44% of the cases.

With regard to a right accessory hepatic artery, the data from the literature show that the incidence is much lower: Michels et al[6] reported an incidence of 9%, Hiatt et al[2] of 10.6%, Araujo Neto et al[1] of 5.1%, and López-Andújar et al[3] of 0.6%.

If we analyze these data based on the authors studied by Hiatt et al[2] and by Chen et al,[7] we can assess that among 15 authors and their results, the rate of the presence of a right accessory hepatic artery is of 12.09%.

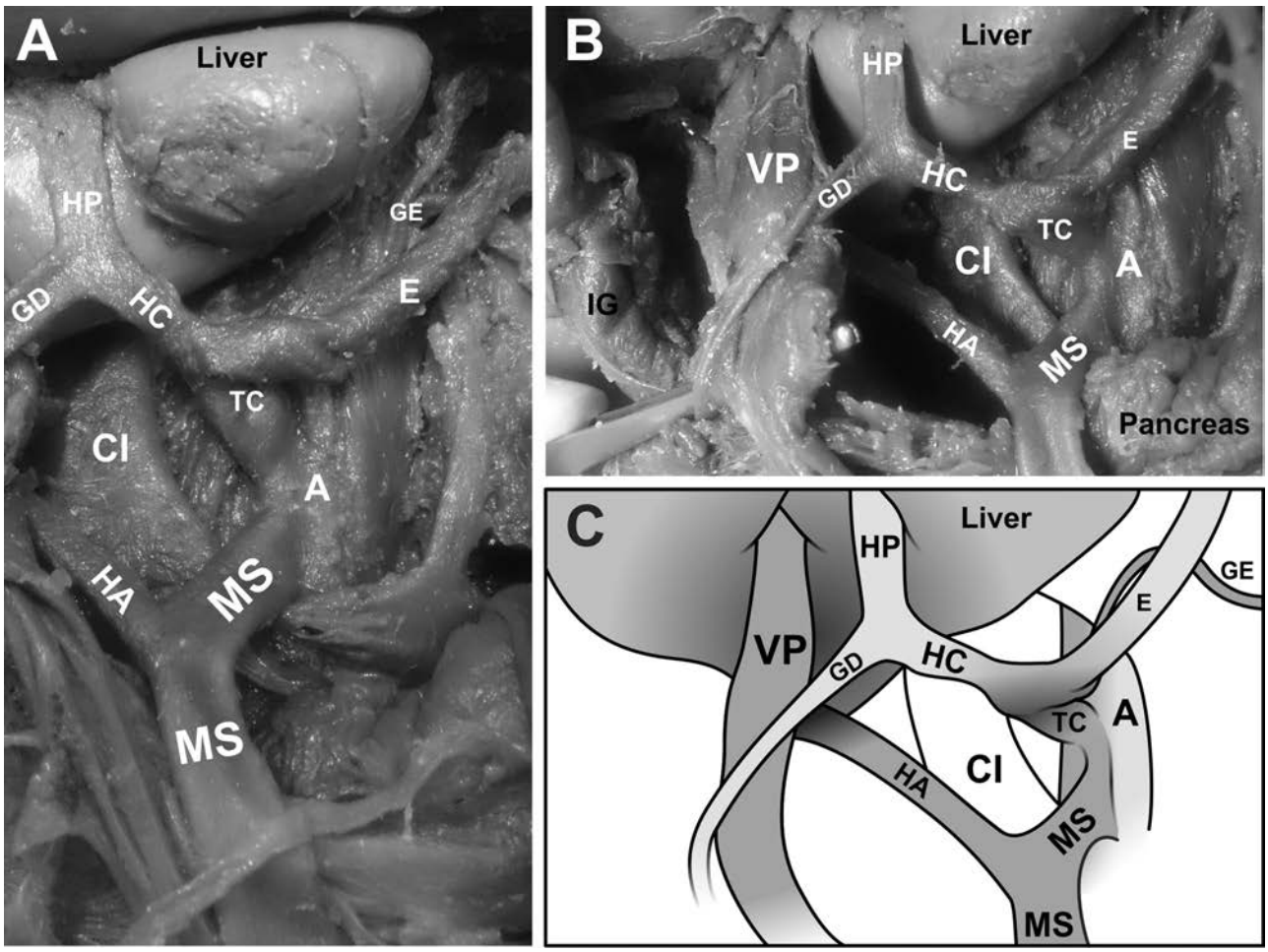

Fig. 1 (**A**, **B**) Photograph of the abdomen, area bellow the liver. (**C**) Schematic illustration based on the photographs. HP: proper hepatic artery; GD: gastroduodenal artery; E: splenic artery; GE: left gastric artery; TC: celiac trunk; A: aorta artery; MS: superior mesenteric artery; HA: accessory hepatic artery; CI: inferior vena cava. VP: portal vein; IG: large intestine.

According to Standring,[5] in general, the right accessory hepatic artery, when present, goes behind the portal vein and the bile duct in the area of the lesser omentum, and can be identified during a surgery through the presence of a pulse behind the portal vein. This artery can be harmed during the resection of the head of the pancreas, since it is very near to the portal vein. This description is identical to the finding of the present article.

Conclusion

The variations of the hepatic artery, as well as of the celiac trunk, have been extensively described in the literature; however there is no pattern to the number of variations found along with the celiac trunk and the common hepatic artery, what leads us to the need of description in each case in which they are found.

Conflicts of Interests
The authors have no conflicts of interests to declare.

References

1 Araujo Neto SA, Franca HA, de Mello Júnior CF, et al. Anatomical variations of the celiac trunk and hepatic arterial system: an analysis using multidetector computed tomography angiography. Radiol Bras 2015;48(06):358–362
2 Hiatt JR, Gabbay J, Busuttil RW. Surgical anatomy of the hepatic arteries in 1000 cases. Ann Surg 1994;220(01):50–52
3 López-Andújar R, Moya A, Montalvá E, et al. Lessons learned from anatomic variants of the hepatic artery in 1,081 transplanted livers. Liver Transpl 2007;13(10):1401–1404
4 Ugurel MS, Battal B, Bozlar U, et al. Anatomical variations of hepatic arterial system, coeliac trunk and renal arteries: an analysis with multidetector CT angiography. Br J Radiol 2010;83(992):661–667
5 Standring S. Gray's Anatomy. The Anatomical Basis of Clinical Practice. 41st ed. New York: Elsevier; 2015
6 Michels NA. Newer anatomy of the liver and its variant blood supply and collateral circulation. Am J Surg 1966;112(03):337–347
7 Chen H, Yano R, Emura S, Shoumura S. Anatomic variation of the celiac trunk with special reference to hepatic artery patterns. Ann Anat 2009;191(04):399–407
8 Song SY, Chung JW, Yin YH, et al. Celiac axis and common hepatic artery variations in 5002 patients: systematic analysis with spiral CT and DSA. Radiology 2010;255(01):278–288

A Rare Case of Absence of the Lateral Cutaneous Nerve of Forearm: Case Report

Helson Freitas da Silveira[1] Jalles Dantas de Lucena[2] Osvaldo Pereira da Costa Sobrinho[3] Roberta Silva Pessoa[3] Gilberto Santos Cerqueira[1] André de Sá Braga Oliveira[4] Howard Lopes Ribeiro Júnior[1]

[1] Department of Morphology, Universidade Federal do Ceará, Fortaleza, CE, Brazil
[2] Postgraduate Program in Morphofunctional Sciences, Universidade Federal do Ceará, Fortaleza, CE, Brazil
[3] Course of Medicine, Universidade Federal do Ceará, Fortaleza, CE, Brazil
[4] Department of Morphology, Universidade Federal da Paraíba, João Pessoa, PB, Brazil

Address for correspondence André de Sá Braga de Oliveira, MD, Centro de Ciências da Saúde, Departamento de Morfologia, Universidade Federal da Paraíba, Campus I, 58059-900, João Pessoa, PB, Brazil (e-mail: andre.sboliveira@gmail.com).

J Morphol Sci 2019;36:129–133.

Abstract

Introduction Variations in the formation and in the branching pattern of the brachial plexus are common. Numerous anastomotic variations between the musculocutaneous nerve (MCN) and the median nerve (MN) have been reported and could be implicated in a wide range of sensory and motor dysfunctions.

Objective To report an uncommon case of an anastomotic variation between the MN and the MCN with a rare absence of the lateral cutaneous nerve of forearm (LCNF).

Material and Methods A dissection of a male cadaver was performed at the Morphology Department of the Universidade Federal do Ceará, Fortaleza, state of Ceará, Brazil. The brachial plexus was exposed.

Results It was observed that the MCN, after its origin in the lateral fasciculus of the brachial plexus, anastomoses with the MN in the middle third of the arm. It diverges from the most prevalent anatomical pattern, in which the MCN continues to pass distally beneath the brachii biceps, originating the LCNF. In this case, the MCN does not emit its main terminal branch, the LCNF, which innervates the lateral portion of the skin of the forearm. In the present case, the innervation of the lateral portion of the skin of the forearm is provided by radial nerve branches. The reported case has practical implications, since the absence of the LCNF could cause hypoesthesia in the skin of the forearm.

Conclusion Thus, the knowledge of the formation and of the branching pattern of the brachial plexus is clinically important for the correct clinical interpretation of the sensory and motor disorders of the upper limbs caused by peripheral nerve injuries, as well as for planning surgical procedures to correct upper limb traumas.

Keywords

- upper limb
- median nerve
- musculocutaneous nerve
- lateral cutaneous nerve of forearm
- brachial plexus

Introduction

Changes in the brachial plexus and in its terminal branches are common, ranging from 12.8 to 53% of the cases.[1,2] The anastomosis between the musculocutaneous nerve (MCN) and the median nerve (MN) are the most common variations observed between brachial plexus branches, corresponding to between 10 and 53.6% of the reports.[3,4]

The normal morphological pattern of the MN is formed by the union of branches of the lateral fasciculus (lateral root of C5, C6 and C7) and also by the contribution of the medial

received
October 23, 2018
accepted
February 15, 2019

DOI https://doi.org/10.1055/s-0039-1685224.
ISSN 2177-0298.

Copyright © 2019 by Thieme Revinter Publicações Ltda, Rio de Janeiro, Brazil

License terms

fasciculus of the brachial plexus (medial root of C8 and T1), following its path through the medial bicipital groove toward the cubital fossa without anastomosis with any other nerve. Mainly, the MN supplies the musculature of the anteromedial compartment of the forearm and part of the muscles and of the skin of the hand.[5]

The MCN originates from the lateral fasciculus of the brachial plexus (lateral root of C5, C6 and C7), where it initially emits a branch to the shoulder and then perforates and innervates the coracobrachialis muscle, follows deep between the biceps brachii and brachialis muscles, and emits a muscle branch for each of these muscles.[6] This nerve extends to the lateral face of the forearm, where it continues as the lateral cutaneous nerve of forearm (LCNF), without any communication with the MN or other nerves.[3]

Although the first reports of communication between the MCN and the MN are dated to the 19th century,[7] knowledge of new anatomical variations between these nerves has neurophysiological, clinical, and surgical implications relevant to the approach to the upper limbs.[2,8,9]

The objective of the present study was to report an uncommon case of an anastomosis between the MCN and the MN with a rare absence of the LCNF, not previously described, and to discuss its possible cause and clinical implications.

Case Report

During a routine dissection of the upper limbs of a glycerin-preserved male cadaver of the Human Anatomy and Dissection Laboratory of the Universidade Federal do Ceará, Fortaleza, State of Ceará, Brazil, an uncommon anatomical variation of the MCN in the right upper limb was observed. The MCN, following the origin of the lateral fasciculus of the brachial plexus, as it is usually seen, pierces the coracobrachialis muscle, traverses between the biceps brachii and brachialis muscles, and sends branches to all of the muscles of the anterior compartment of the arm. However, approximately in the middle third of the arm, the MCN curves medially and anastomoses with the MN, which has a usual path. After the anastomosis between the two nerves, the presence of the LCNF, the terminal branch of the MCN, was not observed, and its agenesis (►**Figs. 1** and **2**) was recorded. Therefore, a careful macroscopic dissection of the arm and of the forearm of the right upper limb was performed to observe the course of the MN after the anastomosis and the other branches of the brachial plexus, revealing that the cutaneous territory that would normally be supplied by the LCNF received innervation from branches originating from the radial nerve. The variation was unilateral, and the innervation pattern of the left upper limb was normal. The arterial pattern in the arm was also normal.

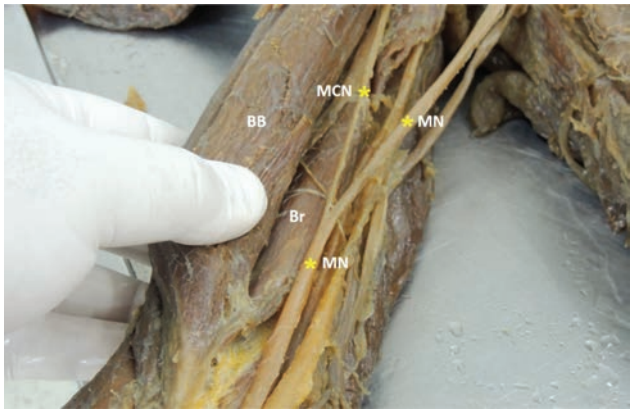

Fig. 1 Communication between the musculocutaneous and the median nerve. MN- median nerve, MCN- musculocutaneous nerve, BB- biceps brachii muscle, Br- brachialis muscle.

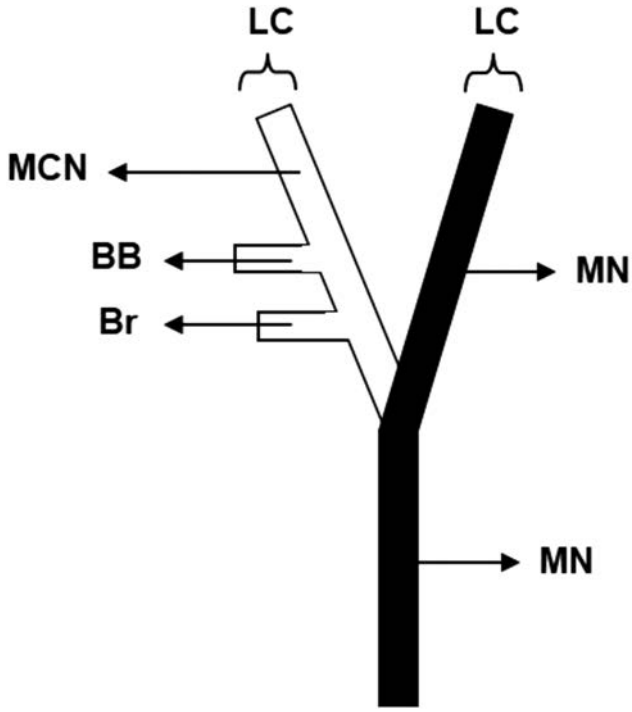

Fig. 2 Schematic diagram showing the communication between the musculocutaneous and the median nerve reported in the present study. LC- lateral cord, MN- median nerve, MCN- musculocutaneous nerve, Br- branch to the brachialis muscle, BB- branch to the biceps brachii muscle.

Discussion

The anastomosis between the MCN and the MN is the most common and frequent anatomical variation found between branches of the brachial plexus.[10] ►**Table 1** describes the communication between the MCN and the MN, and shows the presence of the LCNF in previous studies.

Several classifications of communications between the MCN and the MN were proposed by different authors, based on different criteria.[11] Le Minor[12] classified the communication between the MCN and the MN in five types. In type I, there is no communication between the MCN and the MN; in type II, the lateral fibers of the MN follow those of the MCN in the same sheath, anastomosing with the MN in the middle of the arm; while in type III the fibers of the lateral root of the MN join the MCN and, after some distance, they continue to form the lateral root of the MN. In type IV, the fibers of the MCN join the lateral root of the MN, and after some distance, the MCN arises from the MN. In type V, the MCN is absent, and the muscle fibers supplied by the MCN branch emerge

Table 1 Presentation of the communication between the musculocutaneous nerve and the median nerve, with presence of the lateral cutaneous nerve of forearm in all cases

References	Material analyzed	Communication between the MCN and the MN, and presence of the LCNF
Olave et al, 2000[27]	32 upper limbs of 16 adult cadavers, Brazilian, of both genders	Ten cases of communicating branches between the MCN and the MN, with 9 cases of communicating branch starting from the MCN to the MN, without reports of absence of the LCNF.
Carlotto et al, 2009[28]	Upper left limb of an adult cadaver, Brazilian, male	The MCN originated from the lateral face of the MN, previously crossed the coracobrachialis muscle, to terminate as the LCNF.
Sachdeva et al, 2011[29]	Upper right limb of an adult cadaver, male	The MCN gives a branch to the coracobrachialis muscle, and then anastomoses completely with the MN, no longer appearing. Next, the MN sends branches to the brachialis and brachii biceps muscles, and to the LCNF.
Cerda et al, 2012[11]	Upper limbs of a adult cadaver, Chilean, male	The MCN and the MN had communicating branches in both members. In the right upper limb, the MCN follows the standard anatomy. In the left upper limb, the MCN emits a distal communicating branch to the MN at 15.3 cm from the coracoid process. But, soon after, it terminate as the LCNF.
Radunovic et al, 2013[2]	Upper limb of an adult corpse	Communicating branch of the MCN to the MN was 8.2 cm after the lateral cord branching, inside its passage though the coracobrachial muscle. After the anastomosis, the MCN delivered branches to the brachialis and brachii biceps muscles, and to the LCNF.
Teli et al, 2013[17]	Upper limbs of an adult cadaver, male	Communicating branch of the MCN to the MN. In the middle of the arm, the MCN gave three branches: 1) for the arm, 2) passing between the brachialis and brachii biceps muscles that continued as the LCNF, and 3) for the MN, in both arms.
Cerda, 2014[30]	Upper limbs of an adult cadaver, Chilean, male	In the left upper limb, the MCN penetrated the coracobrachialis muscle and gave three terminal branches in the lower third of the arm; branch to the brachialis muscle, to the LCNF and a communicating branch to the MN. In the right upper limb, the MCN penetrated the coracobrachialis muscle and gave four terminal branches in the lower third of the arm; two branches to the brachialis muscle, one to the LCNF, and a branch communicating to the MN.
Ballesteros et al, 2015[31]	106 upper limbs of 53 adult cadavers, Colombians, male	Communicating branch in 21/106 upper limbs. In 17% of the cases, there was a communication from the MCN to the MN, without report of LCNF agenesis. In 2.8% of the cases, the connection was MN-MCN.
Nascimento et al, 2016[32]	Right upper limb of an adult cadaver, male	In the right upper limb, the MCN passed under the coracobrachialis muscle to then give its first branch to the brachii biceps muscle. It then continued for a further 29.56 mm and provided two more branches: the LCNF and a branch for the brachialis muscle. In the sequence it followed for a further 29.34 mm and attached to the MN, which was 145.90 mm long from its origin to its union with the MCN.

Abbreviations: LCNF; lateral cutaneous nerve of forearm; MCN, musculocutaneous nerve; MN, median nerve.

directly from the MN. The anastomosis between the MCN and the MN in the present study does not correspond to any of the described types, since after the anastomosis of the MCN and the MN, agenesis of the LCNF, the terminal branch of the MCN, was observed.

Choi et al[13] classified the communication between the MCN and the MN in three types. In type I, both nerves are fused. In type II, there is a branch of communication between the MCN and the MN. This type was subdivided into two subtypes based on the number of branches of the MCN that join to form a connection with the MN. In type II a, a single branch of the MCN communicates the two nerves, while in type II b, two or three branches of the MCN join in one anastomotic branch to the MN. In type III, two individual communion branches are present between the MCN and the MN. In the present study, the anastomosis between the MCN and the MN does not correspond to any of the described communication patterns.

Venieratos et al[10] studied 79 cadavers and found a communication between the MCN and the MN in 22 corpses. They reported three types of communication between the MCN and the MN, considering the coracobrachialis muscle as a reference point. In type I, the communication between the MCN and the MN is proximal to the entrance of the MCN in the coracobrachialis. In type II, the communication between the two nerves is distal to the coracobrachialis muscle; and in type III, neither the MCN nor its communicating branches pierce the coracobrachialis. The variation presented in the

present study is morphologically similar to that of type 2 of Venieratos et al,[10] but with two important differences: (1) after the anastomosis with the MN, the MCN does not emit its terminal branch, the LCNF, (2) we suggest that the part of the cutaneous innervation of the forearm that is made by the LCNF is supplied by the posterior antebrachial cutaneous nerve (PACN), a branch of the radial nerve, providing sensory innervation to the skin of the posterior forearm.[14]

Matzi et al[15] reported that, after the separation from the radial nerve, the PACN emerged from the lateral intermuscular septum (LIMS), and immediately pierced the deep fascia after emerging from the LIMS.[16] More distally, its main trunk and branches course in the subcutaneous layer to the posterior forearm, as far as the wrist.[14] Data regarding its anatomy remain insufficient, especially regarding its origin and number of branches.[14]

The anastomotic variability between the MCN and the MN described in the literature suggest that these anastomoses may be attributed to ontogenetic and phylogenetic factors that influence the formation mechanism of muscles and nerves of the upper limbs during embryonic life.[17,18]

Significant variations in nerve patterns may be a result of altered signaling between mesenchymal cells and neuronal growth cones.[19] Chiarapattanakom et al[20] believe that the limb muscles develop from the local mesenchyme, while the axons of the spinal nerves grow distally to reach the muscles or the skin. They point to the lack of coordination between the development of muscles and their innervation as a factor responsible for the emergence of a communicating branch. Tatar et al[21] cite that the common origin of the MCN and of the MN from branches of the lateral fasciculus of the brachial plexus is the explanation for many anastomotic variations between these nerves.

There are also those who believe that the communication between the MCN and the MN is reminiscent of phylogenetic development.[6,17] Comparative anatomy studies have observed similar anastomotic branches in monkeys and in some primates, with the connections representing a primitive innervation of the arm muscles.[6] Chauhan et al[3] suggest the correlation between phylogenetic knowledge and knowledge of the development of nerve structures of the upper limbs for the interpretation of nerve anomalies in the development of the arm.

The PACN innervating the LCNF area is of clinical importance, causing variations in the innervated areas and affecting the electrophysiological study. The knowledge of the formation and of the branching pattern of the terminal branches of the brachial plexus is clinically important in order to avoid iatrogenic PACN injury during surgical procedures at the elbow.[14,22] Portal placement in the elbow arthroscopy could injure the nerve.[23] The PACN injury was diagnosed after the surgical treatment of lateral epicondylitis.[24] Furthermore, preservation of the PACN during harvest of the lateral arm free flap for soft tissue reconstruction was associated with less sensory disturbances.[25]

In cases of brachial plexus injuries with denervation of the muscles supplied by the MCN, it is important to know the morphological variations of this structure to improve its intervention. Muscles supplied by the MCN have a good recovery due to surgical reinnervation after the trauma. This behavior is indicated in cases in which spontaneous recovery of movements such as forearm flexion or adduction of the upper limb does not occur. These approaches aim, for example, to release nerve fibers involved by scar tissue that compress or interpose nerve grafts between compromised MCN regions by microsurgery.[26]

In conclusion, the present article showed a rare case of absence of the LCNF, not previously described in the literature, and an uncommon anastomotic variation between the MCN and the MN. Knowledge of these variations is important in surgical approaches and in the treatment of upper limb injuries. Surgeons and clinicians should always consider possible communicating branches during surgical procedures and clinical investigations of the arm.

Conflicts of Interests

The authors declare that have no conflict of interest that might constitute an embarrassment to the publication of this article.

References

1 Johnson EO, Vekris M, Demesticha T, Soucacos PN. Neuroanatomy of the brachial plexus: normal and variant anatomy of its formation. Surg Radiol Anat 2010;32(03):291–297 10.1007/s00276-010-0646-0
2 Radunovic M, Vukasanovic-Bozaric A, Radojevic N, Vukadinovic T. A new anatomical variation of the musculocutaneous and the median nerve anastomosis. Folia Morphol (Warsz) 2013;72(02):176–179
3 Chauhan R, Roy TS. Communication between the median and musculocutaneous nerve – a case report. J Anat Soc India 2002;51 (01):72–75
4 Guerri-Guttenberg RA, Ingolotti M. Classifying musculocutaneous nerve variations. Clin Anat 2009;22(06):671–683 10.1002/ca.20828
5 Standring S. Gray's Anatomy: The Anatomical Basis of Clinical Practice. In: Pectoral girdle, shoulder region and axilla. 41st ed. New York: Churchill Livingstone Elsevier; 2015:791–822
6 Sahu SK, Baruah P, Choudhury PR, et al. Bilateral communicating branch between musculocutaneous and median nerve. Int J Anat Res. 2015;3(03):1252–1254 10.16965/ijar.2015.205
7 Harris W. The True Form of the Brachial Plexus, and its Motor Distribution. J Anat Physiol 1904;38(Pt 4):399–422. 5
8 Budhiraja V, Rastogi R, Asthana AK, Sinha P, Krishna A, Trivedi V. Concurrent variations of median and musculocutaneous nerves and their clinical correlation–a cadaveric study. Ital J Anat Embryol 2011;116(02):67–72
9 Sawant SP, Shaikh ST, More RM. Study of variant connections of median nerve with musculocutaneous nerve. Int J Med Pharma Sci. 2012;3(03):35–43
10 Venieratos D, Anagnostopoulou S. Classification of communications between the musculocutaneous and median nerves. Clin Anat 1998;11(05):327–331 10.1002/(SICI)1098-2353(1998)11:5<327: AID-CA6>3.0.CO;2-M
11 Cerda A, Suazo Galdames I. Bilateral Communications of the Musculocutaneous and Median Nerves, Morphological Aspects and Clinical Significance. Int J Morphol 2012;30(02):651–655 10.4067/S0717-95022012000200048
12 Le Minor JM. [A rare variation of the median and musculocutaneous nerves in man]. Arch Anat Histol Embryol 1990;73:33–42
13 Choi D, Rodríguez-Niedenführ M, Vázquez T, Parkin I, Sañudo JR. Patterns of connections between the musculocutaneous and median nerves in the axilla and arm. Clin Anat 2002;15(01):11–17 10.1002/ca.1085

14 Chodewaratham P, Chentanez V, Agthong A, Huanmanop T. Anatomy of posterior antebrachial cutaneous nerve related to the lateral epicondyle and interepicondylar line. Int J Morphol 2016;34(03):953–957 10.4067/S0717-95022016000300023
15 Matzi V, Hörlesberger N, Hohenberger GM, et al. Minimally invasive approach to the radial nerve–A new technique. Injury 2015;46(12):2374–2378 10.1016/j.injury.2015.09.017
16 MacAvoy MC, Rust SS, Green DP. Anatomy of the posterior antebrachial cutaneous nerve: practical information for the surgeon operating on the lateral aspect of the elbow. J Hand Surg Am 2006;31(06):908–911 10.1016/j.jhsa.2006.03.013
17 Teli CG, Kadlimatti HS, Kate NN. Bilateral communication between musculocutaneous and median nerve. J Dent Med Sci. 2013;12(06):92–94 10.9790/0853-1269294
18 Kothandaraman U, Lokanadham S. Types of communications between musculocutaneous nerve and median nerve. J Clin Biomed Sci. 2014;4(02):300
19 Abhaya A, Bhardwaj R, Prakash R. Bilaterally Symmetrical Dual Origin of Musculocutaneous Nerve. J Anat Soc India 2006;55(02): 56–59
20 Chiarapattanakom P, Leechavengvongs S, Witoonchart K, Uerpairojkit C, Thuvasethakul P. Anatomy and internal topography of the musculocutaneous nerve: the nerves to the biceps and brachialis muscle. J Hand Surg Am 1998;23(02):250–255 10.1016/S0363-5023(98)80122-6
21 Tatar I, Brohi R, Sen F, Tonak A, Celik H. Innervation of the coracobrachialis muscle by a branch from the lateral root of the median nerve. Folia Morphol (Warsz) 2004;63(04):503–506
22 El Falougy H, Selmeciova P, Kubikova E, Stenova J, Haviarova Z. The variable communicating branches between musculocutaneous and median nerves: a morphological study with clinical implications. Bratisl Lek Listy 2013;114(05):290–294
23 Chaware PN, Santoshi JA, Pakhare AP, Rathinam BA. Risk of nerve injury during arthroscopy portal placement in the elbow joint: A cadaveric study. Indian J Orthop 2016;50(01):74–79 10.4103/0019-5413.173510
24 Iyer VG. Iatrogenic injury to posterior antebrachial cutaneous nerve. Muscle Nerve 2014;50(06):1024–1025 10.1002/mus.24347
25 Ki SH. Lateral arm free flap with preservation of the posterior antebrachial cutaneous nerve. Ann Plast Surg 2016;76(05): 517–520 10.1097/SAP.0000000000000296
26 Rodrigues DB, Viegas MLC, Rogério JS, Pereira ELR. Tratamento cirúrgico das lesões traumáticas do plexo braquial. Arq Bras Neurocir. 2014;33(02):125–131
27 Olave E, Gabrielli C, Braga MTT, Del Sol M, De Souza A. Communicating branch between the musculocutaneous and median nerves in man. Rev Chil Anat 2000;18(02):301–304 10.4067/S0716-98682000000200014
28 Carlotto JRM, Ambros LE, Dal Vesco JA, Reichert PR. Anomalus Origin and Traject of Musculocutaneous Nerve. Int J Morphol 2009;27(02):507–508 10.4067/S0717-95022009000200033
29 Sachdeva K, Singla RK. Communication between median and musculocutaneous nerve. J Morphol Sci. 2011;28(04):246–249
30 Cerda A. Third head of biceps brachii muscle, associated with musculocutaneous and median nerve bilateral communication and with a communicating branch between median nerve roots. Int J Morphol 2014;32(02):510–514
31 Ballesteros LE, Forero PL, Buitrago ER. Communication between the musculocutaneous and median nerves in the arm: an anatomical study and clinical implications. Rev Bras Ortop 2014;50 (05):567–572 10.1016/j.rboe.2014.08.009
32 Nascimento SR, Ruiz CR, Pereira E, Andrades L, de Souza CC. Rare anatomical variation of the musculocutaneous nerve - case report. Rev Bras Ortop 2016;51(03):366–369 10.1016/j.rboe.2015.08.019

Clinical and Anatomical Aspects of Anterior Dislocation of the Pisiform Bone

Carlos Romualdo Rueff-Barroso[1] Fernanda Vieira Botelho Delpupo[1] Valéria Paula Sassoli Fazan[2] Sérgio Ricardo Rios Nascimento[3] Lerud Frosi Nunes[4] Rudi Natalli Montenegro[4] Jorge Luiz Kriger[4] Bernardo Garcia Barroso[4]

[1] Department of Morphology, Centro de Ciências da Saúde, Universidade Federal do Espírito Santo, Vitória, ES, Brazil
[2] Department of Surgery and Anatomy, Faculdade de Medicina de Ribeirão Preto, Universidade de São Paulo, Ribeirão Preto, SP, Brazil
[3] Centro Universitário São Camilo, Ipiranga, SP, Brazil
[4] Orthopedics and Traumatology Institute, Vitória Apart Hospital, Serra, ES, Brazil

Address for correspondence Carlos R. Rueff-Barroso, Doctor in Sciences (Human and Experimental Biology), Master in Morphology, Associate Professor of Anatomy and Neuroanatomy, Departamento de Morfologia, Centro de Ciências da Saúde, Universidade Federal do Espírito Santo, UFES, Av. Marechal Campos, 1468, Maruípe, CEP:29.043-900, Vitória, ES, Brazil (e-mail: carlosrueff@yahoo.com.br).

J Morphol Sci 2019;36:134–137.

Abstract

Introduction The pisiform bone is the fourth bone of the proximal row of the carpal bones, and it is located in the tendon of the flexor carpi ulnaris muscle, being considered a sesamoid bone. Traumatic dislocation of the pisiform bone is a rare condition, which usually results from a trauma in dorsal flexion of the wrist. Its treatment can be conservative or surgical, ending or not with the removal of the pisiform bone.

Objective To report a case of a child who fell from his own height and presented wrist pain, diagnosed with dislocation of the pisiform bone. We emphasize the importance of anatomy knowledge in the evaluation of wrist trauma.

Case Report The anamnesis confirmed that the fall occurred with the wrist in hyperextension. The physical examination showed a slight limitation of movement due to pain. Radiographic exams and a computed tomography (CT) scan of the wrist were performed, in which an anterior deviation/luxation of the pisiform bone was evidenced. A conservative treatment with plaster immobilization for analgesia was performed for 1 week. As there were no symptoms and no signs of trauma consistent with the images, such as edema and local ecchymosis, in addition to the early complete disappearance of pain, the responsible team proposed the hypothesis of asymptomatic chronic dislocation of the pisiform bone.

Conclusion Imaging exams in orthopedic traumatology are fundamental for an accurate diagnosis. Nevertheless, they must be associated with knowledge of the anatomy to correlate the image findings with the anamnesis, leading to a better understanding of silent, asymptomatic, and preexisting conditions in the clinical practice.

Keywords
- anatomy
- pisiform bone
- trauma
- dislocation

Introduction

The pisiform bone, from the Latin *pisum* (pea) and *formis* (form), is the fourth proximal carpal bone, and it is considered by some authors as a sesamoid bone due to its location in the tendon of the flexor carpi ulnaris muscle.[1–5] It is the only carpal bone that has a tendon insertion of a forearm muscle.[6] Fleege et al indicate that the pisiform ossification center usually appears between 7.5 and 10 years of age and is fully developed up to the age of 12 years old, being the last carpal bone to ossify[5] (►**Fig. 1**).

The pisiform bone acts as an important point of fixation of soft tissues (►**Fig. 2**). Pevny et al demonstrated the existence of 10 soft tissue structures related to the pisiform bone,

received
December 8, 2018
accepted
February 10, 2019

DOI https://doi.org/10.1055/s-0039-1683860.
ISSN 2177-0298.

Copyright © 2019 by Thieme Revinter Publicações Ltda, Rio de Janeiro, Brazil

License terms

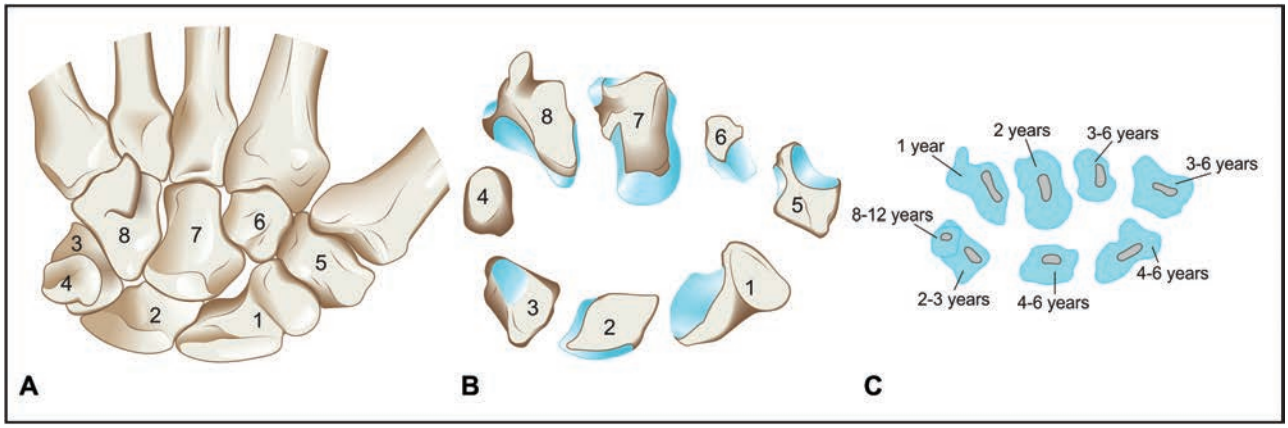

Fig. 1 (A-B) Anatomical arrangement of the carpal bones. Right hand, palmar view. Proximal row: scaphoid (1), lunate (2), triquetrum (3) and pisiform (4). Distal row: trapezium (5), trapezoid (6), capitate (7) and hamate (8). (C) Development of the carpal bones and ossification centers. Based and adapted from Werner Platzer.[7]

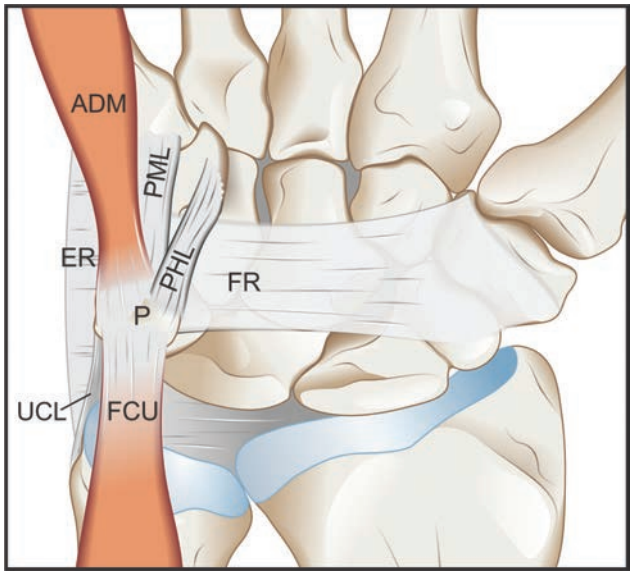

Fig. 2 Main structures attached to the pisiform bone. Right hand, palmar view. Pisiform (P); abductor digiti minimi muscle (ADM), pisometacarpal ligament (PML), pisohamate ligament (PHL), flexor carpi ulnaris muscle (FCU), flexor retinaculum ("transverse carpal ligament") (FR), extensor retinaculum (ER), ulnar collateral ligament of wrist joint (UCL). Based and adapted from Moojen et al.[9]

described as the flexor carpi ulnaris tendon, the extensor retinaculum, the abductor digiti minimi muscle, the flexor retinaculum, the ulnar collateral ligament of the wrist joint, the articular disc of the distal radioulnar joint, the pisohamate ligament, the pisometacarpal ligament, and the pisiform joint capsule, plus a superficial fibrous bundle between the pisiform bone and the hook of hamate.[3,8,9]

The biomechanics of this region contribute to the kinematics of the wrist and of the hand in an indirect and not very relevant way, being the pisiform bone restricted to a fixation point for the aforementioned soft tissues and participating in the joint with the pyramidal bone.[6,10,11] The pisiform bone, like the patella, also acts as a lever and provides increased flexion strength of the wrist and extra stability when the wrist is flexed.[3,6,9]

Historically, the isolated pisiform fracture was identified and described by Guibout in 1847 during a necropsy, along with other carpal fractures.[1,12,13] Although traumatic luxation of the pisiform is a condition reported as rare in the scientific literature, it usually is a result of a trauma in dorsal flexion of the wrist, in which the impact occurs immediately on the hypothenar eminence with the wrist in hyperextension, the forearm in pronation, and the upper limb in adduction.[13,14]

There are also other mechanisms for the pisiform fracture, commonly observed in sports, especially in volleyball players, in which repetitive trauma causes vascular injuries and leads to microfractures and, later, to the evolution to a complete fracture.[1,12,14]

Fractures of the carpal and metacarpal bones represent ~ 6% of all fractures. Isolated fracture of the pisiform is a rare condition, since it is constantly associated with other injuries of the carpus or of the distal end of the radius. In the fracture with concomitant rotation of the pisiform and/or ligament rupture, the treatment can be conservative or surgical, ending up or not with the removal of the pisiform bone.[2,14,15]

The objective of the present study is to report a case of a 9-year-old child who suffered a pisiform dislocation, emphasizing the importance of previous knowledge of the anatomy in the clinical practice, aiming at the correlation of the clinical findings for the correct diagnosis.

Case Report

A 9-year-old male child, led by his parents, presented to the emergency room of the Vitória Apart Hospital reporting pain in the wrist and in the left hand after falling from his own height playing soccer.

During the anamnesis, it was observed that the fall occurred with the wrist in hyperextension and, on the physical examination, there was a slight limitation of the range of motion due to pain. Anteroposterior (AP) and lateral X-ray examinations were performed, showing an anterior deviation of the pisiform bone (►**Figs. 3** and **4**). The child was

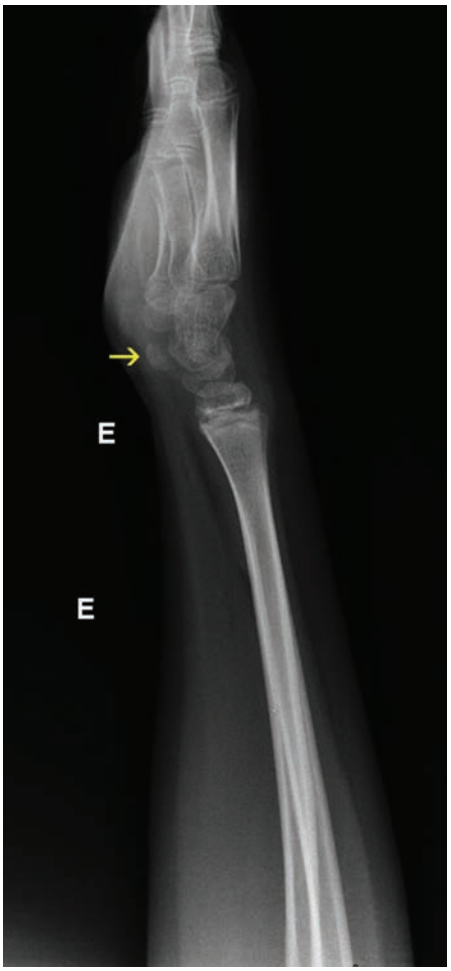

Fig. 3 Lateral radiography view of the left wrist showing the anterior dislocation of the pisiform bone (arrow).

Fig. 4 Lateral radiography view of the right wrist showing a normal anatomical position of the pisiform and carpal bones.

referred for a computed tomography (CT) scan of the wrist with suspected fracture and/or carpal dislocation.

The results of the CT scan showed an anterior dislocation of the pisiform bone; bone irregularity in the pisiform bone with a small adjacent bone fragment measuring 0.2 cm suggestive of microfissure; avulsion or a small ossification nucleus; small joint effusion; slight obliteration of the myotendinous planes; and adipose tissue of the wrist of posttraumatic origin, with preservation of the other bone structures (►**Figs. 5** and **6**).

A conservative treatment with plaster immobilization for analgesia was performed for 1 week. As there were no signs of trauma consistent with the images, such as edema and local ecchymosis, in addition to the early complete disappearance of pain, the responsible team proposed the hypothesis of chronic asymptomatic dislocation of the pisiform bone.

Discussion

The early diagnosis of pisiform fracture is important, since late treatment may result in nonconsolidation and may manifest with chronic pain and limitation of movement.[14] In the present report, the treatment consisted of plaster immobilization for a short period of time that resulted in a good clinical response.

Moojen et al pointed to the fact that traumas of the pisiform bone and of the pisopyramidal joint are not rare. A correct diagnosis, however, is often difficult, in part due to the lack of attention to anatomical structures during the

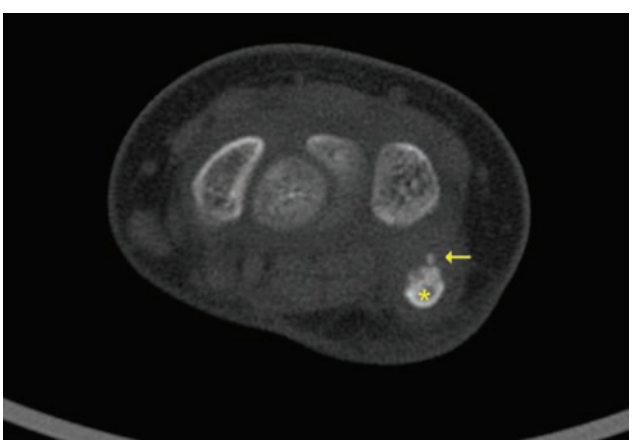

Fig. 5 Axial computed tomography view of the left wrist showing the anterior dislocation of the pisiform bone (*) and a small adjacent bone fragment (arrow).

Fig. 6 Sagittal computed tomography view of the left wrist showing the anterior dislocation of the pisiform bone (*) and a small adjacent bone fragment (arrow).

inspection of the wrist and to the lack of knowledge of the kinematics of the region.[9]

An adequate clinical evaluation and a thorough examination of imaging exams in orthopedic traumatology are essential for an accurate diagnosis. Deep knowledge of the anatomy is essential to correlate the findings of these exams with the anamnesis and to understand the possible existence of silent, asymptomatic, and pre-existent conditions in the clinical practice.

Conflicts of Interest
The authors have no conflicts of interest to declare.

References

1 Kalaria GP, Vora PH, Memon RR. An isolated pisiform fracture: a case report. Int J Res Orthop 2018;4:173–175
2 Verma V, Singh A, Kumar S, Singh MP. Isolated fracture of pisiform: case report of a rare injury of wrist. Int J Medical Update 2016;11(01):19–21
3 Pevny T, Rayan GM, Egle D. Ligamentous and tendinous support of the pisiform, anatomic and biomechanical study. J Hand Surg Am 1995;20(02):299–304
4 Kjosness KM, Hines JE, Lovejoy CO, Reno PL. The pisiform growth plate is lost in humans and supports a role for Hox in growth plate formation. J Anat 2014;225(05):527–538
5 Fleege MA, Jebson PJ, Renfrew DL, Steyers CM Jr, el-Khoury GY. Pisiform fractures. Skeletal Radiol 1991;20(03):169–172
6 Yamaguchi S, Viegas SF, Patterson RM. Anatomic study of the pisotriquetral joint: ligament anatomy and cartilagenous change. J Hand Surg Am 1998;23(04):600–606
7 Werner Platzer. Taschenatlas der Anatomie, in 3 Bãnden. 1: Bewegungsapparat. 9th ed. Stuttgart: Georg Thieme Verlag KG; 2005:137–139
8 Rayan GM, Jameson BH, Chung KW. The pisotriquetral joint: anatomic, biomechanical, and radiographic analysis. J Hand Surg Am 2005;30(03):596–602
9 Moojen TM, Snel JG, Ritt MJPF, Venema HW, den Heeten GJ, Bos KE. Pisiform kinematics in vivo. J Hand Surg Am 2001;26(05): 901–907. Doi: 10.1053/jhsu.2001.26199
10 Raval P, Saeed N, Mahapatra AN. Isolated dislocation of pisiform in an 11-year-old, following a horse bite: a rare injury. Eur Orthop Traumatol 2013;4:273–275
11 Goriainov V, Bayne G, Warwick DJ. Traumatic dislocation of the pisiform: a case report. J Orthop Surg (Hong Kong) 2010;18(03): 389–390
12 Jacobs LG. Isolated fracture of the pisiform bone; a case report. Radiology 1948;50(04):529–531
13 McCARTY V, Farber H. Isolated fracture of the pisiform bone. J Bone Joint Surg Am 1946;28:390–391
14 Applanaidu R. An Isolated Acute Pisiform Fracture. Int J Orthop Surg 2008; 11(01).
15 Hurni Y, Fusetti C, de Rosa V. Fracture dislocation of the pisiform bone in children: a case report and review of the literature. J Pediatr Orthop B 2015;24(06):556–560

Notes on the Accessory Flexor Carpi Ulnaris Muscle: A Rare Supernumerary Variation

Lucas Alves Sarmento Pires[1,2] Graciele de Caro Reis Machado[1] Rodrigo Mota Pacheco Fernandes[1] Jorge Henrique Martins Manaia[1,2] João Francisco Silva Champs[3] Marcio Antonio Babinski[1,2,4]

[1] Department of Morphology, Biomedical Institute, Universidade Federal Fluminense, Niterói, RJ, Brazil
[2] Medical Sciences Postgraduation Program, Hospital Universitário Antonio Pedro, Universidade Federal Fluminense, Niterói, RJ, Brazil
[3] Orthopedics Service, Rede SARAH de Hospitais de Reabilitação, Brasília, DF, Brazil
[4] Traumatology and Orthopaedic Service, Hospital Salgado Filho, Rio de Janeiro, RJ, Brazil

Address for correspondence Lucas Pires, MsC, Departamento de Morfologia, Instituto de Biomedicina da Universidade Federal Fluminense (UFF) Rua Ernani Mello, 101, São Domingos CEP 24.210-150, Niterói, RJ, Brazil (e-mail: lucaspires@id.uff.br).

J Morphol Sci 2019;36:138–140.

Abstract

Variations of the forearm muscles are well described in the literature. In spite of that, reports regarding the accessory flexor carpi ulnaris muscle are scarce due to its rarity. This muscle usually originates from the medial epicondyle of the humerus with the flexor muscle mass and inserts itself into the palmar aponeurosis or the pisiform bone together with the flexor carpi ulnaris muscle. Supernumerary and anomalous muscles of the anterior compartment of the forearm have been associated with ulnar nerve and artery compression. Furthermore, they may also mimic neuromas and soft tissue tumors. The study of supernumerary muscles is necessary, as they may be an option to tendon grafts and muscle flaps. The aim of this paper is to describe the presence of the accessory flexor carpi ulnaris muscle on the left forearm of a cadaver fixated in a phenol solution and discuss its clinical and anthropological significance.

Keywords
- anatomic variations
- flexor carpi ulnaris muscle
- ulnar nerve
- ulnar artery
- anthropology

Introduction

The flexor carpi ulnaris muscle (FCUM) originates from two slips: one from the olecranon and another from the medial epicondyle of the humerus; these muscle bands fuse and forms a fleshy muscle with a strong tendon that inserts itself onto the pisiform bone.[1,2]

The FCUM is innervated by the ulnar nerve (UN), which lies between these fasciculi before they fuse, and it is accompanied by the posterior ulnar recurrent artery. FCUM allows the hand to flex over the forearm and has a slight adductor function.[1,3]

Although variations of the FCUM are rare, it is a clinically significant muscle, as it can cause compression of the UN, and it can be used as a muscle flap for soft tissue reconstruction.[4–6]

Accessory muscles of the forearm can also mimic neuromas or soft tissue tumors, and can contribute to the onset of thrombosis and syndromes such as carpal tunnel. Knowledge of these variations are important to surgery, as most of them are discovered intraoperatively[5,7]

The present work reports the presence of an accessory flexor carpi ulnaris muscle (aFCUM) in a male cadaver and discusses its clinical significance.

Case Report

A male cadaver fixated in a phenol solution was dissected for teaching purposes. The presence of a supernumerary muscle was observed, which was identified as an aFCUM in his left forearm. There were no other associated variations on any side.

received
September 3, 2018
accepted after revision
January 28, 2019

DOI https://doi.org/10.1055/s-0039-1681108.
ISSN 2177-0298.

Copyright © 2019 by Thieme Revinter Publicações Ltda, Rio de Janeiro, Brazil

License terms

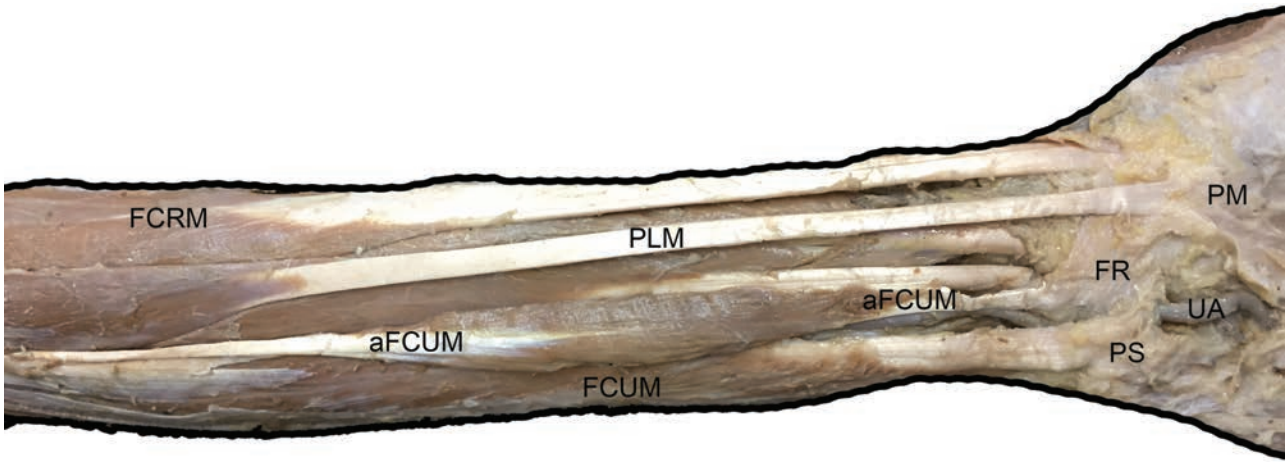

Fig. 1 Anterior view of the dissected forearm. Abbreviations: aFCUM, accessory flexor carpi ulnaris muscle; FCRM, flexor carpi radialis muscle; FCUM, flexor carpi ulnaris muscle; FR, flexor retinaculum; PLM, palmaris longus muscle; PM, palmar aponeurosis; PS, pisiform bone; UA, ulnar artery.

The aFCUM was located medial to the FCUM and lateral to the palmaris longus muscle. Its proximal tendon originated from the medial intermuscular septum together with adjacent muscles, and its distal tendon inserted itself into the flexor retinaculum (►**Fig. 1**). This accessory muscle had a fusiform shape and measured19.8 cm in length.

The ulnar artery and nerve were covered by this accessory muscle during their entire trajectory of the forearm. The floor of the Guyon canal was reinforced by the distal tendon of this muscle (►**Fig. 1**). It was innervated by branches of the UN.

Discussion

Development of the muscles starts with segmentation of the paraxial mesoderm into somites. Each somite has two portions: the sclerotome (which gives origin to bones and cartilages of the thorax and vertebral column) and the dermomyotome (which will form the muscles)[5,8,9]

The myotomes give origin to myoblasts, which go through extensive migration in order to originate the limb muscles. This process starts during the fifth week of development. Then, all myoblasts condense and fuse to form 2 distinct muscle masses on the forearm: the ventral and the dorsal. The ventral mass forms the flexors and pronators, while the dorsal mass forms the extensor and supinator muscles of the forearm.[5,8,9]

Through apoptotic mechanisms and growth factors, each muscle begins to take its shape and current appearance. The presence of supernumerary muscles is usually caused by an increase of cell stimuli, which causes proliferation of muscle tissue and the lack of apoptotic stimuli to cease its growth.[5,8,9]

The FCUM is a fairly consistent muscle that rarely varies (0.02% of all flexor compartment variations). Aberrant origin or insertion, additional slips, partial muscle belly, split tendon, fusion with palmaris longus muscle and the presence of an aFCUM are among reported variations of the FCUM.[1,4,10–12] According to Le Double (1897), the aFCUM was first described by Jarjavay in 1857.[11]

Variations regarding the insertion onto the metacarpals and their joints can be interpreted as regressive dispositions of mammals such as koalas, hyenas and sloths.[11]

Moreover, the ulnar slip of the FCUM is absent in pigs and is in a fibrous state in tapir (*Tapiridae tapirus*). The proximal portion of the FCU is blended with the palmaris longus muscle in rats.[11,13] Its tendon is bifurcated in dogs.[14] Those patterns represent the fact that numerous variations of the FCUM in humans possess similarities with other those of mammals and animals from other species.

Clinically, the presence of supernumerary or abnormally large muscles on the forearm may be the cause of neurovascular bundle compression.[3–5,7,12,15,16] The length, girth, width and the relations of the aFCUM reported herein could predispose an individual to develop compressive neuropathies of the UN not only on the Guyon's canal, but in the whole forearm instead. In addition, the distal insertion on the flexor retinaculum by the aFCUM could compromise the median nerve as well. Furthermore, The aFCUM may simulate a ganglion or a soft tissue tumor.[2]

The ulnar artery could also be a target to compression, as the presence of more muscle mass in the fascial compartment would cause more pressure on this vessel, thus, provoking a decreased local blood flow either during forearm flexion or even in stationary position.[15]

The clinical diagnosis of an accessory muscle belly should be kept in mind when there is a soft and palpable mass at the wrist associated with flexion deformities, albeit not a constant symptom.[16]

Diagnosis often requires imaging techniques, such as CT-scan and MRI. Despite that, most of the muscle anomalies of the forearm are found during surgery or cadaveric dissection. Hence the importance of reporting anatomical variations to provide knowledge and further expand the surgeon's awareness.[2,3]

Furthermore, the FCUM has been used as local and free muscular flap in soft-tissue reconstruction surgery, as well as

in tendon transfer procedures.[5] As the tip of the olecranon has a thin and movable skin, postoperative complications of total elbow arthroplasty are not uncommon. In light of this, FCUM flap has been performed recently due to its regular vascular supply and easy flap obtainment from this muscle.[6] Thus, an aFCUM would also be a good candidate for this procedure, despite its rarity in the general population.

In conclusion, the aFCUM is a clinical and surgical significant variation that should be further studied despite its rare incidence. Nerve compression caused by supernumerary muscles is well described in the literature, specifically in the forearm-hand complex, as the muscles are more prone to vary and the nerves are more exposed due to their relations with the adjacent structures. Supernumerary muscles of the forearm may also confuse diagnosis of soft tissue tumors and neuromas.

Conflicts of Interest

The authors have no conflicts of interest to declare.

Acknowledgments

We wish to thank the body donor and his family for his contribution to the present study.

References

1 Testut L, Latarjet A. Tratado de Anatomía Humana. 8 ed ed. Barcelona: Salvat; 1958
2 Cıftçıoğlu E, Kopuz C, Çorumlu U, Demır MT. Accessory muscle in the forearm: a clinical and embryological approach. Anat Cell Biol 2011;44(02):160–163
3 Campos D, Nazer MB, Bartholdy LM, Souza PL. Accessory flexor carpi ulnaris muscle: a case report of a rare variation in human. Journal of Morphological Sciences. 2010;27(01):30–31
4 Niumsawatt V, Soliman BA, Rozen WM. The aberrant flexor carpi ulnaris and its clinical implications. J Plast Reconstr Aesthet Surg 2013;66(06):e172–e174
5 Sakthivel S, Verma S. Accessory Flexor Carpi Ulnaris and Bilaterally Variant Vascular Anatomy of Upper Limb: An Unusual Presentation. Int J Appl Basic Med Res 2017;7(02):143–145
6 Okamoto S, Tada K, Ai H, Tsuchiya H. Flexor carpi ulnaris muscle flap for soft tissue reconstruction after total elbow arthroplasty. Case Rep Surg 2014;2014:798506
7 Pires L, Perissé JP, Araújo GCS, Manaia J, Fonseca Júnior A, Babinski MA. Hypertrophic reversed palmaris longus muscle: a cadaveric finding. Folia Morphol (Warsz) 2018;77(02):403–405
8 Buckingham M, Bajard L, Chang T, et al. The formation of skeletal muscle: from somite to limb. J Anat 2003;202(01):59–68
9 Schoenwolf G, Bleyl S, Brauer P, Francis-West P. Larsen's Human Embryology. 5th ed. Philadelphia: Churchill Livingstone; 2014:576
10 Tubbs RS, Shoja MM, Loukas M, Eds. Bergman's Comprehensive Encyclopedia of Human Anatomic Variation. Philadelphia: Wiley-Blackwell; 2016
11 Le Double A-F. Traité des variations du système musculaire de l'homme et de leur signification au point de vue de l'anthropologie zoologique. Paris: Schleischer Fréres; 1897
12 Ang GG, Rozen WM, Vally F, Eizenberg N, Grinsell D. Anomalies of the flexor carpi ulnaris: clinical case report and cadaveric study. Clin Anat 2010;23(04):427–430
13 Diogo R, Abdala V, Aziz MA, Lonergan N, Wood BA. From fish to modern humans–comparative anatomy, homologies and evolution of the pectoral and forelimb musculature. J Anat 2009;214 (05):694–716
14 Kuan SY, Smith BA, Fearnside SM, Black AP, Allan GS. Flexor carpi ulnaris tendonopathy in a Weimaraner. Aust Vet J 2007;85(10): 401–404
15 Fröber R, Linss W. Anatomic bases of the forearm compartment syndrome. Surg Radiol Anat 1994;16(04):341–347
16 Iliev A, Georgiev GP, Landzhov B. A rare case of bilateral flexor carpi ulnaris variation: anatomical and clinical considerations and literature review. Revista Argentina de Anatomía Clínica. 2016;8(02):98–103

Sternal Muscle: A Case Report

Pamela Kelly Farias de Aguiar[1] Anna Caroline Duarte Costa Silva[2] André de Sá Braga Oliveira[1] Luciano Edgley dos Santos[2] Felippe Barbosa Gomes[1] Thiago de Oliveira Assis[1,2,3]

[1] Department of Morphology, Universidade Federal da Paraíba, João Pessoa, PB, Brazil
[2] Department of Medicine and Nutrition, Unifacisa, Campina Grande, PB, Brazil
[3] Department of Biology, Universidade Federal da Paraíba, Campina Grande, PB, Brazil

Address for correspondence Thiago de Oliveira Assis, PhD, Departamento de Morfologia, Universidade Federal da Paraíba, Cidade Universitária, S/N, Castelo Branco III - João Pessoa, PB, Brazil, CEP: 58051-900. (e-mail: thiago.oa@hotmail.com).

J Morphol Sci 2019;36:141–144.

Abstract

Introduction The sternal muscle is an anatomical variation found in the anterior region of the thorax.

Objective To report the anatomical characteristics of a new type of sternal muscle.

Case Report This was a dissection study in which the sternal muscle found was unilateral and long.

Discussion Proximal fixation differs from the classification adopted for these cases. Documentation of sternal muscle variations can improve the theoretical database in anatomy as well as aid diagnoses, reducing the probability of the unexpected during clinical and/or surgical thorax-related investigations.

Keywords

- sternal muscle
- anatomical variation
- clinical anatomy

Introduction

The sternal muscle, which is not present in the American population and is more present in the northern China population, presents as an anatomical variation superficially situated at the pectoralis major muscle, usually unilateral, without epidemiological variation in relation to sexual dimorphism.[1] Its low occurrence, estimated to be ~ 8%, and the possibility of confounding it with tumors in the sternal region, justifies its descriptions upon identification. The objective of the present article is to report a case of sternal muscle in a human cadaver.

Case Report

This is an observational dissection study. In the dissection routine at the Anatomy Laboratory of the Morphology Department of the Universidade Federal da Paraíba (Campus I), João Pessoa, state of Paraíba, Brazil, the sternal muscle was found, dissected by routine technique and anatomically characterized.

The most commonly used classification for sternal muscle variations was proposed by Jelev et al[2] and is indicated in ►**Fig. 1**.

The unilateral and long type is the most frequent one, usually originating from the sternocleiomastoid (ECOM) muscle tendon and inserted into the costal cartilages. Silva[3] reported a series of cases in cadavers presenting sternal muscle. In this study, these muscles had origins near the ECOM tendon or even at the manubrium.

In our study, the sternal muscle was dissected through the routine technique and is shown in ►**Fig. 2**.

Our finding reveals a long, unilateral muscle with a length greater than the width and thickness, with proximal fixation in the sternal fascia of the pectoralis major muscle and the distal insertion in the abdominal portion of the pectoralis major muscle.

Discussion

The ontogenesis of the sternal muscle has revealed a muscle as being a reminiscent of four major structures: from the major spinal muscle; from the rectus abdominis muscle; from the musculoskeletal muscle, or from the fleshy panniculus related to the platysma muscle.[4]

Our finding reveals a long, unilateral muscle with a length greater than the width and thickness, with proximal fixation in the sternal fascia of the pectoralis major muscle and the

received
September 5, 2018
accepted
March 28, 2019

DOI https://doi.org/10.1055/s-0039-1688910.
ISSN 2177-0298.

Copyright © 2019 by Thieme Revinter Publicações Ltda, Rio de Janeiro, Brazil

License terms

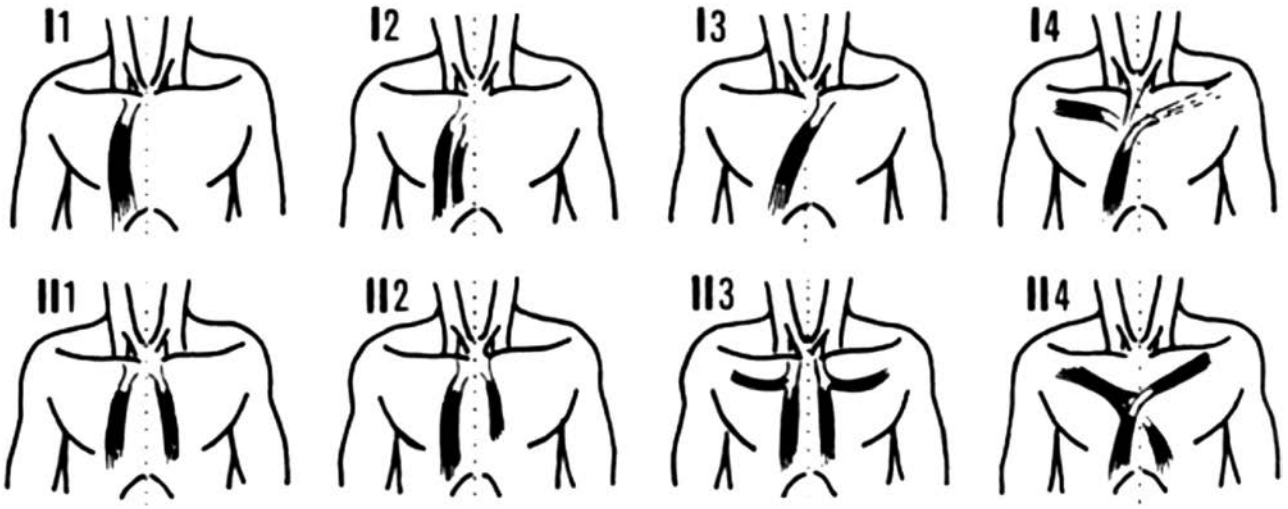

Fig. 1 Variant forms of the sternal muscle previously published by Jelev et al.[2]

Fig. 2 Sternum muscle dissection, anterior to the pectoralis major muscle (A and B). Long muscle with parallel fibers (*).

distal insertion in the abdominal portion of the pectoral muscle. In the classification proposed by Jelev et al,[2] our finding closely resembles type I2, with proximal fixation in the middle axial line of the sternum, but differs in presenting only one venter. Recently, Dudgeon et al[5] also proposed a new variant form to the sternal muscle. This finding was a mixed type with three venters. Therefore, we believe that our finding can also be added to this classification. Interestingly, the phylogenetic theories state that the sternal muscle, when found near the sternum, is derived from primates.[6]

The visualization of the sternal muscle has caused surprise during surgeries.[7] During radical mastectomies in the

treatment of breast carcinomas, the pectoral fascia is folded and the pectoralis major is exposed. In the presence of the sternal muscle, it is necessary to observe its muscular fixations to perform the best cutting plane.[1] In studies using mammography, the sternal muscle was identified, whereas at clinic evaluations it was confused with a mammary lesion.[8]

Therefore, documentation of sternal muscle variations can improve the anatomy theoretical database, as well as aid diagnoses, reducing the probability of the unexpected during clinical and/or surgical thorax-related investigations.

Conflicts of Interests

The authors have no conflicts of interests to declare.

References

1 Povedaa CA, Muñozc EJ, Camargo DC. Músculo esternalis: variante anatómica que simula neoplasia en mamografia. Rev Colomb Cancerol 2013;17(01):46–49

2 Jelev L, Georgiev G, Surchev L. The sternalis muscle in the Bulgarian population: classification of sternales. J Anat 2001; 199(Pt 3):359–363

3 Silva RG. Variação anatômica do músculo esternal: anatomia clínica e revisão da literatura. Salvador: Faculdade de Medicina da Bahia; Universidade Federal da Bahia; 2013:47 (Course conclusion monograph)

4 Raju S, Ragu J, Sreenivasulu RM, Sirisha B, Indira B, Sujata M. Na Unilateral Rectus Sternalis Muscle: It's Clinical Significance. Journal of Surgical Academia 2012;2(01):21–22

5 Dudgeon SN, Marcotte KM, Fox GM, Alsup BK. a previously unclassified variant of sternalis muscle. Surg Radiol Anat 2017: 1–3

6 Bonfiglio NS, Kremer R, Anklam AP, Rios TJ, Guedert DG, Amorim MAP, Lima P. Incidência do músculo esternal em cadáveres dissecados entre os anos de 1989 e 2014 no laboratório de anatomia dafundação universidade regional de Blumenau. FURB.REVISTA SAÚDE E CIÊNCIA online 2015;4(03):98–105

7 Loukas M, Bowers M, Hullett J. Sternalis muscle: a mystery still. Folia Morphol (Warsz) 2004;63(02):147–149

8 Marques EF, Souza JA, Graziano L, Bitencourt AG, Senaga C, Fontes CE. [Sternalis muscle simulating a breast nodule]. Rev Bras Ginecol Obstet 2009;31(10):492–495